KRISTIAN SANDENGEN

PREDICTION OF MINERAL SCALE FORMATION IN WET GAS CONDENSATE PIPELINES AND IN MEG (MONO ETHYLENE GLYCOL) REGENERATION PLANTS

ISBN 82-471-8036-7 (electronic)
ISBN 82-471-8037-5 (printed)

Doctoral Theses at NTNU; 2006:137

This Thesis has been submitted to

Department of Materials Science and Engineering

Norwegian University of Science and Technology (NTNU)

Trondheim

in partial fulfillment of the requirements for the academic degree

PHILOSOPHIAE DOCTOR (PhD)

September 2006

Preface

This work has been carried out at the Department of Materials Science at the Norwegian University of Science and Technology (NTNU), and at the STATOIL research centre at Rotvoll, Trondheim.

Firstly I would like to thank Professor Dr. Tech. Terje Østvold and Dr. Baard Kaasa for being fantastic supervisors and for their support, both professionally and personally. Their enthusiasm has been greatly appreciated for the last three years.

I am grateful for the financial support from STATOIL and NORSK HYDRO and for all the experimental data provided by IFE. I would especially like to thank Marion Seiersten and Arne Dugstad from IFE, and Kari Ramstad and Anne Marie Koren Halvorsen from NORSK HYDRO for useful discussions.

Many thanks are given to Leif Olav Jøsang, Ellen Marie Flaten, Sølvi Slåtten and Peter F. Brown for valuable contributions during the experimental work. I would also like to express my gratitude to all colleagues at STATOIL research centre and at the Materials Science department at NTNU for all support and for nice lunch breaks.

Finally, I thank my parents for believing in me and always inspiring me to take on new challenges. The rest of my family and friends are thanked simply for being who they are, and Sigrid for her love, support and patience.

Summary

Gas hydrate formation is a serious problem in the oil and gas industry, since its formation can plug wells and prevent production. The gas hydrate is a crystalline solid with a natural gas molecule surrounded by a cage of water molecules. It forms at high pressures and low temperatures. This is a problem for offshore gas wells, where the temperature is low in transport lines from well to the production facilities. Mono Ethylene Glycol (MEG) is commonly used as hydrate inhibitor. Classified as a thermodynamic inhibitor, this additive functions just as antifreeze in an automotive radiator.

When producing oil and gas there will in most cases also be produced some water, which can contain dissolved salts. These salts may precipitate and they tend to deposit on surfaces. Deposition of inorganic minerals from brine is called scale.

Generally MEG has the adverse effect of lowering the solubility of most salts. A common method to prevent corrosion in flowlines is to increase pH by adding basic agents (e.g. NaOH, $NaHCO_3$) to the MEG stream. In such cases, carbonate salts are particularly troublesome since an increase in pH by one unit, will reduce the solubility by two orders of magnitude. Thus there will be a trade off between good corrosion protection (high pH) and scale control (low pH).

The aim of this work has been to develop a model that can predict mineral solubility in the presence of MEG. Experimental solubility data, together with thermodynamic data taken from literature, have been utilized to construct empirical functions for the influence of MEG on mineral scale formation. These functions enabled the expansion of an already existing aqueous scale model into a model valid for water+MEG mixed solutions. The aqueous scale model combines an equation of state (gas+oil phase) with the Pitzer ion interaction model (water phase) to describe the multiphase behaviour of gas-oil-water systems. This work describes how MEG has been introduced into the water phase model.

The general idea is that the activity of a specie, *i*, is given as its concentration, *m*, times the activity coefficient, γ, which is divided in two parts. γ^S shall take care of the "Salt effects", and γ^N the "MEG effects";

$$a_i = m_i \gamma_i = m_i \gamma_i^S \gamma_i^N$$

γ^S is calculated by the Pitzer model, as if the solvent was water, and consequently has the same numerical value regardless of the MEG concentration in the water+MEG solvent. γ^N is empirically fitted from solubility data and is obviously a function of MEG concentration. γ^N may also be dependent on temperature and ionic strength.

The pressure dependence of γ^N has not been investigated in this work. All equilibrium constants, $K°$, are independent of MEG concentration. Theoretically this corresponds to a pure water *standard state*. This modelling approach has the advantage that it gives a simple and robust model with reasonable extrapolations outside the range of experimental data. Practically it turns out that the effects of temperature, and that of dissolved species (ionic strength) are almost the same in water+MEG solutions as in water. In such a case a good approximation will be to let the γ^N term merely be dependent on MEG concentration. It has been shown that γ^N for some systems is a function of both temperature and ionic strength in addition to MEG concentration.

The mathematical functions used for curve fitting γ^N were generally arbitrarily chosen polynomials, meaning that they do not have any physical/theoretical basis.

The resulting model has good flexibility and can do exactly the same type of calculations as the aqueous model. It can handle MEG concentrations of up to 99 weight % in the solvent. MEG concentration is commonly specified in the water phase, but the model also accepts MEG input in the gas or oil phase. For conditions encountered in oil and gas transport pipelines and at well heads, the model should function well. It is empirically fitted from solubility data, generally covering the range 0-100°C and 0-100% MEG in the solvent. Hence if the model predicts precipitation of a salt, the ionic strength is normally comparable with the value in the data used for fitting the model. In e.g. a MEG regeneration boiler, however, the temperature is high, and/or several highly soluble species like Na^+, K^+, CO_3^{2-}, Cl^- are present yielding a very high salinity. The model is therefore not suited for calculations at such conditions.

MEG influences the phase distribution of gases. This effect has been included for CO_2, H_2S, CH_4 and the most common organic acids found in the oilfield. CO_2, H_2S, and the organic acids also have MEG dependent dissociation equilibria.

The scale forming minerals included in the model are:

→ $CaSO_4$, $CaSO_4 \cdot 2H_2O$, $BaSO_4$ and $SrSO_4$
→ $CaCO_3$, $FeCO_3$, $BaCO_3$, $SrCO_3$, and $3MgCO_3 \cdot Mg(OH)_2 \cdot 3H_2O$
→ NaCl and KCl
→ $NaHCO_3$ and $KHCO_3$,
→ NaAc and $NaAc \cdot 3H_2O$
→ Na_2CO_3, $Na_2CO_3 \cdot H_2O$ and $Na_2CO_3 \cdot 10H_2O$
→ K_2CO_3 and $K_2CO_3 \cdot 1.5H_2O$
→ FeS
→ $Mg(OH)_2$,

Much new data have been gathered for the water+MEG system, mainly concerning the first dissociation constant of CO_2, the solubilities of the carbonates; $CaCO_3$, $BaCO_3$, $SrCO_3$ and $3MgCO_3 \cdot Mg(OH)_2 \cdot 3H_2O$ as well as the sulphates, $CaSO_4$ and $CaSO_4 \cdot 2H_2O$. These experiments were confined to 20-80°C and ionic strengths of 0-0.7mol/kg.

Hydromagnesite ($3MgCO_3 \cdot Mg(OH)_2 \cdot 3H_2O$) has been included as the only magnesium carbonate mineral in the scale model. Hydromagnesite is actually a meta-stable phase, but the thermodynamically stable magnesite ($MgCO_3$) has been omitted due to its formation being kinetically inhibited. Magnesite of sufficient purity for solubility investigations was not available from commercial suppliers. It was therefore necessary to synthesize it in the laboratory. A new method for synthesizing magnesite from hydromagnesite at atmospheric conditions has been suggested. Mono Ethylene Glycol (MEG) is used to lower the solvent vapour pressure at temperatures above 100°C.

The MEG concentration of an unknown sample is often measured using Gas chromatography (GC). This is an accurate method but has the disadvantage that the sample very often has to be shipped to an external laboratory. A new method for prediction of MEG concentration that is fast, easy and inexpensive has been developed. Values of density, conductivity and alkalinity of an aqueous solution, are used to estimate both MEG and salt contents. The method is valid in the whole concentration interval of 0 to 100 wt% MEG and with ionic strengths from zero to the solubility limits of NaCl and $NaHCO_3$. At intermediate MEG concentrations (40 to 90wt %) the accuracy is regarded as ±2 wt % for MEG content determination. The main limitation is that NaCl and/or $NaHCO_3$ must be the dominating dissolved salts.

pH is an important parameter in carbonate scale prediction. This work summarizes the theoretical foundation and proposes how to work with pH in water+MEG solutions. A pH electrode calibrated only in common aqueous standard solutions, gives a measured value denoted pH_{meas} in this work. pH_{meas} is not reproducible in water+MEG solutions. Calibration also in 0.05m KHPh (Potassium Hydrogen Phtalate) solutions with certain MEG concentrations, gives the calibration value; ΔpH_{MEG}. The actual *pH,* which is reproducible, can thereafter be found from pH_{meas} as;

$$pH = pH_{meas} + \Delta pH_{MEG} + \Delta pH_{Salt}$$

ΔpH_{MEG} has to be determined once for each electrode. ΔpH_{Salt} adjusts for the salt/ionic strength impact on the electrode and is only important at ionic strengths above ~0.5mol/kg.

Table of Contents

1 Introduction

1.1 What is scale?

When producing oil and gas there will in most cases also be produced some water, which contains dissolved salts. These salts may precipitate and they tend to deposit on surfaces. Deposition of inorganic minerals from brine is called scale, and its formation causes flow reduction or even blocking of pipes, valves and other equipment. Common types of scale during oil and gas production are $CaSO_4$, $SrSO_4$, $BaSO_4$ and $CaCO_3$.

Flow reduction can lead to a severe decrease in production rate, and may also lead to safety problems if scale forms e.g. in the down hole safety valve. The economical impact for both prevention and removal of scale can be serious. In some cases the scale may even be radioactive due to small amounts of radium, and must therefore be treated as radioactive waste. Fig. 1.1 shows scale formation in tubing that obviously will constitute a serious flow restriction.

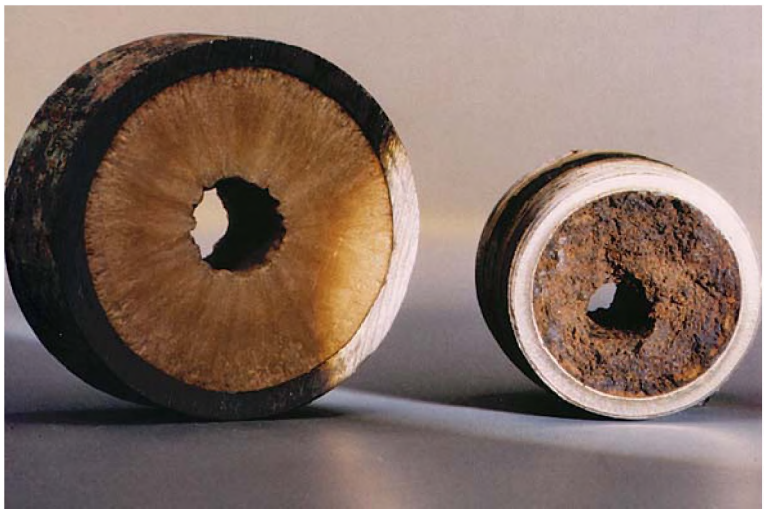

Fig. 1.1: Scale formation in tubing

Scale is not always a problem. Deposition of minerals from brine can be used to seal leaks in concrete and in road tunnels. Another area of application is to bind sand particles together, and scale can be used to stabilize oil field reservoirs[1]. In nature the deposition of $CaCO_3$ is the process forming stalactites found in caves.

1.2 How does scale form?

For scale to form the water solution must first of all be supersaturated. Supersaturation means that the solution contains more dissolved ions than is thermodynamically possible. Thus at a certain time salts have to precipitate. Supersaturation can be achieved in many ways when formation water is produced during oil recovery. Changes in temperature and pressure can cause water evaporation. By removing the solvent (water), salt concentrations obviously increase. Evaporation is the most common cause for deposition of highly soluble minerals like NaCl. Pressure and temperature changes during flow tend to elevate the pH, because of escape of CO_2 from the brine solution. This is particularly troublesome for oil fields with high concentrations of calcium since it results in a solution supersaturated with respect to $CaCO_3$. Another typical example is the mixing of incompatible waters. Sea water is commonly injected into reservoirs to maintain the reservoir pressure and therefore increase oil recovery. It has a high sulphate, SO_4^{2-}, concentration and when this encounters the formation water containing Ca^{2+}, Ba^{2+} and Sr^{2+} it may lead to sulphate precipitation; $CaSO_4$, $SrSO_4$ and $BaSO_4$. This type of scale is usually fairly easy to predict, but $BaSO_4$ is one of the most serious scale forming minerals in the oil industry. The SO_4^{2-} concentration in sea water is therefore frequently reduced prior to injection to avoid such problems. Salt solubility is generally highly temperature dependent, thus temperature changes throughout the productions system is usually a critical factor for scale prediction. Some salts (e.g. $CaCO_3$) have a lower solubility at high temperature and are therefore particularly troublesome on surfaces of heat exchangers and in the hot zone of a well. Others can be troublesome at low temperature.

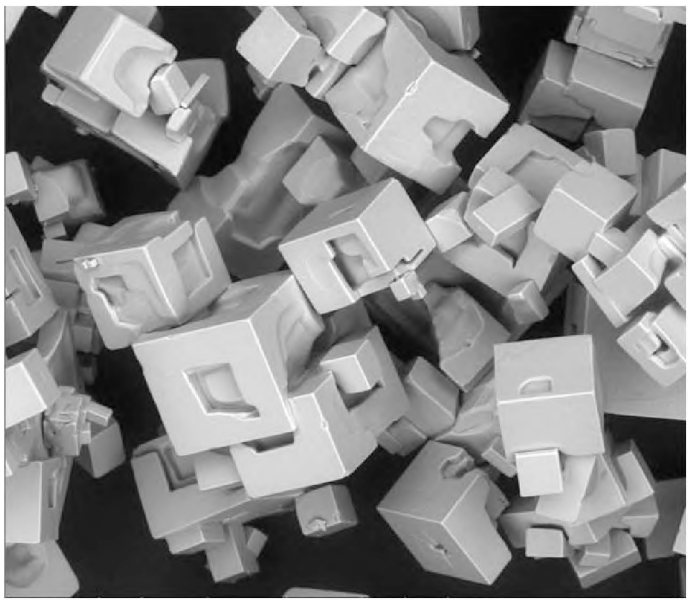

Fig. 1.2: NaCl crystals precipitated from water+MEG (~90wt % MEG), ~140°C. Size 20-100µm.

Even if a solution is supersaturated salt precipitation may not be observed. Kinetics determines how fast precipitation can occur. The rate of precipitation mainly depends on the supersaturation and temperature, but individual salts have very different behaviour. NaCl precipitates almost spontaneously when the solution becomes supersaturated, while e.g. a solution supersaturated with $CaCO_3$ can be left for hours[2] even at 100-120°C without precipitating any solids. Fig. 1.2 shows the nice cube-like structure of a NaCl precipitate.

1.3 Why is Mono Ethylene Glycol (MEG) present?

In the oil and gas industry, gas hydrate formation is a serious problem since its formation can plug wells and prevent production. Gas hydrate is a crystalline solid with a gas molecule surrounded by a cage of water molecules[3]. It forms at high pressures and low temperatures. This is a problem for offshore gas wells, where the temperature is kept low by seawater cooling together with the adiabatic expansion of the gas. Alcohols like Mono Ethylene Glycol (MEG), Ethanol (EtOH) and Methanol (MeOH) are commonly used as hydrate inhibitors. Classified as thermodynamic inhibitors, these additives function just as antifreeze in an automotive radiator, meaning that the freezing point of gas hydrates is lowered.

The main difference between MEG and MeOH is their volatility. MEG has a boiling point of about 200°C and is less volatile than water. Very little MEG will therefore be present in the gas phase. MeOH is more volatile than water and large quantities will be "lost" to the gas phase. This can be a problem for hydrate inhibition, since MeOH must be present at a certain concentration in the aqueous phase. Both from an economic and environmental point of view, these hydrate inhibitors have to be recycled. In this process, however, MeOH can be advantageous. It is simpler and more cost effective to distill MeOH from a water+MeOH solution than water from a water+MEG solution. From a mineral scaling point of view, MEG is generally the better choice since the reduction in salt solubility is less than for MeOH.

1.4 How is scale formation influenced by MEG?

The water molecule is a dipole meaning that it is good at dissolving ionic compounds like inorganic minerals. Alcohols like MEG and MeOH are strong enough dipoles to be miscible with water. Solubility of ionic compounds can be regarded from an electric charge point of view. Between an anion and cation there will be a certain attraction force. If water is put between the ions it counteracts the electric field since it is a dipole and can orientate itself to oppose the field. Thus the force between the ions is reduced. The dielectric constant (=1 for vacuum) is a measure of how effective a solvent is in counteracting the electric field. At room temperature water has a dielectric constant[4] of about 80, which is considerable higher than MEG (~38) and Methanol (~33). This means that ions must be farther away from each other in the alcohols than in water, yielding a lower solubility. Thus generally MEG has the adverse effect of lowering the solubility of most salts. Injection of MEG may therefore cause increased precipitation and scale problems relative to an aqueous solution. A common method to prevent

corrosion in flowlines is to increase pH by adding basic agents (e.g. NaOH, $NaHCO_3$) to the MEG stream. In such cases, carbonate salts are particularly troublesome since an increase in pH by one unit, will reduce the solubility by two orders of magnitude. Thus there will be a trade off between good corrosion protection (high pH) and scale control (low pH). MEG has a complex influence on the solubility of carbonate salts since it changes pH, gas solubility and the CO_2 dissociation.

1.5 This work

Multiscale PVT[5,6] is a thermodynamic scale model mainly developed for oil and gas production applications. It calculates salt solubility (equilibrium conditions) and thereafter scale potential for a wide variety of salts. The Pitzer ion interaction model[7] is used for description of the water and an equation of state for the gas and oil phases. *Multiscale* is merely a thermodynamic model and does not include any kinetic considerations. The aim of this work has been to extend this computer model to include the possibility for predictions in MEG containing solutions.

This work has been divided into several chapters with individual literature reference sections to increase readability. Separate chapters have been given to the topics of "*pH in a mixed solvent*", "*$MgCO_3$ compounds*" and "*A new method for estimation of MEG content*". These subjects have relevance also beyond the scale model of this work, and are therefore presented with separate theoretical and experimental sections.

1.6 References chapter 1

1. Larsen, T. *Sand stabilization with mineral precipitation,* Dr.Ing thesis, Norwegian University of Technology and Science-NTNU, ISBN 82-471-7323-9, (2005)
2. Randhol, P. *Kinetics of calcium carbonate precipitation,* Dr.Ing thesis, Norwegian University of Technology and Science-NTNU, ISBN 82-471-5659-8, (2003)
3. Kan, A. T., Fu, G.,Watson, M. A., Tomson, M. B, "Effect of hydrate inhibitors on oilfield scale formation and inhibition", SPE paper 74657, Proceedings of 2002 Oilfield Scale Symposium, Aberdeen UK (2002)
4. Weast, R.C.,*CRC Handbook of Chemistry and Physics*, 49th ed. (1968), The chemical rubber co.
5. Kaasa, B., *Prediciton of pH, Mineral precipitations and multiphase equilibria during oil recovery*, Dr.Ing thesis, Norwegian University of Technology and Science-NTNU, ISBN 82-471-0339-7(1998)
6. Haarberg, T. *Mineral deposition during oil recovery* Dr.Ing thesis, Norwegian University of Technology and Science-NTNU / NTH, (1989)
7. Pitzer, K. S, Brewer, L. Lewis, G.N., Randall M., *Thermodynamics* 2nd ed. , (1961), McGraw-Hill

2 Theory

This work aims at predicting salt solubility in a mixed MEG+water solvent. Besides temperature and pressure, solubility is dependent on other dissolved species than the salt at question and obviously also on the MEG concentration. This work relies on the same type of *semi-empirical* approach as used by Kan et.al[1,2]. The only main difference is that concentrations in *mol/kg solvent* instead of *mol/kg of water* are used in the modeling, as discussed in detail in section 2.2.3. The term *semi-empirical* is often used in thermodynamic textbooks. It simply implies that a model, although theoretically well founded, includes parameters (extrapolations) that have been fitted from experimental data. The basic idea of this work is that an existing aqueous model shall take care of the main effects of temperature, pressure and salt content/Ionic strength of the solution. On top of this model a purely empirical extension for MEG dependence is added. The MEG dependence is based on experimental data and fitted in a thermodynamic consistent manner.

2.1 Aqueous model

Before discussing the solubility in a mixed solvent it is valuable to look at solubility predictions in an aqueous solution. The basis of this work is the aqueous PVT scale model, *Multiscale*^{tm}, which was developed several years ago. Details can be found in the work of Kaasa[3,4] and Haarberg[5], but the basic thermodynamics and activity coefficient calculation will be given here for the purpose of further discussion. A thorough discussion of thermodynamics of electrolyte solutions can be found in chapter 2 and 9 of Prausnitz et.al[6].

The chemical potential of specie i, μ_i, is related to the activity a_i and fugacity f_i as;

$$\mu_i = \mu_i^o + RT \ln \frac{f_i}{f_i^o} = \mu_i^o + RT \ln a_i \qquad (1)$$

where μ° and f° denotes the chemical potential and fugacity in the standard state respectively. From Eq. 1 it is seen that a_i is unity in the standard state. Either μ° or f° is arbitrary but when one is chosen the other is fixed. Reactions in aqueous solutions usually employ a different standard state for the solvent (water) and the solutes (dissolved species). This is convenient due to the concentration difference of a solvent and a solute. Aqueous solutions typically consist of 99mole% water and pure water is chosen as the standard state for the solvent. This gives a Raoultian standard. By introducing molfraction, x, as concentration measure Eq. 1 becomes;

$$\mu_i = \mu_i^o + RT \ln a_i = \mu_i^o + RT \ln \gamma_i x_i \qquad (2)$$

The activity coefficient, γ, adjusts for the deviation from the ideal case $a_i=x_i$. Water activity is usually found from partial pressure measurements. Dissolved species, however, are usually expressed in terms of molality or molarity, and the activity is defined as;

$$a_i = \frac{f_i}{f_i^o} = \gamma_i \frac{m_i}{m_i^o} \tag{3}$$

f° is the standard fugacity, γ the activity coefficient and m°=1mol/kg solvent, which cancels the dimensionality of m in Eq. 3. The solutes are referred to a *hypothetical ideal solution*[6] of i at system temperature and pressure and at unit concentration. This is known as a Henrian standard state. It is actually a misconception to say that the standard state for the solute is at infinite dilution. At infinite dilution a_i approaches zero, thus the chemical potential of the solute is -∞. The standard state must be at some fixed and non-zero concentration, where unit concentration has been chosen simply since its logarithm is zero. To illustrate this topic regard Fig. 2.1 where the activity of a solute is plotted against the molality, and the hypothetical standard state is shown by point A. The dotted straight line gives the ideal case $\gamma_i=1$.

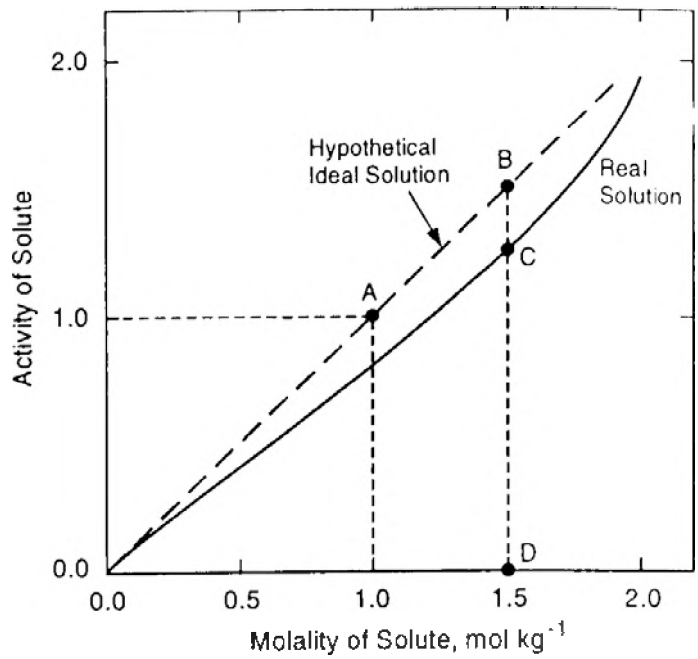

Fig. 2.1: Schematic of the activity, a_i, of a solute as a function of its molality, m_i, from Prausnitz et.al[6].

The difference between the ideal ($m_i = a_i$) and the real solution activity is accounted for by the activity coefficient γ_i. At a molality of 1.5 the actual activity (C) is about 1.3, while the ideal solution has an activity (B) equal to the molality of 1.5, thus the activity coefficient is : $\gamma_i = a_i/m_i = 1.3/1.5 = 0.87$. The practical consequence is that in solutions of very low concentration $a_i = m_i$ while at higher concentration the activity coefficient, γ_i, attains a value different from 1. Thus although the thermodynamic notation may be

confusing the practical use is not very complex. This choice of reference gives that in an ideal solution the *activity* equals the *molality* i.e. $\gamma_i=1$ at all compositions. In a real solution $\gamma_i \to 1$ *as* $m_i \to 0$ i.e. the solution approaches ideality at infinite dilution.

The difference between the Gibbs energy of a real and an ideal solution at the same temperature, pressure and composition is defined as the Excess Gibbs energy[6];

$$G^E = G^{real} - G^{ideal} \tag{4}$$

A model for the Gibbs Excess energy will yield activity coefficients of the solutes i.e. the difference between the dotted and solid line in Fig. 2.1;

$$\ln \gamma_i = \left(\frac{\partial \left(G^E / RT \right)}{\partial n_i} \right)_{T,P,n_{j \neq i}} \tag{5}$$

Several models for Gibbs Excess energy have been published over the years. The Pitzer[7] ion interaction model is probably the most popular and widely used models for electrolyte solutions. On a molality basis it is given by

$$\frac{G^E}{RT} = W_w f(I) + \frac{1}{W_w} \sum_{ij} \lambda_{ij}(I) n_i n_j + \frac{1}{W_w^2} \sum_{ijk} \mu_{ijk} n_i n_j n_k \tag{6}$$

W_w denotes the weight of water, n number of moles, while λ_{ij} and μ_{ijk} corresponds to the second and third virial coefficients in the Pitzer model respectively. *f(I)* must contain the Debye-Hückel limiting law and is consequently a function of ionic strength, temperature and solvent properties like the dielectric constant. This model will not be dealt with in detail here but further information can be found in Pitzer[7]. The equation has a theoretical basis but it contains parameters that must be fitted from experimental data. Hence the final equation is at least partly empirical and the Pitzer model itself must be regarded as a *semi-empirical* approach for modelling of electrolytes. *Multiscale*^{tm} utilizes this Pitzer model for the aqueous phase[3,4].

2.1.1 Supersaturation; Scale Potential

The saturation ratio (SR) is used to describe scale potential for salts. For NaCl it is defined as;

$$SR = \frac{a_{Salt}}{K_{sp}^{o}} = \frac{a_{Na^+} a_{Cl^-}}{K_{sp}^{o}(NaCl)} \tag{7}$$

Eq. 7 gives that SR is equal to the ratio between salt activity and the thermodynamic solubility product. This definition of supersaturation implies that:

SR>1: The salt is supersaturated and may precipitate.
SR=1: At equilibrium
SR<1: The salt is undersaturated. Dissolution occurs if solid is present.

2.2 Mixed solvents

The partial Gibbs free energy for specie *i* is given by the difference in chemical potential between the current state, and that of the chosen standard state, μ_i^o;

$$\mu_i - \mu_i^o = \Delta\overline{G_i} = RT \ln \frac{a_i}{a_i^o} = RT \ln a_i \tag{8}$$

For an ideal system the activity of specie *i* equals the concentration. The transfer from ideal to a real case, or the partial excess Gibbs energy, can be expressed by an activity coefficient γ;

$$\begin{aligned} \Delta\overline{G_i}^{E} &= \Delta\overline{G_i}^{real} - \Delta\overline{G_i}^{ideal} = RT\left(\ln a_i^{real} - \ln a_i^{ideal}\right) \\ &= RT \ln\left(\frac{m_i \gamma_i}{m_i}\right) = RT \ln \gamma_i \end{aligned} \tag{9}$$

In aqueous solutions, the Pitzer model is very well suited for calculating activity coefficients but in a MEG+water mixture the problem is more complex. First one has to consider the standard state. The solute will obviously still be referred to the *hypothetical ideal solution*[6] at concentration of 1molal at system temperature and pressure. However, there exist two good choices for this standard state, since the 1 molal solution can either be in water or in the water+MEG mixture. The latter choice will in principle lead to a different standard state for each concentration of MEG. In this work it was decided to use the water solution reference. This standard is well known, and the thermodynamic constants, $K°$, that are valid in aqueous solutions will consequently remain constant during addition of MEG. The approach is the same as used by Kan et al[1], and is best explained by regarding an example. Eq. 10 gives the

transfer of NaCl from its standard state in water into a real water+MEG solution with salt concentration, *m*, and MEG concentration *x*.

$$NaCl\left(^{\circ},w\right) \rightarrow NaCl\left(m,x_{MEG}\right) \tag{10}$$

(°,w) denotes the standard state of *hypothetical ideal solution* in water as described above. The total Gibbs free energy of transfer for the reaction is given in Eq. 11 where changes in salt and MEG content have individual terms;

$$\Delta\overline{G}^{tot} = \Delta\overline{G}^{ID} + \Delta\overline{G}^{E}_{Salt} + \Delta\overline{G}^{E}_{MEG} \tag{11}$$

Where the terms are

$$\begin{aligned}
\Delta\overline{G}^{ID} &= RT\ln\left(m_{Na^+}m_{Cl^-}\right)\\
\Delta\overline{G}^{E}_{Salt} &= RT\ln\left(\gamma^{S}_{Na^+}\gamma^{S}_{Cl^-}\right)\\
\Delta\overline{G}^{E}_{MEG} &= RT\ln\left(\gamma^{N\pm}_{NaCl}\right)^2
\end{aligned} \tag{12}$$

The activity coefficients γ^S and γ^N shall take care of "salt effects" and "MEG effects" respectively, as discussed below. Fig. 2.2 graphically illustrates the process as the path going first to the right and then down.

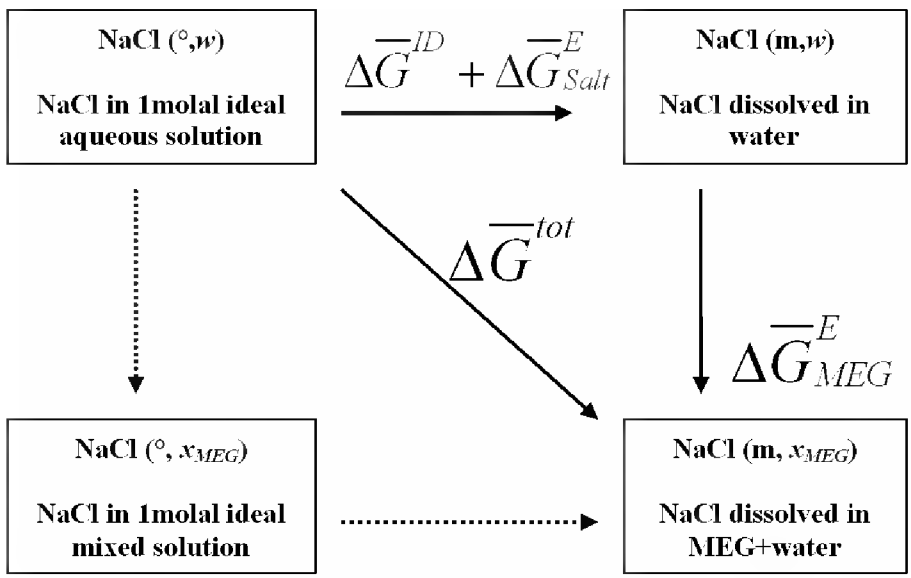

Fig. 2.2: Schematic of the transfer of NaCl from its standard state in water and into an arbitrary NaCl+water+MEG solution.

The first (horizontal) step going from the standard state to the real aqueous solution can be modelled by the Pitzer model since this process does not involve MEG. Going vertically down from this point corresponds to a process where some of the solvent (water) is replaced by MEG. The salt concentration remains constant and Gibbs energy change for the process is given by the $\Delta\overline{G}^{E}_{MEG}$ term. $\Delta\overline{G}^{E}_{MEG}$, however, cannot be equal to the change in standard state from water to a MEG+water solution as it is dependent on the salt concentration. The reason for this can be explained by another possible transfer route going first down and then right in Fig. 2.2.

$$\begin{aligned} NaCl\left(^{o},w\right) &\rightarrow NaCl\left(^{o},x_{MEG}\right) \\ NaCl\left(^{o},x_{MEG}\right) &\rightarrow NaCl\left(m,x_{MEG}\right) \end{aligned} \tag{13}$$

The first step in this process, describes the change in standard state from pure water to the mixed solvent i.e. from the *hypothetical ideal solution*[6] at unit concentration in water (*aqueous* standard) to unit concentration in a mixed solvent (*medium* standard). The second step, from left to right, describes the process of going from the medium standard state to the actual solution, keeping the MEG concentration constant. This process cannot be correctly modelled by the aqueous Pitzer model since the solvent has different properties e.g. the dielectric constant. Thus the two "horizontal" processes in Fig. 2.2 are unequal, and the two "vertical" must consequently also be unequal.

The second route is regarded as the thermodynamic "correct" method, but requires a model for activity coefficients in the mixed solvent. Upgrading the Pitzer model implies that a whole new set of parameters for all MEG+water compositions will have to be constructed[10,13]. This would have been an elaborate job even if all necessary experimental data had been available. Mixed MEG+water data is lacking at present, and such an upgrade of the Pitzer model is therefore virtually impossible. Hence it was decided to use the first approach i.e. the path going first to the right and then down in Fig. 2.2.

Solubility for NaCl in a mixed solution is expressed by Eq. 14, where $K°$ gives the thermodynamic equilibrium constant. m denotes concentration, γ^{S} the aqueous activity coefficient and the $\gamma^{N\pm}$ term describes the MEG dependence that will have to be curve fitted from experimental data.

$$K^{o}_{sp}\left(NaCl\right) = m_{Na^{+}} m_{Cl^{-}} \gamma^{S}_{Na^{+}} \gamma^{S}_{Cl^{-}} \left(\gamma^{N\pm}_{NaCl}\right)^{2} \tag{14}$$

The following procedure was used to construct the model;

- → At each MEG concentration solubility data (*mol/kg solution*) was entered into the aqueous model, which returned γ^{S} values as if the solvent was water.
- → $\gamma^{N\pm}$ was calculated from Eq. 14 using $K°$, the measured solubility m, and the activity coefficients from above.
- → A function for $\gamma^{N\pm}$ was curve fitted as described in detail in Chapter 6

γ^S is independent of MEG and has the same numerical value in a 0.5m NaCl solution containing 99wt% MEG as in water containing 0.5m NaCl. $\gamma^{N\pm}$ consequently contains both the contribution from a change of standard state, as well as the error done by incorrect calculating γ^S as if the solvent was water.

2.2.1 Validity of model

It is most important to note that it is the product of γ^S and $\gamma^{N\pm}$ that is used for solubility calculations, thus their individual values are actually of secondary importance. Generally activity is expressed as molality times an activity coefficient. To calculate it as a product of two parameters is merely a convenient choice, where γ^S shall take care of most of the "salt effects" and $\gamma^{N\pm}$ gives the MEG dependence;

$$\begin{aligned} a_{NaCl} &= m_{Na^+} m_{Cl^-} \gamma^{total}_{NaCl} \\ &= m_{Na^+} m_{Cl^-} \gamma^S_{Na^+} \gamma^S_{Cl^-} \left(\gamma^{N\pm}_{NaCl}\right)^2 \end{aligned} \tag{15}$$

Experimental solubility measurements gives the activity at saturation, thus the total activity coefficient, γ^{total}, will certainly be correct at this point. To investigate what happens at conditions away from saturation it is useful to return to the thermodynamically "correct" route indicated in Fig. 2.2, which is thoroughly described by Mussini and Mazza[8]. By this route the activity of NaCl, referred to an aqueous standard, is given as;

$$a_{NaCl} = m_{Na^+} m_{Cl^-} {}^{sol}\gamma_{Na^+} {}^{sol}\gamma_{Cl^-} {}^{w}_{sol}\gamma^o_{NaCl} \tag{16}$$

${}^{sol}\gamma$ denotes the activity coefficient in the solvent at question and ${}^{w}_{sol}\gamma^o_{NaCl}$ corresponds to the change of standard state as defined below. The top left box in Fig. 2.3 gives the before mentioned *aqueous* standard. Below this is the same type of solution, the only difference being that the solvent is a water+MEG mixture i.e. the *medium* standard. ${}^{sol}\gamma$ denotes the activity coefficient in the *solvent* at question. In the top box it is emphasized that the activity coefficient *in water* is written as γ^S throughout this work. ${}^{sol}\gamma=1$ in the ideal solution, while going from left to right it attains a value in the exact same manner as in an aqueous solution.

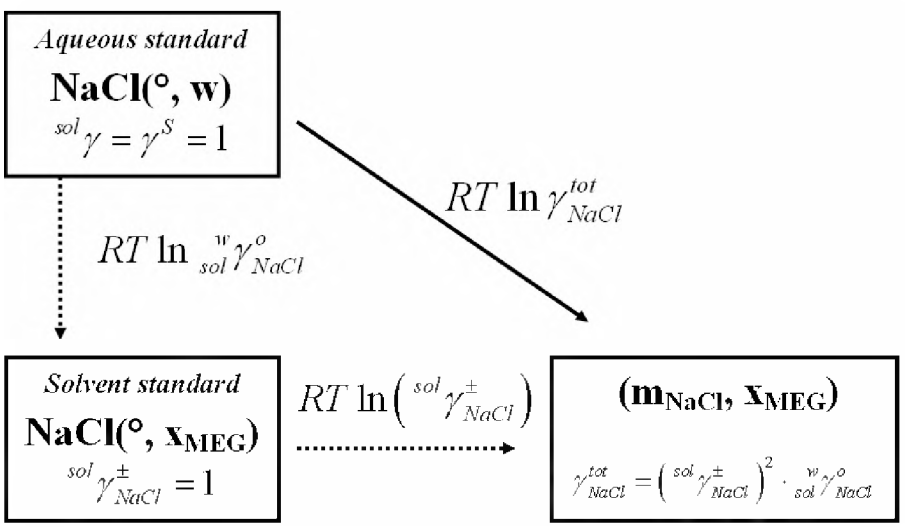

Fig. 2.3: Schematic of the calculation of activity coefficients from an aqueous standard.

The vertical step describes a change of standard state, where ${}^{w}_{sol}\gamma^{o}$ is known as the *primary medium effect* in Owen's terminology[9]. This *primary medium effect* is related to the standard Gibbs' energy change upon transferring NaCl from a *medium* to an *aqueous* standard state as;

$$\ln {}^{w}_{sol}\gamma^{o}_{NaCl} = \left[\Delta \overline{G}^{o}_{\substack{NaCl \\ sol \to w}}\right]\frac{1}{RT} \qquad (17)$$

w denotes water and *sol* the solvent (water+MEG) at question. The change in Gibbs' energy is obviously zero if the solvent is water, and consequently ${}^{w}_{sol}\gamma^{o}_{NaCl} = 1$. Details about how ${}^{w}_{sol}\gamma^{o}_{NaCl}$ is measured by extrapolation to infinite dilution, as well as how activity coefficients are measured by use of an electrochemical cell can be found in Manzoni et. al[11] and Ceccattini et.al[12]. The calculation of ${}^{sol}\gamma$ going from left to right in Fig. 2.3 is generally hindered by lack of data. For KCl and NaCl measurements of the activity coefficient in water+MEG solutions (0-80wt% @25°C) exist[11,12]. Thus for these salts it is possible to directly compare the two approaches in Fig. 2.2. Fig. 2.4 gives the activity coefficient of NaCl in water and in 80wt% MEG i.e. ${}^{sol}\gamma$. The aqueous Pitzer model is given by the solid line. At 80wt% MEG the activity coefficient approaches unity, at low salt content, with a steeper gradient than in water. This is depicted by the Debye Hückel limiting law[6], but unfortunately this equation is valid only for very low (<0.01m) salt contents.

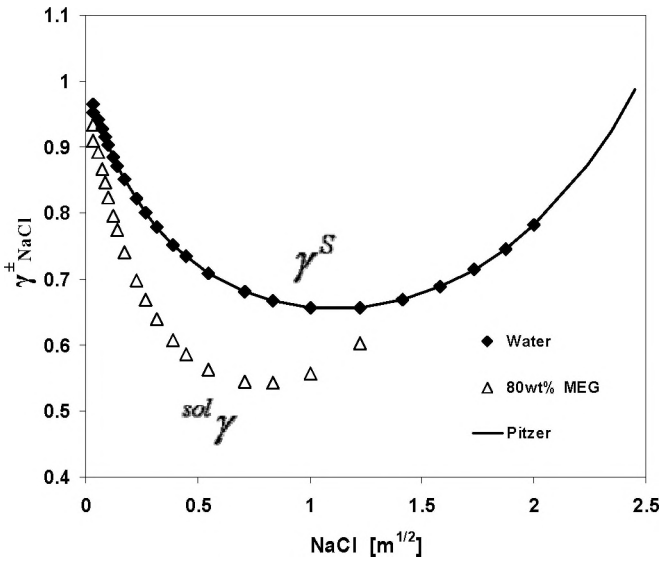

Fig. 2.4: Measured activity coefficients, $^{sol}\gamma^{\pm}$, for NaCl[12] as function of square root of concentration (mol/kg solvent). ♦;water Δ; 80wt% MEG. Solid line; aqueous Pitzer model

γ^S gives the activity coefficient in water, which is calculated by the Pitzer model, while the actual activity coefficient in the solvent at question is written as $^{sol}\gamma$ and it is essential not to confuse the two. It is seen that $^{sol}\gamma$ and γ^S, as expected, are unequal at 80wt% MEG.

$\gamma^{N\pm}$ is fitted at saturation and the two approaches are equal at this point;

$$\begin{aligned} a_{NaCl} &= m_{Na^+} m_{Cl^-} \gamma^{total}_{NaCl} \\ &= m_{Na^+} m_{Cl^-} \gamma^{S}_{Na^+} \gamma^{S}_{Cl^-} \left(\gamma^{N\pm}_{NaCl}\right)^2 \\ &= m_{Na^+} m_{Cl^-} {}^{sol}\gamma_{Na^+} {}^{sol}\gamma_{Cl^-} {}^{w}_{sol}\gamma^{o}_{NaCl} \end{aligned} \tag{18}$$

Because the total activity coefficient is the same it gives that at saturation one can write;

$$\gamma^{S}_{Na^+} \gamma^{S}_{Cl^-} \left(\gamma^{N\pm}_{NaCl}\right)^2 = \gamma^{total}_{NaCl} = {}^{sol}\gamma_{Na^+} {}^{sol}\gamma_{Cl^-} {}^{w}_{sol}\gamma^{o}_{NaCl} \tag{19}$$

This equation summarizes how activities are modeled in MEG+water systems. There are three important points to be made:

- → γ^S and $^{sol}\gamma$ are in principle unequal, thus the curve fitted $\gamma^{N\pm}$ is not equal to the change in standard state given by the *primary medium effect* $^{w}_{sol}\gamma^{o}_{NaCl}$.
- → γ^S and $^{sol}\gamma$ are in principle unequal, thus the Salt/Ionic strength dependence of γ^{tot} (of the left hand side) is wrong at conditions away from saturation.
- → If an ionic strength dependence is included in $\gamma^{N\pm}$, the error in γ^S can be compensated and γ^{total} will be correct at any point.

Using the present model where $\gamma_{NaCl}^{N\pm}$ is only a function of MEG content (see chapter 6), the model will calculate either a too high or too low SR at conditions away from saturation. Ceccattini et.al[12] gives measurements of ${}^{sol}\gamma$ in water+MEG solutions for NaCl at 25°C that were used to calculate the SR of NaCl at a concentration of 80wt% MEG in the solvent. Fig. 2.5 compares these results with the prediction from the model of this work. Both series have been fitted to SR=1 at the solubility limit. The difference between the two is due to γ^S not being equal to the "correct" ${}^{sol}\gamma$.

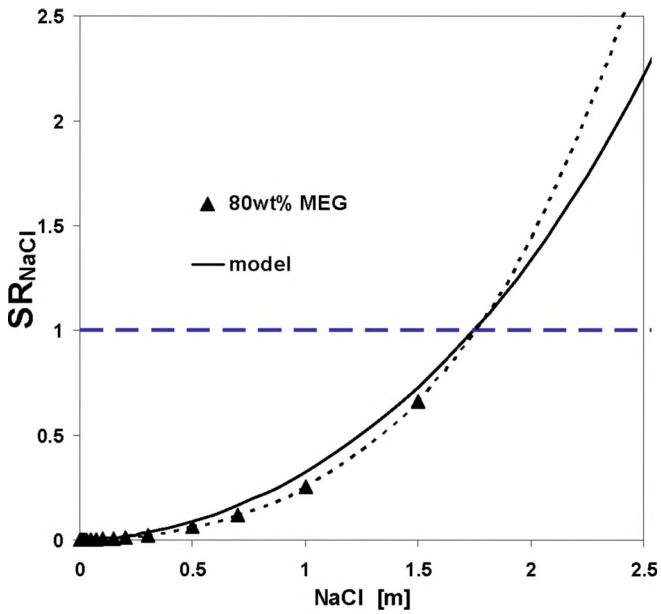

Fig. 2.5: Calculated SR versus NaCl concentration(mol/kg solvent). *Solid line:* This work. *Dotted line:* extrapolation based on data (▲) from Ceccattini et.al[12]

At 80wt% MEG the solubility limit of NaCl is about 1.75m. If the data of Ceccattini et.al[12] are extrapolated to a NaCl concentration of 2.5m the actual SR should be about 2.6, while the model from Eq. 15 gives SR=2.22. Below saturation the model calculates a too high SR, while in highly saline solutions it may consequently predict a too low SR for NaCl. Higher ionic strength than NaCl saturation can be achieved if substantial amounts of other high soluble species are present. e.g. K^+, CO_3^{2-} etc.

The difference between the dotted and solid line can be adjusted with an ionic strength dependence in $\gamma^{N\pm}$, i.e. a coupled MEG-ionic strength effect. Sufficient data to include an ionic strength effect of $\gamma^{N\pm}$ are available for some salts but lacking for others. Further details are given in section 2.2.2 and chapter 6.

2.2.2 Ionic Strength dependence in MEG

It is, as mentioned above, possible to include an ionic strength effect in $\gamma^{N\pm}$ to compensate the error in γ^{S} of Eq. 14. This is merely a question of obtaining enough experimental data but there is actually an obvious limitation. When solubility data is used to determine $\gamma^{N\pm}$, it is impossible to measure the MEG dependence at ionic strengths lower than the solubility of the salt at question. Thus $\gamma^{N\pm}$ is only measurable for ionic strengths at saturation and higher. For highly soluble salts this constitutes a serious limitation, but for low soluble ones like $BaSO_4$ it is no problem. For such cases ionic strength variations can easily be investigated by performing solubility measurements with various additions of e.g. NaCl. For non solid equilibria as CO_2 dissolution and dissociation, there is virtually no lower limit of ionic strength, and the ionic strength dependence can readily be measured.

If equilibrium data are available at various ionic strength the next step will be to curve fit a function. At very low concentrations an activity coefficient model should correspond to the Debye Hückel limiting law[6]. For NaCl and KCl there exists activity data as mentioned above. Data (25°C, 0, 20, 40, 60 and 80wt% MEG) from Manzoni et. al[11] and Ceccattini et.al[12] were used to calculate the ratio ${}^{sol}\gamma/\gamma^{S}$ i.e. the ratio between the activity coefficient in the solvent, ${}^{sol}\gamma$, and in water, γ^{S}. Fig. 2.6 shows this ratio in solutions of 20 and 80wt% MEG. The activity coefficient ratio changes rapidly at low ionic strengths, as depicted by the Debye Hückel limiting law[6]. NaCl and KCl correspond well up to about $I=0.1 mol/kg$, and it was constructed a general equation for the ionic strength effect in water+MEG solutions;

$$\ln\left(\frac{{}^{sol}\gamma}{\gamma^{S}}\right)=\frac{AI^{1/2}}{1+BI^{1/2}}$$

$$A = -1.17w_{MEG} - 0.82w_{MEG}^{2} \qquad (20)$$

$$B = 9.32w_{MEG} - 5.23w_{MEG}^{2}$$

where w denotes weight fraction of MEG in the solvent and I gives the ionic strength (mol/kg). The equation is of the extended Debye Hückel type and mathematically it will approach the limit of A/B at high Ionic strengths.

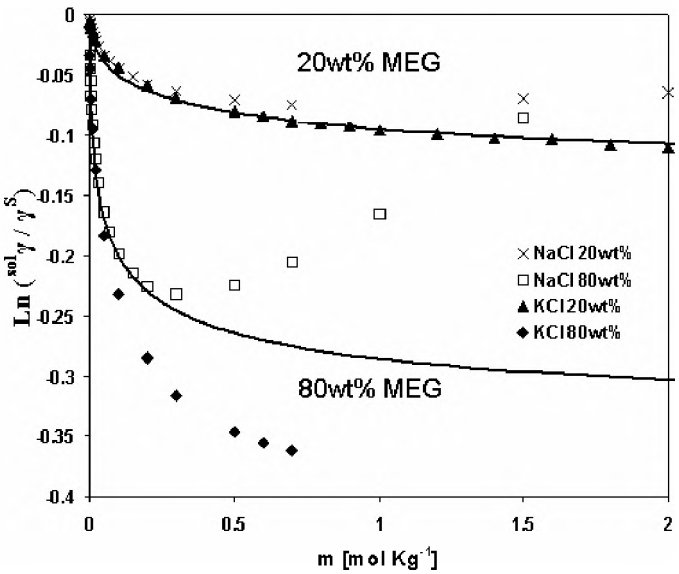

Fig. 2.6: $\ln\left({}^{sol}\gamma / \gamma^{S}\right)$ **for NaCl[11] and KCl[12] at 20 and 80wt% MEG as function of salt concentration. Solid line: Eq. 20**

Eq. 20 is shown as lines for 20 and 80wt% MEG in Fig. 2.6. From *I=1mol/kg* the lines are virtually parallel, meaning that γ^{S} and ${}^{sol}\gamma$ have the same ionic strength dependence after this point. However, at *I>0.1mol/kg* even the two chlorides have a different behaviour and it will certainly be ambitious to use a common equation to describe the ionic strength effect of all equilibria and ions in water+MEG solutions. Thus the coupled MEG-Ionic strength effect was regarded individually in each case, as described in detail in Chapter 6. Fig. 2.6 shows that the effect of any coupled MEG-Ionic strength effect should be most pronounced at low ionic strengths, where $\ln\left({}^{sol}\gamma / \gamma^{S}\right)$ changes rapidly.

2.2.3 Concentration basis

Kan et.al[1,2] generally used the same modeling approach as in this work i.e. Eq. 14 where γ^S was obtained by the aqueous Pitzer model and γ^N was curve fitted from solubility data. The difference is that Kan et.al entered all values of salt solubility with concentrations as *mol/kg water* into the Pitzer model to obtain γ^S. e.g. *1 mol NaCl/kg solvent* equals *5 mol NaCl/kg water* when the solvent composition is 80wt% MEG. Fig. 2.7 shows the resulting activity coefficients in 80wt% MEG.

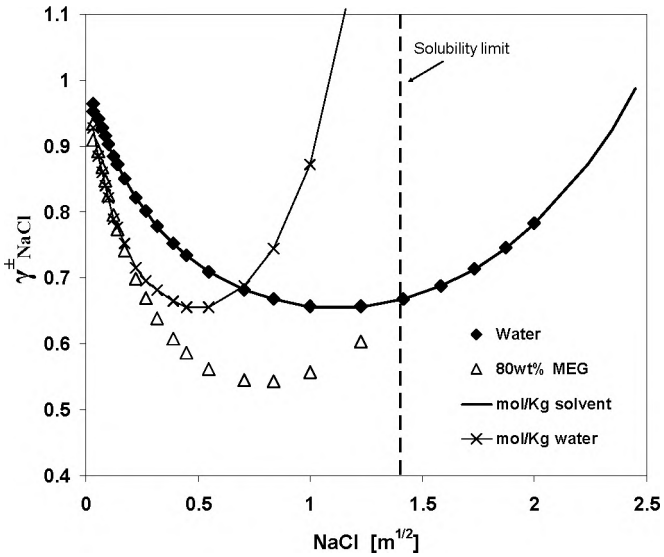

Fig. 2.7: Measured activity coefficients, $^{sol}\gamma^{\pm}$, for NaCl[12] as function of square root of concentration (mol/kg solvent). ♦;water Δ; 80wt% MEG. Lines give Pitzer model with concentrations entered per kg *solvent* (solid), or per kg *water* (solid line with crosses) for a solution of 80wt% MEG.

The experimental data are the same as given in Fig. 2.4, and there is clearly a distinction between the activity coefficients calculated by entering concentrations as *mol/kg water* or *mol/kg solvent*. The former actually very closely resembles the measurements up to about $m^{1/2}=0.25$, which is clearly a motivation to examine this approach. It should be noted that at the solubility limit (about $m^{1/2}=1.4$) there is a large discrepancy between the model (mol/kg water) and the measurements. To further investigate these questions it is valuable to look at the resulting activity plotted in Fig. 2.8, which compares the results to the measured activity of Ceccattini et.al[12].

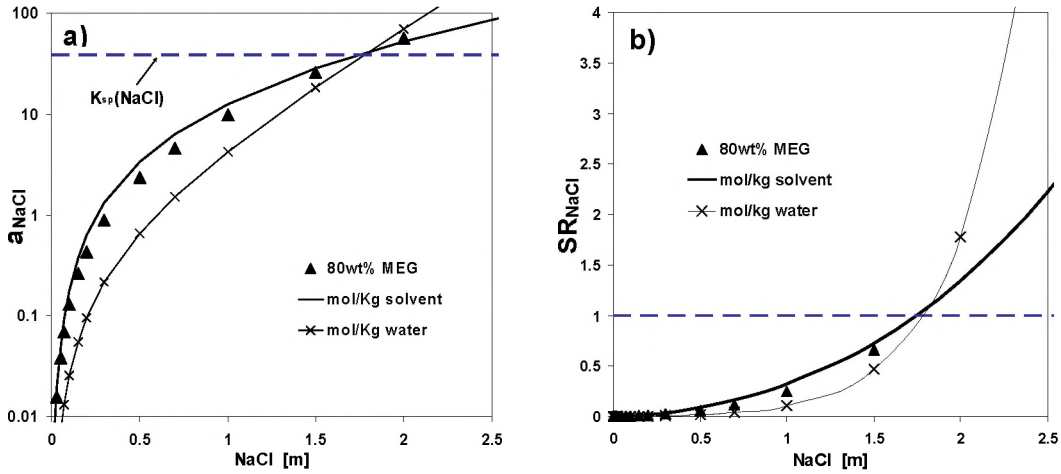

Fig. 2.8: ***a)*** **Activity and** ***b)*** **SR of NaCl[12] at 80wt% MEG referred to an** ***aqueous*** **reference as function of concentration (mol/kg solvent). Solid lines with and without crosses give the model based on** ***mol/kg solvent*****(This work), and** ***mol/kg water*** **respectively.**

It is noted that the models have been fitted at saturation, thus at the solubility limit (~1.8m) the activity exactly equals $K°_{sp}(NaCl)$. At higher and lower values the activity deviates from the measured values and results in a slightly different SR as described above. Although *mol/kg water* closely resembled the measurements in Fig. 2.7 at the lowest concentrations, the activity will actually not do so. In Fig. 2.7 it was observed that the γ^S was much larger than the measured value at the solubility limit. The $\gamma^{N\pm}$ is fitted at this point and will consequently be a small number to compensate for the large value of γ^S. Thus the fitted $\gamma^{N\pm}$ will yield an activity that is too low when NaCl concentration decreases. SR is consequently too low beneath saturation and most likely too high above.

The above example was for the highly soluble NaCl, and in this case the mol/kg solvent approach gives better results than mol/kg water. Salts with low solubility will have different behaviour, but the MEG dependence is in any case empirically fitted at saturation. Hence the choice of *mol/kg water* or *mol/kg solvent* is merely based on what is practically most convenient, and what is believed to give the best results when extrapolating outside of the experimental range. For low concentrations of co-solvent, and for dilution of an aqueous solution by pure MEG, it is reasonable to work with *mol/kg water* as done by Kan et.al[1]. This typically corresponds to the mixing of a MEG rich injection stream with formation water. In cases where salt accumulates in the system, however, the *mol/kg water* notation will lead to salt concentrations approaching infinite when the solvent approaches pure co-solvent. *mol/kg solvent* is therefore better suited for a general model that will have to cope with combinations of high salinity and high MEG contents. The goal of this work is to go up to 99wt% MEG, where e.g. a solution containing *0.5mol NaCl/kg solvent* consequently has a concentration of *50mol NaCl/kg of water*. The latter value will obviously lead to difficulties using the Pitzer model.

2.2.4 Born Equation

The Born equation[14,15] attempts to describe a change in standard state i.e. the first step going vertically down in Fig. 2.3 and ${}^{w}_{sol}\gamma^{o}_{NaCl}$ in Eq. 16. Fig. 2.9 compares the solubility[17-18] of NaCl and KCl in water+MEG mixtures with three different calculations.

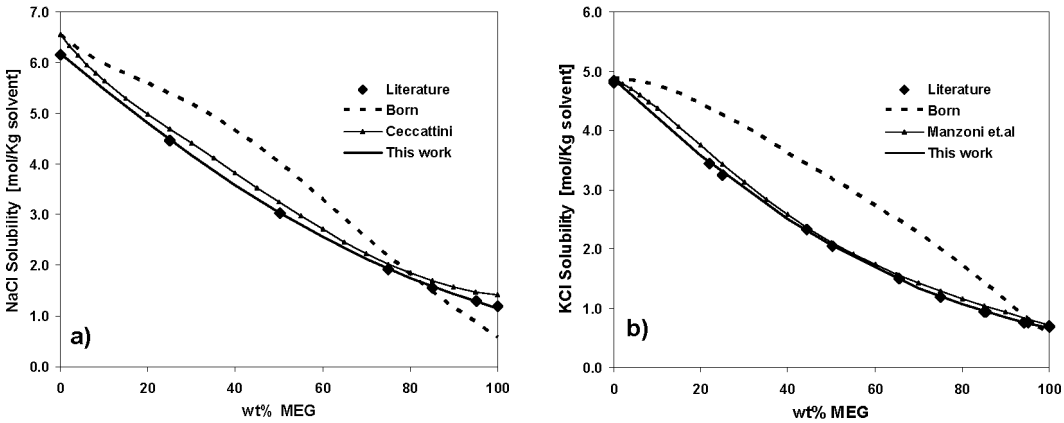

Fig. 2.9: Literature data[17,18] for *a)*NaCl and *b)*KCl solubility versus wt% MEG at 25°C compared to calculations; *Solid line:* This work, *Solid line with triangles:* NaCl data of Ceccattini et.al[12] and KCl of Manzoni et.al[11] *Dotted line:* Born equation for ${}^{w}_{sol}\gamma^{o}$, and literature[11,12] for ${}^{sol}\gamma$.

Predictions (Eq. 16) from Ceccattini et.al[12] and Manzoni et.al[11] give systematically too high values simply because their equations for activity coefficients were not fitted at saturation. The Born equation, however, gives a wrong type of function. This observation is in agreement with several other authors[11,12,14,16] that states that the Born equation fails to completely describe the change of standard state. It is possible to use the form of this equation to curve fit experimental data e.g. by having the ionic radius dependent on MEG content and ionic strength. However, this gives unnecessary complex functions and it was decided to simply use polynomials to fit $\gamma^{N\pm}$ as discussed in chapter 6.

2.3 References chapter 2

1. Kan, A.T Fu,G. Tomson, M.B "Effect of Methanol and Ethylene Glycol on Sulfates and halite Scale Formation" *Ind. Eng. Chem. Res.* **42**, 2399-2408, (2003)
2. Kan, A. T.; Fu, G.; Tomson, M. B. "Effect of Methanol on Carbonate Equilibrium and Calcite Solubility in a Gas/Methanol/Water/Salt Mixed System." *Langmuir*, **18(25)**, 9713-9725, (2002)
3. Kaasa, B., *Prediciton of pH, Mineral precipitations and multiphase equilibria during oil recovery*, Dr.Ing thesis, Norwegian University of Technology and Science-NTNU, ISBN 82-471-0339-7(1998)
4. Kaasa, B., Sandengen, K. and Østvold, T. " Thermodynamic Predictions of Scale Potential, pH and Gas Solubility in Glycol Containing Systems", *SPE 95075, Int. Symposium on Oilfield Scale*, Aberdeen, (2005)
5. Haarberg, T. *Mineral deposition during oil recovery* Dr.Ing thesis, Norwegian University of Technology and Science-NTNU / NTH, (1989)
6. Prausnitz, J.M, Lichtenthaler, R.N, Azevedo, E.G, *Molecular Thermodynamics of Fluid-Phase Equilibria*, chapter 9, 3rd ed. (1999) Prentice Hall
7. Pitzer, K. S, Brewer, L. Lewis, G.N., Randall M., *Thermodynamics* 2nd ed. , (1961), McGraw-Hill
8. Mussini, T., Mazza, F." Medium effects as key electrochemical variables for corrosion and electrochemistry studies in non-aqueous and mixed solvents", *Electrochimica Acta.*, **32(6),** 855-862, (1987)
9. Owen, B.B. "Direct measurement of primary, secondary and total medium effects of acetic acid" *J.Am.Chem.Soc* **54,** 1758-1769, (1932)
10. Yang, J., Pitzer, K.S., "The application of the Ion-Iteraction model to multicomponent 1-1 type electrolytes in mixed solvents", *J. Solution Chemistry,* **18(3),** 201-210, (1989)
11. Manzoni, A., Mussini, P.R., Mussini, T. "Thermodynamics of the amalgam cell {KxHg1-x|KCl(m)|AgCl|Ag} and primary medium effects upon KCl in {ethylene glycol + water}, {acetonitrile + water}, and {1,4-dioxane + water} solvent mixtures" *J. Chem. Thermodynamics* **32,** 107-122, (2000)
12. Ceccattini, P.D., Mussini, P.R., Mussini, T. "Thermodynamics of NaCl in aqueous ethylene glycol, acetonitrile, and 1,4-dioxane mixtures from Emf measurements at 25°C" *J. Solution Chemistry,* **26(12),** 1169-1186, (1997)
13. Ye, S., Xans, P., Lagourette, B., "Modification of the Pitzer model to calculate the mean activity coefficients of electrolytes in a water-alcohol mixed solvent solution" *J. Solution Chemistry,* **23(12),** 1301-1315, (1994)
14. Bates, R.G, *Determination of pH,* 2nd ed. (1973), John Wiley & Sons
15. Tester, J.W., Modell, M. *Thermodynamics and Its Applications*, 3rd ed. Prentice Hall, (1997)
16. Zerres, H., Prausnitz, J.M., "Thermodynamics of Phase Equilibria in Aqueous-Organic Systems with Salt", *AIChE Journal*, **40(4),** 676-91, (1994)
17. Kraus, K.A., Raridon, R.J. and Baldwin,W.H. "Properties of organic-water mixtures." *J. Am. Chem.Soc.,* **86(13),** (1964)
18. Rasmussen, P. Chiavone-Fihlo, C.O., "Solubilities of salts in mixed solvents.", *J. Chem. Eng. data,* **38(3),** 367-369, (1993)

3 Experimental

The experimental work concerning magnesium carbonate solubility is described in chapter 9.2, while density and conductivity measurements are described in chapter 8.3. *pH* measurements are thoroughly discussed in chapter 7.

3.1 General

The MEG(monoethylene glycol) delivered by the suppliers (Acros and Merck) was analyzed with a Methrom 831 KF Karl-Fischer titration equipment, and found to contain less than 500ppm (0.05wt%) of water. All chemicals used in the experimental work are listed in Table 3.1.

Table 3.1: Chemicals used in experimental work

Name	Formula / Concentration	Quality	Manufacturer
Potassium Hydrogen Phtalate	KHPh	p.a. 99.8%	Merck
Sodium bicarbonate	$NaHCO_3$	p.a. 99.5%	Merck
Potassium bicarbonate	$KHCO_3$	p.a. 99.5%	Merck
Sodium Carbonate	Na_2CO_3 (anhydrate)	p.a. 99.9%	Merck
Potassium Carbonate	K_2CO_3	p.a. 99%	Merck
Sodium hydroxide	NaOH	p.a. 99%	Merck
Magnesium chloride	$MgCl_2 \cdot 6H_2O$	p.a 99-102%	Merck
Sodium chloride	NaCl	p.a 99.5%	Merck, Baker
HCl standard solutions	HCl(aq) 0.1-0.01M	Titrisol Ampoule	Merck
NaOH standard solutions	NaOH(aq) 0.1-1M	Titrisol Ampoule	Merck
EDTA standard solutions	0.01M-0.1M	Titriplex Ampoule	Merck
Mg^{2+} standard solution	as $MgCl_2$ (aq)	Titrisol Ampoule	Merck
Monoethylene Glycol (MEG)	$C_2H_4(OH)_2$	p.a. 99.5%	Merck
Monoethylene Glycol (MEG)	$C_2H_4(OH)_2$	p.a. 99.9%	Acros
Acetic Acid	HAc (conc. liquid)	p.a. >99.8%	Merck
Strontianite	$SrCO_3$	p.a 99.8%	Baker
Witherite	$BaCO_3$	p.a 99.3%	Baker
Calcite	$CaCO_3$	p.a 99%	Merck
Hydromagnesite	$3MgCO_3 \cdot Mg(OH)_2 \cdot 3H_2O$	z.a 99.5%	Merck
Carbon Dioxide	CO_2 gas	4.0 (99.99%)	AGA
Calmagite	C.A.S. 3147-14-6	indicator grade	Acros
Gypsum	$CaSO_4 \cdot 2H_2O$	p.a. 99-102%	Merck
Anhydrite	$CaSO_4$	p.a 99%	Aldrich
Brucite	$Mg(OH)_2$	ultra pure >>99%	Fluka
Water	H_2O - distilled	$\kappa < 2.5 \mu S/cm$	

pH was measured using a Mettler Toledo (3M KCl bridge) glass electrode (SC-111) at low temperature (0-50°C), while a special high temperature glass electrode from Innovative sensors (GT-DJ) was used at 50-90°C. The electrodes were calibrated in aqueous IUPAC standard solutions, and in 0.05m KHPh (Potassium Hydrogen Phtalate) solutions containing the same concentration of MEG as the sample (see chapter 7). The KHPh solutions were prepared from dried (100°C, 3h) KHPh salt.

Both HCl and EDTA (only for Ca^{2+}) titration analyses were performed with an automatic titration system (Mettler Toledo DL50). For alkalinity titration a common pH electrode (Mettler Toldeo SC-111) was used for end point determination. A calcium sensitive electrode (Radiometer ISE25Ca) in combination with a Ag/AgCl reference electrode was used during EDTA titration. End points were read manually from the titration curve and its 1. derivative. This gave a random error of about 0.5-1%. Ma and Tsang[1] proposed to use a simple *arctan* curve fit to evaluate titration end points. A common spreadsheet was used to construct this fit. It did, however, not give any better results and was significantly slower than to simply read the end points directly.

3.2 $CaSO_4$ solubility

Solid gypsum was used directly in the experiments while the anhydrite delivered by Aldrich was stirred in a saline aqueous solution (0.5m NaCl, 50°C) for one day, filtered, washed with ethanol and dried at 200°C. This was done to remove any traces of hemi-hydrate. Both starting materials were checked using X-ray Diffraction (XRD) and found to have no traces of hemi-hydrate.

MEG+water+NaCl solutions (0-100%MEG, 0-0.7mol NaCl/kg solvent) were made gravimetrically in 1L flasks. Sample bottles (100-250ml) were filled with this solution and put in a water bath for temperature control (25-85°C). Excess solid $CaSO_4$(1-2g), either as gypsum or as the anhydrite, was thereafter added. The solutions were vigorously stirred for 1-14days before being filtered through 0.2μm filters and analysed for Ca^{2+} using EDTA(0.01M) titration. The analysis was checked against Ca^{2+} standard solutions delivered by Merck. Solids were collected by vacuum filtration, washed with ethanol, and run through XRD analysis. In selected samples Ca^{2+} was regularly measured each day to establish the time needed to reach equilibrium conditions.

If Anhydrite is dissolved under conditions were gypsum is actually the stable phase, the X-ray pattern should yield traces of gypsum and vice versa. It was also anticipated that precipitation is a slower process[2] than dissolution. Thus anhydrite dissolves until its solubility limit is reached. At the same time gypsum will precipitate, but so slowly that the calcium and sulphate concentrations remain on the solubility limit of anhydrite.

3.3 Carbonate system

In our laboratory a series of measurements have been performed to establish the first and second dissociation constant of the carbonic acid as well as solubility of $CaCO_3$, $BaCO_3$, $SrCO_3$ and three magnesium carbonate containing compounds (see chapter 9). CO_2 gas solubility was measured during the determination of the first dissociation constant. Stock solutions (MEG+water+NaCl 0-100%MEG, 0-1mol NaCl/kg solvent) were made gravimetrically in 1L flasks.

3.3.1 CO_2 flow and pressure

CO_2 was bubbled through solutions at a flow rate of about 20-50ml/min, with the flask being open to atmospheric pressure. The gas passed through cleaning bottles with the same MEG+water+NaCl content as the sample before the inlet of the reaction flask. This was done to equilibrate the CO_2(g) with solvent vapour, and in this way minimize evaporation of solvent during the experiments.

The CO_2 partial pressure was calculated by subtracting MEG+water vapour pressure from the atmospheric pressure. Vapour pressures of salt free water+MEG solutions are available in the literature[3-7] at temperatures (25, 50, 60, 90.3, 98, 110 and 122)°C. For experiments at other temperatures than found in the literature, and/or with salt present, vapour pressure had to be estimated. This was done by using ideal behaviour i.e. Raoult's law given as:

$$\begin{aligned} P_{solvent} &= P_{H_2O} + P_{MEG} \\ &\approx P^o_{H_2O} x_{H_2O} + P^o_{MEG} x_{MEG} \end{aligned} \tag{21}$$

where P denotes partial pressure, x mole fraction in the liquid and $P°$ the pressure of pure water and MEG at the given temperature. MEG has a boiling point of about 200°C, thus water is the more volatile component and the gas phase consists of mostly water($P°_{MEG}$~0.02bar at 100°C). It was found that the vapour pressure of a water+MEG solution could be approximated by the H_2O partial pressure, given by Eq. 22, when operating beneath 90°C and 98wt% MEG.

$$P_{solvent} \approx P_{H_2O} = P^o_{H_2O} x_{H_2O} \tag{22}$$

Eq. 22 reproduced the experimental data for solvent vapour pressure within 0.01bar up to 90°C. At higher temperatures it is necessary to also include the vapour pressure of MEG (~$x_{MEG}P°_{MEG}$). Fig. 3.1 shows the total vapour pressure[3-7] divided by the vapour pressure of water[8] at temperatures of (25 to 98)°C. The solid line corresponds to ideal behaviour.

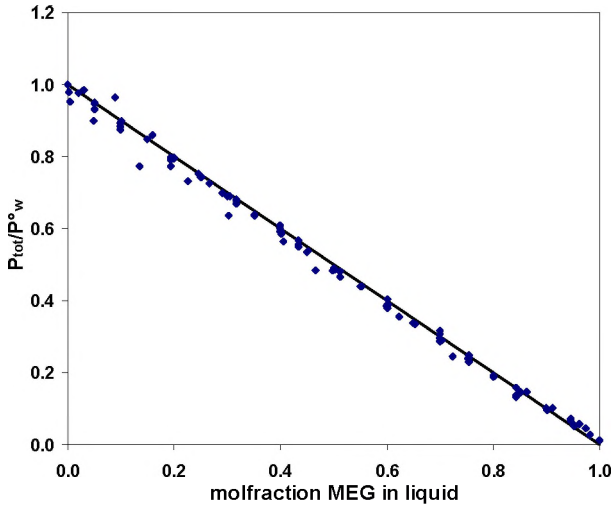

Fig. 3.1: Vapour pressure[3-7], P_{tot}, of water+MEG solutions divided by pure water partial pressure[8], $P°_w$, at temperatures of (25 to 98)°C. Solid line gives ideal behaviour depicted by Eq. 22.

There are no data for vapour pressures of water+MEG+salt solutions available at present. When salt is present, the molfraction of water (and MEG) is reduced, thus it was anticipated that Eqs. 21-22 gave a good approximation also in saline solutions. In this work the solutions were not highly saline and the influence on the vapour pressure should therefore be small. During the experiments CO_2 pressure is directly dependent on the atmospheric pressure. It was recorded at the time samples were taken, and generally varies between 0.97 and 1.03bar. The uncertainty in the CO_2 pressure determination was estimated to ±0.01bar.

3.3.2 K1 and KH determination

A MEG+water+NaCl solution (~250g) of known concentration was filled into a three neck round flask and magnetically stirred Solid $NaHCO_3$(~10mmol/kg solvent) was added and the flask put in a water bath for temperature control(25-90°C). CO_2 gas was continuously bubbled through the solution with the flask being open to atmospheric pressure. When pH had stabilized (1-5h), samples (20-50g) were withdrawn using a plastic syringe. Two different types of samples were collected. In the first type the syringe was filled with a small amount of degassed NaOH(~5ml, 0.2M) solution before use. In the second type the samples were withdrawn directly from the flask with no further treatment. The samples were titrated with HCl(0.01-0.1M) to establish total alkalinity.

3.3.3 K_2 determination

A titration method was used to measure the second dissociation constant. MEG+H_2O+NaCl stock solution was filled into a round flask (100-250ml). About equal amounts of solid Na_2CO_3 and $NaHCO_3$ were added (5-25mmol/kg solvent of each). The flask was equipped with a pH electrode and closed. The solution was stirred on a water bath (25-80°C) for a few hours until all solids had dissolved. When pH had stabilized the Mettler Toledo DL50 titration system was utilized to construct a curve of measured

pH versus amount of added HCl(0.01-0.1M). The flask was open to atmospheric pressure through a syringe needle. Gas volume in the flask was about 10% of the liquid volume.

3.3.4 $CaCO_3$, $BaCO_3$ and $SrCO_3$ solubility

Excess solid $BaCO_3$ (~3g) was put into three neck flasks containing MEG+H_2O+NaCl solutions (250-300g). A water bath was used for temperature control (4-80°C). The solutions were vigorously stirred for 1-14days using a magnetic stirrer. CO_2 was continuously bubbled through the solution. The gas was saturated by passing it through a cleaning flask containing the same MEG+Water+NaCl solution as the sample. Samples (15-25g) were withdrawn using a plastic syringe, filtered through syringe mounted filters (0.2µm, Schleicher & Schuell) and titrated with HCl (0.01M) to establish the total alkalinity. When $BaCO_3$ is dissolved, alkalinity equals twice the Ba^{2+} concentration. The titration analysis was calibrated using $KHCO_3$ and $NaHCO_3$ standard solutions made gravimetrically from the solid salts. At 80°C the samples were quenched in distilled water(~20g) to minimize evaporation during weighing. The same experimental method was used for $SrCO_3$ and $CaCO_3$.

ETDA analysis for direct measurement of Ca^{2+} concentration was used as the primary analysis during $CaCO_3$ experiments. Selected samples were also analysed for total alkalinity, to check that the measured calcium concentration corresponded to ½ of the alkalinity.

All starting materials were analysed by X-ray diffraction (XRD) and no impurities could be observed. Solids were collected from samples in water as well as in 90wt% MEG, and XRD analysis showed no phase change.

To estimate the time needed to reach equilibrium, salt concentrations were measured as function of time for some samples. The presence of MEG was found to significantly lower the reaction rate. It is noted that MEG has a much higher viscosity than water. This suggests a lower diffusivity[2] that can be rate determining for the dissolution process. Fig. 3.2 shows measured cation concentration as function of elapsed time at high MEG contents. Based on such measurements it was found that solutions of 50-90wt% MEG should be left for at least 5-6 days at 25°C, while solutions with 90wt% MEG or more, were left for at least 7 days. 2-3 days were sufficient for equilibrium to be reached at MEG concentrations lower than 50wt%. Higher temperature increases the reaction rate and at 80°C 2 days was found to be sufficient for all cases.

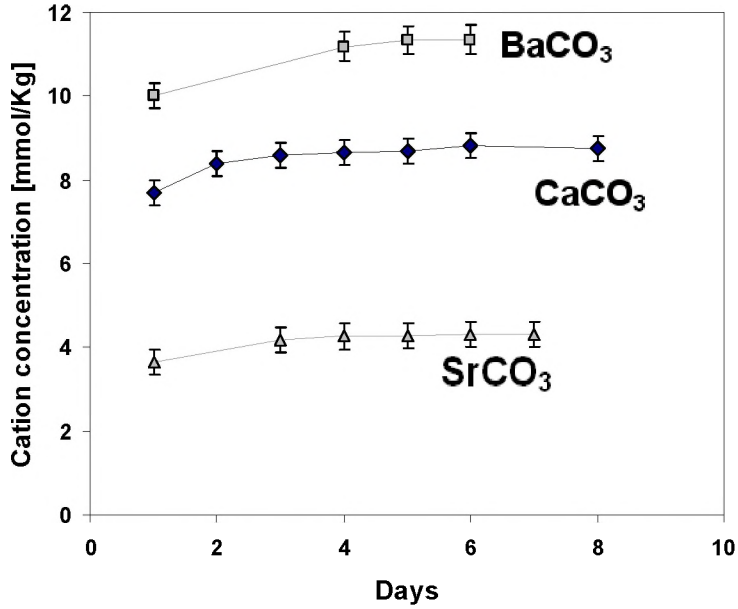

Fig. 3.2: Cation concentration (mmol/kg solvent) versus time. Dissolution of $CaCO_3$ (90wt% MEG, 0.5m NaCl), $BaCO_3$ (80wt% MEG, 0.5m NaCl) and $SrCO_3$ (90wt% MEG, 0.16m NaCl) at 25°C under CO_2 bubbling P_{tot}~1atm.

Ideally solubility should be determined both by dissolution and precipitation. In the case of $CaCO_3$ only dissolution experiments were performed since precipitation can lead to the formation of the metastable aragonite or vaterite. For $SrCO_3$ and $BaCO_3$ also precipitation was performed; by raising the temperature of saturated solutions from room temperature and allowing them to reestablish equilibrium at a higher temperature (50-80°C).

3.3.5 $NaHCO_3$ and $KHCO_3$ solubilities

Saturated sodium bicarbonate solutions were prepared at room temperature by dissolving $NaHCO_3$ (~250ml solvent, 60 and 90wt% MEG) under continuous CO_2 bubbling with the flask being open to atmospheric pressure. The same solutions were thereafter transferred to a cooling bath such that $NaHCO_3$ precipitated at the low temperature. It was in addition run an experiment where $NaHCO_3$ was dissolved at 4°C, 90wt% MEG under CO_2 bubbling. Samples (25-50g) were withdrawn using a plastic syringe and filtered through 0.2μm syringe mounted filters. Total alkalinity was analyzed using HCl (0.504M) titration on a Mettler Toledo DL50 automatic titration system.

$KHCO_3$ solubility was measured in a cooling bath at 0°C. Three neck round flasks were filled with solvent (0, 60 and 97.5wt% MEG) and continuously bubbled with CO_2. When the solution had cooled to 0°C, excess solid $KHCO_3$ was added. It was also done one precipitation experiment with 60wt% MEG. In this solution ~1mol $KHCO_3$/kg solvent was dissolved at 50°C before the solution was put in the cooling bath at 0°C. The solutions were vigorously stirred for 5-10days.

3.3.6 Application and testing; pH

These experiments were performed to test the pH prediction and therefore also the carbonic acid equilibria in the model. A KCl ceramic bridge glass electrode from Metrohm (Unitrode) and a combined electrode with a sleeve type of liquid junction from Radiometer (pHC2601), were utilized for pH measurements. A MEG+water solution of known composition (60 or 90wt% MEG) was put into a 250ml three neck round flask, and the solution magnetically stirred. A water bath was used for temperature control (4, 25, 50, 80°C). CO_2 was continuously bubbled through the solution with the flask being open to atmospheric pressure. When the pH reading was stable (~1h), known amounts of $NaHCO_3$ or $KHCO_3$ were added to the solution. pH was recorded after each addition and the procedure continued until the solubility limit had been reached (4-48hours).

3.4 $Mg(OH)_2$ solubility

250-500ml flasks were filled with MEG+water+NaCl solutions and put in a water bath (20-80°C). The solutions were thereafter degassed using a water jet pump, before solid $Mg(OH)_2$ was added(1-3grams) and the flasks corked. After the solutions had been vigorously stirred for 2-7 days, the stirring was stopped and the solids left to settle for 1-2 days. Samples(100-200g) were thereafter withdrawn using a plastic syringe, filtered through syringe mounted filters (0.2μm) and titrated with HCl (0.100±0.0003M) to establish the alkalinity. The titration analysis was calibrated using $KHCO_3$ and $NaHCO_3$ standard solutions made gravimetrically from the solid salts. At low temperature (20-25°C) and high MEG concentration (70-90wt%) the solutions were too viscous to be pressed through the filters. In these solutions the solids were removed by centrifuging. After the samples had been titrated with HCl, they were analysed for Mg^{2+} with EDTA (0.01M±0.0003M) titration. The analysis was performed on a hot plate(50-60°C) since the reaction is slow at room temperature. Calmagite was used as colour indicator and the titration was calibrated using standard $MgCl_2$ solutions from Merck.

The starting material and samples that had been stirred in water and 90wt% MEG were analysed using X-ray diffraction (XRD). No phase change was observed.

3.5 pH at known H^+ concentration

pH was measured in solutions of known H^+ concentration to obtain a relation between *molality* and *activity*. Solutions of known HCl (~0.001M) concentration were made by weighing the contents of HCl ampoules together with degassed distilled water and MEG into 1L bottles. Samples were filled into 250ml round flasks and continuously stirred on a water bath (25°C). pH was measured as portions of NaCl(s) were added (0-0.7m).

3.6 HAc titration

Solid NaCl (~50mmol/kg) and $NaHCO_3$ (~50mmol/kg) were, together with the solvent (0, 50 and 90wt% MEG), weighed into 1L bottles. The solutions were stirred at room temperature under continuous CO_2 flow. Concentrated HAc (0-200mmol/kg) was titrated into solution and pH measured as function of added acid to verify the dissociation constant of HAc.

3.7 References chapter 3

1. Ma, N. L., Tsang, C. W. "Curve-fitting approach to potentiometric titration using spreadsheet" *J. Chem. Ed.* **75(1),** 122-123, (1998)
2. Mullin, J. W. *Crystallization 4th ed.*, (2001), Butterworth Heinemann
3. Trimble, H.M., Potts, W. "Glycol-water mixtures. Vapor pressure-boiling point-composition relations." *Ind. and Eng. Chem*, **27**, 66-68, (1935)
4. Villamanan,M.,A., Gonzalez, C., Van Ness, H.C. "Excess thermodynamic properties for water/ethylene glycol." *J. Chem. Eng. Data*, **29(4)**,427-429, (1984)
5. Gonzalez, C., Van Ness, H.C. "Excess thermodynamic functions for ternary systems. 9. Total-pressure data and GE for water/ethylene glycol/ethanol at 50°C.", *J. Chem. Eng. Data*, **28(4)**,410-412, (1983)
6. Nath,A., Bender,E., *J.Chem.Eng.Data*, "Isothermal vapor-liquid equilibriums of binary and ternary mixtures containing alcohol, alkanolamine, and water with a new static device." **28(4)**,370-375,(1983)
7. Lancia,A., Musmarra,D., Pepe,F., "Vapor-liquid equilibria for mixtures of ethylene glycol, propylene glycol, and water between 98° and 122°C." *J. Chem. Eng of Japan*, **29(3),** 449-455, (1996)
8. Lide, D. R. *CRC Handbook of Chemistry and Physics*, 84th ed. (2003)

4 Results

The data for magnesium carbonate solubility are given in chapter 9. Conductivity and density of water+MEG+NaCl+$NaHCO_3$ solutions are given in chapter 8.3.

All salt concentrations are given per kg of *solvent*. MEG concentrations are given as molfraction or weight % in the *salt free solvent*. Solvent denotes water+MEG.

4.1 Experimental error

In most of the experimental work titration analysis were used for alkalinity or for Ca^{2+} concentration determinations. Parallel samples generally gave a variation of less than 1%. Samples withdrawn hours/days apart, however, showed larger variations than 1% even in identical solutions. This is due to uncertainties introduced during weighing, filtering, sampling etc. The random error in the experiments was therefore estimated from observed variations as well as comparison with literature values in water. This is discussed in each section below. Accuracy of the pH measurement is estimated as ±0.05pH units at 4-25°C, and ±0.1 units at 50-90°C (see chapter 7). The determination of CO_2 pressure is within 0.01bar (see section 3.3.1)

4.2 $CaSO_4$ solubility

Calcium concentrations in equilibrium with solid calcium sulphate, either as anhydrite ($CaSO_4$) or gypsum ($CaSO_4 \cdot 2H_2O$), were analysed by EDTA titration. The random error in the experiments was estimated to ±3%, but never less than 0.2mmol/kg. At high MEG contents the analysis is more troublesome and the solubility lower, thus percent is not a suitable measure. At high MEG contents the random error was estimated to ±0.2mmol/kg.

All results are given in Table 4.1 - Table 4.3, where the latter column gives the phase analysis of the collected solid performed by X-ray diffraction (XRD).

4.3 Carbonate system

4.3.1 K_1 and K_H

pH was measured at a given CO_2 pressure and bicarbonate concentration to investigate the MEG effect upon the first dissociation constant of carbonic acid, K_1. From the same experimental setup it was possible to measure the amount of dissolved CO_2 gas, yielding the Henry's constant, K_H. When CO_2 is bubbled through the solution, bicarbonate dominates the alkalinity i.e. $[HCO_3^-] >> [CO_3^{2-}]$ and $[OH^-]$. The reported

bicarbonate concentration in Table 4.4-Table 4.7 is therefore virtually equal to the alkalinity. Samples from the same solution were added excess NaOH such that both the dissolved CO_2 and HCO_3^- reacted to CO_3^{2-}. HCl (alkalinity) titration of such samples give the *total dissolved* CO_2 content. The amount of dissolved CO_2 was thereafter found as the difference between *total dissolved* CO_2 and bicarbonate concentration (see section 6.4). All concentrations are given per kg of salt free solvent. The experimental error is discussed in chapter 6.4.2.

4.3.2 K_2; second dissociation constant of CO_2

The experimental method is discussed in detail in chapter 6.4.3. Table 4.8 gives pH measured at certain ratios of carbonate to bicarbonate concentration. When titrating the carbonate/bicarbonate solution with HCl, there will be a half-way titration point where HCO_3^- equals CO_2(aq) concentration. The measured pH at this point equals the stochiometric first dissociation constant of carbonic acid, and is denoted "pH K_1" in Table 4.9.

4.3.3 $CaCO_3$, $BaCO_3$ and $SrCO_3$ solubilities

Solubilities of $SrCO_3$ (Table 4.11) and $BaCO_3$ (Table 4.10) were obtained by alkalinity titrations, while EDTA titration was the main analysis for $CaCO_3$ (Table 4.12) data. All measurements were performed with continuous CO_2 bubbling of the solutions.

Systematic error can be caused by impurities in the starting material. From the information provided by the supplier the possible error was estimated to be less than 0.15mmol/kg for $BaCO_3$, which contained the highest amount of impurities. Another source of error could be that solids passed through the 0.2μm filter, but this is not easily quantified. Comparison with literature data in water did not indicate any systematic error for $BaCO_3$ or $CaCO_3$. The $SrCO_3$, data, however, were systematically slightly higher than reported by Busenberg et.al[1], as discussed in detail in chapter 5.1. To investigate the difference between the data of Busenberg et.al[1] and the present data, one test was performed. Two solutions for determination of $SrCO_3$ solubility was set up at 25°C (Table 4.11). One was added over 10 times as much $SrCO_3$(s) as the other. A large amount of solids should give higher measured solubility if the solid contained impurities or solids passed through the filter. The results showed no differences between the two. Concentration changes can occur if solvent evaporates, which will cause NaCl content to rise and consequently increase the solubility. If water evaporates relative to MEG, this will in addition cause the MEG concentration to rise and generally the solubility to decrease. The evaporation problem was minimized by saturating the gas before the inlet of the sample flask, but no further analysis was run to quantify this problem. It was run three parallels for each alkalinity determination and the error between parallels was generally within 1%.

The error in the Ca, Sr, and $BaCO_3$ solubility determination was estimated to ±3-4% but never less than ±0.2mmol/kg. This latter value was introduced since the error in the end point determination (~0.1-0.2mmol/kg.) alone accounts for more than 3% when MEG contents are high and measured concentrations small.

4.3.4 $NaHCO_3$ and $KHCO_3$ solubilities

Both $NaHCO_3$(Table 4.13) and $KHCO_3$(Table 4.14) solubilities were measured at a given CO_2 pressure. Precipitation experiments were performed by dissolving the salts at higher temperature. Thereafter the reaction vessels were cooled. The total pressure was in all cases equal to the atmospheric pressure. Salt concentrations were determined by alkalinity titration. Low temperature was the main problem during these measurements, as it gives low reaction rates. The solubility measured in the precipitation experiments, were slightly higher than the values obtained by dissolving the solid at the same conditions. This indicates that equilibrium probably have not been reached after 8 days at these low temperatures. The error was estimated to ±5 % in the measured values.

4.3.5 Application and testing; pH

pH was measured as function of $NaHCO_3$ (and $KHCO_3$) content to check if the model calculated correct pH in the whole concentration interval up to saturation. The experiments also gave approximate values for the solubility of $NaHCO_3$ and $KHCO_3$. When saturation is reached, further addition of bicarbonate does not change the pH. Thus solubility is read from the break in the pH curve as described in detail in chapter 7. In Table 4.19 the asterisk denotes that the solubility limit certainly has been reached, due to solids being observed when pH was measured. Salt concentrations were weighed into solution with an accuracy of ±0.15mmol/kg.

4.4 $Mg(OH)_2$ solubility

$Mg(OH)_2$ solubility was investigated by dissolving the solid in degassed water+MEG+NaCl solutions. Samples were analyzed with EDTA titration for Mg^{2+} and with HCl titration for OH^-. As discussed in detail in chapter 5.1.7 there seemed to be a problem with CO_2 in the system. OH^- concentration in Table 4.20 is therefore most likely *too high*.

The amount of total CO_2 in the system, given in the latter column, was calculated by subtracting the measured OH^- concentration from 2 times the Mg^{2+} concentration (see chapter 5.1.7). The amount of starting material, which may have contained some carbonate, was not constant in the experiments. This could have resulted in a variation in the CO_2 contents. At 100°C an experiment was run where the solution (with solids) was refluxed to boil off CO_2. The solution was thereafter cooled to 80°C. These experiments, at the bottom of Table 4.20, are marked with ^{r}. Reproduced samples in water showed a variation in the Mg^{2+} analysis (EDTA titration) of only about 5 % in the measured values. This is good given the low concentrations and large sample volumes that have to be filtered. Samples that had to be centrifuged to remove the solids seemed to have higher total carbonate contents. This was expected due to handling in air for longer time than when filtered. After filtering/centrifuging the samples were immediately analyzed with HCl titration. Some contact with air is inevitable, in the present experimental setup, and some of the CO_2 may have been introduced at this point. The random error for the end point determination during HCl titration was estimated to 5% of the measured value.

4.5 pH at known H^+ concentration

pH was measured to get a relation between H^+ molality and activity. The accuracy was estimated to ±0.05pH units and the HCl content was within 0.005mmol/kg.

4.6 References chapter 4

1. Busenberg, E., Plummer, L.N., Parker, V.N "The solubility of Strontianite in CO_2-H_2O solutions between 2 and 91°C, the association constants of $SrHCO_3^+$(aq) and $SrCO_3$°(aq) between 5 and 80°C, and an evaluation of the thermodynamic properties of Sr^{2+}(aq) and $SrCO_3$ at 25°C and 1 atm total pressure" *Geochimica et. Cosmo. Acta* **48,** 2021-2035, (1984)

Table 4.1: Experimental results with $CaSO_4$ (*A*) as starting material. *A* indicates Anhydrite and *G* Gypsum. Concentration given per kg solvent (water+MEG)

T °C	Time[a] days	MEG wt%	NaCl mol/kg	$[Ca^{2+}]$ mmol/kg	XRD
22	7	0	0.5	36.40	**G**
22	3	0	0.5	36.50	
22	1	0	0.5	41.26	**A + G**
22	7	30	0.5	19.16	**A + G**
22	11	50	0.5	12.10	**A**
22	11	70	0.5	6.86	**A**
22	11	90	0.5	3.67	**A**
22	8	95	0.5	3.01	
21	2	0	0	24.09	
50	2	0	0.5	34.30	
50	3	30	0.5	15.64	
50	3	50	0.5	8.70	
50	3	70	0.5	4.60	
50	11	90	0.5	2.51	
50	5	95	0.5	2.08	
50	7	95	0.5	1.89	
50	4	100	0.5	1.62	
50	2	0	0	14.57	**A**
50	4	50	0	1.72	**A**
50	4	90	0	0.35	**A**
50	2	0	0.1	21.50	
50	2	50	0.1	4.23	
50	4	90	0.1	1.15	
80	2	0	0.5	24.46	**A**
80[p]	3	0	0.5	25.21	
80	2	30	0.5	11.53	
80[p]	2	50	0.5	6.46	**A**
80[p]	2	50	0.5	6.48	
80[p]	2	90	0.5	1.52	**A**
80	2	95	0.5	1.46	

[a]Elapsed time before final Ca^{2+} analysis. [p]precipitation experiments

Table 4.2: Experimental results with $CaSO_4 \cdot 2H_2O$ (Gypsum) as starting material. Calcium concentration given in mmol/kg solvent.

T °C	MEG wt%	NaCl [m]	Ca^{2+}	T [°C]	MEG wt%	NaCl [m]	Ca^{2+}
25	0.0	0	15.44	40	0.0	0.5	36.40
25	20.0	0	8.10	40	20.0	0.5	23.06
25	40.0	0	4.00	40	50.0	0.5	12.27
25	50.0	0	2.82	40	50.0	0.5	12.25
25	50.0	0	2.82	40	50.0	0.5	12.38
25	50.0	0	2.81	40	80.0	0.5	9.74
25	60.0	0	2.01	40	99.8	0.5	29.82
25	70.0	0	1.54	40	0.0	0.7	40.68
25	80.0	0	1.26	40	20.0	0.7	26.54
25	90.0	0	1.72	40	50.0	0.7	14.63
25	95.0	0	3.74	40	79.9	0.7	20.20
25	97.5	0	7.59	40	79.9	0.7	20.03
25	99.9	0	9.54	40	89.9	0.7	34.63
25	0.0	0.5	36.42	40	99.8	0.7	29.76
25	20.0	0.5	23.12	65	0.0	0	14.57
25	50.0	0.5	12.98	65	20.0	0	7.17
25	80.0	0.5	9.31	65	40.0	0	3.21
25	99.8	0.5	29.04	65	50.0	0	2.19
25	0.0	0.7	40.35	65	60.0	0	1.44
25	20.0	0.7	26.43	65	70.0	0	0.97
25	50.0	0.7	15.21	65	80.0	0	0.77
25	79.9	0.7	21.10	65	99.9	0	2.01
25	89.9	0.7	35.93	65	0.0	0.5	36.00
25	99.8	0.7	30.02	65	20.0	0.5	22.69
40	0.0	0	15.76	65	50.0	0.5	11.48
40	20.0	0	7.68	65	80.0	0.5	7.12
40	40.0	0	3.73	65	99.8	0.5	30.34
40	50.0	0	2.53				
40	60.0	0	1.65				
40	70.0	0	1.32				
40	80.0	0	1.05				
40	90.0	0	1.42				
40	95.0	0	3.42				
40	97.5	0	4.74				
40	99.9	0	5.54				

Table 4.3: Experimental results at 44±0.3°C in water with either Gypsum (G) or anhydrite(A) as starting material. Samples stirred for 2 days.

Temp °C	NaCl m	$[Ca^{2+}]$ mmol/kg	START	XRD
44	0	16.38	**A**	**A+G**
44	0.5	37.52	**A**	**A+G**
44	0	15.43	**G**	**G**
44	0.5	36.08	**G**	**G**

Table 4.4: Measurements of CO_2 dissolution and dissociation at 25°C

MEG[a] wt%	NaCl[b] [m]	pCO_2 [bara]	pH	HCO_3^- [mmol/kg][c]	CO_2 [mmol/kg][c]
0.0	0.0	0.97	5.86	11.25	30.84
30.0	0.0	0.99	6.10	11.89	26.45
50.0	0.0	0.98	6.25	10.65	
95.0	0.0	1.01	4.69	0.00	33.89
99.9	0.0	1.01	3.97	0.00	35.92
50.0	0.1	0.98	6.07	9.35	23.08
60.0	0.1	0.97	6.43	13.88	22.44
80.0	0.1	0.99	6.66	12.47	
80.0	0.1	1.01	6.66	12.49	26.26
90.0	0.1	1.00	6.70	9.31	
97.5	0.1	1.00	6.93	7.79	33.10
0.0	0.5	0.98		14.06	31.25
0.0	0.5	0.96	5.63	10.06	
0.0	0.5	0.97	5.62	9.99	30.32
0.0	0.5	0.97	5.63	10.92	28.64
0.0	0.5	0.96	5.63	10.06	28.71
30.0	0.5	0.98	5.82	9.77	25.65
30.0	0.5	0.98	5.82	9.69	24.50
30.0	0.5	0.96	5.82	9.72	24.13
30.0	0.5	0.97	5.80	9.53	24.39
30.0	0.5	0.97	5.87	11.02	23.16
50.0	0.5	0.98	6.02	8.73	21.65
50.0	0.5	0.97	6.02	9.63	21.68
50.0	0.5	0.97	6.02	9.58	21.56
50.0	0.5	0.97	6.02	9.65	22.06
60.0	0.5	0.98	6.30	13.81	
60.0	0.5	0.98	6.31	13.66	21.21
70.0	0.5	0.97	6.29	9.81	21.94
70.0	0.5	0.99	6.31	10.76	22.23
70.0	0.5	0.99	6.29	10.65	22.43
80.0	0.5	0.99	6.67	16.02	23.48
80.0	0.5	1.00	6.49	12.87	28.43
90.0	0.5	1.00	6.59	9.25	
90.0	0.5	1.00	6.60	9.94	29.87
90.0	0.5	1.00	6.61	9.94	27.75
95.0	0.5	1.00	6.89	10.89	26.61
99.9	0.5	1.00	6.97	12.43	31.20
50.0	0.7	0.98	6.01	10.19	21.34
60.0	0.7	0.98	6.19	10.80	21.19
80.0	0.7	0.99	6.60	13.74	22.69
80.0	0.7	1.01	6.50	10.98	22.50
90.0	0.7	0.99	6.65	10.65	24.98

[a]wt% in salt free solvent. [b]mol/(kg solvent). [c]mmol/(kg solvent)

Table 4.5: Measurements of CO_2 dissolution and dissociation at 50°C

MEG wt%	NaCl [m]	pCO_2 [bara]	pH	HCO_3^- [mmol/kg]	CO_2 [mmol/kg]
0.0	0.1	0.89	5.90	9.50	18.69
50.0	0.1	0.92	6.36	12.24	19.74
50.0	0.1	0.92	6.51	16.00	15.04
70.0	0.1	0.95	6.56	9.75	15.98
80.0	0.1	0.96	6.84	9.96	18.54
95.0	0.1	1.00	7.17	10.43	21.59
97.5	0.1	1.01	7.30	11.38	22.38
97.5	0.1	1.01	7.19	8.90	22.51
0.0	0.5	0.88	5.93	12.42	14.49
0.0	0.5	0.89	5.89	13.16	17.04
30.0	0.5	0.90	6.09	10.52	
50.0	0.5	0.91	6.36	10.82	
70.0	0.5	0.94	6.64	12.16	14.57
80.0	0.5	0.96	6.71	10.41	16.48
80.0	0.5	0.96	6.77	11.63	18.87
90.0	0.5	0.97	7.02	12.46	20.26
90.0	0.5	0.99	6.92	9.74	23.00
95.0	0.5	0.99	7.15	10.01	19.77
95.0	0.5	1.00	7.09	9.95	19.84
0.0	0.7	0.89	5.86	10.15	15.53
30.0	0.7	0.91	6.14	11.03	14.87

Table 4.6: Measurements of CO2 dissolution and dissociation at 80°C

MEG wt%	NaCl [m]	pCO_2 [bara]	pH	HCO_3^- [mmol/kg]	CO_2 [mmol/kg]
0.0	0.1	0.55	6.44	12.43	
0.0	0.1	0.55	6.46	13.00	7.50
50.0	0.1	0.65	6.76	10.16	8.15
70.0	0.1	0.73	7.17	10.70	10.19
80.0	0.1	0.80	7.29	10.04	11.81
90.0	0.1	0.89	7.50	10.71	
90.0	0.1	0.89	7.58	11.80	17.26
97.5	0.1	0.98	7.77	10.28	16.91
99.9	0.1	1.02	7.78	12.09	16.88
0.0	0.5	0.55	6.22	10.42	
0.0	0.5	0.55	6.44	13.56	8.61
30.0	0.5	0.59	6.61	11.79	7.25
60.0	0.5	0.69	6.88	10.10	8.55
70.0	0.5	0.74	7.09	10.97	9.19
80.0	0.5	0.79	7.20	10.05	7.76
80.0	0.5	0.80	7.26	12.56	10.61
95.0	0.5	0.94	7.61	11.63	14.45
95.0	0.5	0.95	7.68	15.12	17.91
0.0	0.7	0.56	6.29	10.61	6.26
70.0	0.7	0.75	7.10	12.10	9.58
80.0	0.7	0.80	7.17	9.59	13.18
90.0	0.7	0.89	7.46	12.48	12.22

Table 4.7: Measurements of CO_2 dissolution and dissociation at 65 and 90°C

MEG wt%	Temp °C	NaCl [m]	pCO_2 [bara]	pH	HCO_3^- [mmol/kg]	CO_2 [mmol/kg]
30.0	65	0.1	0.79	6.38	10.58	11.70
50.0	65	0.1	0.82	6.61	11.96	11.80
90.0	65	0.1	0.93	7.12	9.22	17.33
95.0	65	0.1	0.98	7.37	14.57	16.44
97.5	65	0.1	1.00	7.47	10.75	18.80
0.0	65	0.5	0.77	6.11	12.87	20.38
70.0	65	0.5	0.87	6.71	9.77	11.98
80.0	65	0.5	0.88	7.04	12.27	19.97
50.0	90	0.1	0.48	7.02	10.66	6.55
50.0	90	0.1	0.48	6.94	11.09	6.55
90.0	90	0.1	0.82	7.73	14.37	12.03
70.0	90	0.7	0.61	7.16	12.20	

Table 4.8: Data for second dissociation constant of carbonic acid. The carbonate concentration ratio corresponds to the point at which pH is measured. Total dissolved carbonate is about 50mmol/(kg solvent).

Temp °C	MEG wt%	NaCl m	$m_{CO_3^{2-}} / m_{HCO_3^-}$	pH
20.5	0	0.05	1.15	10.01
20.5	0	0.50	1.01	9.70
20.5	30	0.50	0.95	9.98
20.5	40	0.50	0.91	10.15
20.5	50	0.50	1.05	10.37
20.5	60	0.50	0.98	10.52
20.5	90	0.50	0.83	11.43
22.0	0	0.00	1.02	10.05
22.0	0	0.10	1.02	9.92
22.0	50	0.00	1.00	10.71
22.0	50	0.00	1.00	10.69
22.0	90	0.00	0.80	11.64
22.0	90	0.00	0.80	11.61
22.0	90	0.14	0.80	11.44
22.0	90	0.14	0.80	11.32
22.0	90	0.50	0.80	11.32
22.0	90	0.50	0.80	11.26
22.5	0	0.00	1.10	10.02
22.5	50	0.00	0.98	10.73
22.5	90	0.00	1.03	11.69
50.0	0	0.00	1.05	9.85
50.0	50	0.00	0.91	10.55
50.0	90	0.00	0.83	11.32
80.0	0	0.00	1.06	9.76
80.0	0	0.00	1.06	9.70
80.0	50	0.00	0.99	10.18
80.0	50	0.00	0.99	10.13
80.0	90	0.00	0.82	10.85
80.0	90	0.00	0.82	10.89

Table 4.9: Titration results for determination of carbonate dissociation at 25°C. The carbonate concentration ratio corresponds to the point at which pH is measured. Total dissolved carbonate is about 10mmol/kg. The latter column gives the pH for determination of K_1.

MEG wt%	NaCl m	$m_{CO_3^{2-}} / m_{HCO_3^-}$	pH	pH K_1
0	0.5	0.85	9.69	6.13
0	0.5	0.81	9.64	6.14
0	0.5	0.92	9.71	6.10
0	0.5	0.95	9.74	6.07
50	0.5	0.98	10.45	6.39
60	0.5	0.98	10.61	6.49
60	0.5	0.93	10.50	6.47
70	0.5	0.98	10.66	6.59
90	0.5	0.30	10.82	7.07
50	0.1	0.98	10.67	6.48
60	0.1	0.98	10.82	6.63
60	0.1	0.94	10.71	6.59
70	0.1	0.96	10.81	6.69
90	0.1	0.50	11.22	7.14

Table 4.10: $BaCO_3$ solubility [mmol/kg solvent]. Continuous CO_2 bubbling at P_{tot}~1atm, and with varying NaCl (mol/kg solvent) contents. ^{P}=Precipitation

T °C	MEG wt%	NaCl m	P_{CO2} bar	$BaCO_3$ mmol/kg	pH
4	0	0.50	1.00	17.52	5.91
23	0	0.05	0.98	10.09	6.02
23	50	0.05	1.00	6.61	6.24
23	90	0.05	1.00	7.08	6.94
25	0	0.15	0.97	11.91	6.00
25	0	0.50	0.97	14.94	6.08
25	0	0.50	0.97	14.41	6.08
25	30	0.50	0.99	11.54	6.20
25	30	0.50	0.99	11.69	6.20
25	50	0.50	1.00	10.57	6.28
25	70	0.50	1.00	10.75	6.51
25	80	0.50	1.00	11.20	6.76
25	90	0.50	1.00	12.14	7.01
25	97.5	0.50	1.00	15.27	
25	0	0.95	0.97	16.20	6.05
37.5	0	0.50	0.94	12.80	
50	0	0.50	0.88	11.14	
50	50	0.50	0.91	7.40	
50^P	90	0.50	0.97	8.41	
50	90	0.50	0.97	7.99	
80	0	0.50	0.54	7.36	6.3
80	50	0.50	0.64	4.78	
80^P	50	0.50	0.63	4.63	
80	90	0.50	0.87	4.70	

Table 4.11: $SrCO_3$ solubility [mmol/kg solvent]. Continuous CO_2 bubbling at P_{tot}~1atm, and with varying NaCl (mol/kg solvent) contents.

T °C	MEG wt%	NaCl m	P_{CO2} bar	$SrCO_3$ mmol/kg	pH
23	0	0.05	0.97	6.03	5.80
23	50	0.05	1.00	3.70	5.92
23	90	0.05	1.00	2.96	6.54
25[a]	0	0.00	0.97	4.91	
25[b]	0	0.00	0.97	4.91	
25	90	0.16	0.99	4.32	6.66
25	0	0.19	0.98	7.32	5.81
25	0	0.50	0.97	8.61	5.83
25	0	0.50	0.97	8.60	5.83
25	30	0.50	0.98	6.33	5.86
25	30	0.50	0.98	6.55	5.97
25	50	0.50	0.99	5.85	6.04
25	70	0.50	1.00	5.45	6.30
25	80	0.50	1.00	5.50	6.49
25	90	0.50	1.00	5.46	6.68
25	97.5	0.50	1.00	6.17	
25	0	1.03	0.97	9.52	5.83
37.5	0	0.50	0.94	7.36	
50	0	0.50	0.88	6.36	
50	50	0.50	0.91	3.93	
50	50	0.50	0.91	3.97	
50	90	0.50	0.97	4.06	
50[p]	90	0.50	0.97	4.05	
80	0	0.50	0.53	4.08	
80	50	0.50	0.64	2.46	
80[p]	90	0.50	0.87	2.24	

[a] Contained 0.8g of starting material $SrCO_3$(s). [b]Contained 12.1g of $SrCO_3$(s). [p]Precipitation

Table 4.12: $CaCO_3$ solubility [mmol/kg solvent]. Continuous CO_2 bubbling at P_{tot}~1atm, and with varying NaCl (mol/kg solvent) contents.

T °C	MEG wt%	NaCl m	P_{CO2} bar	$SrCO_3$ mmol/kg	pH
25	0	0.1	0.96	10.58	6.05
25	0	0.5	1.00	14.71	
25	0	0.5	0.98	14.68	
25	0	0.7	0.97	14.55	6.07
25	30	0.5	1.00	11.97	6.22
25	30	0.7	0.97	11.02	6.22
25	50	0.1	0.98	7.96	6.31
25	50	0.5	1.00	10.41	6.39
25	50	0.7	0.99	10.94	6.34
25	50	0.7	0.97	9.88	6.35
25	60	0.5	0.99	10.06	6.44
25	70	0.5	0.99	9.50	6.55
25	80	0.5	0.99	8.90	6.72
25	90	0.1	1.01	6.99	6.87
25	90	0.5	0.99	8.75	6.86
25	95	0.5	1.00	9.19	7.01
37.5	0	0.5	0.95	12.34	
50	0	0.5	0.89	9.87	
50	50	0.7	0.90	7.04	
50	90	0.1	0.99	3.34	
60	0	0.5	0.80	8.30	
60	30	0.5	0.82	6.20	
60	50	0.5	0.83	5.25	6.43
60	60	0.5	0.87	4.90	6.65
60	70	0.5	0.88	4.17	6.73
60	90	0.5	0.95	4.10	6.93
80	0	0.5	0.53	5.30	
80	0	0.5	0.54	5.47	
80	30	0.5	0.59	4.19	
80	70	0.5	0.95	2.82	
80	90	0.1	0.89	1.90	
80	90	0.5	0.95	2.66	

Table 4.13: $NaHCO_3$ solubility. T ± 0.2°C.

T °C	Time days	MEG wt%	$NaHCO_3$ mmol/kg	P_{CO2} Bar	pH
21.9	2	60	419	0.96	7.79
21.9	2	90	373	0.97	8.32
4.0[p]	8	90	342	0.99	8.01
4.0	11	90	323	1.00	8.04
4.0[p]	11	60	366	0.99	9.62

[p]Precipitation

Table 4.14: $KHCO_3$ solubility

Time days	MEG wt%	$KHCO_3$ mmol/kg	P_{CO2} Bar
5	0	2253	0.99
8	60	820	1.00
8	60[p]	849	1.00
5	97.5	1034	1.00

[p]Precipitation

Table 4.15: Measured pH at 25°C in solutions of 60 and 90wt% MEG. Salt concentration given in mmol/kg solvent. P_{CO2} denotes CO_2 pressure in bar

$NaHCO_3$	p_{CO2}	60wt%	$NaHCO_3$	p_{CO2}	90wt%
0.0	0.98	4.13	0.0	0.99	4.88
19.9	0.98	6.58	1.0	0.99	5.90
99.4	0.98	7.21	9.0	0.99	6.80
199.0	0.98	7.49	47.0	0.99	7.45
298.9	0.98	7.65	104.3	0.99	7.82
399.5	0.98	7.77	164.1	0.99	7.96
599.0	0.98	7.80	216.9	0.99	8.10
			270.2	0.99	8.20
			313.1	0.99	8.22
			378.5	0.99	8.29
			514.1	0.99	8.30

Table 4.16: Measured pH at 4°C in solutions of 60 and 90wt% MEG. Salt concentration given in mmol/kg solvent. P_{CO2} denotes CO_2 pressure in bar

$NaHCO_3$	p_{CO2}	60wt%	$NaHCO_3$	p_{CO2}	90wt%
0.00	1.00	4.01	0.00	1.01	5.02
0.06	1.00	4.68	0.13	1.01	5.03
1.9	1.00	5.48	0.59	1.01	5.60
9.4	1.00	6.11	1.7	1.01	5.97
44.7	1.00	6.69	12.4	1.01	6.78
93.1	1.00	6.98	50.0	1.01	7.33
158.8	1.00	7.20	100.5	1.01	7.59
227.7	1.00	7.35	214.8	1.01	7.87
280.9	1.00	7.44	452.4	1.01	8.03
337.7	1.00	7.52	897.5	1.01	8.03
422.9	1.00	7.52			

Table 4.17: Measured pH at 50°C in solutions of 60 and 90wt% MEG. Salt concentration given in mmol/kg solvent. P_{CO2} denotes CO_2 pressure in bar

$NaHCO_3$	p_{CO2}	60wt%	$NaHCO_3$	p_{CO2}	90wt%
0.00	0.92	4.39	0.00	0.94	5.10
0.23	0.92	4.50	0.17	0.94	5.56
1.2	0.92	5.62	1.3	0.94	6.32
9.1	0.92	6.54	9.0	0.94	7.12
58.5	0.92	7.31	65.2	0.94	7.90
112.9	0.92	7.56	165.4	0.94	8.27
192.6	0.92	7.79	265.2	0.94	8.50
267.5	0.92	7.94	432.5	0.94	8.63
321.5	0.92	7.98	644.2	0.94	8.65
377.2	0.92	8.04	964.4	0.94	8.65
434.2	0.92	8.10			
503.0	0.92	8.15			
556.3	0.92	8.18			
609.4	0.92	8.22			
672.4	0.92	8.23			

Table 4.18: Measured pH at 80°C in solutions of 60 and 90wt% MEG. Salt concentration given in mmol/kg solvent. P_{CO2} denotes CO_2 pressure in bar

$NaHCO_3$	p_{CO2}	60wt%	$NaHCO_3$	p_{CO2}	90wt%
0.00	0.72	4.76	0.00	0.88	5.40
3.8	0.72	6.69	0.96	0.88	6.59
12.8	0.72	7.21	8.8	0.88	7.53
60.1	0.72	7.81	46.1	0.88	8.16
114.3	0.72	8.04	92.9	0.88	8.34
273.2	0.72	8.37	180.56	0.88	8.59
394.9	0.72	8.47	297.2	0.88	8.74
584.2	0.72	8.58	452.2	0.88	8.88
751.9	0.72	8.62	666.8	0.88	8.95
1005.5	0.72	8.63	925.1	0.88	8.95
1368.9	0.72	8.64			

Table 4.19: Measured pH at 25°C in solutions of 60 and 90wt% MEG. $KHCO_3$ concentration given in mmol/kg solvent. P_{CO2} denotes CO_2 pressure in bar

$KHCO_3$	p_{CO2}	60wt%	$KHCO_3$	p_{CO2}	90wt%
0.0	0.98	4.22	0.0	0.99	4.96
0.2	0.98	4.55	0.2	0.99	5.50
1.3	0.98	5.46	0.8	0.99	5.92
11.4	0.98	6.40	12.3	0.99	7.03
42.1	0.98	6.94	41.3	0.99	7.49
78.2	0.98	7.19	85.8	0.99	7.76
152.8	0.98	7.46	158.5	0.99	7.99
236.1	0.98	7.64	314.9	0.99	8.26
338.2	0.98	7.79	505.2	0.99	8.45
451.1	0.98	7.90	857.3	0.99	8.69
671.2	0.98	8.06	1153.5*	0.99	8.74
994.3	0.98	8.20	1725.9*	0.99	8.74
1127.6	0.98	8.27			
1459.7*	0.98	8.32			

*Solubility limit reached

Table 4.20: Measured OH^- and Mg^{2+}(mmol/kg solvent) concentrations from dissolution of $Mg(OH)_2$. NaCl given as mol/kg solvent.

T °C	MEG wt%	NaCl m	"OH^-" [d] mmol/kg	Mg^{2+} mmol/kg	CO_2 [b] mmol/kg
22	0	0.5	0.59	0.43	0.27
22	0	0.5	0.56	0.44	0.31
22	30	0.5	0.69	0.47	0.25
22	30	0.5	0.63	0.51	0.39
22[a]	50	0.5	0.72	0.46	0.19
22[a,c]	50	0.5	0.59	0.56	0.53
22	60	0.5	0.70	0.49	0.28
22[c]	90	0.5	0.39	0.50	0.61
22	0	0	0.26	0.28	0.30
22	0	0	0.21	0.26	0.31
22	0	0	0.23	0.27	0.31
22	30	0	0.36	0.29	0.23
22	50	0	0.39	0.34	0.29
22[c]	70	0	0.30		
22[c]	90	0	0.14	0.30	0.47
50	0	0.5	0.44	0.35	0.26
50	30	0.5	0.33	0.34	0.35
50	40	0.5	0.26	0.43	0.60
50	50	0.5	0.41	0.37	0.33
50	90	0.5	0.32	0.32	0.31
80	0	0.5	0.65	0.61	0.57
80	50	0.5	0.44	0.78	1.12
80	90	0.5	0.19	0.63	1.07
80[r]	0	0.5	1.31	0.60	
80[r]	0	0.5	1.10	0.63	0.16
100[r]	0	0.5	0.65	0.35	0.04

[a]same sample either filtered or centrifuged. [b]estimated CO_2 content (see section 5.1.7)
[c]centrifuged. [d](see section section 5.1.7) [r]Refluxed at 100°C to remove CO_2.

Table 4.21: Measured pH at 25°C in solutions of 0.98mmol HCl /kg (-log(0.00098)=3.01) at various NaCl contents

MEG	NaCl / mol kg^{-1}			
wt%	0	0.1	0.5	0.7
0	3.03	3.11	3.12	3.11
50	2.94	3.08	3.11	3.09
70	2.92	3.08	3.10	3.08
90	2.56	2.71	2.75	2.73

5 Thermodynamic data

5.1 Thermodynamic equilibrium constant

The basis for the scale model is the thermodynamic solubility product. For some of the salts in the present work these thermodynamic solubility products $K°_{sp}$ were not previously available in the aqueous model[1,2]. Thus before any MEG dependence could be calculated the $K°_{sp}$ had to be included. $K°_{sp}$ was calculated from aqueous solubility data by use of Eq. 23, where NaCl is used as an example. m and γ denotes concentrations (mol/kg solvent) and activity coefficients respectively. m is measured at saturation and γ found from the Pitzer ion interaction model[1,3].

$$K^o_{sp}(NaCl) = m_{Na^+} m_{Cl^-} \cdot \gamma_{Na^+} \gamma_{Cl^-} \tag{23}$$

This is the same approach as used by Marion[4] and Königsberger et.al.[5] Solubility is highly temperature dependent and the solubility products were fitted with the function given in Eq. 24 unless stated otherwise.

$$\ln K^o_{sp} = \frac{K_1}{T} + K_2 + K_3 \ln T + K_4 T + \frac{K_5}{T^2} \tag{24}$$

T denotes absolute temperature (K), while K_1-K_5 are curve fitted constants given in Table 5.1. This equation is "physically correct" and can be deduced from the Gibbs' energy change for the dissolution reaction;

$$NaCl(s) = Na^+(aq) + Cl^-(aq) \tag{25}$$

$$\begin{aligned} \Delta G &= \mu_{Na^+(aq)} + \mu_{Cl^-(aq)} - \mu_{NaCl(s)} \\ &= \mu^*_{Na^+(aq)} + \mu^*_{Cl^-(aq)} - \mu^o_{NaCl(s)} + RT \ln \frac{a_{Na^+} a_{Cl^-}}{a_{NaCl(s)}} \\ &= \Delta G^o + RT \ln \frac{a_{Na^+} a_{Cl^-}}{a_{NaCl(s)}} \end{aligned} \tag{26}$$

The superscript * refers to the infinite dilution based standard state and ° to the Raoultion standard, as described in chapter 2. $a_{NaCl(s)}=1$ when NaCl is the pure solid phase. At equilibrium ($\Delta G=0$) the dissolution of NaCl can be related to the change in standard Gibbs free energy;

$$\ln K_{sp}^{o}\left(NaCl\right)=\frac{-\Delta G^{o}}{RT}=\ln a_{Na^{+}}+\ln a_{Cl^{-}} \tag{27}$$

By inserting the enthalpy and entropy Eq. 28 is obtained. If $\Delta H°$ and $\Delta S°$ are regarded as constants, the right hand side will equal the two first terms in Eq. 24.

$$\begin{aligned}\ln K_{sp}^{o} &= \frac{-\Delta G^{o}}{RT}=\frac{-\Delta H^{o}}{RT}+\frac{\Delta S^{o}}{R}\\ &= \frac{K_1}{T}+K_2\end{aligned} \tag{28}$$

The temperature dependence of the enthalpy and entropy is given from the heat capacity. T denotes the temperature in question while $T°$ corresponds to the reference, usually 298K;

$$\Delta H_T^o=\Delta H_{T^o}^o+\int_{T^o}^{T}\Delta C_p dT \tag{29}$$

$$\Delta S_T^o=\Delta S_{T^o}^o+\int_{T^o}^{T}\frac{\Delta C_p}{T}dT \tag{30}$$

If the change in heat capacity is regarded as constant i.e. not a temperature function, this will give a lnT term from the entropy relation in Eq. 30. Thus Eq. 28 becomes;

$$\begin{aligned}\ln K_{sp}^{o} &= \frac{-\left[\Delta H^{o}+\Delta C_p\left(T-T^{o}\right)\right]}{RT}+\frac{\left[\Delta S^{o}+\Delta C_p\ln\frac{T}{T^{o}}\right]}{R}\\ &= \frac{K_1}{T}+K_2+K_3\ln T\end{aligned} \tag{31}$$

Eq. 31 corresponds to the first three terms of the general Eq. 24, and is equivalent with the expression used by Prausnitz et al.[6]. The temperature function of C_p is commonly[1] included by a function such as given by Eq. 32.

$$C_p=\alpha+\beta T+\frac{\gamma}{T^2} \tag{32}$$

By performing the above integration with this function, one will arrive at an equation with the same form as the general function in Eq. 24. In some cases it was found that one or more of the K parameters in Eq. 24 could be omitted without this having a negative effect on the curve fit. From Table 5.1 it is consequently seen that some salts have parameters set to 0. The fitting should, however, at least include parameters K_1 and K_2, which corresponds to enthalpy and entropy respectively. Eq. 27-31 also shows that solubility can be calculated from calorimetric data.

Table 5.1 gives all the parameters for the $K°_{sp}$ functions. The latter two columns give the literature references used for fitting the equation, and the temperature range that they cover.

Table 5.1: Parameters for calculation of $K°_{sp}$ in Eq. 24

Salt	K_1	K_2	K_3	K_4	K_5	T / °C[a]	Ref.[b]
KCl[c]	494.26[c]	-5.8585	2.4552E-2	-4.2553E-5	2.6066E-8	0-300	7-9
NaAc·3H$_2$O	1.5994	117.49	-26.359	0.12141	1.1220E-2	0-58	8-10
NaAc	-9653.9	185.40	-24.242	-2.5292E-2	0	0-120	8-10
NaHCO$_3$	-3.6367	-77.250	14.575	-2.2468E-2	0	-3-95	8,12-18
KHCO$_3$	2.2403	69.658	-17.016	9.2964E-2	0	0-70	4,8-11,19-20
K$_2$CO$_3$·1.5H$_2$O	6.6460	191.93	-44.847	0.23565	0	0-250	8-11,21
K$_2$CO$_3$	-39.805	-1160.4	244.78	-0.68681	0	0-250	8-11,21
Na$_2$CO$_3$·10H$_2$O	-8006.9	25.093	0	0	0	-2-40	8.14,22,23
Na$_2$CO$_3$·H$_2$O	3016.7	-274.98	55.483	-0.16629	-0.082013	30-100	8,18,22-24
Na$_2$CO$_3$	-17483	462.07	-70.047	-1.5459E-3	-4.2439E-3	100-300	18
BaCO$_3$	-46077	1399.1	-236.68	0.28289	0	0-90	26
SrCO$_3$	-16669	362.71	-57.996	8.3170E-3	0	0-90	25,35
CaSO$_4$	-9536.5	239.87	-38.258	0	0	20-250	27-34,TW
Mg(OH)$_2$	-10621	240.71	-40.444	0	0	18-300	8,10,36,TW
HydMg[d]	3555.62	-85.022	0	0	0	0-80	4,5,38,TW

[a]Temperature range of *experimental data* [b]Literature references. TW=This work
[c]Parameters for *Fourth order polynomial* given in Eq. 34
[d]Solid phase included in model is Hydromagnesite with formula; 3MgCO$_3$·Mg(OH)$_2$·3H$_2$O

5.1.1 KCl

Potassium chloride has been thoroughly studied through the years and its aqueous solubility is tabulated in the literature[7-9]. The thermodynamic solubility product is given as;

$$K_{sp}^{o}(KCl) = m_{KCl}^{2} \cdot \gamma_{K^+} \cdot \gamma_{Cl^-} \tag{33}$$

m_{KCl} corresponds to the solubility data taken from the literature[7-9]. The activity coefficients, γ, were calculated by the Pitzer model mentioned above. It is noted that the form of the fitting equation (Eq. 24) is a direct consequence of the chosen expression for C_p. For KCl, however, Eq. 24 gave a poor fit, thus possibly caused by a different temperature function for the heat capacity. The results shown in Fig. 5.1 were fitted with the 4th order expression given in Eq. 34. T is in degree K, and the fitting constants K_1-K_5 are given in Table 5.1. This function is the same as used for NaCl by Kaasa[1];

$$K_{sp}^{o}(KCl) = K_1 + K_2 T + K_3 T^2 + K_4 T^3 + K_5 T^4 \tag{34}$$

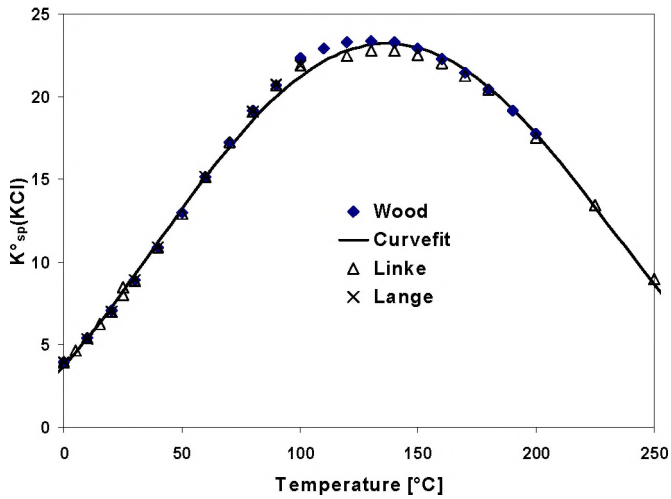

Fig. 5.1: The thermodynamic solubility product of KCl versus temperature. Curve fit of Eq. 34 compared with literature data[7-9]

It is generally known that such numerically fitted equations can give improbable extrapolations compared to "physically correct" equations like Eq. 24. Because the fitting in addition is performed on K_{sp} rather than lnK_{sp}, such polynomials may even give negative values for the solubility product i.e. physically impossible. The polynomial expression was therefore forced to always be greater than 0 and to have a reasonable extrapolation from -50 to 300°C.

5.1.2 NaAc

Sodium acetate can exist in two different crystal modifications. At high temperature anhydrate, NaAc, is the stable phase, while at temperatures lower than about 58°C the trihydrate, NaAc·3H_2O, is the stable phase in aqueous solutions. Thus for the latter case the activity of water must be included in the calculation of K_{sp}° and Eq. 23 becomes;

$$K_{sp}^{o}\left(NaAc \cdot 3H_2O\right) = m_{Na^+} m_{Ac^-} \gamma_{Na^+} \gamma_{Ac^-} a_{H_2O}^{3} \quad (35)$$

$$K_{sp}^{o}\left(NaAc\right) = m_{Na^+} m_{Ac^-} \gamma_{Na^+} \gamma_{Ac^-} \quad (36)$$

Activity coefficients and water activities were calculated by the mentioned *Multiscale* model[1]. The NaAc concentration in Eq. 35-36 is written as Na^+ and Ac^- to emphasize that the negative ion is actually a base and consequently in equilibrium with acetic acid, HAc. When NaAc is dissolved in water, however, the HAc concentration is negligible and Na^+ and Ac^- concentrations are virtually equal. Tabulated data[8-10] from different sources correspond well as shown in Fig. 5.2 and have probably been taken from the same original works. A rough extrapolation gave a phase shift from NaAc·3H_2O to anhydrous NaAc at about 60°C.

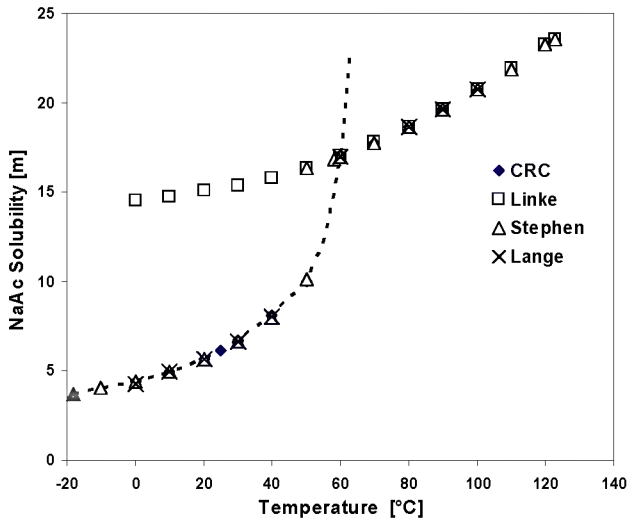

Fig. 5.2: Solubility[8-10] of NaAc (mol/kg water) in aqueous solutions as function of temperature.

The calculated values were fitted to Eq. 24 and gave two functions for K_{sp}^{o}, one for the trihydrate and one for the anhydrous salt with the parameters given in Table 5.1. Fig. 5.3a) shows the two functions, where the equation does not give a perfect fit for the highly soluble anhydrate. It was, however, chosen to use Eq. 24 since this equation gives a reasonable extrapolation as mentioned above. From Fig. 5.3a) it seems that the change in phase stability occurs at about 100°C, which is misleading. The reason for this is that the water activity is included for NaAc·3H_2O, but obviously not for the anhydrate, NaAc. To directly compare the two, the solubility product of NaAc·3H_2O is divided by the water activity as shown in Eq. 37. The right hand side is now the same as

for the anhydrate expression and Fig. 5.3b) gives, as expected, an intersection at about 58°C.

$$\frac{K_{sp}^{o}\left(NaAc\cdot 3H_2O\right)}{a_{H_2O}^{3}} = m_{Na^+} m_{Ac^-} \gamma_{Na^+} \gamma_{Ac^-} \tag{37}$$

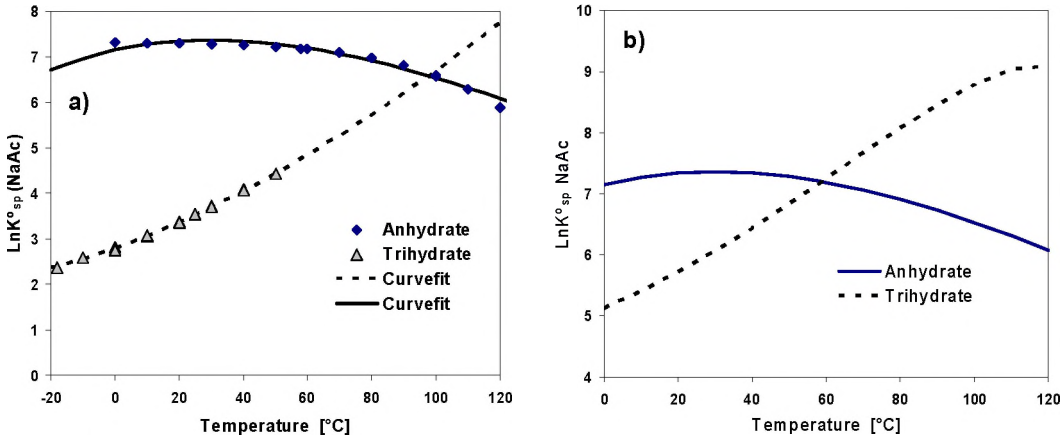

Fig. 5.3: ***a) Ln K°$_{sp}$*** **of NaAc and NaAc·3H$_2$O as function of temperature.** ***b)*** $\ln K_{sp}^{o}\left(NaAc\right)$ **and** $\frac{\ln K_{sp}^{o}\left(NaAc\cdot 3H_2O\right)}{a_{H_2O}^{3}}$ **versus temperature.**

5.1.3 NaHCO$_3$ and KHCO$_3$

The thermodynamic solubility product of NaHCO$_3$ was calculated from literature solubility data[8,12-18] that covered –2.5 to 95°C. For sodium bicarbonate it is necessary to separate the anion and cation concentrations, thus Eq. 23 becomes;

$$K_{sp}^{o}\left(NaHCO_3\right) = m_{Na^+} m_{HCO_3^-} \gamma_{Na^+} \gamma_{HCO_3^-} \tag{38}$$

If the solubility measurements are performed by dissolving NaHCO$_3$, alkalinity will equal sodium concentration but not necessarily the bicarbonate concentration. Bicarbonate can dissociate according to Eq. 39, where carbonate and CO$_2$ is formed.

$$2HCO_3^- = CO_3^{2-} + CO_2 + H_2O \tag{39}$$

At high temperature and low CO$_2$ pressure the reaction is shifted towards the right, thus bicarbonate concentration will not equal Na^+ concentration or alkalinity. If the Bicarbonate concentration have not been measured directly it has to be calculated, and the existing aqueous scale model[1,2] was used for this purpose. Wegscheider et.al.[16] measured both bicarbonate and carbonate concentrations, which were in good agreement with the model calculations. Data from the CRC handbook[11] (above 40°C) did not correspond well with the other sources and was not utilized for the curve fitting.

This reference[11] did not clearly state how the experiments had been performed, and therefore it was not evident how to calculate the carbonate equilibria.

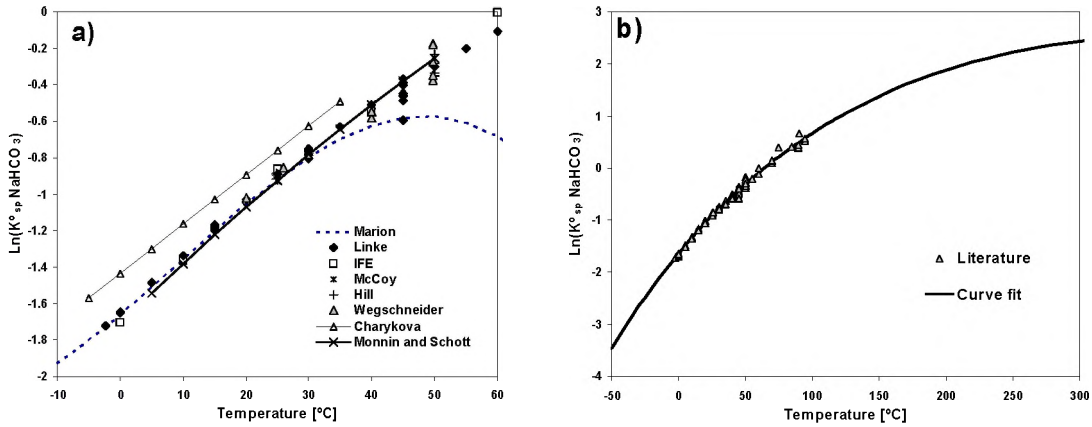

Fig. 5.4: ***a)*** **Calculated lnK_{sp}° of $NaHCO_3$ from literature data[8,12-18] versus temperature, compared with low temperature models of Marion[4], Charykova[15] and Monnin and Schott[17]. b) Calculated lnK_{sp}° of $NaHCO_3$ from literature data[8,12-18] and the extrapolation of the curve fit.**

Fig. 5.4a) shows the calculated values of lnK_{sp}° compared to models found in the literature. Both Marion[4] and Monnin and Schott[17] fitted models from solubility data by use of the Pitzer ion interaction model in an equivalent manner as in this work. It is noted that Marion[4] was only concerned with low temperature systems, and the model consequently deviates at 40°C and above. Monnin and Schott[17] only used data from 5 to 50°C but their simple extrapolation seems much more reliable outside this range. Charykova[15] used the same approach, but the model is systematically higher than the calculations in this work. Charykova used own data for the fitting of parameters in the Pitzer model. It is noted that the choice of model for the activity coefficients will consequently lead to a different value of K_{sp}°. There will, however, always be internal consistency in the model since it obviously reproduces the solubility data it has been fitted from.

The work of Waldeck, Lynn and Hill[18] is the only available reference for solubility at 100-200°C. It was stated that they had problems with CO_2 leaving the system, and the total pressures in their closed bomb experiments are not given. Thus it was not evident how to interpret their measurements for calculation of activity coefficients and bicarbonate concentration. It was, however, given approximate values for the CO_2 pressure at 190 and 200°C, and based on these a rough calculation of the carbonate equilibria was performed. It did, however, not correspond well with the measured bicarbonate concentration, which may be due to uncertainties in the model. $NaHCO_3$ and $KHCO_3$ were included in this work since it is desirable to calculate solubility of these salts in MEG injection pipelines at seabed temperature. High temperature and concentrations up to 10m can be found in MEG regeneration plants. These conditions, however, are at present well outside the scope of this work. Further development, to enable calculations in process plants, is a possible future extension of this work. This will probably require reinvestigation of the Pitzer ion interaction model when these

extremely high concentrations are encountered. At present it was chosen to only use the data at below 100°C.

The thermodynamic solubility product of $KHCO_3$ was calculated similarly as done for $NaHCO_3$. Solubility data found in the literature[4,8-11,19,20] covered 0 to 70°C, and with a few exceptions the data corresponded well.

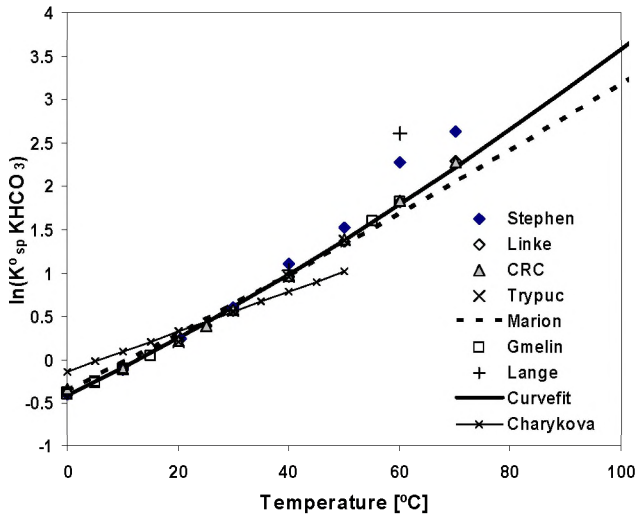

Fig. 5.5: lnK_{sp}° for $KHCO_3$ versus temperature, calculated from literature data[4,8-11,19,20] The curve fit is compared with equations from Marion[4] and Charykova[15]

Fig. 5.5 shows that the calculation is in agreement with the findings of Marion[4], while Charykova[15] gives a different temperature function. The work of Charykova, however, was primarily done at 25°C and it is, as in the case of $NaHCO_3$, pointed out that since Charykova use a slightly different model for activity coefficients, it leads to a different solubility product. It was chosen to use the same type of extrapolation as for $NaHCO_3$ and all parameters are given in Table 5.1.

5.1.4 K_2CO_3 and Na_2CO_3

As in the case of bicarbonate salts, anions and cations have to be separated in the calculation of K^o_{sp} for carbonates. Eq. 40 gives the solubility product for potassium carbonate, and the expression for the sodium salt will be equivalent. The water activity must be introduced for phases including crystal water, where y denotes the number of moles of crystal water.

$$K^o_{sp}\left(K_2CO_3 \cdot yH_2O\right) = m^2_{K^+} m_{CO_3^{2-}} \gamma^2_{K^+} \gamma_{CO_3^{2-}} a^y_{H_2O} \qquad (40)$$

Solubility data for potassium carbonate found in several handbooks[8-11] are plotted in Fig. 5.6 versus temperature(°C). High temperature data is given by Moore et.al[21]. The thermodynamic solubility product was calculated from Eq. 40 with carbonate ion concentration from the aqueous model described in previously. At ambient

temperatures $K_2CO_3 \cdot 1.5H_2O$ is the stable phase, while the anhydrate, K_2CO_3, is only stable in aqueous solutions above ≈152°C.

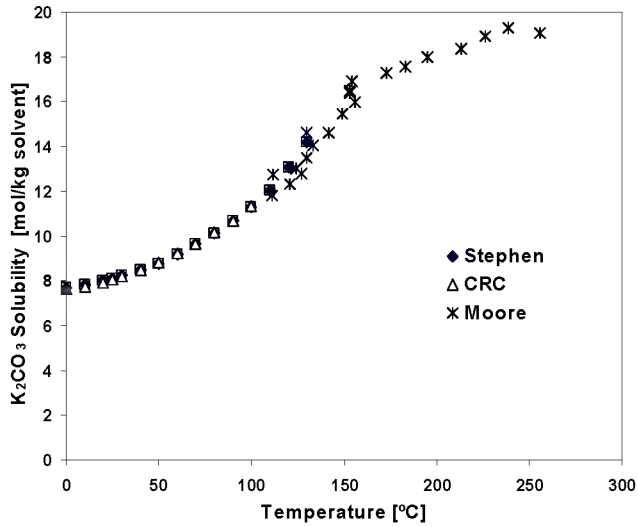

Fig. 5.6: Solubility of K_2CO_3 in aqueous solutions versus temperature from Stephen[10], CRC Handbook[11] and Moore et. al.[21]

It should be noted that the calculated activity coefficient of the carbonate ion is about 850 at 150°C, while it drops to 10^{-2} at 250°C. The model seems to be questionable for use in these highly saline solutions at high temperature. Calculated K_{sp}^{o} values were fitted with two equations as shown in Fig. 5.7. As in the case of NaAc the water activity dependence of one of the salts, result in a misleading intersection of the two K_{sp}^{o} functions. Phase change is in fact predicted at about 154°C. The anhydrate function does not give a very good fit, but given the uncertainties both in measurements and modelling at these conditions, a more sophisticated equation did not seem warranted.

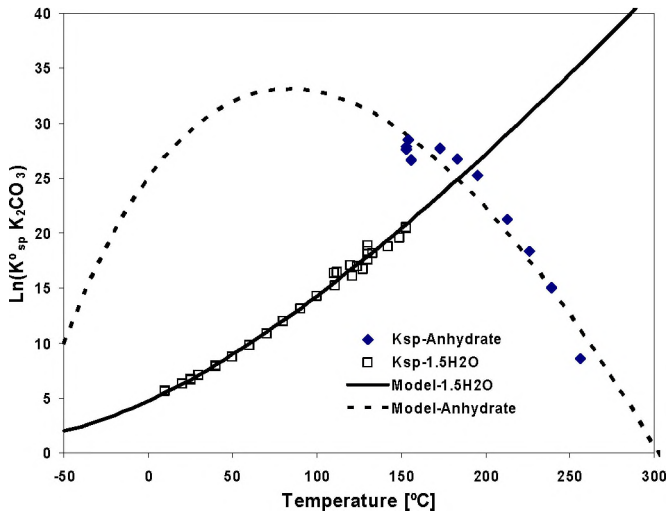

Fig. 5.7: lnK_{sp}^{o} of $K_2CO_3 \cdot 1.5H_2O$ and K_2CO_3 versus temperature, compared with the fitted equations

Three solid phases of Na_2CO_3 were included in the model;

→ decahydrate $Na_2CO_3 \cdot 10H_2O$
→ monohydrate $Na_2CO_3 \cdot H_2O$
→ anhydrate Na_2CO_3.

In aqueous solutions the anhydrate is not stable at temperatures below about 100-120°C. When MEG is added to the system, however, water activity drops and anhydrate becomes stable at lower temperatures. Thus the thermodynamic solubility product of anhydrate has to be included in the model. The data found in the literature corresponded well, and the stability shift from deca to monohydrate is clearly seen in Fig. 5.8a) Wells and McAdam[23] found a short temperature interval where the heptahydrate $Na_2CO_3 \cdot 7H_2O$ was stable as shown in the segment given in Fig. 5.8b). Apelblat and Manzurola[22], however, did not include the heptahydrate, $Na_2CO_3 \cdot 7H_2O$, in their work. In the present work it was also chosen to omit this phase from the modeling due to its narrow stability range.

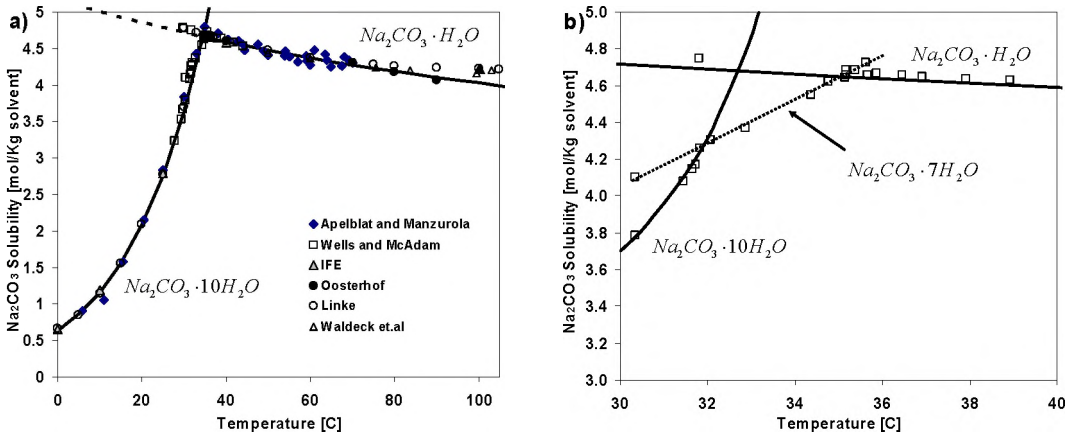

Fig. 5.8: a)Solubility (mol/kg water) of Na_2CO_3 in aqueous solutions as function of temperature from various sources[8,10,14,22-24], lines correspond to functions given by Apelblat and Manzurola[22]. b) Segment at 30-40°C with data from Wells and McAdam[23]

K_{sp}^{o} values were calculated from solubility data in the literature[8,10,14,22-24], where carbonate concentration, water activity and activity coefficients were calculated with the aqueous model as described above.

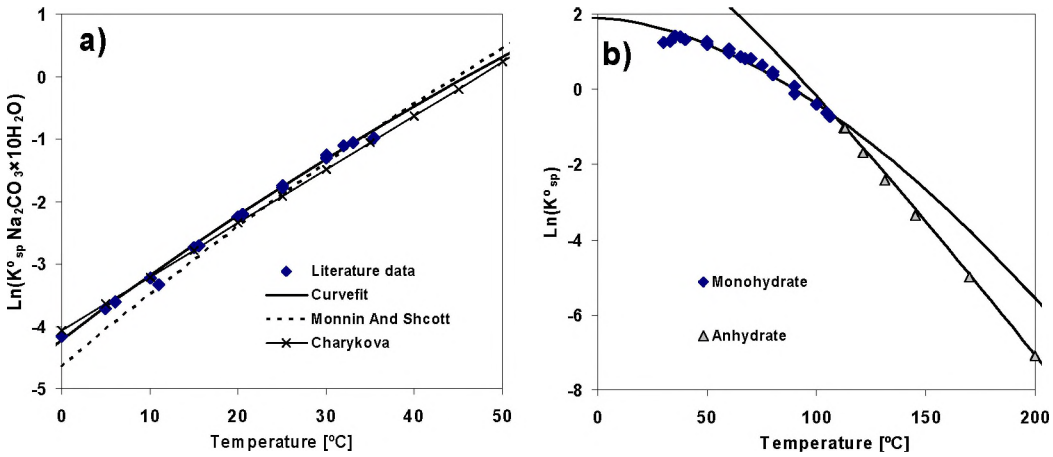

Fig. 5.9: a) $LnK_{sp}°$ of decahydrate $Na_2CO_3·10H_2O$ as function of temperature compared with functions of Monnin and Schott[17] and Charykova[15]. b) $LnK_{sp}°$ of monohydrate $Na_2CO_3·H_2O$ and anhydrate Na_2CO_3 versus temperature. This work: solid lines

Fig. 5.9 shows the curve fit of the three solubility products, where all parameters are given in Table 5.1. For $Na_2CO_3·10H_2O$ the function was found to correspond well with the findings of Monnin and Schott[17] and Charykova[15]. These equations predict a shift from deca to monohydrate at about 36°C and from mono to anhydrate at 102°C. The former corresponds well with the findings of Apelblat and Manzurola, while the latter is slightly lower than the 112°C predicted by Waldeck et.al[18]. It should be noted that due to one of the salts in Fig. 5.9b) containing crystal water, the intersection is misleading and will not equal the transformation temperature as described in detail for NaAc above.

5.1.5 $BaCO_3$ and $SrCO_3$

There exist a few publications concerning $BaCO_3$ and $SrCO_3$ solubility in aqueous solutions. The elaborate works of Busenberg and Plummer[25-26] review available data and give $K°_{sp}$ values between 0-90°C based on measurements with controlled a CO_2 pressure. Millero et.al[35] gave $K°_{sp}$ values at 25°C from measurements without CO_2(g), with 0.1 to 6mol NaCl/kg water. Satisfactory results were obtained using the Pitzer model in the whole ionic strength interval. Busenberg et.al[25-26], however, included the $BaHCO_3^+$, $BaCO_3°$, $SrHCO_3^+$ and $SrCO_3°$ complexes in their modified Debye-Hückel equation to calculate activity coefficients. By evaluating the equilibrium constants of the complexes they could calculate free Ba^{2+} and HCO_3^- concentrations and finally find the desired thermodynamic $K°_{sp}$. Kaasa[1] found that if the $CaHCO_3^+$ complex was included for prediction of calcite ($CaCO_3$) solubility, the calculated solubility became too high at higher CO_2 pressures.

When solubility data is used for calculating $K°_{sp}$, the value consequently depends on the chosen model for the activity coefficients. In the present work the Pitzer ion interaction model was used. i.e. a different model than used by Busenberg et.al[25-26]. It was therefore necessary to recalculate the thermodynamic $K°_{sp}$.

The equilibrium between solid $BaCO_3$ and the dissolved species under CO_2 pressure is conveniently given by Eq.41. In solutions saturated with CO_2, bicarbonate concentration dominates and virtually equals alkalinity. It is therefore reasonable to work with an equation that includes HCO_3^- concentration rather than CO_3^{2-}. Eq.42 gives the corresponding thermodynamic equilibrium constant, where *a, m,* and γ corresponds to activity, concentration and activity coefficients, respectively. P_{CO2} denotes partial pressure of CO_2 with the corresponding fugacity coefficient φ.

$$Ba^{2+} + 2HCO_3^- = CO_2(g) + BaCO_3(s) + H_2O \tag{41}$$

$$K^o_{Eq.42} = \frac{K^o_2}{K^o_{sp} K^o_H K^o_1} = \frac{f_{CO_2} a_{H_2O}}{a_{Ba^{2+}} a^2_{HCO_3^-}} = \frac{p_{CO_2} \varphi_{CO_2} a_{H_2O}}{m_{Ba^{2+}} \gamma_{Ba^{2+}} \left(m_{HCO_3^-} \gamma_{HCO_3^-} \right)^2} \tag{42}$$

Eq.42 is modified to give the desired $K°_{sp}$ as shown in Eq.43 where φ is set equal to 1.

$$K^o_{sp} = \frac{K^o_2}{K^o_H K^o_1} \cdot \frac{m_{Ba^{2+}} \gamma_{Ba^{2+}} \left(m_{HCO_3^-} \gamma_{HCO_3^-} \right)^2}{p_{CO_2} a_{H_2O}} \tag{43}$$

When the solubility is measured by dissolution of $BaCO_3$(s), the alkalinity (see section 6.4) equals two times the barium concentration.

$$A_T = 2m_{Ba^{2+}} = m_{HCO_3^-} + m_{CO_3^{2-}} + m_{OH^-} - m_{H^+} \tag{44}$$

New $K°_{sp}$ values were calculated from Eq.43 based on data from Busenberg et.al[25-26], where $[HCO_3^-]$ was set equal to 2 times the $[Ba^{2+}]$. The $K°_{sp}$ functions were modeled with the same type of expressions (see Table 5.1) as originally used by Busenberg et.al.[25-26]. Fig. 5.10 shows that the deviation increases with temperature, which is consistent with introduction of the complexes described above.

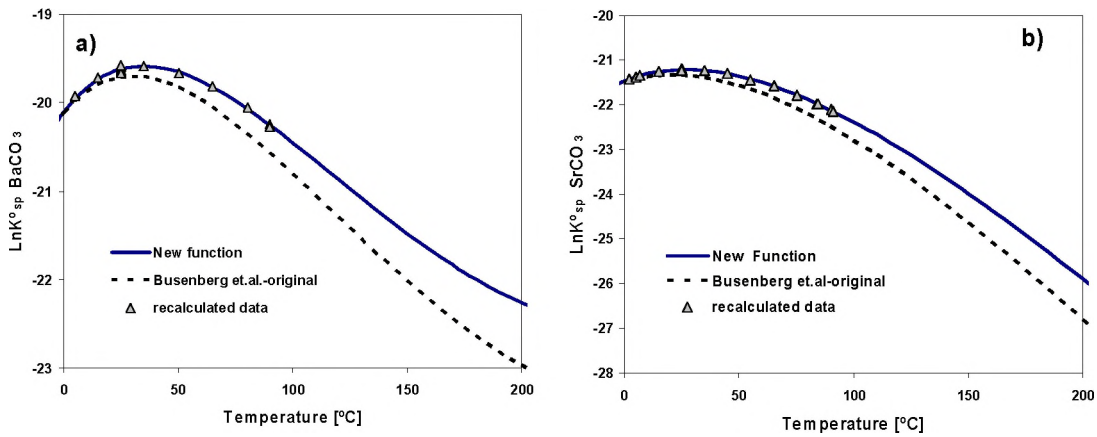

Fig. 5.10: ***a)*** **ln$K°_{sp}$ of $BaCO_3$** ***b)*** **ln$K°_{sp}$ of $SrCO_3$ versus temperature. New values compared to the original function of Busenberg et.al.[25-26].**

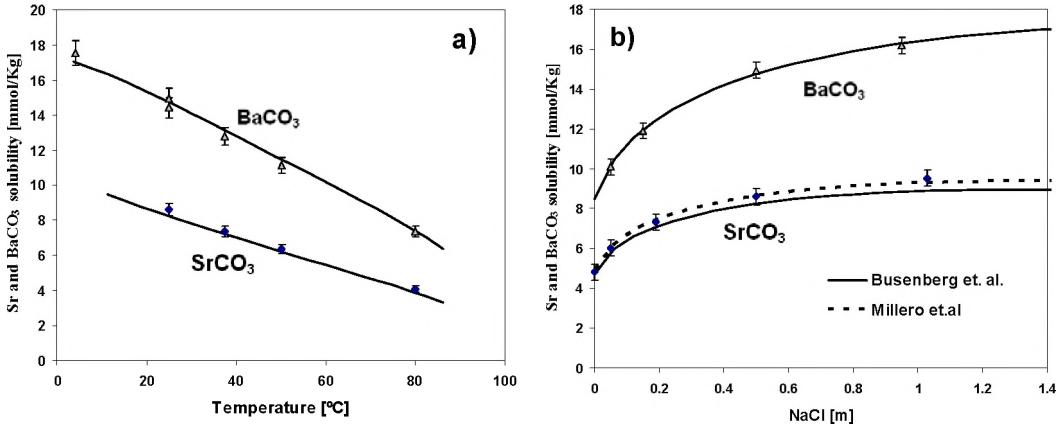

Fig. 5.11: Measured (mmol/kg solvent) $BaCO_3$ and $SrCO_3$ solubility in CO_2 saturated solutions at atmospheric pressure (Table 4.10 and Table 4.11) *a)* with 0.5mol NaCl/kg at 4-80°C *b)* with 0-1.05m NaCl at 25°C *Solid line:* Calculation *Dotted line:* Calculation with $K°_{sp}$ from Millero et.al[35]

Fig. 5.11 compares the data from this work (see Table 4.10 and Table 4.11) with calculations based on the new $K°_{sp}$ functions. The data in Fig. 5.11a) have been measured in solutions containing 0.5m NaCl, and generally corresponds well with the model. For $SrCO_3$, however, there is seen that the data are systematically slightly higher than the calculation. The systematic deviation is easier observed in Fig. 5.11b) at higher ionic strengths (25°C). Because $BaCO_3$ data did not show discrepancies, the deviation should not come from the experimental setup or impurities in the NaCl(s). Impurities in the starting material $SrCO_3$ could, however, be a cause for the observed deviation, and possibly also that fines passed through the filter. To test this it was set up two solutions at 25°C, where one was added over 10 times as much $SrCO_3$(s) as the other. A large amount of solids should give a higher measured solubility if solids passed the filter or the starting material contained impurities. The results given in Table 4.11 showed no differences between the two. Busenberg et.al[26] found that aging of the $SrCO_3$ starting material had an influence on solubility measurements; hence this could be the reason for the differences. The data measured in this work imply a slightly higher $K°_{sp}$, but it was decided to use a conservative approach i.e. the function developed from the data of Busenberg et.al[26]. It is noted that the $K°_{sp}$ value given by Millero et.al[35] is in good agreement with the findings of this work, as shown in Fig. 5.11b).

5.1.6 $CaSO_4$

When performing new experimental work on calcium sulphate anhydrite, $CaSO_4$, it was discovered that the existing aqueous model predicted a slightly too low solubility compared with the measured data (see Table 4.1). For gypsum, $CaSO_4 \cdot 2H_2O$, there was good agreement between measured data and the model.

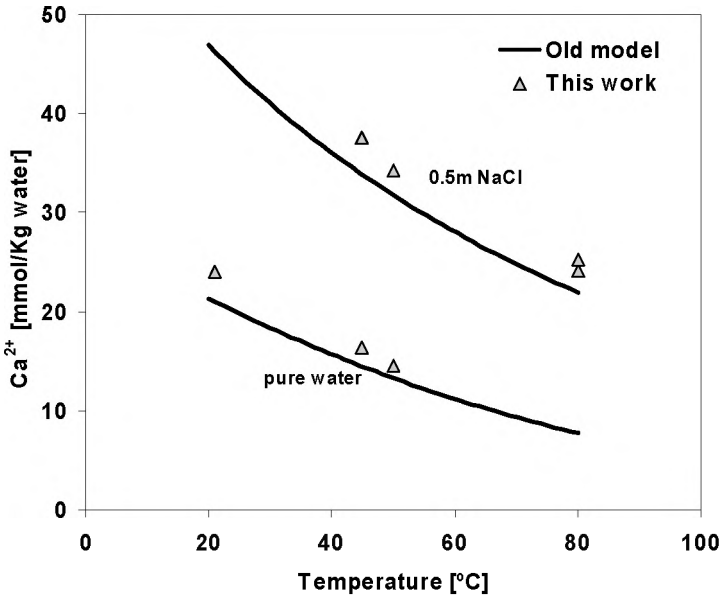

Fig. 5.12: Measured $CaSO_4$ anhydrite solubility at 0 and 0.5mNaCl versus temperature compared with model predictions.

Fig. 5.12 shows that the experimental data were slightly higher than the predictions, and a comparison with Møller[27] also indicated that the model systematically returned too low solubilities. Because gypsum was in good agreement, this indicated that the Pitzer model functioned well but that the $K°_{sp}$ function of $CaSO_4$ was too low. Thus it was decided to construct a new curve fit from the new solubility measurements in Table 4.1, as well as literature values[27-34].

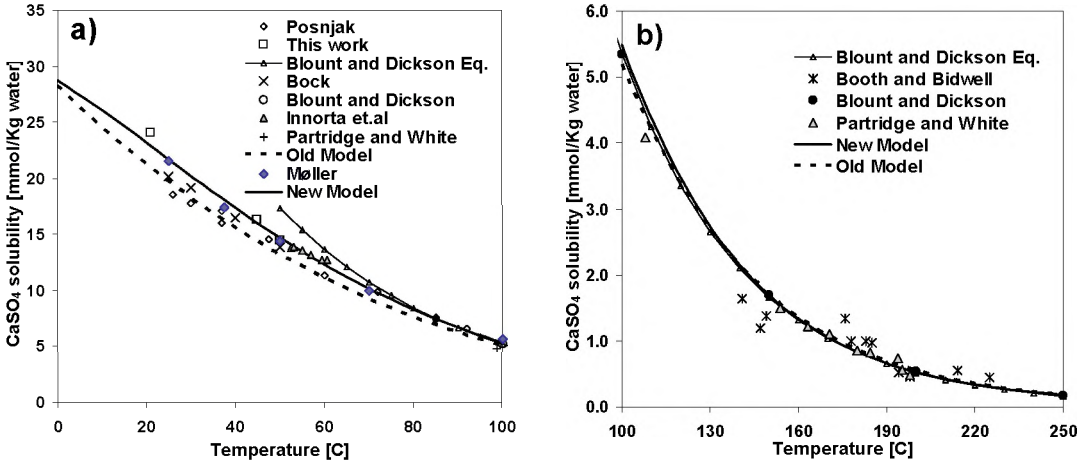

Fig. 5.13: Measured anhydrite $CaSO_4$ solubility and literature[27-34] data compared with models a) low temperature b) high temperature.

Fig. 5.13 compares the model predictions with experimental data for the solubility of $CaSO_4$ in pure water. *Old model* denotes the original function given by Kaasa[1], while *New model* corresponds to the curve fitting performed in the present work. The points from Møller[27] have been read from figure 3 in that work. The *old* and *new* models are virtually equal at high temperature, and also in good agreement with the equation given by Blount and Dickson[32]. Low temperature data of Posnjak[28] (26-50°C) were not used in the curve fitting, since these data were systematically lower than values from other sources. It is noted that although the difference between the old and new model may seem insignificant, it becomes noticeable in solutions of higher ionic strength. The old model predicted the gypsum-anhydrite phase stability shift at about 42°C in pure water, which corresponded well with the 42±1°C predicted by Posnjak[28]. New experimental measurements of this work (see Table 4.3) did, however, show that gypsum was the stable phase at 44°C, thus the transformation point should be higher than this. This supports the conclusion that the old model predicts a too low solubility for the anhydrite $CaSO_4$. The new model predicts the gypsum-anhydrite shift at 46.7°C, which is closer to the 49.5±2.5°C estimated by Innorta et.al.[29].

5.1.7 $Mg(OH)_2$

The solubility of Brucite, $Mg(OH)_2$, is very low and therefore troublesome to measure. A further complication is that CO_2 present in solution will react with OH^- to form carbonate in a high pH solution;

$$2OH^- + CO_2 = H_2O + CO_3^{2-} \qquad (45)$$

Thus CO_2 removes hydroxide ions and thereby increases the solubility of $Mg(OH)_2$ in contact with the solution. Experimentally this means that the solutions must either be CO_2 free or alternatively the individual concentrations of OH^- and Mg^{2+} must be known to calculate the solubility product;

$$Mg(OH)_2(s) = Mg^{2+} + 2OH^- \quad (46)$$

$$K^o_{sp}\left[Mg(OH)_2\right] = m_{Mg^{2+}} m^2_{OH^-} \gamma_{Mg^{2+}} \gamma^2_{OH^-} \quad (47)$$

In this work solid $Mg(OH)_2$ was dissolved in degassed distilled water. Filtered samples were analysed both for Mg^{2+} by EDTA titration and alkalinity by HCl titration. For each Mg^{2+} going into solution there are also two hydroxide ions, as seen from Eq. 46. Thus the total alkalinity (see section 6.4) is always two times the magnesium concentration. When performing solubility measurements in water it was found that the HCl titration gave an end point that did not correspond with twice the Mg^{2+} concentration, as seen from Table 4.20. A possible reason for this is given in Fig. 5.14a) that shows theoretical HCl titration curves for a solution with an alkalinity of 0.6mmol/kg without any CO_2 present, and with 0.2mmol/kg of CO_2.

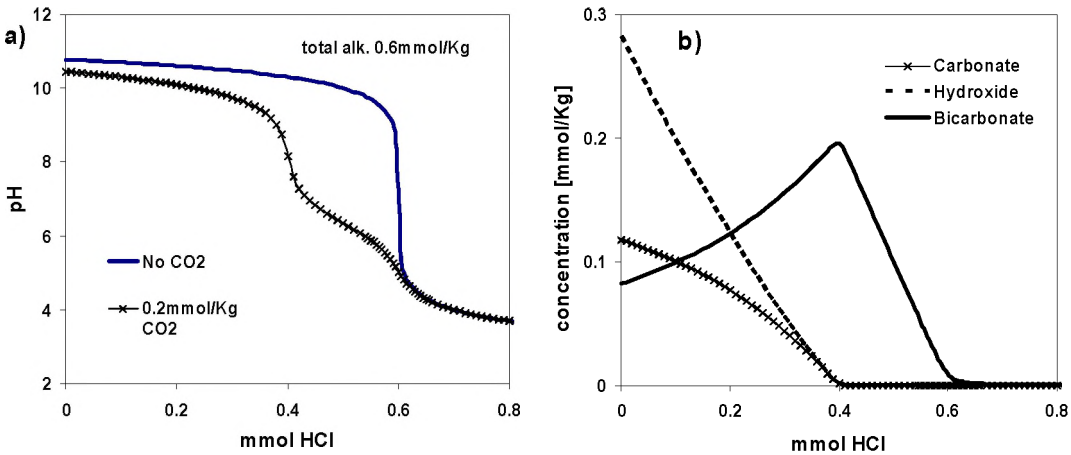

Fig. 5.14: ***a)*** **Theoretical titration curve of pH versus added HCl for solution having an alkalinity of 0.6mmol/kg, with (0.2mmol/kg) and without CO_2** ***b)*** **Concentrations of CO_3^{2-}, HCO_3^- and OH^- for the case with 0.2mmol/kgCO_2 in a)**

In a solution without carbonate the titration end point is very distinct at pH=7, while with CO_2 there will be two break points. Investigation of the HCl titration curves showed that there was most likely some CO_2 in the system during this work. "OH^-" reported in Table 4.20 probably corresponds to this first breakpoint (at 0.4mmol HCl) and is consequently lower than twice the Mg^{2+} concentration. The second breakpoint (at 0.6mmol HCl) was virtually invisible due to the low concentrations and could not be used as a titration end point during the laboratory work. Fig. 5.14b) shows the concentrations of OH^-, HCO_3^- and CO_3^- in solution during the alkalinity titration as function of added HCl. By neglecting H^+ the alkalinity of the solution is at the start given by Eq. 48, and equal to two times the Mg^{2+} concentration;

$$\begin{aligned} A_T &= m_{OH^-} + m_{HCO_3^-} + 2m_{CO_3^{2-}} \\ &= 2m_{Mg^{2+}} \end{aligned} \quad (48)$$

It should be noted that the difference between the two end points (0.6 – 0.4mmolHCl) gives the total amount of CO_2 in solution (0.2mmolHCl). The second end point was invisible in the HCl titration but since it corresponds to the total alkalinity it consequently equals twice the Mg^{2+} concentration. Hence by using the magnesium concentration to find the second end point, the total amount of carbonate could be estimated during the analysis, as given in Table 4.20. Fig. 5.14b) shows that the 0.4mmolHCl added up to the first end point, has reacted with carbonate to form bicarbonate and also neutralized OH^-. If the total amount of CO_2 is assumed to be in the form of carbonate (i.e. CO_3^{-}>> HCO_3^-) at the beginning of the titration the actual amount of OH^- at this point can be found simply by subtracting total CO_2 (0.2mmol) from the added amount of HCl at the first end point(0.4mmol). Then OH^- concentration in the solution is estimated as 0.2mmol/kg. When pH is high this is a reasonable assumption but Fig. 5.14b), however, shows that this is actually not valid in this case. Bicarbonate is not negligible and by subtracting total CO_2 from alkalinity the obtained OH^- concentration (0.2mmol/kg) will therefore be *too low*. The other extreme case will be to set OH^- equal to the alkalinity, which will give a *too high* value(0.6mmol/kg). These extremes were used to construct the error bars in Fig. 5.15.

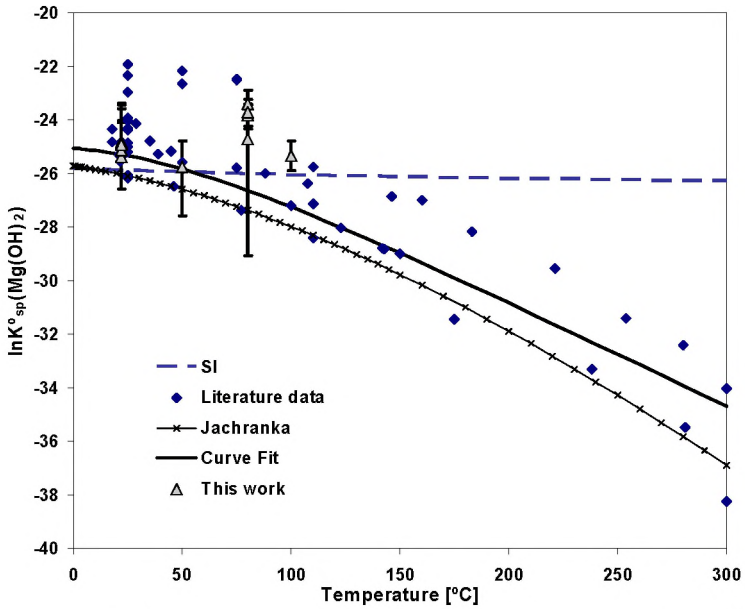

Fig. 5.15: ln$K°_{sp}$ of $Mg(OH)_2$ versus temperature; calculated from literature[8,10,36], and from this work. The line gives the curve fit of this work. The dotted line corresponds to calculation from enthalpy and entropy dissolution data[43]. Solid line with crosses gives model from literature (Lambert page 102)[36]

Evidently there is a large uncertainty in the thermodynamic solubility product of $Mg(OH)_2$. $K°_{sp}$ was calculated from the literature values[8,10,36] by use of the Pitzer model as described in previous sections, and a large variation is observed. The dotted line "SI" corresponds to calculation from enthalpy and entropy data given in SI Chemical data[43] at 298K i.e. calculated by assuming constant(independent of T) $\Delta H°$ and $\Delta S°$ for the dissolution reaction in Eq. 46. This simplification actually corresponds reasonably well up to 100°C but is, as expected, seen to deviate from experimental data at very high

temperature. In this work the presence of CO_2 complicated the analysis, and it could be that the starting material itself contained a small amount of carbonate that did not show in the X-ray pattern that was used to check this material. At 100°C the solution was refluxed for 2 days after the starting material had been added. This was done to remove CO_2 and this experiment seemed to have much less carbonate present (See Table 4.20). For this point at 100°C the error bars actually correspond to the analysis error and not the CO_2 assumptions discussed above.

The accuracy of the experimental method used in this work was obviously not satisfactory, but although the error bars are large the results are at least in the same range as literature data. For better results CO_2 control is vital. Another possibility could be to deliberately introduce carbonate in the form of a buffered solution, to decrease the pH of the system. Lower pH leads to larger Mg^{2+} concentrations that are more easily analysed. This method requires the use of a model to calculate the low OH^- concentration. Further $Mg(OH)_2$ solubility experiments would be time consuming and it was decided to focus on other aspects of the scale model instead. Thus the function for $K°_{sp}$ was simply drawn through the scattered datapoints in Fig. 5.15.

5.1.8 $MgCO_3$ compounds

It was decided to include hydromagnesite ($3MgCO_3 \cdot Mg(OH)_2 \cdot 3H_2O$) as the only solid magnesium carbonate compound, as described in detail in chapter 9. $K°_{sp}$ was calculated from solubility data in an equivalent manner as for the other salts. All parameters in the curve fit equation are given in Table 5.1

5.2 Pressure dependence of K_{sp}

The Pressure dependence of the solubility product is related to the partial molar volume as[1,6,45];

$$\left(\frac{\partial \Delta G^o}{\partial P}\right)_T = -RT\left(\frac{\partial K^o}{\partial P}\right)_T = \Delta \overline{V}^o \tag{49}$$

$$\ln\left(\frac{K^o_{sp,P}}{K^o_{sp,P_o}}\right)_T = \frac{-\Delta \overline{V}^o \left(P - P_o\right)}{RT} \tag{50}$$

P denotes pressure, P_o standard pressure, R the universal gas constant and T the absolute temperature. $\Delta \overline{V}^o$ corresponds to the change in partial molar volume at infinite dilution and can, for the dissolution of the arbitrary salt MX, be calculated[45] as given in Eq. 51.

$$\Delta \bar{V}^o = \bar{V}^o\left(M^+, X^-\right) - \bar{V}\left[MX\left(s\right)\right] \tag{51}$$

These individual ion volumes have been calculated from the convention that the partial molar volume of H^+ is set to zero[46]. In this work the partial molar volume of the solid phase was calculated from the density at 25°C and assumed to be independent of temperature. Millero[45] found that the temperature effect over an interval of 50°C was about 0.04cm^3/mol, which should give a change of only about 0.2-0.3 cm^3/mol from 0 to 300°C. The effect of pressure on $V°$ for the solid phase is negligible[45] below 1000bars. It is known that the partial molar volume can change with the ionic strength of the solution[45], but due to lack of data the ionic strength dependence was not included in this work. For salts containing crystal water it is necessary to include the partial molar volume of water[11,48] in Eq. 51.

The change in molar volume of the ions is also a function of pressure, and is related to the compressibility, κ, as;

$$\Delta \overline{V}^o_{T,P} = \Delta \overline{V}^o_{T,P_o} + \Delta \overline{\kappa}^o_T \left(P - P_o\right) \tag{52}$$

Compressibility is calculated from products and reactants in an equivalent manner as for the change in partial molar volume, and is in addition assumed pressure independent;

$$\Delta \bar{\mathrm{K}}^o = \bar{\kappa}^o\left(M^+, X^-\right) - \bar{\kappa}\left[MX\left(s\right)\right] \tag{53}$$

Combination of Eq. 50 with Eq. 52 gives the same expression for the pressure dependence as utilized by Millero[45];

$$\ln\left(\frac{K^{o}_{sp,P}}{K^{o}_{sp,P=P_o}}\right)=\frac{-\Delta\overline{V}^{o}_{P_o}\left(P-P_o\right)+0.5\Delta\overline{\kappa}^{o}_{P_o}\left(P-P_o\right)^2}{RT} \tag{54}$$

$\Delta\overline{V}^{o}_{P_o}$ and $\Delta\overline{\kappa}^{o}_{P_o}$ corresponds to the partial molar volume and compressibility changes respectively at the reference pressure P_o. For the model in this work P_o has been set[1,37] to 1 atm below 100°C and equal to the water vapour pressure[11] at higher temperatures. This choice is advantageous when it comes to interpreting actual experimental measurements, since the molar volumes are usually measured at these conditions. Thus the measured values can be used directly in Eq. 54, while if a reference of 1atm is chosen for all temperatures the measured values will have to be recalculated using Eq. 52. The water vapour pressure depends on ionic strength of the solution as well as total pressure and is therefore not exactly 1 atm at 100°C. Thus the standard pressure will have a small shift either up or down at this point i.e. a discontinuity occurs at 100°C. From a practical point of view, however, this is unimportant and the discontinuity is merely a modeling oddity.

Because both the volume and compressibility changes are temperature dependent a temperature function must be constructed. For this purpose Eq. 55 was used, as in the work of Kaasa[1].

$$f(t)=q_o+q_1t+q_2t^2+q_3t^3+q_4t^4 \tag{55}$$

f(t) corresponds to either partial molar volume or compressibility and q_o is the value at 0°C. *t* denotes temperature in °C and $q_{1\text{-}4}$ are the curve fitted constants given in Table 5.2 and Table 5.3. Literature data for the compressibility are scarce and in several cases it was chosen to simply use the typical value[1] of $-15\cdot10^{-3}$ [cm^3/mol bar]. The partial molar volume at high temperature was obtained from Tanger and Helgeson[44], while for low temperature this work relied on the data from Millero[45-46].

Molar volume data were, except for KCl and the bicarbonates, only available from 0-50°C. The extrapolation outside of this region is therefore uncertain. It was decided to use similar trends as for other salts described by Kaasa[1], where all parameters are given in Table 5.2 and Table 5.3. Hydromagnesite has a change in partial molar volume that is 5-10 times larger than the others, which is due to it being a much more complex structure with 4 moles of Mg^{2+} in the formula. Both the solubility product and the pressure dependence will obviously depend on how the structure of the solid is expressed. In this work it was utilized the notation $3MgCO_3\cdot Mg(OH)_2\cdot 3H_2O$ from Marion[4], while e.g. Königsberger et al.[5] use the chemical formula $4MgCO_3\cdot Mg(OH)_2\cdot 4H_2O$.

Ionic compressibility data were generally only available at 25°C. When the compressibility was calculated at this temperature, it was found to be between $-7 \cdot 10^{-3}$ and $-17 \cdot 10^{-3}$ [cm^3/mol bar] for all salts except KCl and Hydromagnesite. $\Delta\kappa_{KCl}$ was fitted as shown in Fig. 5.16, using the same extrapolation as done for NaCl in the work of Kaasa[1]. $\Delta\kappa_{hydromagnesite}$ was assumed temperature independent and set to $-44 \cdot 10^{-3}$ [cm^3/mol bar]. All other salts were set to the typical value of $-15 \cdot 10^{-3}$ [cm^3/mol bar] as seen in Table 5.3.

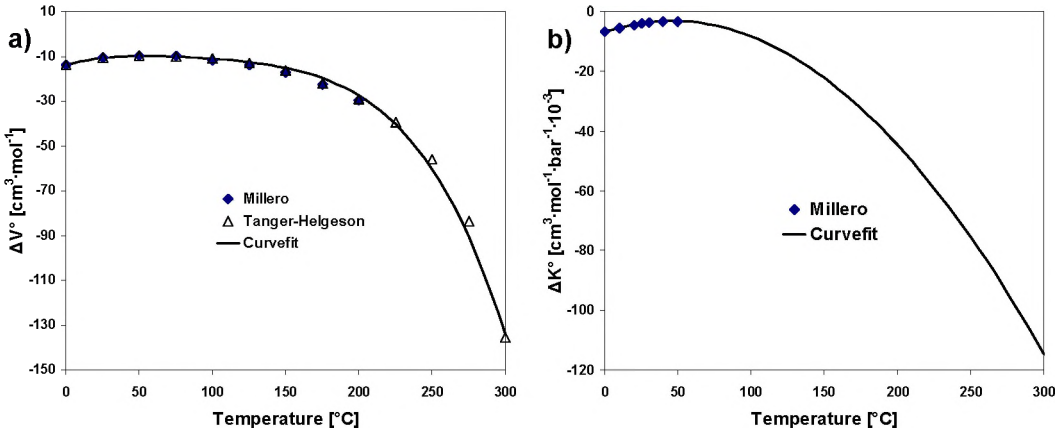

Fig. 5.16: a) $\Delta V°$ and b) $\Delta K°$ of KCl in aqueous solutions versus temperature. Data from Millero[45,46] and Tanger and Helgeson[44]. *Solid lines*; curvefit

5.2.1 Magnitude of pressure dependence

Generally the effect of the compressibility term is insignificant at pressures below about 500bar. Fig. 5.17 shows the lnK_{sp} ratio of Eq. 54 as function of gage pressure for two salts. The lines marked with "No compression" are calculated with the compression term set to zero, hence the pressure dependence is given directly from the partial molar volume. $BaCO_3$ is much more influenced by pressure than KCl, but the contribution from the compressibility term is in both cases insignificant below 500bar. Omitting $\Delta\kappa°$ will give a slightly too high estimate of the solubility product at high pressures.

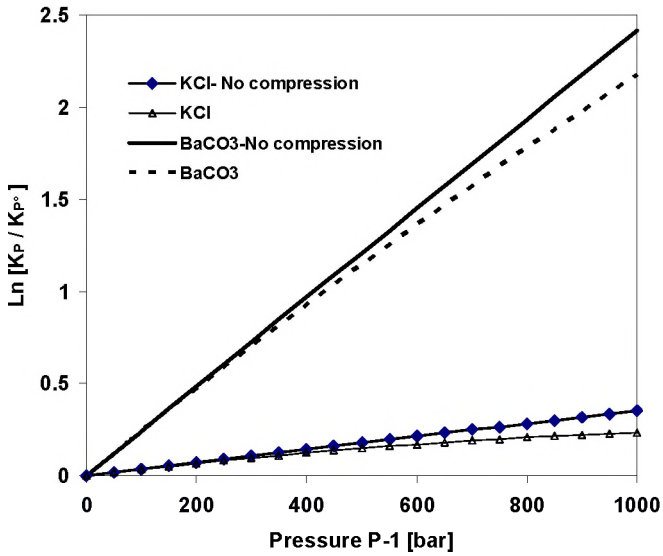

Fig. 5.17: $\ln\left(\frac{K^{o}_{sp,P}}{K^{o}_{sp,P_o}}\right)$ **as function of gage pressure for the solubility of KCl and $BaCO_3$, with and without compressibility term at 100°C.**

Table 5.2: $\Delta V°$ [cm^3 mol^{-1}] change in partial molar volume for dissolution reaction. Parameters for Eq. 55

Salt	q_o	q_1	q_2	q_3	q_4	T/°C[a]	Ref.[b]
KCl	-13.872	0.18489	-2.8645E-3	1.7896E-5	-4.9516E-8	0-300	44-46
$NaAc{\cdot}3H_2O$	-10.402	0.47490	-5.1003E-3	8.2925E-6	0	25	46
NaAc	-24.459	0.47490	-5.1003E-3	8.2925E-6	0	25	46
$NaHCO_3$	-21.032	0.30255	-3.9696E-3	2.1067E-5	-4.9727E-8	0-300	44-47
$KHCO_3$	-17.460	0.27154	-3.6733E-3	1.9973E-5	-4.7611E-8	0-300	44-47
$K_2CO_3{\cdot}1.5H_2O$	-48.684	0.47490	-5.1003E-3	8.2925E-6	0	0-50	45
K_2CO_3	-51.898	0.47490	-5.1003E-3	8.2925E-6	0	0-50	45
$Na_2CO_3{\cdot}10H_2O$	-33.075	0.47490	-5.1003E-3	8.2925E-6	0	0-50	45
$Na_2CO_3{\cdot}H_2O$	-52.481	0.47490	-5.1003E-3	8.2925E-6	0	0-50	45
Na_2CO_3	-57.335	0.47490	-5.1003E-3	8.2925E-6	0	0-50	45
$BaCO_3$	-68.479	0.34776	-3.1762E-3	0	0	0-50	45
$SrCO_3$	-71.623	0.28142	-2.9200E-3	0	0	0-50	45
$Mg(OH)_2$	-62.308	0.47490	-5.1003E-3	8.2925E-6	0	0-50	45
HydMg[c]	-230.18	0.21170	-2.7943E-3	0	0	0-50	45

[a]Temperature range of *experimental data* [b]Literature reference.
[c]Solid phase included in model is Hydromagnesite with formula $3MgCO_3{\cdot}Mg(OH)_2{\cdot}3H_2O$

Table 5.3: Parameters for calculation of $\Delta\kappa°$ [10^{-3} cm^3 mol^{-1} bar^{-1}] in Eq. 55

Salt	q_o	q_1	q_2	q_3	q_4	T/°C[a]	Ref.[b]
KCl	-6.8700	0.16365	-1.8094E-3	2.1853E-7	0	0-50	45,46
$NaAc{\cdot}3H_2O$	-15	0	0	0	0		no data
NaAc	-15	0	0	0	0		no data
$NaHCO_3$	-15	0	0	0	0	25	45
$KHCO_3$	-15	0	0	0	0	25	45
$K_2CO_3{\cdot}1.5H_2O$	-15	0	0	0	0	25	45,47
K_2CO_3	-15	0	0	0	0	25	45
$Na_2CO_3{\cdot}10H_2O$	-15	0	0	0	0	25	45,47
$Na_2CO_3{\cdot}H_2O$	-15	0	0	0	0	25	45,47
Na_2CO_3	-15	0	0	0	0	25	45
$BaCO_3$	-15	0	0	0	0	25	45
$SrCO_3$	-15	0	0	0	0	25	45
$Mg(OH)_2$	-15	0	0	0	0	25	45
HydMg[c]	-44	0	0	0	0	25	45,47

[a]Temperature range of *experimental data* [b]Literature reference.
[c]Solid phase included in model is Hydromagnesite with formula $3MgCO_3{\cdot}Mg(OH)_2{\cdot}3H_2O$

5.3 References chapter 5

1. Kaasa, B., *Prediciton of pH, Mineral precipitations and multiphase equilibria during oil recovery,* Dr.Ing thesis, Norwegian University of Technology and Science-NTNU, (1998)
2. Kaasa, B., Sandengen, K. and Østvold, T. " Thermodynamic Predictions of Scale Potential, pH and Gas Solubility in Glycol Containing Systems", *SPE 95075, Int. Symposium on Oilfield Scale,* Aberdeen, (2005)
3. Pitzer, K. S. *Thermodynamics* 3rd ed., (1995), McGraw-Hill
4. Marion, M.G.; Carbonate mineral solubility at low temperatures in the Na-K-Mg-Ca-H-Cl-SO_4-OH-HCO_3-CO_3-CO_2-H_2O system; *Geochim. Cosmochim. Acta*, **65(12)**, 1883-1896, (2001)
5. Königsberger, E.; Königsberger, L.; Gamsjäger, H.; Low-temperature thermodynamic model for the system Na_2CO_3-$MgCO_3$-$CaCO_3$-H_2O; *Geochim. Cosmochim. Acta* , **63(19/20),** 3105-3119, (1999)
6. Prausnitz, J.M, Lichtenthaler, R.N, Azevedo, E.G, *Molecular Thermodynamics of Fluid-Phase Equilibria*, chapter 9, 3rd ed. (1999) Prentice Hall
7. Wood, J R. ." Thermodynamics of brine-salt equilibriums. II. The system sodium chloride-potassium chloride-water from 0 to 200°C." , *Geochim. Cosmochim. Acta.* **40**, 1211-20, (1976)
8. Linke, W. F. *Solubilities, Inorganic and metal-organic compounds 4th ed.* (1965) Am. Chem. Soc. Washington D.C
9. Dean, J.A., Lange, N. A. *Lange's handbook of Chemistry* 15th ed. (1999) McGraw-Hill
10. Stephen H., *Solubilities of inorganic and organic compounds Vol.1*, (1963) Pergamon Press
11. Lide, D. R. *CRC Handbook of Chemistry and Physics*, 84th ed. (2003)
12. McCoy,H.N. Test, D. "Equilibrium between Alkali-earth Carbonates, Carbon Dioxide and Water" *J.Am.Chem.Soc* **33**, 473-6. (1911)
13. Hill, A.E., Bacon, L.R. "Ternary systems. VI. Sodium carborate, sodium bicarbonate and water." *J.Am.Chem.Soc*, **49**, 2487. (1927)
14. Seiersten, M., *Institute For Energy technology, Norway* Private communications.
15. Charykova, M. V. "Calculation of Phase equilibria in water-salt systems simulating the natural carbonate brines", *Geochemistry international*, **38(s2)**, s206-s213, (2000)
16. Wegschneider, R., Mehl, J. *Monatshefte für Chemie*, **49**, 283-315, (1928)
17. Monnin, C., Schott, J. *Geochim. Cosmochim. Acta* , **48**, 571-581, (1984)
18. Waldeck, W. F., Lynn, G.; Hill, A. E. "Aqueous solubility of salts at high temperatures. II. The ternary system Na_2CO_3-$NaHCO_3$-H_2O from 100° to 200°C" *J.Am.Chem.Soc*, **56**, 43-7 (1934)
19. Pietsch, E., *Gmelins Handbook der anorganischen Chemie*, (1938), Vol 55
20. Trypuc, M., Kielkowska, U., Stefanovic, D. "Solubility Investigations in the KHCO3 + NH4HCO3 + H2O System" *J. Chem. Eng. Data.* **46,** 800-804, (2001)
21. Moore, R.C., Mesmer, R. E., Simonson, J. M. "Solubility of Potassium Carbonate in Water between 384 and 529 K Measured Using the Synthetic Method." *J. Chem. Eng. Data*, **42**, 1078-1081, (1997)
22. Apelblat, A., Manzurola, M., " Solubilities and vapour pressures of saturated aqueous solutions of sodium tetraborate, sodium carbonate, and magnesium sulfate and freezing-

temperature lowerings of sodium tetraborate and sodium carbonate solutions. " *J. Chem. Thermodynamics*, **35**, 221-238, (2003)

23. Wells, R. C., McAdam Jr, D. J. ." Phase Relations of the System Sodium Carbonate and Water." *J. Am. Chem. Soc.* **29**, 721-727, (1907)
24. Oosterhof, , H., Witkamp, G.J., van Rosmalen, G.M. "Some antisolvents for crystallisation of sodium carbonate", *Fluid Phase Eq.* **155,** 219-227, (1999)
25. Busenberg, E., Plummer, L.N., Parker, V.N "The solubility of Strontianite in CO_2-H_2O solutions between 2 and 91°C, the association constants of $SrHCO_3^+$(aq) and $SrCO_3$°(aq) between 5 and 80°C, and an evaluation of the thermodynamic properties of Sr^{2+}(aq) and $SrCO_3$ at 25°C and 1 atm total pressure" *Geochimica et. Cosmo. Acta* **48,** 2021-2035, (1984)
26. Busenberg, E., Plummer, L.N. "The solubility of $BaCO_3$ (witherite) in CO_2-H_2O solutions between 0 and 90°C, evaluation of the association constants of $BaHCO_3^+$(aq) and $BaCO_3$°(aq) between 5 and 80°C and a preliminary evaluation of the thermodynamic properties of Ba^{2+}" *Geochimica et. Cosmo. Acta* **50,** 2225-2233, (1986)
27. Møller, N, "The prediction of mineral solubilities in natural waters: A Chemical equilibrium model for the Na-Ca-Cl-SO_4-H_2O system, to high temperature and concentration"" *Geochimica et. Cosmo. Acta* **52,** 821-°837, (1988)
28. Posnjak, E. "The system, $CaSO_4$-H_2O", *Amer. J. Sci.* **35A,** 247-272, (1938)
29. Innorta, G., Rabbi, E., Tomadin, L. "The gypsum-anhydrite equilibrium by solubility measurements", *Geochimica et. Cosmo. Acta* **44,** 1931-1936, (1980)
30. Partridge, P., White, A.H., "The solubility of calcium sulfate from 0 to 200°C" . *J. Am. Chem. Soc.* **51,** 360-370, (1929)
31. Blount C.W., Dickson, F.W. "The solubility of anhydrite in NaCl-H_2O from 100 to 450°C and 1 to 1000bars" *Geochimica et. Cosmo. Acta* **33,** 227-245, (1969)
32. Blount C.W., Dickson, F.W."Gypsum-Anhydrite equilibria in systems $CaSO_4$-H_2O and $CaSO_4$-NaCl-H_2O" *Amer. Mineralogist,* **58,** 323-331, (1973)
33. Booth, H.S, Bidwell, R.M, "Solubilities of salts in water at high temperatures", *J. Am. Chem. Soc.* **72,** 2567-2575, (1950)
34. Bock, E. "On the solubility of anhydrous calcium sulphate and gypsum in concentrated solutions of sodium chloride at 25, 30, 40 and 50°C" *Canadian J. Chem.* **39,** 1746-1751, (1973)
35. Millero, F.J., Milne, P.J., Thurmond, V.L. "The solubility of calcite, strontianite and witherite in NaCl solutions at 25°C", *Geochim. Cosmochim. Acta,* **48,** 1141-1143, (1984)
36. Lambert, I. Clever, H.L *Solubility Data Series* vol.52, 57-109, (1992), Pergamon Press
37. Haarberg, T. *Mineral deposition during oil recovery* Dr.Ing thesis, Norwegian University of Technology and Science-NTNU / NTH, (1989)
38. Yanat'eva, O.K. "The metastable equilibrium in the system $CaCO_3$-$MgCO_3$-H_2O", translation of *Izvestiya Akademii Nauk SSSR,* **1,** 180-182, (1960)
39. Johnston, J. "The solubility constant of calcium and magnesium carbonates", *J. Am. Chem. Soc.*, **37,** 2001-20, (1915)
40. Langmuir, D. "Stability of carbonates in the system MgO-CO_2-H_2O", *Journal of Geology,* **73,** 730-754, (1965)
41. Christ, C.L. Hostetler, P.B., "Studies in the system MgO-SiO_2-CO_2-H_2O: the activity product constant of Magnesite", *Am.J.Sci.* **268,** 439-453, (1970)
42. Mullin, J. W. *Crystallization 4th ed.*, (2001), Butterworth Heinemann
43. Aylward, G. Findlay, T. *SI Chemical Data* 3rd ed. (1994) John Wiley & Sons

44. Tanger, J.C and Helgeson, H.C. "Calculation of the thermodynamic and transport properties of aqueous species at high pressures and temperatures" *American Journal of Science* 288,19-98, 1988

45. Millero,F.J. "The effect of pressure on the solubility of minerals in water and seawater" *Geochim. et Cosmochim. Acta,* **46**, 11-22, (1982)

46. Millero,F.J. "The molal volumes of electrolytes" *Chemical Rev.* 71(21), 147-176, (1971)

47. Poisson, A., Chanu, J. "Semi-empirical equations for the partial molar volumes of some ions in water and in seawater", *Marine Chemistry*, **8(4)**, 289-98, (1980)

48. Olofsson, G., Heppler, L.G. "Thermodynamic of ionization of water over wide ranges of temperature and pressure" *J. Sol. Chem.,* **4(2),** 127-142, (1975)

6 MEG dependence

In this chapter the MEG dependences, $\gamma^{N\pm}$, are given for all equilibria included in the model. The first section concerning chloride solubility, will serve as a general overview on how the model was made. Solubility is given as *mol/kg solvent*, and MEG concentration in the *salt free solvent*, unless otherwise stated.

The mathematical functions used for curve fitting are generally arbitrarily chosen polynomials i.e. they do not have any physical/theoretical basis. Polynomials have the disadvantage that they can yield extremely improbable values, e.g. approach 0, -∞ or +∞, when they are extrapolated well outside of the range covered by the experimental data. Such values will obviously cause the model to fail. All functions have therefore been fitted in the whole 0-100% MEG (in water+MEG solvent) interval. They are also forced not to have physically improbable values at -50-300°C and at ionic strengths up to 25mol/kg solvent.

6.1 NaCl and KCl

The thermodynamic solubility product of NaCl is given by Eq. 56. $\gamma^{N\pm}$ denotes the MEG influence, which equals unity in water. In the simplest case $\gamma^{N\pm}$ is only a function of the MEG concentration. *m* (mol/kg solvent) denotes the equilibrium concentrations, while the aqueous activity coefficients γ^{S} were calculated using the Pitzer model (see chapter 2)

$$K_{sp}^{o}\left(NaCl\right) = m_{Na^+} m_{Cl^-} \gamma_{Na^+}^{S} \gamma_{Cl^-}^{S} \left(\gamma_{NaCl}^{N\pm}\right)^2 \qquad (56)$$

The $\gamma_{NaCl}^{N\pm}$ term was calculated from water+MEG+NaCl solubility data found in the literature[1-5] as described in detail in chapter 2, page 24. Table 3 in Masoudi et.al[3] does not correspond with the data in their first figure. Their figure, however, corresponded well with other literature data. Fig. 6.1 shows $\ln \gamma_{NaCl}^{N\pm}$ as function of MEG concentration. A temperature independent straight line satisfactory models $\ln \gamma_{NaCl}^{N\pm}$ in the 10-90°C range.

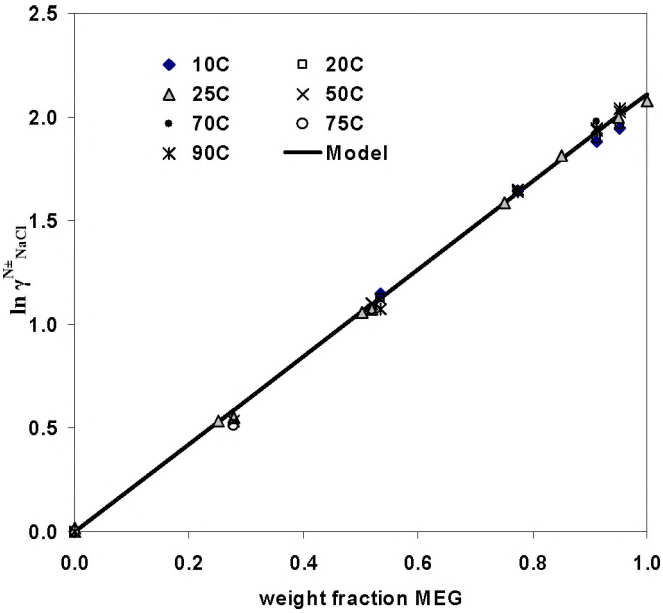

Fig. 6.1: $\ln \gamma_{NaCl}^{N\pm}$ **versus weight fraction MEG in solvent. Literature data[1-5] compared with model. Temperature in the (10-90)°C range.**

The MEG dependence of the NaCl solubility is given by Eq. 57 where w_{MEG} denotes weight fraction of MEG in the salt free MEG+water solvent.

$$\ln \gamma_{NaCl}^{N\pm} = 2.110 \cdot w_{MEG} \qquad (57)$$

Data for the KCl solubility found in the literature[2,4,5] cover the whole co-solvent interval 0-100w% MEG at four temperatures from 25 to 75°C. Seiersten[1] provided data at 50-95wt%MEG and 0-80°C. The calculated $\gamma_{KCl}^{N\pm}$ values were fitted with a function being slightly temperature dependent;

$$\ln \gamma_{KCl}^{N\pm} = 1.589 w_{MEG} + \left(-0.114 + 0.00158\mathrm{T}\right) w_{MEG}^2 \qquad (58)$$

T denotes the temperature in degree Kelvin. Fig. 6.2 shows the small temperature dependence, where model predictions at 10°C(solid) and 80°C(dotted) are drawn as lines. The data at 0°C deviates from the others. This data set[1] did not include measurements in water, and the large values may come from a systematic error in the measured values. It was therefore decided to exclude this data set from the model. If the data were included they implied an improbable large temperature effect between 0 and 10°C, with an opposite direction than observed between 10 and 80°C.

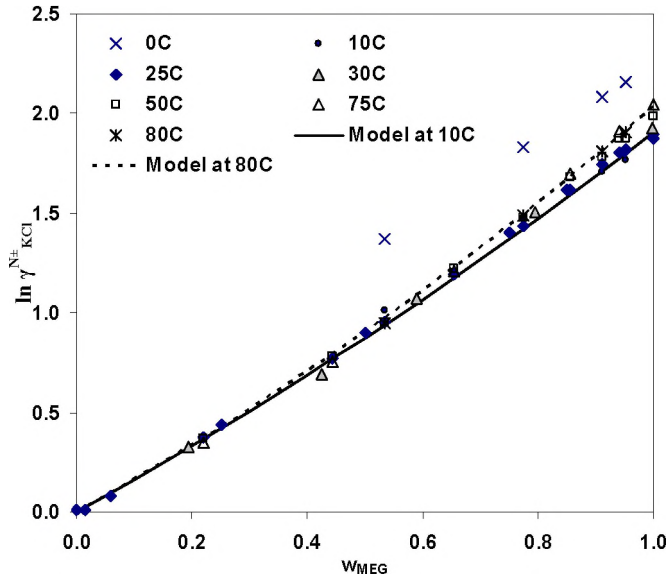

Fig. 6.2: $\ln \gamma_{KCl}^{N\pm}$ **versus weight fraction MEG in solvent at temperatures (0-80)°C. Literature data[1,2,4,5] compared with model.**

Fig. 6.3 compares literature data[1-5] with model predictions at 25°C. Good agreement is observed since the model is based on the same data sets. NaCl and KCl show a MEG dependence that is typical for many salts in water+MEG solutions. The solubility decreases virtually linearly (as function of wt% MEG) up to about 50-60wt%. In pure MEG the solubility is still quite high, which gives a more upward trend at high MEG concentrations.

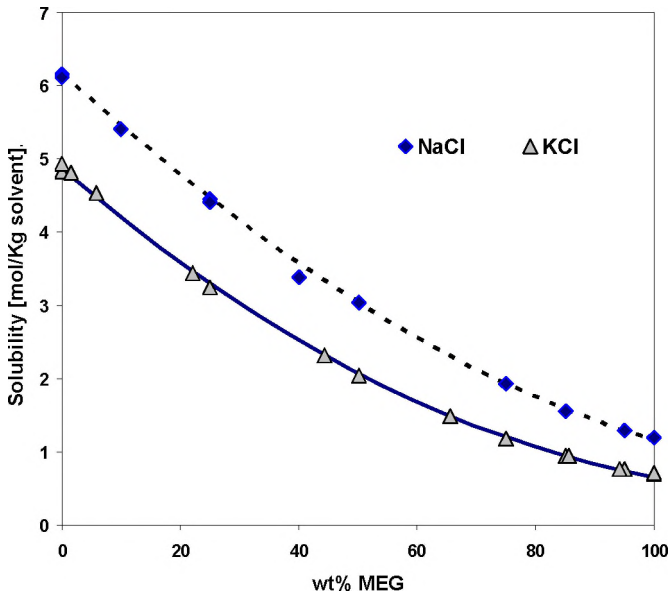

Fig. 6.3: Solubility of KCl and NaCl at 25°C (mol/kg solvent)[2-5] versus wt% MEG in solvent. ***Dotted line:*** **NaCl model.** ***Solid line:*** **KCl model**

In chapter 2 it was described that since $\gamma^{N\pm}$ is merely a function of MEG content and temperature, the model gives SR values that are too high when ionic strength is lower than NaCl (or KCl) saturation. At low ionic strengths the model will consequently be a conservative approach. To calculate accurate SR values at conditions well below saturation is in any case not the emphasis in a scale model. Higher ionic strengths than the NaCl (or KCl) solubility can, however, be achieved in e.g. boilers where several highly soluble species are present; Na^+, K^+, Cl^-, CO_3^{2-} etc. It was shown (chapter 2) that the calculated SR could be too high at such conditions. There is, however, no data available for such mixtures and the model is neither well suited for calculation in boilers. Thus it was chosen to use the simple approach with an ionic strength independent $\gamma^{N\pm}$.

6.2 Water activity

The water activity decreases with MEG concentration. A decreased water activity gives a lower vapour pressure, but it is also important for salt solubility. Salts containing crystal water will be directly influenced, while e.g. carbonates are indirectly influenced because H_2O is present in the first dissociation reaction of CO_2. Vapor pressures of salt free water+MEG solutions are available in the literature[7-11] at temperatures (25 to 125)°C, but only Trimble and Potts[7] and Lancia et.al[11] give the actual gas phase composition. The data showed close to ideal behaviour, which according to Raoults' law gives Eq. 59;

$$a_{H_2O} \approx x_{H_2O} \approx \frac{P_{H_2O}}{P^o_{H_2O}} \tag{59}$$

where P denotes partial pressure, x mole fraction of water in the liquid and $P°$ the partial pressure of the pure component at the given temperature. There were no data available for the vapour pressure of water+MEG+salt mixtures. It was arbitrarily chosen to use the same deviation from ideality in water+MEG solutions as in water without MEG, giving Eq. 60 for the water activity;

$$a_{H_2O} = x_{H_2O}\gamma^S_{H_2O} \tag{60}$$

x corresponds to the molfraction of water in a water+MEG+salt solution, while γ^S is the activity coefficient from the aqueous Pitzer ion interaction model described in chapter 2.1. At present the MEG activity was simply set equal to the molfraction of MEG in the aqueous phase. These simplifications should be looked into in future investigations by obtaining more activity/vapour pressure data. In the oil and gas industry there is much focus on the amount of MEG and H_2O present in a gas phase, e.g. for tuning of PVT models. Thus new experimental data will probably be available in near future.

6.3 Sulphates

The $\gamma^{N\pm}$ terms of the sulphates were modelled by the equation;

$$\ln \gamma^{N\pm}_{Sulphates} = \left(s_1 + s_4 I^{1/3}\right)x_{MEG} + \left(s_2 + s_5 I^{1/3}\right)x^2_{MEG} + s_3 x^3_{MEG} \qquad (61)$$

I denotes ionic strength, x molfraction of MEG in solvent, while $s_{1\text{-}5}$ are constants given in Table 6.1. The 1/3 exponential term was included to reduce the effect of I at very high ionic strengths, in such a way that the model did not return improbable values. Gypsum solubility is dependent on the water activity. In this work it was chosen to include water activity directly in the $\gamma^{N\pm}$ function as discussed in detail below.

In the literature there are no data available for the solubility of $SrSO_4$ in MEG+water solutions, hence at present it was decided to simply use the same MEG dependence as for $CaSO_4$.

Table 6.1: Parameters for calculation of $ln\gamma^{N\pm}$ for sulphates in Eq. 61

Salt	s_1	s_2	s_3	s_4	s_5	T /°C[a]	Ref.[b]
$CaSO_4 \cdot 2H_2O$[c]	7.9421	-8.3573	0.99658	-2.7225	1.8547	22-65	This work
$CaSO_4$	7.9753	-7.2016	2.1404	-1.9139	1.7072	22-85	This work,14
$SrSO_4$	7.9753	-7.2016	2.1404	-1.9139	1.7072		No data
$BaSO_4$	6.8799	-10.064	4.3410	0	0	25	12

[a]Temperature range of experimental data [b]References for solubility data.[c] see Eq. 64

6.3.1 $CaSO_4$

The main difficulty with $CaSO_4$ solubility measurements is not a very low solubility, but rather that calcium sulphate can exist in three different phase modifications. In this work only gypsum($CaSO_4 \cdot 2H_2O$) and anhydrite ($CaSO_4$) were investigated since they are the thermodynamically stable phases at the chosen conditions. Hemihydrate ($CaSO_4 \cdot 0.5H_2O$) is a metastable phase in aqueous solutions, but is easily made by drying gypsum at 140-150°C. Heating at higher temperature yields $CaSO_4$. The reaction between the two stable solid phases can be expressed by the reaction;

$$CaSO_4(s) + 2H_2O = CaSO_4 \cdot 2H_2O(s) \qquad (62)$$

The phase stability in aqueous solutions is predominantly given by the temperature. At low temperature Eq. 62 is shifted to the right, and gypsum is the stable phase, while anhydrite is stable at higher temperature. In pure water the transition occurs at ~45°C. If, however, some of the water is exchanged with MEG, the water activity is lowered. This will shift Eq. 62 towards the left, which means that anhydrite is stable also at temperatures lower than ~45°C. Salts generally have a decreasing solubility with increasing MEG content, but since gypsum includes crystal water, an increase in the gypsum solubility is expected at high MEG contents. When measuring solubility at high MEG contents the reaction in Eq. 62 is shifted to the left as mentioned above. Thus when dissolving gypsum at such conditions it is not the stable phase, and the

"solubility" is actually that of a non-stable phase. Usually dissolution is a faster reaction than precipitation[19]. This means that if gypsum is added to a solution of high MEG concentration it starts to dissolve, and at the same time anhydrite is precipitating as it is the stable phase. Because precipitation is the rate determining step the amount of dissolved calcium sulphate will, however, remain on the solubility product of gypsum. When $CaSO_4 \cdot 2H_2O$ has been completely removed the calcium concentration drops to the value in equilibrium with $CaSO_4$.

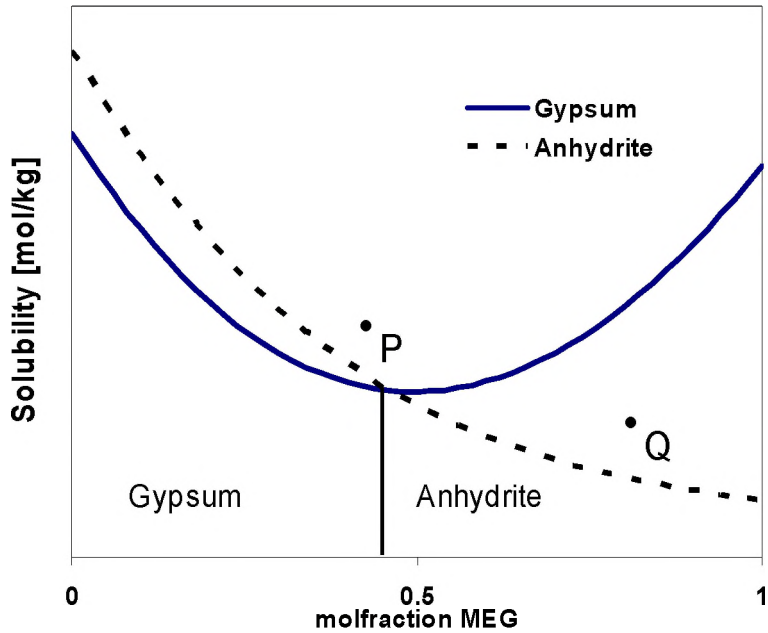

Fig. 6.4: Schematic of $CaSO_4$ solubility versus x_{MEG} at a temperature <45°C.

The relative stability in the Ca-SO_4-H_2O-MEG system is shown schematically in Fig. 6.4 at an arbitrary temperature < 45°C. Gypsum has the lowest solubility in water i.e. is the stable phase at this point. Anhydrite is the stable phase at the high MEG end where the gypsum "solubility" rapidly increases due to the decrease in water activity. At some point the two curves must intersect. Regard a solution with dissolved $CaSO_4$ at composition given by point *Q* i.e. supersaturated with respect to anhydrite but not saturated with respect to gypsum. Anhydrite will start to precipitate and the concentration of $CaSO_4$ in solution drops (Q moves vertically down) until the solubility limit is reached. Point P gives a supersaturated solution with a MEG concentration slightly below the stability area of anhydrite. The stable phase is now gypsum, but when precipitating one molecule of gypsum, also two water molecules are removed from the solution. Thus as gypsum is precipitating the MEG concentration will increase and the point moves towards the right in the diagram. When the MEG concentration becomes 0.5, there is a shift of stability and the rest of the dissolved calcium sulphate will have to precipitate as $CaSO_4$. Two phases, $CaSO_4$ and $CaSO_4 \cdot 2H_2O$ are now actually coexisting. If solid gypsum dissolves and precipitates as $CaSO_4$ the MEG concentration decreases and one consequently moves to the left in the diagram, i.e. into an area where gypsum is stable and the reaction has to be reversed. If anhydrite dissolves one correspondingly moves into the area of anhydrite stability and the

reaction again has to be reversed. This is theoretically interesting since the system is actually maintaining itself at the borderline; $CaSO_4$-$CaSO_4 \cdot 2H_2O$. From a practical view, however, the solubility of $CaSO_4$ is so low that dissolving/precipitating such small amounts of gypsum will change the composition of the solvent very little. Thus such a situation with coexistence of the two phases will be rare. For a highly soluble salt on the other hand, such as sodium carbonate, the change in MEG concentration can be considerable when hydrated salts are precipitating/dissolving. Na_2CO_3 and its hydrated phases are discussed in section 6.6.2

After a careful investigation of the solubility data in a previous publication[14], it was found that the measured values of anhydrite solubility in aqueous solutions were systematically too high. This could have been caused by hemi-hydrate ($CaSO_4 \cdot 0.5H_2O$) in the starting material, combined with a too short reaction time for the dissolved hemihydrate to precipitate as anhydrite. It was consequently decided to perform new experimental measurements in the whole water+MEG interval. The new results are given in Table 4.1 while the old data can be found in the literature[14]. When comparing the two data sets, it was found that only the data in water seemed to be too high. These data points were therefore removed and the rest of the series[14] (see also Appendix 3), together with the results in Table 4.1-Table 4.2, were used to fit the MEG dependence of this work.

The transition temperature from gypsum to anhydrite is ~45°C in water. Experiments above this temperature were consequently used to construct the MEG dependence for anhydrite, $CaSO_4$, while low temperature experiments were similarly used to construct the MEG dependence of gypsum, $CaSO_4 \cdot 2H_2O$. The MEG correction term, $\gamma^{N\pm}$, was calculated from Eq. 63-64 in an equivalent manner as for NaCl/KCl. It should be noted that the water activity a^S_{H2O} in Eq. 64 is the activity calculated by the Pitzer model i.e. adjusting only for the decrease due to salinity. The change in water activity as function of MEG concentration is included in the $\gamma^{N\pm}$ term. This is an arbitrary choice, which has the positive effect that the model will not approach infinity when the solvent approaches 100% MEG.

$$K^o_{sp}(A) = m_{Ca^{2+}} m_{SO_4^{2-}} \gamma^S_{Ca^{2+}} \gamma^S_{SO_4^{2-}} \cdot \left(\gamma^{N\pm}_{CaSO_4(A)}\right)^2 \tag{63}$$

$$K^o_{sp}(G) = m_{Ca^{2+}} m_{SO_4^{2-}} \gamma^S_{Ca^{2+}} \gamma^S_{SO_4^{2-}} \left(a^S_{H_2O}\right)^2 \cdot \left(\gamma^{N\pm}_{CaSO_4(G)}\right)^2 \tag{64}$$

A and G denotes anhydrite and gypsum respectively. The most general approach, however, would be to have the water activity dependent on MEG, and also let the $\gamma^{N\pm}$ functions for anhydrite and gypsum be equal. This gave good results up to about 50wt% MEG. With this model it was, however, difficult to reproduce experimental data at higher MEG contents.

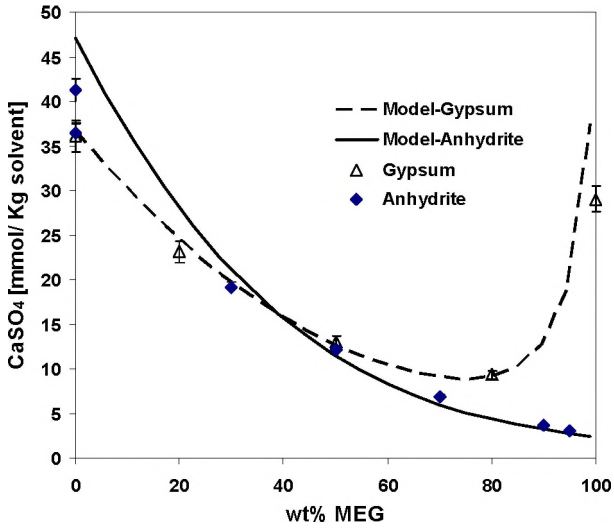

Fig. 6.5: Gypsum(25°C) and anhydrite (22°C) solubilities versus wt% MEG in solutions containing 0.5m NaCl (Table 4.1-Table 4.2). *Solid line;* anhydrite model, *Dotted line;* gypsum model

In Fig. 6.5 model calculations are compared with experimental data at room temperature. It should be noted that the phase change occurs at about 40wt% MEG. This corresponds well with the XRD data in Table 4.1, which gives transformation between 30 and 50wt%. At 0 and 30wt% MEG the experiments with anhydrite as starting material lie on the gypsum solubility line. This indicates that the anhydrite has transformed to gypsum.

6.3.2 $BaSO_4$

$\gamma^{N\pm}(BaSO_4)$ is given in Eq. 65 in an equivalent manner as for calcium sulphate.

$$K_{sp}^{o}\left(BaSO_4\right) = m_{Ba^{2+}} m_{SO_4^{2-}} \gamma_{Ba^{2+}}^{S} \gamma_{SO_4^{2-}}^{S} \left(\gamma_{BaSO_4}^{N\pm}\right)^2 \qquad (65)$$

The $BaSO_4$ solubility is extremely low and therefore troublesome to measure. At present the only available data in water+MEG solutions are provided by Kan et.al[12], covering 0-70wt % MEG at 25°C. These measurements were performed in solutions containing 1 and 3 *mol NaCl/kg water,* which correspond to 0.3 and 0.9 *mol/kg solvent* at 70wt%MEG, respectively.

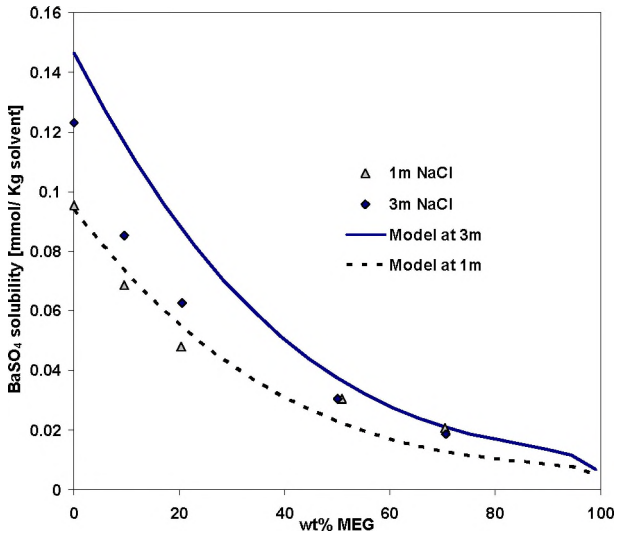

Fig. 6.6: $BaSO_4$ solubility[12] at 25°C with 1 and 3 mol NaCl/(kg water) versus wt% MEG. *Solid line:* model at 3mol NaCl /(kg water). *Dotted line:* Model at 1mol NaCl /(kg water).

Fig. 6.6 shows the solubility of $BaSO_4$ versus MEG concentration at 25°C for two NaCl containing solutions. The model clearly deviates some from the measured values of Kan et.al[12]. In water the model corresponds well for the solution containing 1mol NaCl/kg water, but is too high for the 3m NaCl solution. The aqueous model[13] is based on experimental data, where e.g. Templeton[17] measured a solubility of 0.144mmol/kg in a 3m NaCl solution. Thus it is a possibility that the data[12] at 3mol NaCl/kg water are systematically too low. It was therefore decided to use the relative change in the measured data to calculate the $\gamma^{N\pm}(BaSO_4)$ given in Table 6.1. This meant that the MEG dependence was calculated relative to the *measured* concentration in water, rather than the thermodynamic $K°_{sp}$ i.e. the measured trend as function of MEG was used, not the absolute values. In Fig. 6.6 this is clearly seen from the first three points in the 3m NaCl series being systematically lower than the model.

At high MEG contents there is a clear break in the 3m curve. This is not due to an irregularity in the $\gamma^{N\pm}$ term, but is caused by the calculation being done with a constant NaCl content as *mol/kg water,* while the plot is as *mol/kg solvent.* In a solution containing 99wt% MEG, the NaCl concentration is only 0.03*mol/kg solvent,* while *3mol/kg water.* When ionic strength approaches zero, $\gamma^{S} \rightarrow 1$ in Eq. 65 and the solubility therefore rapidly decreases, as shown in Fig. 6.6. Thus the break is actually due to the NaCl concentration, on a mol/(kg solvent) basis, not being constant.

6.4 Carbonate system

The carbonic acid equilibria given in Eq. 66-68 directly influence the scale potential for carbonate salts and must be well established in the model. Each equilibrium has a certain thermodynamic equilibrium constant, $K°$;

$$CO_2(g) = CO_2(aq) \qquad K_H^o \qquad (66)$$

$$CO_2(aq) + H_2O = H^+ + HCO_3^- \qquad K_1^o \qquad (67)$$

$$HCO_3^- = H^+ + CO_3^{2-} \qquad K_2^o \qquad (68)$$

$$Ca^{2+} + CO_3^{2-} = CaCO_3 \qquad K_{sp}^o \qquad (69)$$

The CO_2 pressure in a gas phase in contact with the solution will obviously influence precipitation of carbonate salts. This was the main reason for integrating a PVT model in the aqueous scale prediction model, as described in detail by Kaasa[13,14]. Introduction of MEG into the aqueous phase changes the CO_2 gas solubility, acidity and pH. In the following sections the determination of this MEG effect is presented. pH measurements have been performed as described in chapter 7. The main analysis method during these investigations was the alkalinity titration. It is therefore valuable to first regard the alkalinity in a carbonate system and how it is measured.

6.4.1 Alkalinity and analysis

A throughout discussion of alkalinity, and how it can be measured, is given by Kaasa and Østvold[21]. Alkalinity is commonly defined as the *sum of all titratable bases*, and for the carbonate system it is given by Eq. 70. Another important quantity is the *total dissolved CO_2*, which is given in Eq. 71 as the sum of dissolved gas, bicarbonate and carbonate.

$$A_T = m_{HCO_3^-} + 2m_{CO_3^{2-}} + m_{OH^-} - m_{H^+} \qquad (70)$$

$$m_{CO_2}^{tot} = m_{HCO_3^-} + m_{CO_3^{2-}} + m_{CO_2(aq)} \qquad (71)$$

Fig. 6.7 shows a log-log diagram of the carbonate system in water. An arbitrary solution having equal amounts of Na_2CO_3 and $NaOH^-$ will be at point 0 in the figure and have a pH of 12-13. As HCl is added one moves to the left in the diagram. Point *i*, 1 and 2 are possible equivalence points. Point *i*, however, is not a well suited end point as it has too high buffer capacity to give a very distinct pH change and is in addition concentration dependent. When concentration, *c*, increases the point will move to the right and vice versa.

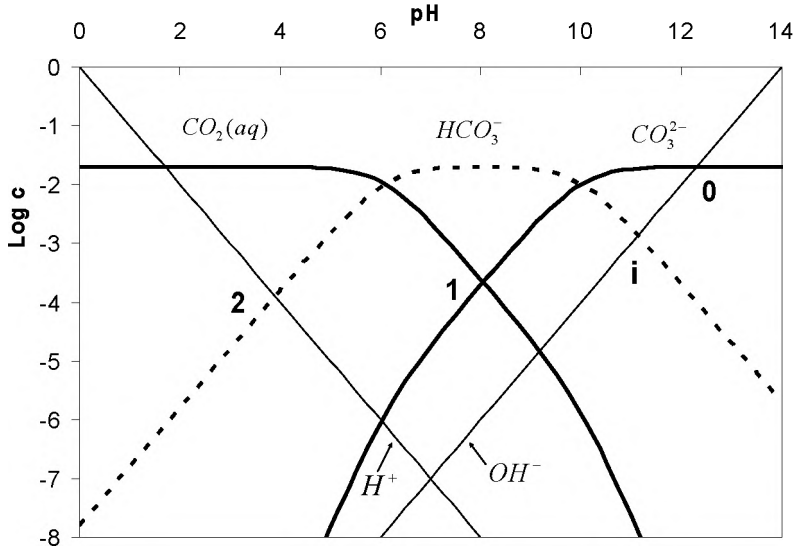

Fig. 6.7: Logarithmic plot of the carbonic acid (total CO_2 concentration 0.02M) dissociation as function of pH. c denotes concentration

A typical titration curve is shown in Fig. 6.8, where the two distinct end points correspond to point 1 and 2 in the logarithmic diagram. From the start and up to point 1, HCl is reacting with CO_3^{2-} to form HCO_3^-. Between point 1 and 2 this bicarbonate is neutralized to form CO_2(aq). In point 1 virtually all carbonates will be present as HCO_3^-, and at point 2 as CO_2(aq). The *total alkalinity* (of Eq. 70) is measured by titrating to point 2, while the total amount of carbonate can be found from the difference between point 1 and 2.

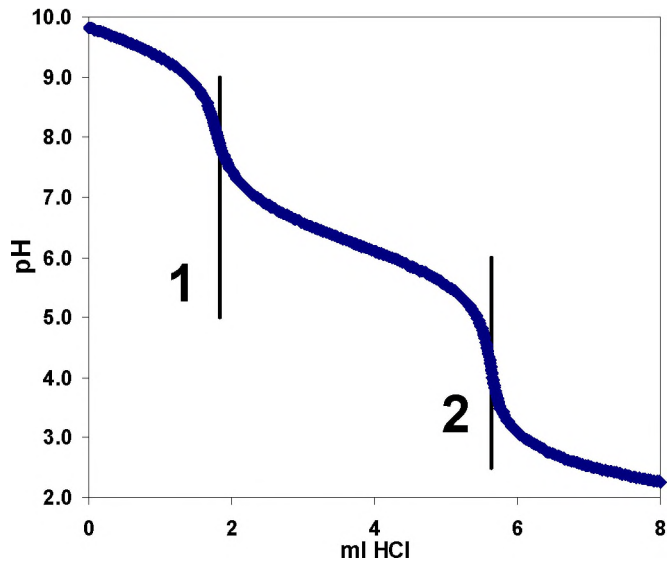

Fig. 6.8: Typical titration curve of an aqueous Na_2CO_3/$NaHCO_3$ mixture at 25°C. pH as function of added HCl.

The alkalinity at a certain point on the curve is given by the distance to point 2. Regard the point where 1ml HCl has been added and pH is about 9.5. CO_2(aq), OH^- and H^+ concentrations are negligible compared to the bicarbonate/carbonate and the alkalinity and total amount of carbonate are consequently given as;

$$A_T \approx m_{HCO_3^-} + 2m_{CO_3^{2-}} \tag{72}$$

$$m_{CO_2}^{tot} \approx m_{HCO_3^-} + m_{CO_3^{2-}} \tag{73}$$

Hence with two equations and two unknowns it is possible to calculate both carbonate and bicarbonate concentrations at this point. For this case the carbonate ratio can be expressed as;

$$\frac{m_{CO_3^{2-}}}{m_{HCO_3^-}} = \frac{A_T - m_{CO_3}^{tot}}{m_{CO_3}^{tot} - \left(A_T - m_{CO_3}^{tot}\right)} = \frac{A_T - m_{CO_3}^{tot}}{2m_{CO_3}^{tot} - A_T} \tag{74}$$

In most of the data collected in this work, however, solutions were continuously bubbled with CO_2. This situation is not described by Fig. 6.7. In this case pH is about 6-8, and HCO_3^- is consequently dominating the alkalinity i.e. HCO_3^- >> CO_3^{2-} and OH^- concentrations. CO_2(aq) obviously has a certain value and Eq. 70 and Eq. 71 becomes;

$$A_T \approx m_{HCO_3^-} \tag{75}$$

$$m_{CO_2}^{tot} \approx m_{HCO_3^-} + m_{CO_2(aq)} \tag{76}$$

Thus an alkalinity titration directly yields the bicarbonate concentration. It is also possible to measure the total dissolved CO_2. This can be done by adding excess NaOH to a sample such that the dissolved gas reacts into CO_3^{2-} and/or HCO_3^-. Performing a HCl titration of this sample yields a titration curve like Fig. 6.8, where the total amount of carbonate is found from the difference between equivalence point 1 and 2. The amount of dissolved gas can thereafter be found by subtracting Eq.75 from Eq. 76.

6.4.2 CO_2 dissolution

The CO_2 solubility (see reaction 66) had previously been measured by the Institute for Energy Technology (IFE)[1] in MEG+Water solutions. The experiments were performed in a closed container with known volumes of gas and liquid over a broad range of conditions (5-125°C and 0-100wt% MEG). CO_2(aq) concentration was found from the pressure drop accompanying dissolution in the water+MEG solution. The pressure drop gives the total amount of CO_2 that goes from the gas phase and into the solution. Some of the CO_2 will dissociate into HCO_3^-. However, when CO_2 dissolves in the solution the carbonic equilibria will adjust such that the system is in point 2 in the logarithmic diagram (Fig. 6.7). At this point (pH~4) the HCO_3^- concentration is negligible compared to CO_2(aq). Higher CO_2 pressures moves the point to the left i.e. to a lower pH, and the ratio of CO_2(aq)/ HCO_3^- increases. MEG and temperature alter the diagram slightly, but bicarbonate concentration is still negligible compared to CO_2(aq).

$\gamma^N_{CO2(aq)}$ was calculated from Eq. 77 where m denotes molality of dissolved gas and γ^Scorresponds to the aqueous activity coefficient described above. Fugacity, f, is given by the product of partial pressure, P, and the fugacity coefficient, φ. *Multiscale*[13] was used to calculate f, $K°_H$, γ^S, and φ, while the measurements[1] gave m and P.

$$K_H^o = \frac{a_{CO_2(aq)}}{f_{CO_2(g)}} = \frac{m_{CO_2(aq)} \cdot \gamma^S_{CO_2(aq)}}{P_{CO_2(g)} \cdot \varphi_{CO_2(g)}} \cdot \gamma^N_{CO_2(aq)} \tag{77}$$

$\gamma^N_{CO2(aq)}$ was fitted with the third order polynomial shown in Eq. 78, where x_{MEG} denotes the molfraction of MEG in the solvent. The constants $a_{1\text{-}3}$ are temperature dependent and must be calculated from Eq. 79, where T denotes absolute temperature (K). Parameters in the temperature function, $p_{1\text{-}4}$, are given in Table 6.2. Fig. 6.9 shows that the model generally corresponds well with literature data[20] and the results from this work described below.

$$\gamma^N_{CO_2(aq)} = 1 + a_1 x_{MEG} + a_2 x^2_{MEG} + a_3 x^3_{MEG} \tag{78}$$

$$a = p_1 + p_2 \ln(T) + \frac{p_3}{T} + p_4 T \tag{79}$$

Table 6.2: Parameters for calculation of $a_{1\text{-}3}$ using Eq. 79

	p_1	p_2	p_3	p_4
a_1	-2034.4	336.28	71381	-0.39693
a_2	2708.5	-445.17	-97897	0.50547
a_3	-1189.3	195.38	43120	-0.22046

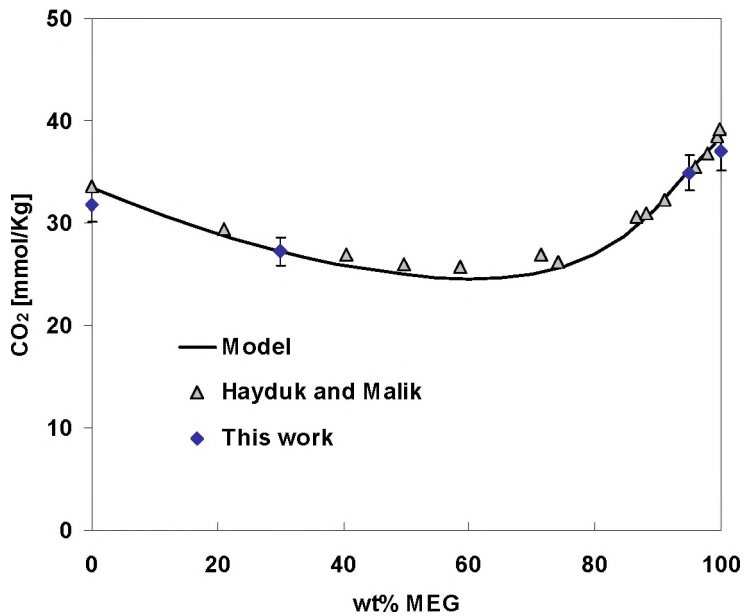

Fig. 6.9: CO_2 solubility (25°C and pCO_2=1bar) as function of wt% MEG in solvent. Model compared with literature data[20] and results in this work with no added NaCl (Table 4.4).

The main goal of the experiments of this work (see section 4.3.1 and 3.3.2) was to investigate the dissociation of CO_2. It was, however, also possible to obtain gas solubility data from the same experimental setup. This was done by adding NaOH to obtain the *total dissolved* CO_2, $m^{tot}_{CO_2}$, as described above (see Eq.75-76). The amount of dissolved gas was thereafter found by subtracting the bicarbonate concentration from (total dissolved CO_2). Fig. 6.10 shows calculated $\gamma^N(CO_2)$ from the results (Table 4.4-Table 4.7) of this work, compared with the model described above. A large variation in the results, especially at $x_{MEG}>0.53$ (=80wt% MEG), is observed. The trend, however, is reasonable.

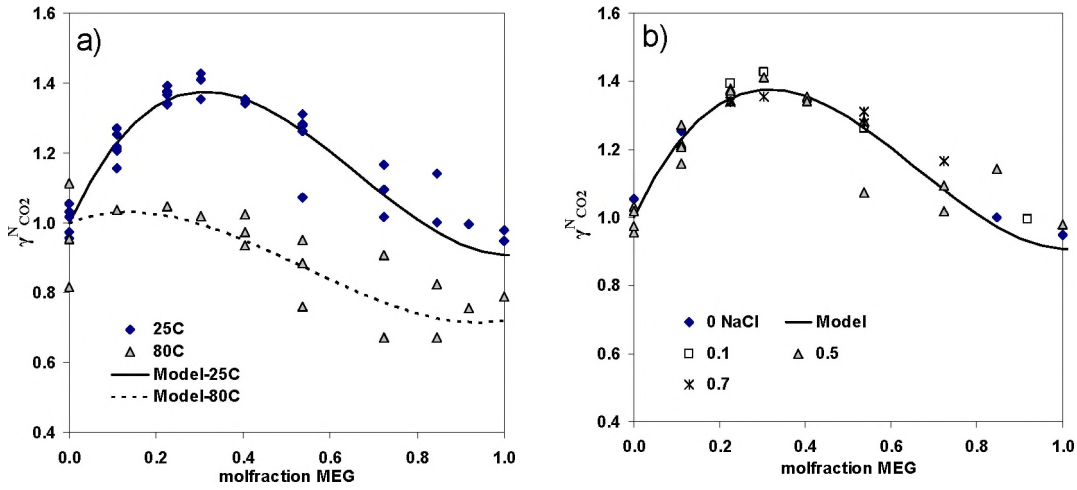

Fig. 6.10: $\gamma^N_{CO_2}$ as function of molfraction MEG in solvent. From data in Table 4.4-Table 4.7 *a)* All results at 25°C and 80°C. *b)* Results at 25°C in solutions of 0-0.7m NaCl. Model (Eq. 78) given by lines.

The main uncertainty came from the addition of NaOH. If too little is added all CO_2(aq) will not be converted to CO_3^{2-} and/or HCO_3^- yielding a *too low* value of gas solubility. If, however, the NaOH solution adsorbs some CO_2 from the air before being used this would lead to *too high* measurements of gas solubility. The gas bubbling was in addition not completely stopped when the samples were withdrawn. Thus it is a possibility that gas was sucked into the syringe yielding a *too high* value for dissolved CO_2 and consequently a too low value of $\gamma^N(CO_2)$. Addition of NaOH and a subsequent alkalinity titration is the same approach as used by Hayduk and Malik[20]. The method is believed to be sound and with better control of the NaOH addition, it should be well suited for future investigations. The main goal of new measurements should be to obtain a throughout investigation of the ionic strength dependence for a wider interval. The results at different ionic strength shown in Fig. 6.10b) did not indicate any systematic ionic strength effect in $\gamma^N(CO_2)$, and it was decided too keep $\gamma^N(CO_2)$ as function only of temperature and MEG content.

6.4.3 Carbonic Acid Dissociation

Carbonic acid equilibria are critical in the model because the concentrations of bicarbonate and carbonate directly influence the scale potential of many salts. Curve fitting was performed with Eq. 80, where all parameters are given in Table 6.3.

$$\ln \gamma^N = (r_1 + t_1[T-298])x_{MEG} + (r_2 + t_2[T-298])x_{MEG}^2 + (r_3 + t_3[T-298])x_{MEG}^3 \quad (80)$$

H^+ and OH^- are included in Table 6.3, and discussed in sections 6.4.4 and 6.4.5.

Table 6.3: Parameters for γ^N functions of OH^-, HCO_3^- and CO_3^{2-} from Eq. 80.

Specie	r_1	r_2	r_3	t_1	t_2	t_3	T / °C	Ref.[a]
HCO_3^-	3.4648	-1.7839	-1.3926	2.0977E-2	6.7566E-3	-1.9826E-2	25-90	TW
CO_3^{2-}	11.240	-9.7739	4.0510	0	0	0	25-80	TW
H^+		See Eq. 88					25-50	TW,1
OH^-	-6.6801	11.953	-8.2732	0	0	0	25-50	1

[a]References for experimental data. TW denotes this work

First dissociation constant

Table 4.4-Table 4.7 give the results from the experiments where pH was recorded in a solution of known bicarbonate content at a given CO_2 pressure. Combination of reaction (66) and (67) yields Eq. 81, where m is the measured concentration and the fugacity of CO_2 has been set equal to the partial pressure, P;

$$K_H^o K_1^o = \frac{a_{H^+} m_{HCO_3^-} \gamma_{HCO_3^-}^S \gamma_{HCO_3^-}^N}{P_{CO_2} a_{H_2O}} \quad (81)$$

The measured pH gives the H^+ activity directly, while the water activity and the activity coefficient $\gamma_{HCO_3^-}^S$ were calculated as described above. The resulting $\gamma_{HCO_3^-}^N$ term was fitted using Eq. 80, which is a function of MEG content and temperature. There was no need to include an ionic strength term in $\gamma_{HCO_3^-}^N$, meaning that $\gamma_{HCO_3^-}^S$ satisfactory adjusted for the ionic strength variations in the data. The error in the experimental data is mainly determined by the accuracy of the pH measurement. In Fig. 6.11 the error bars are calculated from an expected accuracy of ±0.05pH units at 25°C and 0.07 at 80°C. A detailed description of the pH measurements is given in chapter 7. Fig. 6.11 compares the measured $\ln \gamma_{HCO_3^-}^N$ with the model as function of MEG concentration. The decrease at the high MEG end is caused by the decline in water activity, which becomes zero in pure MEG.

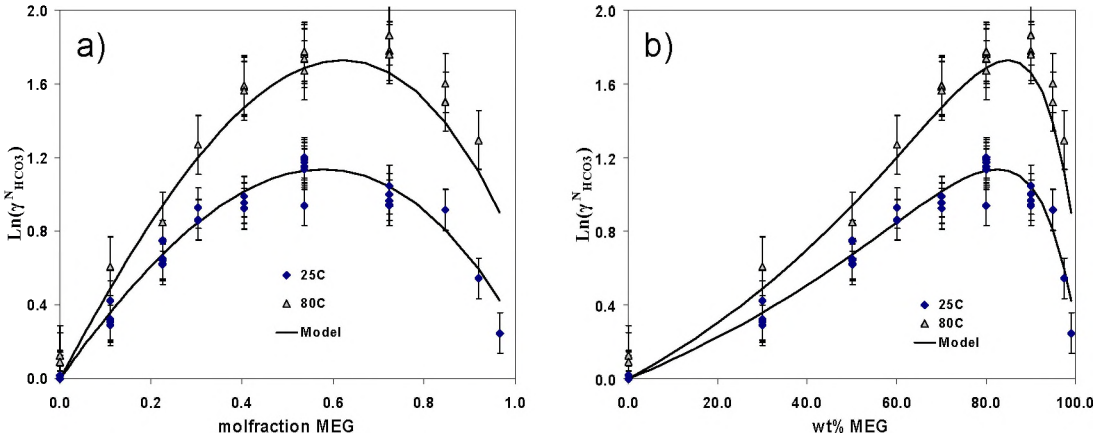

Fig. 6.11: $\ln \gamma^{N}_{HCO_3^-}$ **versus MEG content at 25 and 80°C. a) versus x_{MEG} in solvent b) versus wt% MEG in solvent**

A pure water standard state has been chosen (see section 2.2), and the water activity therefore approaches 0 when the MEG content approaches 100%. It is possible to measure pH in ~100% MEG although the electrode has a slow and less stable response, but the interpretation of such a measurement is not evident. If there is no water present pH can certainly not be defined from the activity of H^+ *(*H_3O^+*)*. A pure water standard state is obviously not defined in 100% MEG, but as long as there is some water present the method is consistent. In principle this amount of water could be infinitesimal. In practice this is ambitious, and the modeling difficulties can be explained by regarding Eq. 81. When approaching pure MEG, a measured pH gives the H^+ activity, which is therefore a finite value. *m* and $\gamma^{S}_{HCO_3^-}$ are certainly finite. a_{H_2O}, however, approaches zero, thus $\gamma^{N}_{HCO_3^-}$ consequently also has to approach zero ($\ln \gamma^{N}_{HCO_3^-} = -\infty$) in pure MEG. In Fig. 6.11 the two highest MEG contents at 25°C are 97.5wt% (x_{MEG}=0.92) and 99wt% (x_{MEG}=0.97). If the model should be correct up to ~100% MEG the curve would have to go to -∞ between x=0.97 and x→1. Practically the effect of this declining water activity is that the model is invalid above ~99wt %MEG.

Another experimental setup to determine $\gamma^{N}_{HCO_3^-}$ was also investigated. The first dissociation constant is given as;

$$K_1^o = \frac{a_{H^+} m_{HCO_3^-} \gamma^{S}_{HCO_3^-} \gamma^{N}_{HCO_3^-}}{m_{CO_2(aq)} \gamma^{S}_{CO_2} \gamma^{N}_{CO_2} a_{H_2O}} \qquad (82)$$

γ^S values, γ^N of CO_2(aq) and water activity can be obtained as described above. $\gamma^{N}_{HCO_3^-}$ is therefore directly obtained from Eq. 82 if pH is measured at a known ratio of the HCO_3^- and CO_2(aq) concentration.

From the logarithmic equilibrium plot in Fig. 6.7 the concentration of dissolved CO_2 equals the concentration of HCO_3^- at the point around pH=6 between equivalence point 1 and 2. A typical titration curve was described in Fig. 6.8 above, and the halfway-point between 1 and 2 in this figure corresponds to the condition of equal concentrations; $[HCO_3^-] = [CO_2(aq)]$. Thus if pH is measured at this point, the equilibrium constant (or $\gamma^N_{HCO_3^-}$) can be directly obtained. Such data are given in Table 4.8. However, the CO_2 concentration in solution will at this point become higher than anticipated from the CO_2 pressure in the laboratory atmosphere. Thus $CO_2(aq)$ is not in equilibrium with the surrounding air, and should therefore leave the solution. Such an experiment will therefore give slightly different results depending on how fast the titration is performed, the opening in the experimental cell to the atmosphere, gas-liquid ratio in the cell etc.

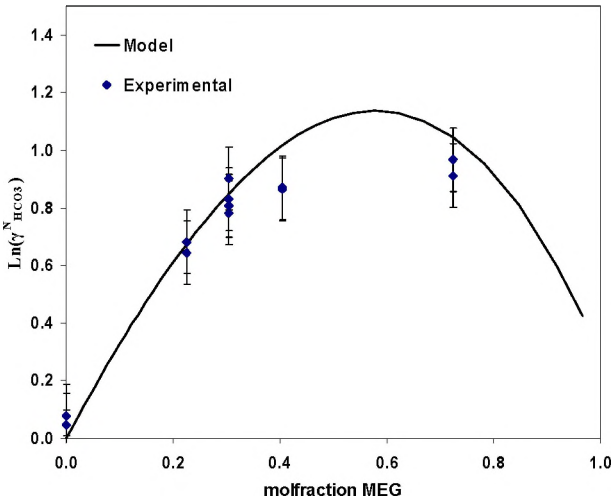

Fig. 6.12: $\ln \gamma^N_{HCO_3^-}$ **from titration measurements in Table 4.9 versus** x_{MEG} **at 25°C.** ***Solid line:*** **model (Eq. 80)**

$\gamma^N_{HCO_3^-}$ values were calculated from the data in Table 4.8. A comparison with the model is given in Fig. 6.12. With one exception, the measurements actually correspond well with the model. This may indicate that the experimental setup successfully kept the CO_2 in solution during the titration. CO_2 leaving the solutions and going into the gas phase is a slow process. This is well known from beverage cans that have to be vigorously shaken to get all CO_2 out of the liquid. Further improvement and investigation of this method was not examined, since the method with constant CO_2 bubbling was used for determination of the first dissociation constant in this work.

Second dissociation constant

The second dissociation constant was investigated by the same titration as described in Fig. 6.8. From Eq. 83 it is seen that the $\gamma^N_{CO_3^{2-}}$ term is simply determined by measuring pH at a known carbonate/bicarbonate ratio. The γ^S terms and $\gamma^N_{HCO_3^-}$ can be calculated as described above.

$$K_2^o = \frac{a_{H^+} \cdot m_{CO_3^{2-}} \gamma^S_{CO_3^{2-}} \gamma^N_{CO_3^{2-}}}{m_{HCO_3^-} \gamma^S_{HCO_3^-} \gamma^N_{HCO_3^-}} \tag{83}$$

When known amounts of $NaHCO_3$ and Na_2CO_3 are added to a solution the carbonate/bicarbonate ratio is, however, in principle unknown. When mixing a solution in the laboratory, it will be exposed to a certain CO_2 pressure from the air, and carbonate will react with dissolved CO_2 to form bicarbonate. But more importantly carbonate and bicarbonate will obviously react to achieve the equilibrium given by Eq. 83. The carbonate/bicarbonate ratio is therefore not equal to the added molar ratio. In this work titration was used to find the $m_{CO_3^{2-}} / m_{HCO_3^-}$ ratio, as described on page 96.

Two slightly different approaches were undertaken. One was to let the electrode stabilize before the titration, read the pH, and thereafter titrate reasonably fast (~30min) to obtain the concentration ratio at the start of the titration. These results are given in Table 4.8. The other approach was to titrate slowly (1-4hours) and let the electrode stabilize at each point during the titration (see Table 4.9). A long time was needed since the electrode has a slow response at high MEG concentration. These experiments were run with additional NaCl such that the activity coefficients, γ^S, remained virtually constant. At a given MEG concentration and ionic strength the γ^N terms are also constant. This meant that the activity coefficients could be regarded as a constant term. The titration curve then gave the "quasi stochiometric" constant, K_2* at any titration point;

$$K_2^* = K_2^o \cdot \left(\frac{\gamma^S_{CO_3^{2-}} \gamma^N_{CO_3^{2-}}}{\gamma^S_{HCO_3^-} \gamma^N_{HCO_3^-}} \right)^{-1} = \frac{a_{H^+} \cdot m_{CO_3^{2-}}}{m_{HCO_3^-}} \tag{84}$$

Fig. 6.13a) shows the results obtained in water with two distinct end points at about 1.8 and 5.6ml added acid.

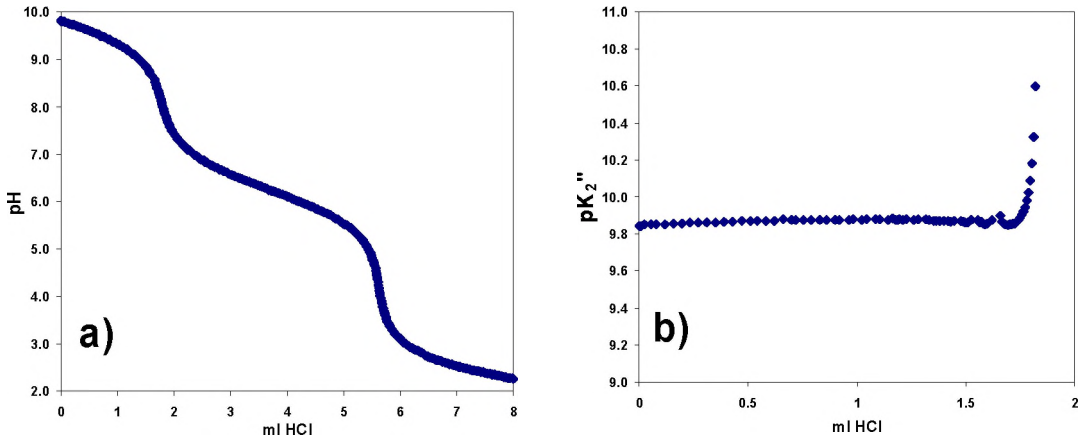

Fig. 6.13: ***a)*** **Titration curve for an aqueous solution of $NaHCO_3$(~5mmol/kg) and Na_2CO_3(~5mmol/kg) with 0.1m NaCl.** ***b)*****Calculated pK_2* (Eq. 84) versus ml added HCl.**

Fig. 6.13b) shows the calculated "quasi stochiometric" constant up to the first end point. The carbonate/bicarbonate ratio is calculated from Eq. 74. Eq. 74 is not valid when approaching the endpoint since the concentration of dissolved CO_2 is no longer neglectable compared to carbonate. This experiment, with water as solvent, is obviously an ideal case, where the measured pK_2* is virtually the same during the titration. Fig. 6.14 shows an experiment with 90wt%MEG (x_{MEG}=0.72), where the "quasi stochiometric" constant was lower at the start before it increased to a reasonable constant value. This was most likely caused by the OH^- concentration not being negligible in Eq. 72, which is consistent with a lower value of K_2*. Thus the calculated carbonate/bicarbonate ratio used in the "quasi stochiometric constant" shown in Fig. 6.14 is therefore not correct at the beginning of the titration.

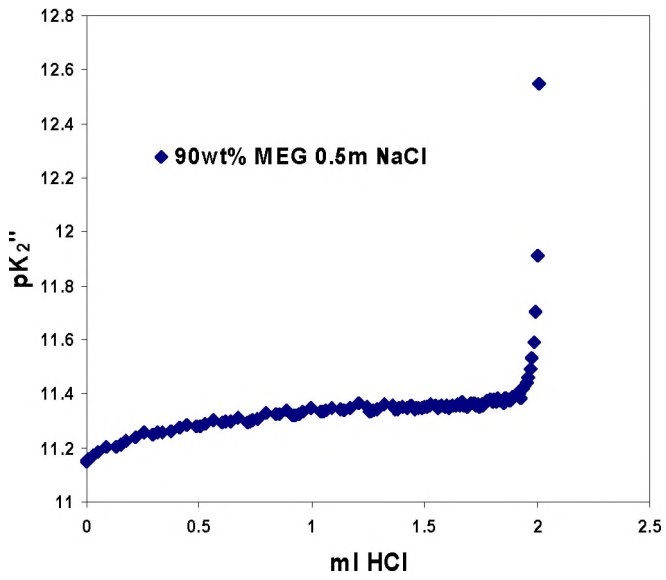

Fig. 6.14: pK_2* in for a solution of 90wt% MEG at 25°C versus ml HCl added.

Plots like the one shown in Fig. 6.14 were constructed to determine K_2*. When K_2* had been determined, $\gamma^N_{CO_3^{2-}}$ was calculated by inserting values for γ^S and $\gamma^N_{HCO_3^-}$ in Eq. 84. All data for $\ln \gamma^N_{CO_3^{2-}}$ are summarized in Fig. 6.15 where the model fit is given by the solid line.

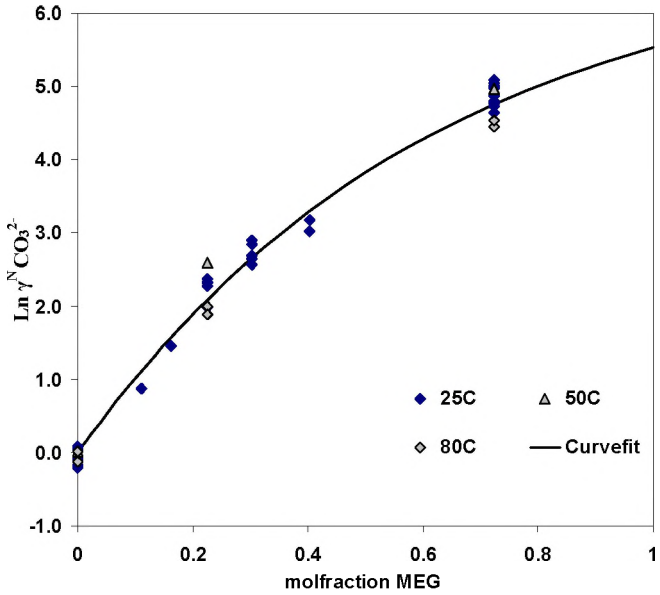

Fig. 6.15: $\ln \gamma^N_{CO_3^{2-}}$ **as function of** x_{MEG} **from 25 to 80°C (Table 4.8 and Table 4.9).** ***Solid line;*** **model (Eq. 80)**

The curve fit is merely a function of MEG concentration as given in Eq. 80 and Table 6.3. In water the method functioned well, but at higher MEG contents some scattering in the data is observed. This is believed to come mainly from the uncertainties in the pH measurement. pH was observed to be much less stable in these solutions than during measurements of the first dissociation constant. This can be due to the much lower hydrogen ion activity. The scatter shown in the data at 90wt% (x_{MEG}=0.72) in Fig. 6.15, corresponds to a variation in pH of 0.15-0.2units. There is in addition some uncertainty in the carbonate/bicarbonate ratio determination, due to the OH^- concentration not being negligible, as discussed above. Thus these data might be improved in future investigations of the system. Titrations as used in this work should be well suited for this purpose. Measuring both pH and the carbonate/bicarbonate ratio in the vicinity of the first equivalence point will certainly give a negligible OH^- concentration, but the buffer capacity will also be low yielding a more unstable pH measurement.

6.4.4 MEG dependence of H^+

This section gives the relation between the H^+ *activity* (given by the pH measurement) and the *molality*. For the purpose of this work the *molalities* of H^+ and OH^- are important only in the acidic and basic region respectively. In an acidic solution OH^- is negligible and vice versa. At intermediate pH values (6-8) both are usually negligible compared to e.g. the concentration of carbonate species. The relation between pH and H^+ concentration in a water+MEG solvent is given as;

$$a_{H^+} = m_{H^+}\gamma^S_{H^+}\gamma^N_{H^+} = 10^{-pH} \tag{85}$$

where the activity of H^+ is given as the molality times an activity coefficient product. γ^S is the before mentioned aqueous activity coefficient, and $\gamma^N_{H^+}$ corresponds to the MEG dependence. $\gamma^N_{H^+}$ equals 1 in water and its value in MEG+water can be found simply by measuring pH at a given molality of H^+. The results from Table 4.21 and Seiersten[1,22] are given in Fig. 6.16.

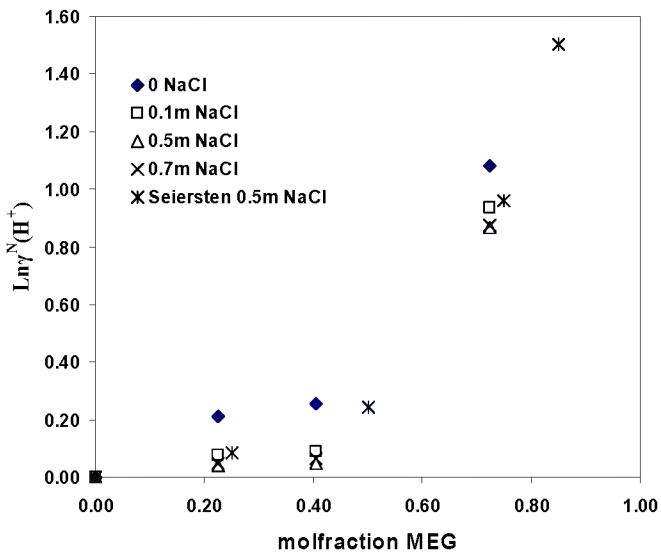

Fig. 6.16: $\ln\gamma^N_{H^+}$ versus x_{MEG} at 25°C 0-0.7m NaCl (mol/kg solvent) from Table 4.21 and from Seiersten[1,22] (0.5m NaCl).

In water all measurements are consistent and $\gamma^N_{H^+} = 1$. There is also reasonable agreement between the data obtained in this work and those of Seiersten et.al.[1,22]. However, the results with no added NaCl deviate from the other data. This is consistent with the discussion concerning a coupled ionic strength + MEG effect in section 2.2.2. Ionic strength effects are expected to be most pronounced at low ionic strengths (0-0.1mol/kg), and can explain the observation in Fig. 6.16.

A pH electrode is influenced by ionic strength/salt content as described in detail in chapter 7. The result is that a measured pH must be corrected with a quantity ΔpH_{salt} to obtain the actual pH. ΔpH_{salt} is found by measuring the change in pH relative to a solution of 0.1mol NaCl/kg solvent. The measurements are interpreted by the equation;

$$\begin{aligned}\Delta pH_{Salt} &= \left(pH^{0.1}_{meas} - pH^{x}_{meas}\right) + \left(pH^{0.1} - pH^{x}\right) \\ &= \left(pH^{0.1}_{meas} - pH^{x}_{meas}\right) + \log\frac{a_{H^+(0.1)}}{a_{H^+(x)}}\end{aligned} \tag{86}$$

All quantities are defined in chapter 7 (*See Eq. 147-148, Page 148*). The superscripts 0.1 and x, denotes the reference ionic strength (mol/kg solvent) and a solution with a different ionic strength respectively. In the calculation there will consequently be a term with a H^+ activity ratio. This ratio corresponds to the activity of H^+ at the reference ionic strength (0.1mol NaCl/kg solvent), divided by the activity at the actual ionic strength (x mol NaCl/kg). Using Eq. 85 for the two solutions with ionic strengths of 0.1 and x, Eq. 87 is obtained;

$$\frac{a_{H^+(0.1)}}{a_{H^+(x)}} = \frac{m_{H^+(0.1)}\gamma^{S}_{H^+(0.1)}\gamma^{N}_{H^+(0.1)}}{m_{H^+(x)}\gamma^{S}_{H^+(x)}\gamma^{N}_{H^+(x)}} \tag{87}$$

It should be noted that to find ΔpH_{salt}, $\gamma^{N}_{H^+}$ must be known or vice versa. In this work it was arbitrarily chosen to use the same ΔpH_{salt} in water+MEG as in water (see section 7.3.3). This choice will thereafter give consistent values for $\gamma^{N}_{H^+}$. In appendix 2 pH measurements in HCl+water+MEG+NaCl solutions are given. The experiments were run with constant H^+ concentration, thus *m* cancels in Eq. 87. If $\gamma^{N}_{H^+}$ is ionic strength independent, the $\gamma^{N}_{H^+}$ terms also cancel at each MEG concentration and the $\gamma^{S}_{H^+(0.1)} / \gamma^{S}_{H^+(x)}$ ratio will be the same in water+MEG as in water. Using this approximation the ΔpH_{salt} is calculated (data in Appendix 2), as shown in Fig. 6.17a). The results in Fig. 6.17a) may seem insignificant since pH is usually measured with an accuracy of about ±0.05-0.1pH units. Although an *absolute* pH determination usually has an error of about ±0.05-0.1pH units, a *relative* measure, however, is much more accurate.

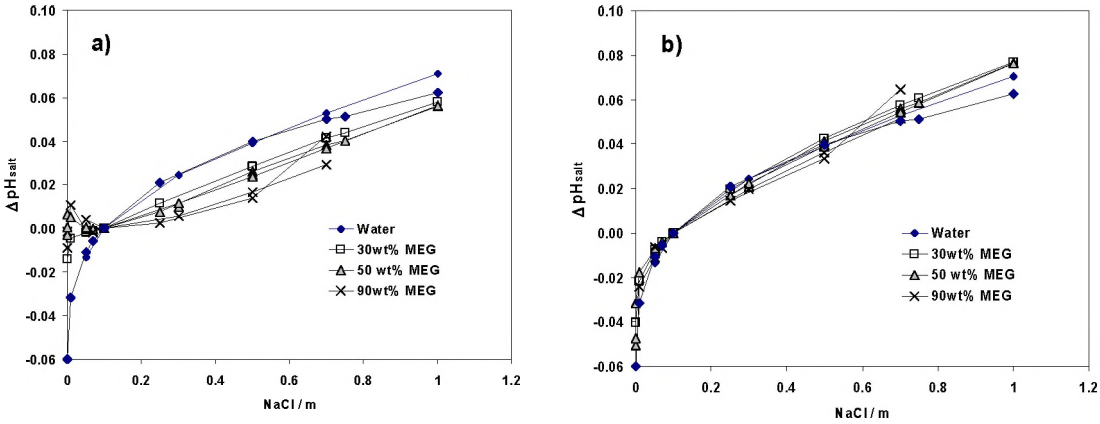

Fig. 6.17: ΔpH_{salt} at 0-90wt% MEG as function of NaCl content(mol/kg solvent) at 25°C. (data from Appendix 2) *a)* Calculated with $\gamma^N_{H^+}$ ionic strength *independent* *b)* calculated from Eq. 88

ΔpH_{salt} is not the same in 30, 50 and 90wt% MEG as in water, although the trend from about NaCl=0.3m and higher is virtually identical. Thus the deviation is, as expected, most evident at low ionic strengths. The deviation is due to a coupled Ionic strength-MEG effect, as discussed in detail in section 2.2.2. Based on the observations in Fig. 6.16 and Fig. 6.17a) it was decided to include an ionic strength dependence in $\gamma^N_{H^+}$;

$$\ln \gamma^N_{H^+} = 1.4457 x_{MEG} - 3.9428 x^2_{MEG} + 5.6753 x^3_{MEG} + \frac{AI^{1/2}}{1+BI^{1/2}}$$

$$A = -1.17 w_{MEG} - 0.82 w^2_{MEG}, \qquad (88)$$

$$B = 9.92 w_{MEG} - 3.65 w^2_{MEG}$$

x_{MEG} and w_{MEG} denotes molfraction and weight fraction of MEG in the solvent, respectively. The last term in Eq. 88 gives the coupled MEG-Ionic strength effect, and corresponds to the general equation developed in section 2.2.2. This term is mathematically advantageous since it approaches the limit A/B at high ionic strengths (*see Fig. 2.6 on Page 30*). When applying Eq. 88 the ΔpH_{salt} function is virtually the same in 30-90wt% MEG as the one for pure water, as seen in Fig. 6.17b).

Seiersten et.al[1,22] also provided data at 50 and 80°C where the results at 50°C for $\gamma^N_{H^+}$ closely resembled those at 25°C. In Fig. 6.18 an inconsistency is observed at 80°C. The difference observed for x_{MEG}>0.5 between the data at 80°C and 25-50°C, corresponds to a difference in pH of about 0.25 units. It was chosen not to include any temperature function of $\gamma^N_{H^+}$ based on these data, since there could be a systematic deviation due to an error in the pH calibration.

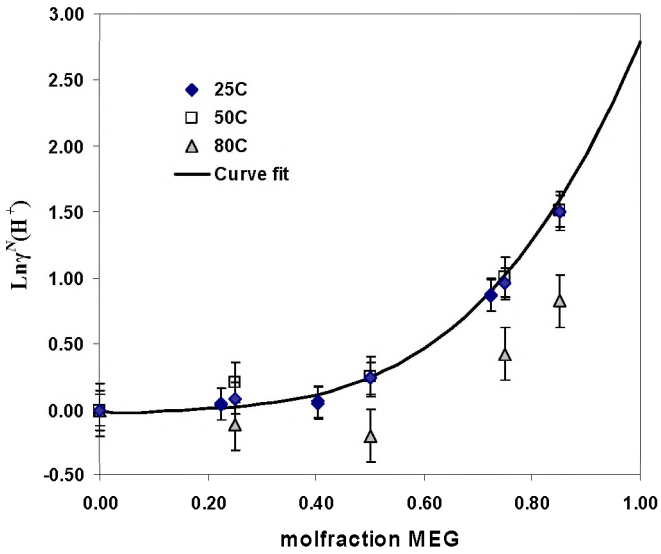

Fig. 6.18: $\gamma^{N}_{H^+}$ values from Seiersten et.al[1,22] and from this work versus x_{MEG}. 25-80°C with 0.5m NaCl. *Solid line:* Eq. 88

6.4.5 The autoprotolysis of water

For calculation of acid/base equilibria it is in addition necessary to include the autoprotolysis of water;

$$2H_2O = H_3O^+ + OH^- \tag{89}$$

The thermodynamic autoprotolysis constant of water $K°_w$ is in an aqueous solution given as;

$$K^o_w = \frac{a_{H^+}a_{OH^-}}{a_{H_2O}} = \frac{m_{H^+}\gamma^S_{H^+}m_{OH^-}\gamma^S_{OH^-}}{a_{H_2O}} \tag{90}$$

When the solvent is a MEG+water solution it is not obvious how to interpret this equation. In pure MEG, the autoprotolysis obviously cannot be expressed by reaction (89). Banjaree et.al[24] gave that the autoprotolysis of mono ethylene glycol (GH) could be expressed with reaction (91). In a MEG-water mixture both GH and H_2O ionize, but the total equilibrium can be denoted by reaction (92) where SH denotes the solvent at question.

$$GH + GH = GH_2^+ + G^- \tag{91}$$

$$SH + SH = SH_2^+ + S^- \tag{92}$$

The autoprotolysis of a MEG+water solvent (SH) can be measured by electrochemical methods as described in detail by Rondinini et.al[23] and Banjaree et.al[24]. The tabulated

autoprotolysis constants of the solvent, K_{ap}, have a standard state chosen such that the activity of the undissociated solvent (SH) is unity in the pure solvent, i.e. a *medium reference* as described in chapter 2.2. In this work it was decided to use an aqueous standard state, and since introduction of new glycol ions (GH_2^+, G^-) in the model would only complicate it further, it was simply chosen to use Eq. 90 directly as described below. Thus the model does not contain any ionization model of MEG.

pH is a key parameter in scale calculations for some minerals thus the model must calculate pH correctly also in the basic region where OH^- is dominating. The link between pH and *molality* of OH^- is provided by the autoprotolysis constant in Eq. 90. By introducing the MEG effect, γ^N, the equation is given as;

$$K_w^o = \frac{m_{H^+}\gamma_{H^+}^S\gamma_{H^+}^N m_{OH^-}\gamma_{OH^-}^S\gamma_{OH^-}^N}{a_{H_2O}} \tag{93}$$

$\gamma_{OH^-}^N$ can be found by measuring pH at a given hydroxide concentration m_{OH};

$$\gamma_{OH^-}^N = K_w^o \frac{a_{H_2O}}{m_{OH^-}\gamma_{OH^-}^S \cdot 10^{-pH}} \tag{94}$$

The activity of water is calculated as described in section 6.2. Seiersten et.al[22] gave a method for pH calibration where the raw data[1] from their work was in the form of titration curves. These curves gave pH at certain OH^- and H^+ concentrations, and the data could be used to find $\gamma_{OH^-}^N$ from Eq. 94, as well as $\gamma_{H^+}^N$ described above. The $\gamma_{OH^-}^N$ values at 25 and 50°C were similar, while the data at 80°C showed a systematic deviation, as seen in Fig. 6.19. It is unfortunate that the data set[1,22] did not contain measurements in water for reference purposes, hence it is a possibility for a systematic error.

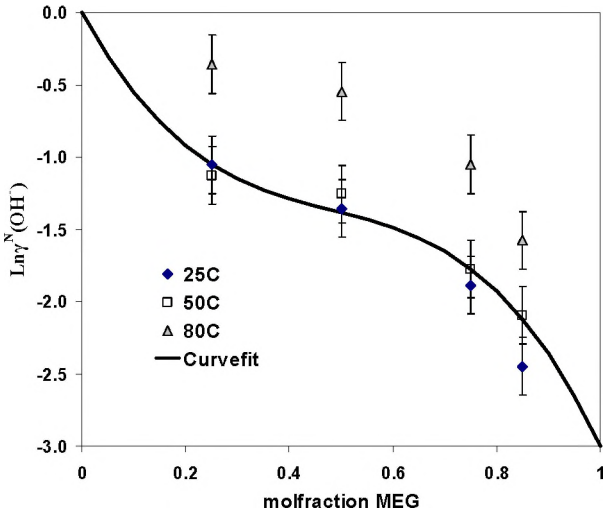

Fig. 6.19: $\ln \gamma^N_{OH^-}$ **at 25-80°C as function of MEG. Data from Seiersten[1,22]. Solid line gives model in Eq. 80**

The raw data are the same as those used for the calculation of $\gamma^N_{H^+}$ (see Fig. 6.18). Due to the inconsistency in the data it was chosen not to include a temperature function for OH^-. There are no measurements at various ionic strengths available at present, hence the $\gamma^N_{OH^-}$ is modeled as ionic strength independent. Generally the data for the determination of $\gamma^N_{H^+}$ and $\gamma^N_{OH^-}$ at other temperatures than 25°C are scarce.

6.5 Carbonate solubility

Carbonate solubility data were used to fit $\gamma^N_{M^{2+}}$ by the general polynomial;

$$\ln \gamma^N_{M^{2+}} = c_1 x_{MEG} + c_2 x^2_{MEG} + c_3 x^3_{MEG} + c_4 x^4_{MEG} \tag{95}$$

where $c_{1\text{-}4}$ are constants given in Table 6.4, x_{MEG} denotes molfraction in solvent and M^{2+} the mineral cation. A fourth degree polynomial was necessary to satisfactory fit the function at high MEG concentration. This is due to the choice of water as the reference, since the water activity approaches zero at this point. From Table 6.4 it is seen that $c_{1\text{-}4}$ for Fe^{2+} have arbitrarily been set equal to those of Ca^{2+}. This is due to lack of data. The $FeCO_3$ solubility is troublesome to measure[1], mainly due to slow kinetics.

Table 6.4: Parameters for γ^N of 2 valent ions forming carbonate scale

Specie	c_1	c_2	c_3	c_4	Temp [°C]	Ref.[a]
Ca^{2+}	-1.0841	-12.619	23.486	-12.766	25-80	TW
Fe^{2+}	-1.0841	-12.619	23.486	-12.766	50	1
Ba^{2+}	2.3152	-32.243	51.994	-26.785	25-80	TW
Sr^{2+}	0.4169	-17.748	25.677	-11.545	25-80	TW
Mg^{2+} [b]	3.3238	-7.0198	18.6567	-8.6400	25-80	TW[b]

[a]References for experimental data. TW denotes this work.
[b]Solid phase is Hydromagnesite ($3MgCO_3 \cdot Mg(OH)_2 \cdot 3H_2O$)

6.5.1 $CaCO_3$, $SrCO_3$ and $BaCO_3$

The equilibrium between calcite ($CaCO_3$) and the dissolved species can be expressed as;

$$Ca^{2+} + 2HCO_3^- = CO_2(g) + CaCO_3(s) + H_2O \tag{96}$$

This equation is convenient when a CO_2 rich gas phase is present, and is obtained by combining the equilibria (66-69). The corresponding equilibrium constant is given as;

$$\begin{aligned} K^o_{Eq.96} &= \frac{K^o_2}{K^o_H K^o_1 K^o_{sp}} = \frac{f_{CO_2} a_{H_2O}}{a_{Ca^{2+}} a^2_{HCO_3^-}} \\ &= \frac{p_{CO_2} \varphi_{CO_2} a_{H_2O}}{m_{Ca^{2+}} \gamma^S_{Ca^{2+}} \gamma^N_{Ca^{2+}} \left(m_{HCO_3^-} \gamma^S_{HCO_3^-} \gamma^N_{HCO_3^-} \right)^2} \end{aligned} \tag{97}$$

where γ^S denotes the activity coefficient in water, γ^N denotes the MEG dependence, φ fugacity coefficient and $K°$ are the common thermodynamic equilibrium constant for

each reaction (66-69). The activity of water is calculated as described in section 6.2. P_{CO2} corresponds to the partial pressure of CO_2. γ^N for the bicarbonate ion was modeled as described above and $\gamma^N(Ca^{2+})$ could consequently be found directly from the measured data in Table 4.12 where Ca^{2+} concentrations are measured at a given CO_2 pressure. At these conditions the HCO_3^- concentration virtually equals the alkalinity of the solution and consequently 2 times the calcium concentration. By a different combination of equilibria, it is possible to calculate $\gamma^N(Ca^{2+})$ directly from the measured pH and the Ca^{2+} concentration;

$$\gamma^N_{Ca^{2+}} = \frac{K^o_{sp}}{K^o_2 K^o_1 K^o_H} \cdot \frac{a^2_{H^+}}{m_{Ca^{2+}} \gamma^S_{Ca^{2+}} p_{CO_2} \varphi_{CO_2} a_{H_2O}} \tag{98}$$

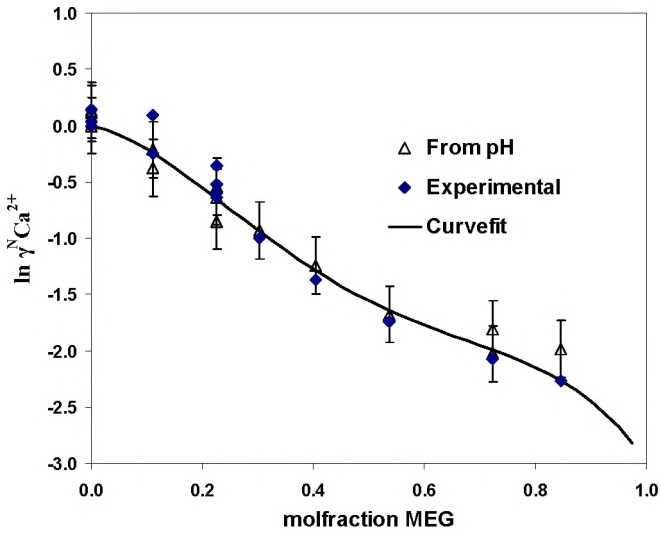

Fig. 6.20: $\ln \gamma^N_{Ca^{2+}}$ **versus** x_{MEG} **at 25˚C from experimental data given in Table 4.12. Calculated from either Eq. 97(*experimental*) or Eq. 98(*from pH*). Error bars determined from measured pH.**

Fig. 6.20 shows the calculated MEG dependence at 25˚C both from Eq. 97 and 98. The two routes generally correspond well. This indicates that the model for the carbonic acid equilibria is consistent. From the measured data it was not observed any systematic effect of ionic strength or temperature upon the MEG dependence. $\gamma^N_{Ca^{2+}}$ was therefore merely a function of MEG concentration. The downward extrapolation at high MEG content was necessary to counteract the decrease in the water activity.

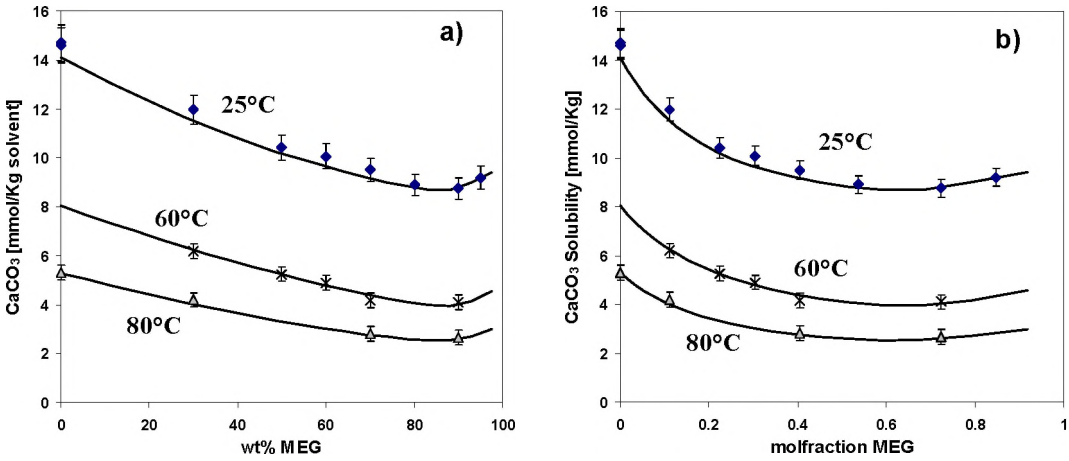

Fig. 6.21: $CaCO_3$ (Calcite) solubility (mmol/kg solvent) versus MEG concentration in solutions saturated with CO_2 at p_{tot}=1atm (25-80°C and 0.5m NaCl see Table 4.12) *Solid lines;* model predictions. MEG concentration as *a)* wt% and *b)* molfraction

Fig. 6.21 shows the measured and calculated solubility of $CaCO_3$(calcite) at three temperatures in water+MEG solutions containing 0.5m NaCl. MEG reduces the solubility that seems to pass through a minimum at about 85wt% MEG. The increase at high alcohol content can, however, not be explained by formation of a Ca^{2+}-MEG complex since this increase was not observed for $CaSO_4$ (anhydrite).

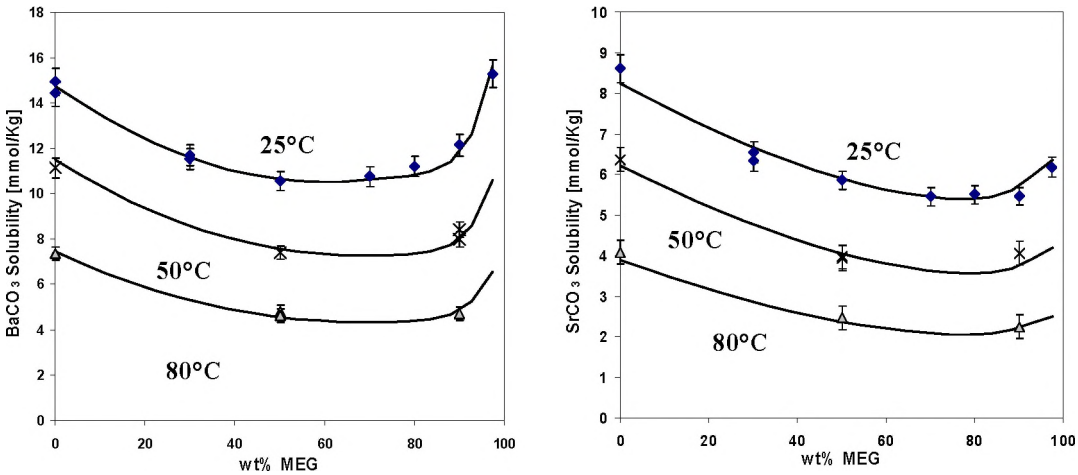

Fig. 6.22: $BaCO_3$ (Witherite) and $SrCO_3$ (Strontianite) solubility (mmol/kg solvent) in solutions saturated with CO_2 at p_{tot}=1atm (25-80°C and 0.5m NaCl). Solid lines; Model predictions

The same approach was used to model Ba and $SrCO_3$ solubilities. Fig. 6.22 compares model predictions with the measured data in Table 4.10 and Table 4.11. $SrCO_3$ has a very similar behaviour as $CaCO_3$, while $BaCO_3$ has a smaller solubility decrease with increasing MEG concentration than the other two. At 97.5wt% MEG the $BaCO_3$ solubility was actually found to be higher than in water.

6.5.2 Hydromagnesite

Magnesium carbonate can exist in several different modifications as described in chapter 9. In this work it was chosen to only include hydromagnesite ($3MgCO_3 \cdot Mg(OH)_2 \cdot 3H_2O$), as this is the compound that probably will occur during oilfield operations. It has a complex solid structure with a mixture of carbonate and hydroxide, where $K°_{sp}$ is given from the reaction;

$$3MgCO_3 \cdot Mg(OH)_2 \cdot 3H_2O(s) = 4Mg^{2+} + 3CO_3^{2-} + 2OH^- + 3H_2O \quad (99)$$

As for the other carbonates the solubility was measured under constant CO_2 pressure i.e. at conditions where the alkalinity is mainly determined by the bicarbonate concentration. Thus the results are best interpreted by an equation including only bicarbonate and Mg^{2+}, as well as the CO_2 pressure. By combination of Eq. 99 with the carbonic acid equilibria of Eq. 66-68 the desired relation is found;

$$3MgCO_3 \cdot Mg(OH)_2 \cdot 3H_2O(s) + 5CO_2 = 4Mg^{2+} + 8HCO_3^- \quad (100)$$

It should be noted that although the solid phase includes crystal water, Eq. 100 describes the equilibrium merely by CO_2(g) and the dissolved ions. Thus the solubility is actually not directly dependent on the water activity. A pronounced solubility increase as water activity decreases is therefore not expected. Fig. 6.23 does, as expected, not show any increased solubility at the high MEG end as was observed for gypsum ($CaSO_4 \cdot 2H_2O$).

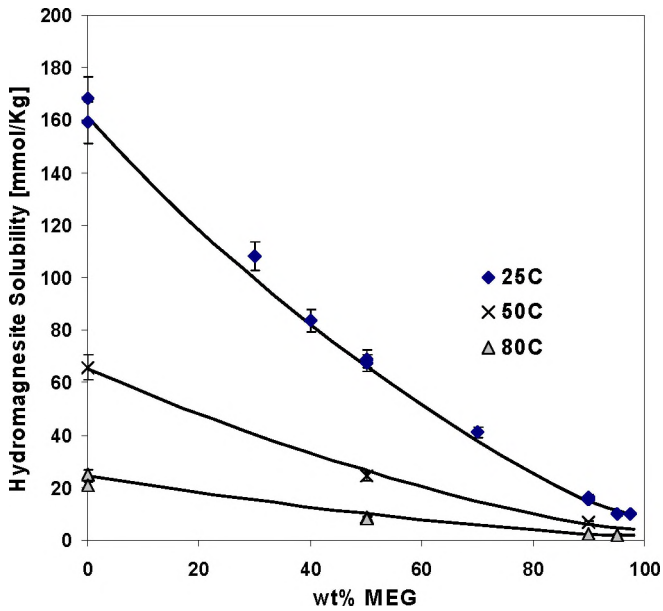

Fig. 6.23: Hydromagnesite ($3MgCO_3 \cdot Mg(OH)_2 \cdot 3H_2O$) solubility (mmol/kg solvent, Table 9.1) versus wt% MEG in solutions saturated with CO_2 at p_{tot}=1atm (25-80°C). *Solid line:* model

MEG has in addition a much more severe influence on hydromagnesite solubility than for the other carbonates. The obvious difference between hydromagnesite and the other carbonates is that OH^- is incorporated in the solid phase. With a given CO_2 pressure and alkalinity the model of this work calculates a higher OH^- concentration in MEG than in water. At 90wt% MEG the OH^- concentration is in the order of 50 times higher and this is consistent with the much lower solubility of hydromagnesite. Due to a more complex structure the calculation of $\gamma^N(Mg^{2+})$ was slightly more complicated than for the other carbonates as shown in Eq. 101-102. The method is, however, exactly the same and all parameters are given in Table 6.4.

$$K^o_{Eq.100} = \frac{K^o_{sp}\left(K^o_H K^o_1\right)^5}{\left(K^o_w\right)^2\left(K^o_2\right)^3} = \frac{a^4_{Mg^{2+}} a^8_{HCO_3^-}}{f^5_{CO_2}} \tag{101}$$

$$\gamma^N_{Mg^{2+}} = \left(\frac{K^o_{sp}\left(K^o_H K^o_1\right)^5}{\left(K^o_w\right)^2\left(K^o_2\right)^3} \cdot \frac{P^5_{CO_2}\varphi^5_{CO_2}}{m^4_{Mg^{2+}} m^8_{HCO_3^-}\left(\gamma^S_{Mg^{2+}}\right)^4\left(\gamma^S_{HCO_3^-}\gamma^N_{HCO_3^-}\right)^8} \right)^{\frac{1}{4}} \tag{102}$$

It should be noted that magnesium may also precipitate in Mg+Ca mixed phases such as dolomite, but no such phase have been included in the model at present.

6.6 Solubility of Na and K carbonates

The highly soluble carbonates were included in the model in a slightly different manner than the low soluble carbonate salts described above. Instead of fitting a function for the cation directly, a $\gamma^{N\pm}$ was used to fit the MEG dependence for each salt. Experimental solubility data are usually given as dissolved amount of salt. For $NaHCO_3$ or Na_2CO_3 this means that the Na^+ concentrations are given. The bicarbonate or carbonate concentrations, however, have to be calculated. The solubility product of $NaHCO_3$ is given as;

$$K^o_{sp} = m_{Na^+} m_{HCO_3^-} \gamma^S_{Na^+} \gamma^S_{HCO_3^-} \left(\gamma^{N\pm}_{NaHCO_3}\right)^2 \tag{103}$$

$K°_{sp}$, the thermodynamic solubility product, is unaffected by MEG due to the choice of aqueous standard state. The activity coefficient product $\gamma^S_{Na^+}\gamma^S_{HCO_3^-}$ is calculated by the model as described earlier. Solubility data gives the m_{Na^+} concentration. $m_{HCO_3^-}$ has to be calculated as it is dependent on temperature, MEG concentration etc. This is done using the model for carbonic acid equilibria described above. When both m_{Na^+} and $m_{HCO_3^-}$ concentrations are known, $\gamma^{N\pm}_{NaHCO_3}$ can be calculated.

$CaCO_3$ and the other low soluble carbonates can precipitate over a wide pH range (~5-14) i.e. at conditions where either bicarbonate, carbonate or even CO_2(aq) is the

dominating dissolved carbonate specie. For the low soluble carbonate salts it was found that a model with a γ^N term for each ion gave a consistent model. This was believed to yield a reasonable extrapolation in the pH ranges not covered by the experimental data. Sodium and potassium carbonates on the other hand precipitate as bicarbonate at medium pH and as carbonate at high pH. Thus each salt can only exists in an area where either HCO_3^- or CO_3^{2-} is the dominating specie as seen from Fig. 6.7. An alternative could be to fit a common $\gamma^N_{Na^+}$ function, meaning that $\gamma^N_{Na^+}$ calculated from $NaHCO_3$ solubility data, should be the same as calculated from Na_2CO_3 solubility data. This, however, was not the case and it was therefore decided to construct a $\gamma^{N\pm}$ function for each salt.

The general fitting equation given in Eq. 104 was used for all salts except for the two sodium carbonates containing crystal water. $r_{1\text{-}3}$ and $t_{1\text{-}3}$ are constants given in Table 6.5.

$$\ln \gamma^{N\pm}_{Salt} = (r_1 + t_1[T-298])x_{MEG} + (r_2 + t_2[T-298])x^2_{MEG} + (r_3 + t_3[T-298])x^3_{MEG} \tag{104}$$

For $Na_2CO_3{\cdot}H_2O$ and $Na_2CO_3{\cdot}10H_2O$ simpler functions could be used by utilizing weight fraction MEG instead of molfraction;

$$\ln \gamma^{N\pm}_{Na_2CO_3 \cdot yH_2O} = r_1 w_{MEG} + r_2 w^2_{MEG} + r_3 w^3_{MEG} \tag{105}$$

w_{MEG} denotes weight fraction of MEG in the solvent, while y corresponds to either 1 or 10 crystal waters.

Table 6.5: Parameters for $\gamma^{N\pm}$ of highly soluble carbonates. For use in Eq. 104-105

Salt	r_1	r_2	r_3	t_1	t_2	t_3	T[a] /°C	Ref.[c]
$NaHCO_3$	4.278	-5.441	1.817	0	2.936E-2	-2.699E-2	0-90	1,25-27
$KHCO_3$	3.847	-3.817	0.5601	0.0290	-0.0207	0	0-80	1,TW
K_2CO_3	9.669	-12.867	7.001	0.1077	-0.1712	0.0950		no data
$K_2CO_3{\cdot}1.5H_2O$	9.669	-12.867	7.001	0.1077	-0.1712	0.0950	0-80	1
Na_2CO_3	6.950	-5.793	1.371	0	0	0	0-90	1,26,28
$Na_2CO_3{\cdot}H_2O$[b]	3.863	-2.354	1.341	0	0	0	0-90	1,26,28
$Na_2CO_3{\cdot}10H_2O$[b]	2.400	0	0	0	0	0	0-25	1

[a]Temperature range of experimental data [b] Modeled as function of weight fraction Eq.105.
[c]Literature references. TW denotes This Work

6.6.1 $NaHCO_3$ and $KHCO_3$

The solubility of sodium bicarbonate is expressed by Eq. 103. The elaborate works of Gärtner et.al[25-27] (15-90°C) together with investigations at IFE[1] (0-90°C), provide solubility data for $NaHCO_3$ in MEG+water solutions. Gärtner et.al. did measurements in closed containers, while IFE used continuous CO_2 flow during their experiments. The total alkalinity was measured using acid titration by both groups, and the results corresponded well. $\gamma^{N\pm}_{NaHCO_3}$ values were calculated as described above and thereafter curve fitted as given in Table 6.5.

In oilfield applications MEG is transported to the wellhead through a pipeline. It typically contains a solution of 90wt% MEG, which is called "lean MEG". During testing of the model it was discovered that the solubility of $NaHCO_3$ in "lean MEG" may be an important limiting factor when it comes to adjustment of the alkalinity. To verify the experimental data it was decided to perform a few additional solubility measurements at low temperature. The measurements from this work (Table 4.13) corresponded well with the data from IFE[1] and the model predictions, as seen in Fig. 6.24.

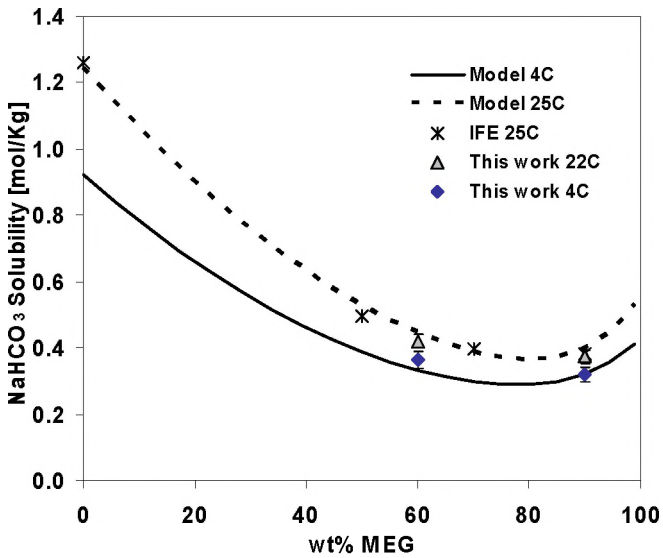

Fig. 6.24: $NaHCO_3$ solubility (mol/kg solvent) versus wt% MEG at 4 and 25°C. Data from this work and IFE[1]. *Solid line:* model at 4°C. *Dotted line:* model at 25°C

At seabed temperature the solubility of $NaHCO_3$ is less than 400mmol/(kg solvent) (A_T~24000mg/kg) in the range 50-95wt% MEG. This will be most important for design and operation of systems containing MEG as a hydrate inhibitor. The $NaHCO_3$ solubility at higher temperature is less important for transport lines since its solubility increases rapidly with temperature, but may be of interest in other parts of the production system e.g. in the MEG reclaiming unit.

The MEG dependence of the $KHCO_3$ solubility was included in the same manner as described for the sodium salt. Experimental data from 0 to 80°C were provided by IFE[1], but unfortunately their work did not contain any water reference data. The measurements at the highest MEG concentrations and lowest temperatures also seemed to be too low. It was therefore decided to perform a few additional $KHCO_3$ solubility measurements in our lab at 0°C (see Table 4.14). These data are included in Fig. 6.25 and support the same type of function as obtained for $NaHCO_3$ with an increased solubility at the high MEG end. From the pH data given in Table 4.19 $KHCO_3$ solubilities in 60 and 90wt% MEG at 25°C were estimated.

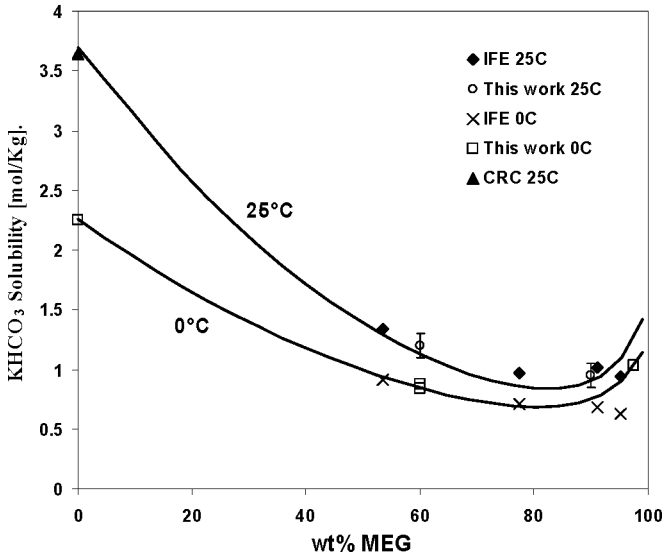

Fig. 6.25: a) $KHCO_3$ solubility (mol/kg solvent) versus wt% MEG in solutions saturated with CO_2 at p_{tot}=1atm (0-25°C). Data from IFE[1] and Table 4.14. Solid lines; model predictions (Table 6.5). ▲; Aqueous data from CRC handbook (see section 5.1.3)

$KHCO_3$ solubility may be of interest for MEG injection pipelines at low temperature. Future investigations of the $KHCO_3$ solubility should therefore focus on 0-25°C. Aqueous reference measurements should always be performed.

6.6.2 Na_2CO_3 and K_2CO_3

The solubility of the sodium carbonate is expressed as;

$$K_{sp}^{o} = m_{Na^+}^2 m_{CO_3^{2-}} \left(\gamma_{Na^+}^{S}\right)^2 \gamma_{CO_3^{2-}}^{S} \left(\gamma_{Na_2CO_3 \cdot yH_2O}^{N\pm}\right)^3 \cdot a_{H_2O}^{y} \qquad (106)$$

where y denotes number of crystal waters of the solid phase ($y=0,1$ *or* 10). Solubility data were taken from the elaborate studies of Gärtner et.al[25-27] and Oosterhof[28-30], who give data mainly at high temperature (40-90°C). IFE[1] provided data at low temperature (0-40°C). All calculations of activity coefficients, CO_3^{2-} concentrations etc. were calculated as for $NaHCO_3$ described above. The resulting MEG dependences, $\ln \gamma_{Na_2CO_3 \cdot yH_2O}^{N\pm}$, were curve fitted with the parameters in Table 6.5 .

The sodium and potassium carbonate salts are highly soluble and will probably not precipitate in MEG injection pipelines, and certainly not if a CO_2 containing gas phase is present. In process plants where CO_2 is removed and the MEG concentration is increased, however, there is a possibility for carbonate precipitation. Data for sodium carbonate is interesting for MEG regeneration plants where the salt can deliberately be precipitated at high temperature, high MEG and low CO_2 conditions. Sodium carbonate will form either as monohydrate, $Na_2CO_3 \cdot H_2O$, or as anhydrate, Na_2CO_3, under MEG regeneration conditions. Na_2CO_3 is an important constituent in glass and it was for glass manufacturing that Gärtner et.al[25-27] and Oosterhof[28-30] did their solubility investigations. There are principally three different phases of sodium carbonate that have to be regarded in connection with MEG regeneration;

→ **Decahydrate** $Na_2CO_3 \cdot 10H_2O$
→ **Monohydrate** $Na_2CO_3 \cdot H_2O$
→ **Anhydrate** Na_2CO_3

Each salt was fitted with its own $\gamma^{N\pm}$ function (see Table 6.5) to obtain the model.

Fig. 6.26 shows model calculations at 25 and 80°C. The discontinuity in the curve at 25°C and about 45wt% MEG is due to the shift from $Na_2CO_3 \cdot 10H_2O$ to $Na_2CO_3 \cdot H_2O$, as the stable phase. An increase at the high MEG end is due to the declining water activity. This rise in solubility is not observed at 80°C. At 80°C the temperature is high enough that anhydrate, Na_2CO_3, is the stable phase. This can be seen as a small discontinuity in the curve at 70wt% MEG corresponding to a shift from $Na_2CO_3 \cdot H_2O$ to Na_2CO_3.

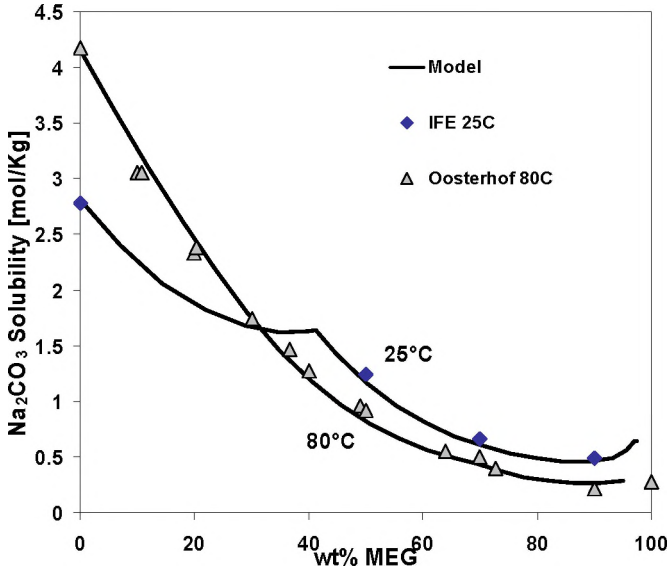

Fig. 6.26:Na_2CO_3 solubility[1,28] (mol/kg solvent) at 25 and 80°C versus wt% MEG. *Solid lines;* model

At low temperature the decahydrate, $Na_2CO_3 \cdot 10H_2O$, is the stable phase, and it is evident that if water is added to Na_2CO_3 at low temperature it may transform into this phase. This is an important observation for oilfield operation where Na_2CO_3 is used. 100kg of Na_2CO_3 can absorb 170kg of water to form the solid $Na_2CO_3 \cdot 10H_2O$. Thus systems containing Na_2CO_3 should simply be flushed with warm and not cold water to avoid formation of the decahydrate.

In section 6.3.1 dealing with $CaSO_4$ it was described that $CaSO_4$ with and without crystal water in principle could co-exists. It is very unlikely that this can happen due to the low solubility. In the case of $Na_2CO_3 \cdot 10H_2O$, however, it is actually not that improbable since each mole of precipitated solid will remove 10 moles i.e. 180grams of water from solution. In a laboratory one can deliberately choose a MEG concentration of about 40%, add 3mole of sodium carbonate, and the precipitating deca-hydrate should remove enough water from the solvent that one reaches the stability field of mono-hydrate. This can be seen from Fig. 6.26.

Solubility data for potassium carbonate was provided by IFE[1] (0-80°C). It was, however, not investigated whether the solid phase in equilibrium with the aqueous phase was K_2CO_3 or $K_2CO_3 \cdot 1.5H_2O$. Measurements had neither been performed in water such that a comparison with literature data could be made. In aqueous solutions the transformation from $K_2CO_3 \cdot 1.5H_2O$ into the anhydrate occurs at about 154°C. At temperatures <80°C the solubility of K_2CO_3 should be very high as seen in chapter 5.1.4. The data[1] did not show any sign of discontinuities that would indicate a phase shift. Thus it was most likely $K_2CO_3 \cdot 1.5H_2O$ that had been present in all the experiments at IFE[1]. $\gamma^{N\pm}$ of $K_2CO_3 \cdot 1.5H_2O$ was calculated in the same manner as done for the sodium salts above, and curve fitted with the parameters given in Table 6.5. The same function was used for the MEG dependence, $\gamma^{N\pm}$, of the anhydrate K_2CO_3.

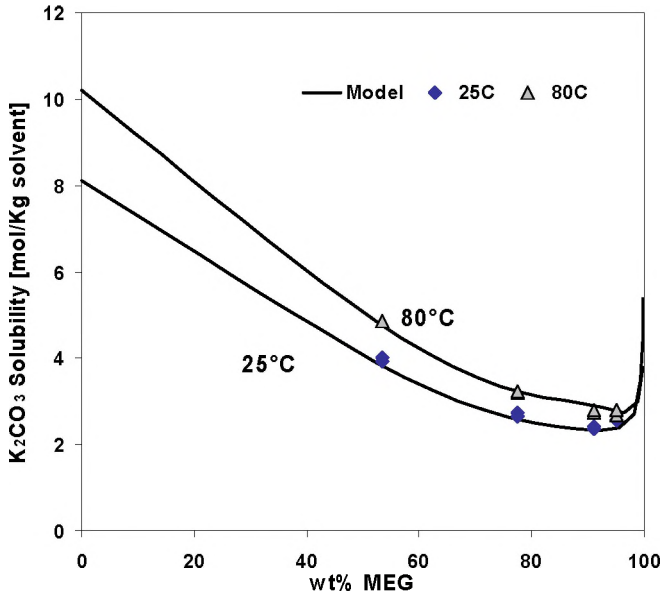

Fig. 6.27: $K_2CO_3 \cdot 1.5H_2O$ solubility[1] (mol/kg solvent) at 25 and 80°C as function of wt% MEG. *Solid lines:* model (Eq. 104)

Fig. 6.27 shows the steep increase in the $K_2CO_3 \cdot 1.5H_2O$ solubility close to 100% MEG. This is due to the rapid decrease in water activity. The anhydrate K_2CO_3 is not predicted to be the stable phase even at the highest MEG concentrations (>95wt% MEG). This is due to the very high value of $K°_{sp}(K_2CO_3)$ (see chapter 5.1.4). In future investigations phase analysis should be performed to determine which solid phase that is actually in equilibrium.

6.6.3 Other solid phases in the Na-HCO_3^--CO_3^{2-} system

The elaborate works of Gärtner et.al[25-27] also concern the solid phases *Trona* ($Na_2CO_3 \cdot NaHCO_3 \cdot H_2O$) and *Wegscheiderite* ($Na_2CO_3 \cdot 3NaHCO_3$). It was, however, decided not to include these in the present model, since these compounds are believed to be of little importance for oilfield applications. The data contained in the literature should be sufficient to include both solids in the model. This is a possible future extension that can be done if the need should arise. These salts contain both carbonate and bicarbonate ions and the calculation of precipitated amounts can be a challenge in the scale model. Since these salts have high solubilities, precipitation may be in the order of many moles per kg solvent. This will have a large influence on activity coefficients. Mutual ions are a problem since precipitation of one solid could lower the SR of other salts so much that they become under saturated. The model can therefore end up in oscillations between precipitation/dissolution. In such a situation it may be mathematically difficult to find a suitable iteration procedure.

6.7 $Mg(OH)_2$ solubility

The stochiometric solubility product K'_{sp} of $Mg(OH)_2$ (brucite) is given as;

$$K'_{sp} = m_{Mg^{2+}} m^2_{OH^-} \tag{107}$$

If the solid is dissolved in solutions without CO_2 present, the OH^- concentration will equal two times the Mg^{2+} concentration and K'_{sp} can be written as;

$$\begin{aligned} K'_{sp} &= m_{Mg^{2+}} m^2_{OH^-} \\ &= 4m^3_{Mg^{2+}} \end{aligned} \tag{108}$$

The stochiometric constant can then be found directly from the measured Mg^{2+} concentration. As discussed in detail in chapter 5.1.7 , CO_2 was observed in the solutions during the $Mg(OH)_2$ solubility studies. There is a question concerning how and when this CO_2 was introduced. If it came from air in contact with the sample during analysis (filtering/weighing etc.), there is actually no problem since the measured Mg^{2+} concentration can be used directly in Eq. 108. If, on the other hand, CO_2 was present during the dissolution process, CO_2 would have reacted with OH^- to form carbonate. Using Mg^{2+} concentration directly in this case, yields a too high solubility product, since the m_{OH^-} is in fact lower than $2m_{Mg^{2+}}$. Unfortunately the main part of the CO_2 was most likely present in the system during the dissolution reaction, either from remaining gas in solution, or simply due to small amounts of carbonate in the $Mg(OH)_2$(s). Thus using Mg^{2+} concentration in Eq. 108 probably yields a *too high* solubility product. The OH^- concentrations given in Table 4.20 are also most probably *too high* (see chapter 5.1.7).

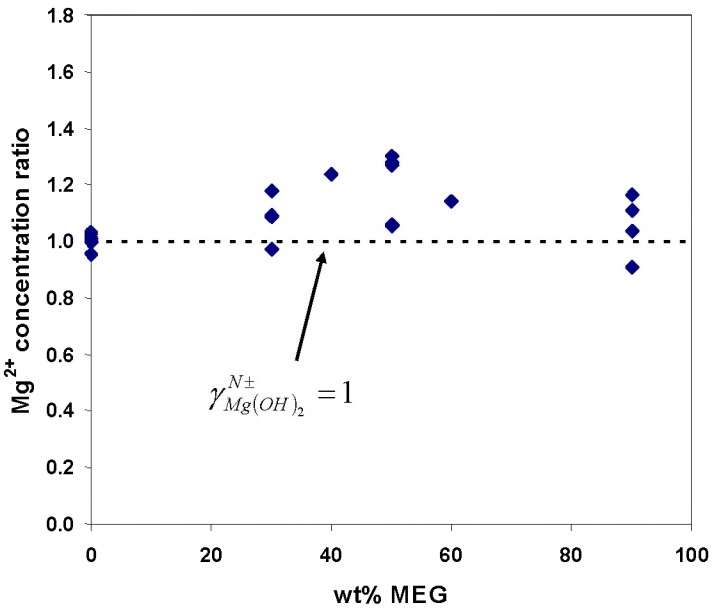

Fig. 6.28: Mg^{2+} concentration ratio $m_{Mg^{2+}(MEG)} / m_{Mg^{2+}(H_2O)}$ (Table 4.20) versus wt% MEG; Temperature (22-80°C) NaCl content (0-0.5mol/kg).

Fig. 6.28 shows the measured saturation concentration of Mg^{2+} divided by the measured saturation concentration in water at the same temperature(22-80°C) and NaCl content(0 and 0.5m). From this plot it looks like the solubility increases up to 50wt% MEG and then drops to a value comparable with water at 90wt% MEG. This is the only salt that has shown such behaviour. The magnesium concentration alone is, however, not necessarily representing the solubility as described above. Given the uncertainties in the data it was decided to neglect the MEG dependence for $Mg(OH)_2$ i.e. $\gamma^{N\pm}_{Mg(OH)_2}$ for the dissolution equilibrium of $Mg(OH)_2$ was simply set to 1;

$$K^{o}_{sp}\left[Mg(OH)_2\right] = m_{Mg^{2+}} m^2_{OH^-} \gamma^{S}_{Mg^{2+}} \left(\gamma^{S}_{OH^-}\right)^2 \left(\gamma^{N\pm}_{Mg(OH)_2}\right)^3 \qquad (109)$$

This means that the solubility product is independent of MEG concentration. The actual solubility ($m_{Mg^{2+}}$) will, however, not always be unaffected by MEG. This is due to the OH^- concentration being dependent on the pH, which in turn is dependent on MEG concentration.

From Eq. 107 it is seen that a decrease in pH by one unit, will increase the solubility 100times ($K'_{sp} \sim 10^{-12}$). At pH=7 ($m^2_{OH^-} \approx 10^{-14}$) the concentration of Mg^{2+} has to be in the order of 100mol/kg for $Mg(OH)_2$ to precipitate. $Mg(OH)_2$ precipitation can therefore only be a problem when pH is 8-9 or higher.

6.8 Acetic acid, NaAc, H_2S and FeS

The MEG dependence, $\gamma^{N\pm}$, was fitted with the general Eq. 110 unless otherwise stated. All parameters are given in Table 6.6. Data were supplied by IFE[1].

$$\ln\gamma^{N\pm} = (r_1 + t_1[T-298])x_{MEG} + (r_2 + t_2[T-298])x_{MEG}^2 + (r_3 + t_3[T-298])x_{MEG}^3 \quad (110)$$

The MEG dependence for the organic acids that normally appear in formation waters was set equal to that of HAc (Acetic), since water+MEG data were not available for the other acids.

Table 6.6: Parameters for γ^N from Eq. 110. All data from IFE[1]

Specie	r_1	r_2	r_3	t_1	t_2	t_3	T /°C
HAc	2.8663	-4.3518	0	-0.02409	0.07166	0	25-70
K_1-HAc	6.4869	-2.4993	0	-0.01743	-0.00671	0	2-70
NaAc	2.113	0	0	0	0	0	0-90
NaAc·3H_2O	4.467	-3.806	0	0	0	0	0-40
H_2S	Fitted by Eq. 78-79. Parameters in Table 6.7						5-125
HS^-	1.260	-0.3828	0	-0.01427	0	0	25-80
FeS	0	0	0	0	0	0	No data

6.8.1 Acetic acid

Henry's constant for acetic acid is in MEG containing solutions given as;

$$K_H^o(HAc) = \frac{a_{HAc}}{f_{HAc}} = \frac{m_{HAc}\gamma_{HAc}^S}{P_{HAc}\varphi_{HAc}}\gamma_{HAc}^N \quad (111)$$

$$K_H'(HAc) = \frac{m_{HAc}}{P_{HAc}} \quad (112)$$

The Henrian constant gives the ratio between the activity in the aqueous phase, a_{HAc}, and the fugacity, f_{HAc}, in the gas phase. P denotes pressure [bar] while the other parameters are defined previously. In an equivalent manner as for CO_2 dissolution, the MEG dependence, γ_{HAc}^N, was measured[1] (25, 40 and 70°C) by recording partial pressure at a certain aqueous concentration m_{HAc}. The resulting parameters for the γ_{HAc}^N function are given in Table 6.6. At a given concentration of HAc in the aqueous phase, the amount of HAc in the gas increases with temperature. i.e. the stochiometric constant, K_H', decreases.

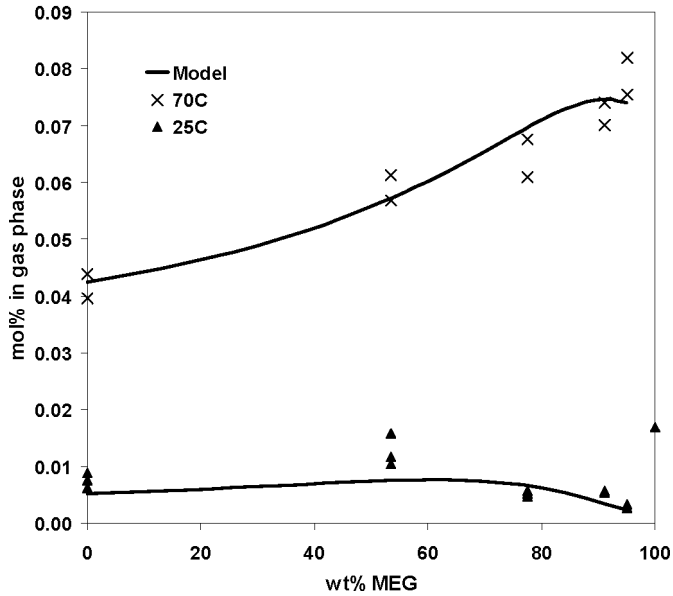

Fig. 6.29: mol% HAc in gas phase in equilibrium with water+MEG+HAc versus wt% MEG. HAc concentrations in the liquid phase are 130-150mmol/kg solvent at 70°C and 170-190mmol/kg solvent at 25°C. P_{tot}=1bar. N_2 used as inert gas.

Fig. 6.29 shows the mol% of acetic acid in the gas phase at two temperatures, as function of wt% MEG. The data[1] show some scattering but corresponds well with the model in water. It should be noted that HAc is not very volatile and most of the acetic acid will be in present the aqueous phase. There is a need for more data in water+MEG solutions to tune the model.

The dissociation of acetic acid takes place according to Eq. 113, where the MEG dependence is introduced by the γ^N term as for all other equilibria. a_{H^+} is directly measured by a pH electrode.

$$K_1^o(HAc) = \frac{a_{H^+}a_{Ac^-}}{a_{HAc}} = \frac{a_{H^+}\cdot m_{Ac^-}\gamma^S_{Ac^-}}{m_{HAc}\gamma^S_{HAc}}\cdot\frac{\gamma^N_{Ac^-}}{\gamma^N_{HAc}} \qquad (113)$$

Data for NaOH titrations of a solution containing HAc were obtained from IFE[1]. The pH meter was calibrated in KHPh as described in chapter 7. At the half titration point the concentrations of HAc and Ac^- are equal and cancel in Eq. 113. Thus the ratio $\gamma^N_{Ac^-}/\gamma^N_{HAc}$ can be found directly from the pH measurement. This ratio was denoted $\gamma^N_{K_1-HAc}$ and Eq. 113 can, at the half titration point, be rewritten as;

$$K_1^o(HAc) = a_{H^+}\cdot\frac{\gamma^S_{Ac^-}}{\gamma^S_{HAc}}\cdot\gamma^N_{K_1-HAc} \qquad (114)$$

The measurements were run in series with constant HAc concentration and ionic strength (NaCl), meaning that the γ^S ratio remained constant when MEG was added. $\gamma^N_{K_1-HAc}$ could consequently be found directly from the observed change in pH when MEG was introduced.

It was chosen to construct a model for $\gamma^N_{K_1-HAc}$ instead of the Ac^- ion ($\gamma^N_{Ac^-}$). This is advantageous for two reasons. Firstly it enables a simpler curve fit function and secondly it will be unaffected of changes in the gas dissolution equilibrium i.e. if a new function for γ^N_{HAc} is made. $\gamma^N_{K_1-HAc}$ was calculated from the data at various MEG concentrations (0-95wt%) and fitted with Eq. 110 (parameters in Table 6.6).

In our own laboratory three experimental series were preformed to check the IFE data. Solutions containing approximately 50mmol/kg of both $NaHCO_3$ and NaCl were continuously bubbled with CO_2 at room temperature (22°C) and atmospheric conditions. Concentrated HAc was titrated into this solution and pH recorded when the signal had stabilized.

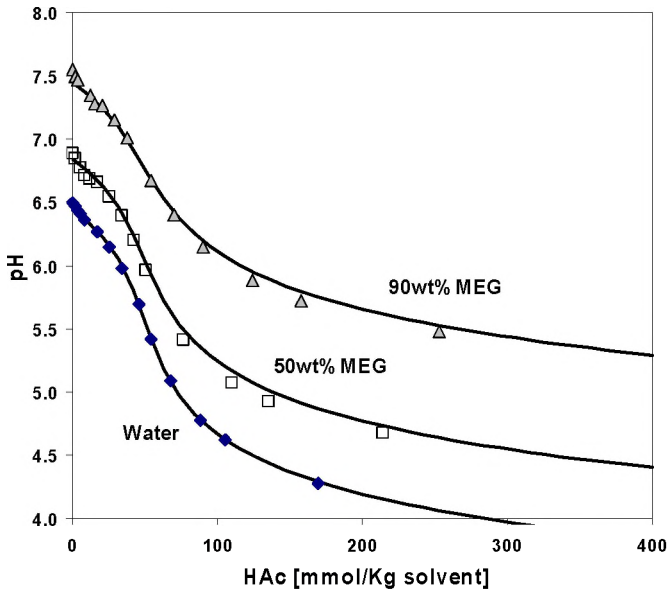

Fig. 6.30: pH as function of added HAc at 22°C compared with model predictions (solid lines). The solutions were saturated with CO_2 at 1atm (~0.05m $NaHCO_3$ and NaCl)

Fig. 6.30 compares the data for 0, 50 and 90wt% MEG with model predictions. It should be noted that these data have not be used to fit the model. These solutions are also closer to what will be encountered during practical operation, as they have a certain alkalinity and are saturated with CO_2. The correctly modeled pH at zero added HAc, has obviously nothing to do with the dissociation of acetic acid, but indicates that the carbonic acid equations and pH calibration are correct. Some discrepancies are observed at 50 and 90wt% MEG, but it was concluded that the model satisfactory reproduced the measured data.

6.8.2 NaAc solubility

The MEG dependence was calculated from solubility data provided by IFE[1], in a similar manner as for all other salts, according to Eq. 115-116

$$K_{sp}^{o}(NaAc) = m_{Na^+} m_{Ac^-} \gamma_{Na^+}^{S} \gamma_{Ac^-}^{S} \left(\gamma_{NaAc}^{N\pm}\right)^2 \quad (115)$$

$$K_{sp}^{o}(NaAc \cdot 3H_2O) = m_{Na^+} m_{Ac^-} \gamma_{Na^+}^{S} \gamma_{Ac^-}^{S} \left(\gamma_{NaAc\cdot 3H_2O}^{N\pm}\right)^2 a_{H_2O}^{3} \quad (116)$$

The water activity is important for salts containing crystal water, and is calculated as given in section 6.2. A good approximation, however, is simply the molfraction of water in the solvent. It should be evident that with water activity to the third power, the solubility will rapidly increase at high MEG concentrations, as long as NaAc·3H_2O is the stable phase. At room temperature the *tri hydrate* is stable in water but will consequently become the less stable salt as the water activity decreases. The curve fitted $\gamma^{N\pm}$ terms are given in Table 6.6. Fig. 6.31 shows experimental data and the resulting model. At 70-90wt% MEG the curves have distinct break points. These correspond to a shift in stability from NaAc·3H_2O at low MEG concentrations to NaAc at high MEG concentrations.

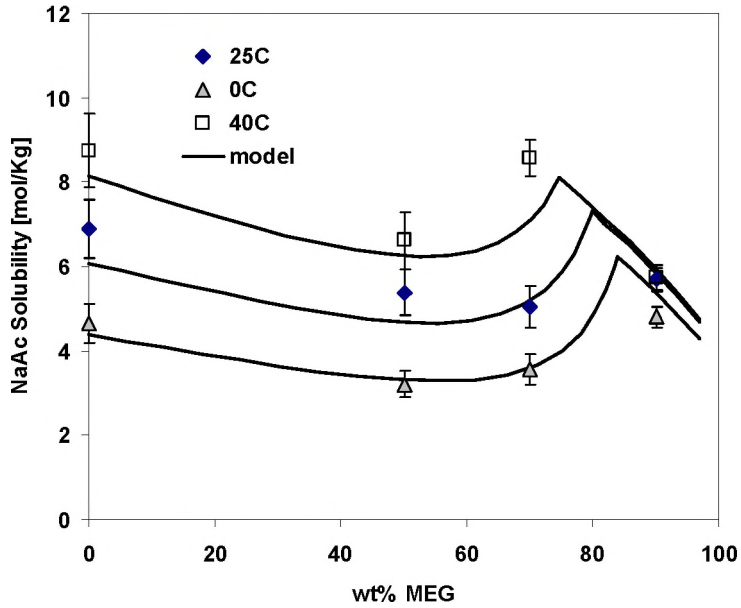

Fig. 6.31: NaAc solubility[1] at 0-40°C versus wt% MEG compared with model lines.

At IFE the solubility was measured by dissolving NaAc. Thus the NaAc solubility was measured by dissolution and NaAc·3H_2O by precipitation. The experimental error was regarded as ±5% and ±10%, respectively. In water the data are systematically higher than predicted by the model. This may be due to that the precipitation reaction has not reached equilibrium. At 40°C and 70wt% MEG, the measurement is much higher than the model prediction. Either the model calculates the stability shift from NaAc·3H_2O to NaAc at a slightly too high MEG concentration or anhydrate was present in a

metastable condition. The latter implies that if the experiment had been left for longer time, a lower solubility closer to the $NaAc{\cdot}3H_2O$ curve would have been observed.

In oilfield operation NaAc (or as $NaAc{\cdot}3H_2O$) formation is most unlikely, due to the very high solubility also at low temperature. When MEG is circulated, however, salt concentrations can become very high at certain points in the system e.g. in boilers. If there is considerable amounts of acetic acid in the well, NaAc precipitation can actually be feasible.

6.8.3 H_2S dissolution and dissociation

Measurements of the $H_2S(g)$ solubility in MEG+water solutions had previously been performed at the IFE[1]. The amount of dissolved gas was calculated from the pressure decrease in a closed cylinder of known volume as for the CO_2 studies described above. The γ^N term in Eq. 117 gives the MEG dependence of the gas solubility.

$$K_H^o(H_2S) = \frac{a_{H_2S(aq)}}{f_{H_2S}} = \frac{m_{H_2S} \cdot \gamma^S_{H_2S}}{P_{H_2S} \cdot \varphi_{H_2S}} \cdot \gamma^N_{H_2S} \tag{117}$$

The activity coefficient, γ^S, and fugacity coefficient, φ, were both calculated by *Multiscale*[13]. It was used the same type of polynomial to fit the MEG dependence, $\gamma^N(H_2S)$, as for CO_2. The polynomial is given in Eq. 78 and Eq. 79, with the corresponding parameters in Table 6.7.

Table 6.7: K_H of H_2S. Parameters for Eq. 78-79

	p_1	p_2	p_3	p_3
a_1	33.587	-7.1744	1.2701	0.022654
a_2	222.78	-46.776	8.3516	0.14202
a_3	317.03	-63.537	11.134	0.16386

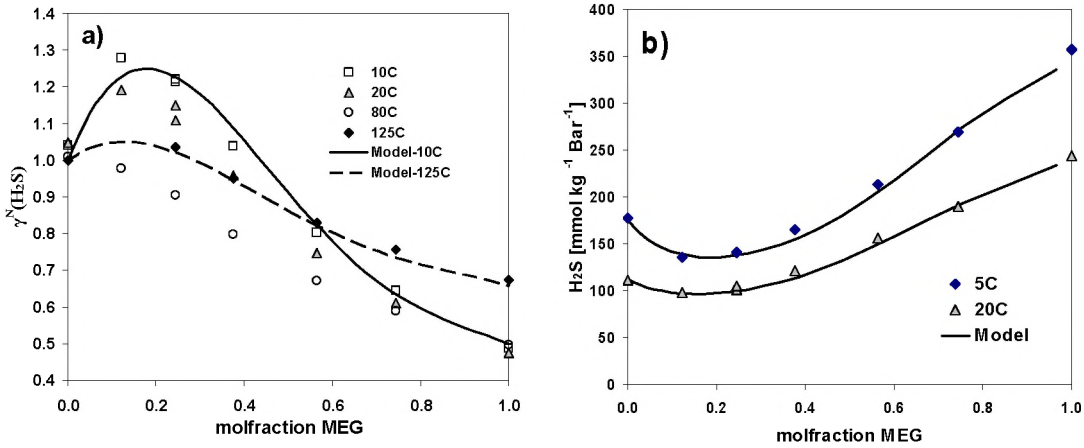

Fig. 6.32: ***a)*** $\gamma^N(H_2S)$ **at four temperatures(10-125°C) versus** x_{MEG}**. Model predictions at 10 and 125°C are shown as lines.** ***b)*** **Measured solubility[1] [mmol·kg^{-1}·bar^{-1}] versus** x_{MEG} **compared to model at 5 and 20°C** P_{tot}**=1bar**

Fig. 6.32a) shows $\gamma^N(H_2S)$ at four selected temperatures. Fig. 6.32b) compares the measured solubility (as mmol·kg^{-1}·bar^{-1}) with the model calculations. It should be noted that the solubility of H_2S is much larger than for CO_2 (~27mmol/kg in x_{MEG}=0.72, ~30mmol/kg in water @20°C, P_{CO2}=1bar) also in MEG containing solutions.

The first dissociation constant of the hydrogen sulfide acid, was calculated from Eq. 118

$$K_1^o = \frac{m_{H^+}\gamma^S_{H^+}\gamma^N_{H^+}\cdot m_{HS^-}\gamma^S_{HS^-}}{m_{H_2S}\gamma^S_{H_2S}}\cdot\frac{\gamma^N_{HS^-}}{\gamma^N_{H_2S}} \qquad (118)$$

$$K_1^{'} = \frac{m_{H^+}m_{HS^-}}{m_{H_2S}} \qquad (119)$$

Titration experiments[1] gave m_{H^+} at the half titration point where concentrations of HS^- and H_2S are equal. The *molality* of H^+ was directly measured using a pH electrode that had been calibrated as described by Seiersten et.al[22]. At half-way titration, concentrations of HS^- and H_2S cancels and the H^+ molality equals the stochiometric equilibrium constant K_1'. γ^S values, $\gamma^N_{H_2S}$ and $\gamma^N_{H^+}$ were calculated as described above and inserted in the thermodynamic constant, Eq. 118. The resulting $\gamma^N_{HS^-}$ was curve fitted as given in Table 6.6. Calculated and measured stochiometric constants (Eq. 119) for the dissociation of H_2S in water+MEG mixtures are compared in Fig. 6.33.

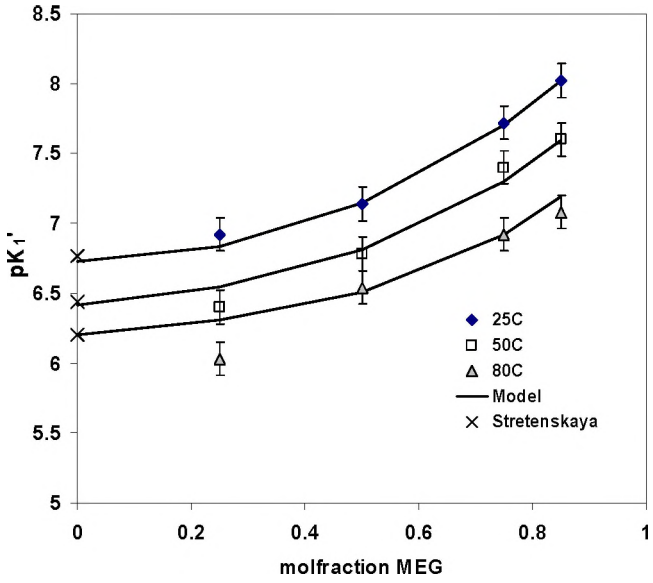

Fig. 6.33: $pK_1'(H_2S)$[1,31] versus x_{MEG}, at temperatures (25, 50 and 80)°C; in solutions of 0.5m (mol/kg solvent) NaCl and about 2.5mmol/kg of total H_2S. *Solid lines:* model

Unfortunately IFE[1] had not performed measurements in water, thus in Fig. 6.33 the aqueous predictions are compared with data of Strentenskaya[31]. The data of Strentenskaya[31] was recalculated to a solution of 0.5m NaCl using the Pitzer ion interaction model. At x_{MEG}=0.25 there was some variation between the three temperatures, while at higher MEG concentrations the measurements at 25, 50 and 80°C gave virtually the same trend.

6.8.4 Solubility of FeS

Data are not available for the FeS solubility in water+MEG at present. Consequently it was decided to simply set the $\gamma^{N\pm}$ term of FeS equal to 1 i.e. the solubility product will have the same value in MEG containing solutions as in water. The actual solubility of FeS, however, will vary slightly due to change in the H_2S equilibria with MEG concentration.

6.9 Methane solubility

There are much data available for CH_4 solubility in pure MEG[32-34](-9-125°C), but in mixed water+MEG solutions, the available data[33] are scarce (10-30°C). The solubility in water+MEG solutions is modeled in the same manner as done for the other gas equilibria. The thermodynamic Henrys' constant is given as;

$$K_H^o(CH_4) = \frac{a_{CH_4}}{f_{CH_4}} = \frac{m_{CH_4}\gamma^S_{CH_4}\gamma^N_{CH_4}}{P_{CH_4}\varphi_{CH_4}} \tag{120}$$

All parameters are defined in previous sections. Wang et.al.[33] and Zheng et.al.[32] give solubility of methane, m_{CH_4}, at certain total pressures. The partial pressure of the solvent is, however, in all cases so low that total pressure virtually equals the partial pressure of methane, P_{CH_4}. $\gamma^S_{CH_4}$ and φ_{CH_4} were calculated by *Multiscale*[13] to obtain the unknown $\gamma^N_{CH_4}$. The calculated values of the MEG dependence, $\gamma^N_{CH_4}$, were thereafter curve fitted by the equation;

$$\ln\gamma^N_{CH_4} = Aw_{MEG} + Bw_{MEG}w_{H_2O} + Cw^2_{MEG}w_{H_2O} \tag{121}$$

w_{MEG} and w_{H2O} denote weight fraction of MEG and water in the solvent, respectively. The temperature dependent constants A,B and C are calculated as;

$$A = a_1 + a_2T + \frac{a_3}{T} \tag{122}$$

T denotes temperature in degree Kelvin and the parameters $a_{1\text{-}3}$, $b_{1\text{-}3}$ and $c_{1\text{-}3}$ are given in Table 6.8.

Table 6.8: K_H of CH_4. Parameters for Eq. 121-122

Parameter	value	Parameter	value	Parameter	value
a_1	-18.19	b_1	-55.56	c_1	1.899
a_2	0.02194	b_2	0.07652	c_2	0
a_3	3327	b_3	9990	c_3	0

Both Fig. 6.34 and Fig. 6.35 show CH_4 solubility (mol/kg solvent) versus total pressure. Total pressure is given as $P_{tot}=P_{CH4}+P_{MEG}+P_{water}$, but the partial pressure of the solvent (water+MEG) is generally so low that P_{tot} virtually equals P_{CH4}. Fig. 6.34 compares the model calculations with the data of Wang et.al.[33] for 40, 80, and 100wt% MEG at 20°C. The aqueous data are calculated by the model for comparison. In Fig. 6.34 the model corresponds well with the data in the whole pressure interval. Fig. 6.35, however, shows some slight discrepancies between the data and the model for these pure MEG solutions. For 125°C the model actually predicts a too high solubility at 100-200bar, but a too low solubility at >300bar. Thus there seems to be a pressure dependence for the effect of MEG, i.e. $\gamma^{N}_{CH_4}$ should be pressure dependent. This observation, however, can also be caused by the PVT part of the model that calculates the fugacity of the gas phase. There is a need for more data to investigate these effects further.

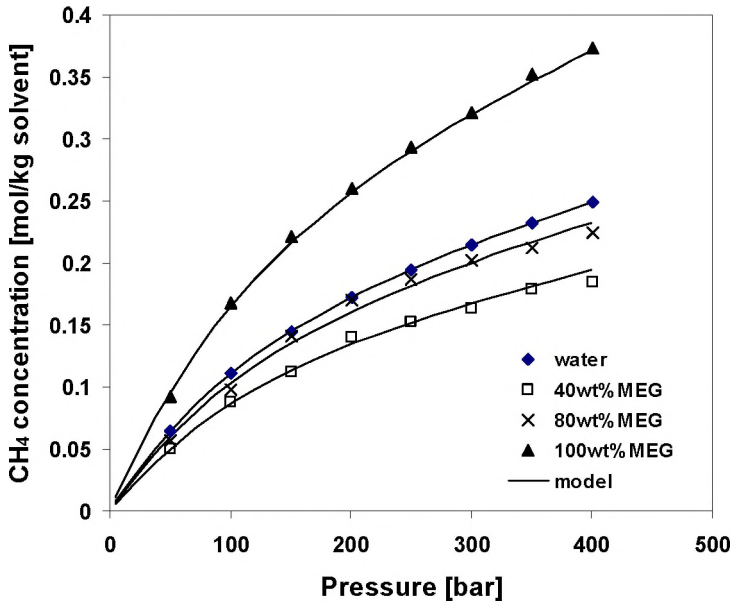

Fig. 6.34: CH_4 solubility[33] (mol/kg solvent) versus total pressure (bar) at 20°C and 0-100wt% MEG. *Solid lines:* model

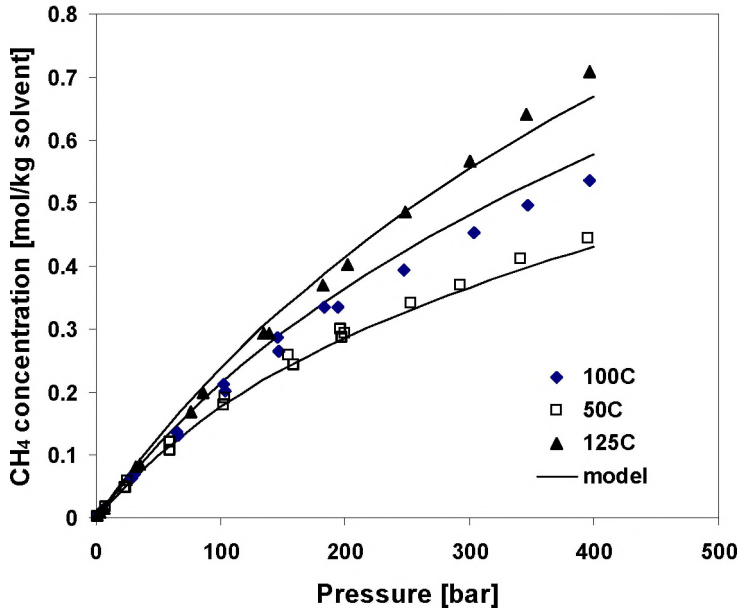

Fig. 6.35: CH_4 solubility[34] (mol/kg solvent) versus total pressure (bar) at 50-125°C with 100wt% MEG as solvent. *Solid lines:* model

6.10 References in Chapter 6

1. Seiersten, M., Institute For Energy technology(IFE), Norway Private communications.
2. Kraus, K.A., Raridon, R.J. and Baldwin,W.H. "Properties of organic-water mixtures." *J.Am.Chem.Soc.,* **86(13),** (1964)
3. Masoudi, R., Tohidi, B., Anderson, R., Burgass, R.W., Yang, J. "Experimental measurements and thermodynamic modeling of chlathrate hydrate equilibria and salt solubility in aqueous ethylene glycol and electrolyte solutions" *Fluid Phase Equilibria*, **219**, 157-163, (2003)
4. Linke, W. F. *Solubilities* 4th ed, (1965), Am Chem Soc Washington D.C
5. Rasmussen, P. Chiavone-Fihlo, C.O., "Solubilities of salts in mixed solvents.", *J. Chem. Eng. data,* **38(3),** 367-369, (1993)
6. Curme, G.O, Johnston, F. *Glycols*, New York (1952), Reinhold Publishing co.
7. Trimble, H.M., Potts, W. "Glycol-water mixtures. Vapor pressure-boiling point-composition relations." *Ind. and Eng. Chem*, **27**, 66-68, (1935)
8. Villamanan,M.,A., Gonzalez, C., Van Ness, H.C. "Excess thermodynamic properties for water/ethylene glycol." *J. Chem. Eng. Data*, **29(4)**,427-429, (1984)
9. Gonzalez, C., Van Ness, H.C. "Excess thermodynamic functions for ternary systems. 9. Total-pressure data and GE for water/ethylene glycol/ethanol at 50°C.", *J. Chem. Eng. Data*, **28(4)**,410-412, (1983)
10. Nath,A., Bender,E., *J.Chem.Eng.Data*, "Isothermal vapor-liquid equilibriums of binary and ternary mixtures containing alcohol, alkanolamine, and water with a new static device." **28(4)**,370-375,(1983)
11. Lancia,A., Musmarra,D., Pepe,F., "Vapor-liquid equilibria for mixtures of ethylene glycol, propylene glycol, and water between 98° and 122°C." *J. Chem. Eng of Japan*, **29(3),** 449-455, (1996)
12. Kan, A.T Fu,G. Tomson, M.B "Effect of Methanol and Ethylene Glycol on Sulfates and halite Scale Formation" *Ind. Eng. Chem. Res.* **42**, 2399-2408, (2003)
13. Kaasa, B., *Prediciton of pH, Mineral precipitations and multiphase equilibria during oil recovery*, Dr.Ing thesis, Norwegian University of Technology and Science-NTNU, (1998)
14. Kaasa, B., Sandengen, K. and Østvold, T. " Thermodynamic Predictions of Scale Potential, pH and Gas Solubility in Glycol Containing Systems", *SPE 95075, Int. Symposium on Oilfield Scale*, Aberdeen, (2005)
15. Manzoni, A., Mussini, P.R., Mussini, T. "Thermodynamics of the amalgam cell {KxHg1-x|KCl(m)|AgCl|Ag} and primary medium effects upon KCl in {ethylene glycol + water}, {acetonitrile + water}, and {1,4-dioxane + water} solvent mixtures" *J. Chem Thermodynamics* **32,** 107-122, (2000)
16. Ceccattini, P.D., Mussini, P.R., Mussini, T. "Thermodynamics of NaCl in aqueous ethylene glycol, acetonitrile, and 1,4-dioxane mixtures from Emf measurements at 25°C" *J. Solution Chemistry,* **26(12),** 1169-1186, (1997)
17. Templeton, C. C. "Solubility of Barium sulfate in sodium chloride solutions from 25 ° to 95°C." *J. Chem. Eng. data* **5(4),** 514-516, (1960)
18. Lide, D. R. *CRC Handbook of Chemistry and Physics*, 84th ed. (2003)
19. Mullin, J. W. *Crystallization 4th ed.*, (2001), Butterworth Heinemann

20. Hayduk, W. Malik, V.K. "Density, Viscosity, and Carbon Dioxide solubility and diffusivity in aqueous ethylene glycol solutions" *J. Chem. Eng. Data.* **16(2),** 143-146, (1971)
21. Kaasa, B, Østold, T, "Alkalinity in Oil Field Waters. What Alkalinity is and How it is Measured", *Int. Symp. Oilfield Chemistry SPE 37277*, Houston 18-21 Feb., (1997)
22. Seiersten, M., Dugstad, A., Gulbrandsen, E. "Conditions for scaling in pipelines-pH in glycol solutions", *SPE 80393, Int. Symposium on Oilfield Scale, Aberdeen*, (2003)
23. Rondinini, S., Longhi, P., Mussini, P.R., Mussini, T. "Autoprotolysis constants in nonaqueous solvents and aqueous organic solvent mixtures", *Pure & Appl. Chem.* **59(12),** 1693-1702, (1987)
24. Banjaree, S.K., Kundu, K.K., Das, M.N. "Autoprotolysis constants of ethylene glycol-water mixtures at different temperatures and related thermodynamic quantities ", *J.Chem.Soc.(A).*166-169, (1967)
25. Gärtner, R. S., Seckler, M.M, Witkamp, G-J, " Reactive Recrystallization of Sodium Bicarbonate" *Ind. Eng. Chem. Res.*, **44**, 4272-4283, (2005)
26. Gärtner, R. S., Seckler, M.M, Witkamp, G-J, " Solid Phases and their solubilities in the system Na_2CO_3+$NaHCO_3$+Ethylene Glycol+water from 50to90°C" *J. Chem. Eng. Data.*, **49**, 116-125, (2004)
27. Gärtner, R. S. *Mixed Solvent Reactive Recrystallization of Sodium Carbonate,* ISBN 90-901-6165-8, PhD Thesis, University of Delft, (2005)
28. Oosterhof, H., Witkamp, G.J., van Rosmalen, G.M. "Some antisolvents for crystallisation of sodium carbonate", *Fluid Phase Eq.* **155,** 219-227, (1999)
29. Oosterhof, H., Witkamp, G.J., van Rosmalen, G.M. "Evaporative Crystallization of Anhydrous Sodium Carbonate at Atmospheric Conditions", *ALChE* **47(10),** 2220-2225, (2001)
30. Oosterhof, H., Witkamp, G.J., van Rosmalen, G.M. "Antisolvent Crystallization of Anhydrous Sodium Carbonate at Atmospherical Conditions", *ALChE* **47(3),** 602-608, (2001)
31. Stretenskaya, N.G., "Electrical conductivity of aqueous solutions of hydrogen sulfide and the first dissociation constant of hydrogen sulfide at different temperatures", *Geochemistry Int.* 681-687, (1974)
32. Zheng, D.; Ma, W.; Wei, R.; Guo, T. "Solubility study of methane, carbon dioxide and nitrogen in ethylene glycol at elevated temperatures and pressures". *Fluid Phase Eq.*, **155(2),** 277-286, (1999)
33. Wang, L.; Chen, G.; Han, G.; Guo, X.; Guo, T.; "Experimental study on the solubility of natural gas components in water with or without hydrate inhibitor." *Fluid Phase Eq.* **207,** 143-154, (2003)
34. STATOIL data. Private communications with Baard Kaasa (May 2006)

7 pH in a mixed solvent

pH in water+MEG (Monoethylene Glycol / 1,2-ethane-diol) solutions is an important parameter. In the literature there are several publications[1-9] dealing with calibration, measurements and interpretation of pH in such mixed solvent solutions. This chapter summarizes the theoretical foundation and proposes how to handle pH in practical work. The present work is based on calibration values given by Mussini et. al.[1-3], and the calibration method is virtually equivalent with the treatment in water+methanol mixtures described by Kan.et.al[4]. All symbols are defined in Appendix 1.

7.1 Theory

It is most important to note that pH is not an absolute quantity. It has to be measured relative to a certain reference (standard solution). With a suitable choice of reference solution, any electrode should yield the same measured pH. If different electrodes are calibrated in aqueous standard solutions at 25°C and thereafter used to measure pH in another solvent at 200°C, they will most likely give very different results. This is obviously due to a bad choice of reference. Generally a pH measurement is uncertain if the test solution is much different from the standard solution in which the electrode has been calibrated. e.g. different MEG content, temperature, salt contents etc.

7.1.1 pH electrodes

A typical combined glass electrode is shown in Cell-I, where the liquid junction is indicated by double vertical lines and the boundaries of the glass membrane are indicated by single vertical lines.

Sensing electrode | test solution. || Reference electrode

(Cell-I)

Ag;AgCl;H^+(aq) | *glass* | test solution || KCl(3M);AgCl;Ag

The sensing electrode consists of a pH-responsive glass with a solution of known pH on the inside. KCl (3M) solution in contact with silver/silver chloride is a common reference electrode. To create electrical contact it is necessary to introduce a liquid junction. It is typically made of a ceramic material that allows a small flow of KCl solution from the reference electrode into the test solution. The electrode potential is according to Nernst equation given by

$$E(T) = E^o(T) + \frac{RT}{nF} \ln a_{H^+} \qquad (123)$$

$E°$ is the standard potential and is specific for each glass electrode. R, T and F correspond to the gas constant, temperature in Kelvin and the Faraday constant, respectively. n is the number of charges (in this case n=1) and a_{H^+} denotes the activity of H^+. The electrodes do not follow the Nernst slope perfectly, and to correct for the non-ideal behaviour the sensitivity, s, is introduced. Using the definition of pH, $pH = -\log a_{H^+}$, Eq. 124 is obtained;

$$E(T) = E^o(T) - s\frac{R'T}{F}pH \tag{124}$$

R' corresponds to $R \cdot ln10$, while the two unknown parameters $E°$ and s can be found by measuring E in at least two solutions with known pH. There are several commercial standard solutions available that have been given a specified pH_S (pH Standard) as described in detail by Covington et al[10] and Buck et.al[11]. A typical calibration is shown in Fig. 7.1.

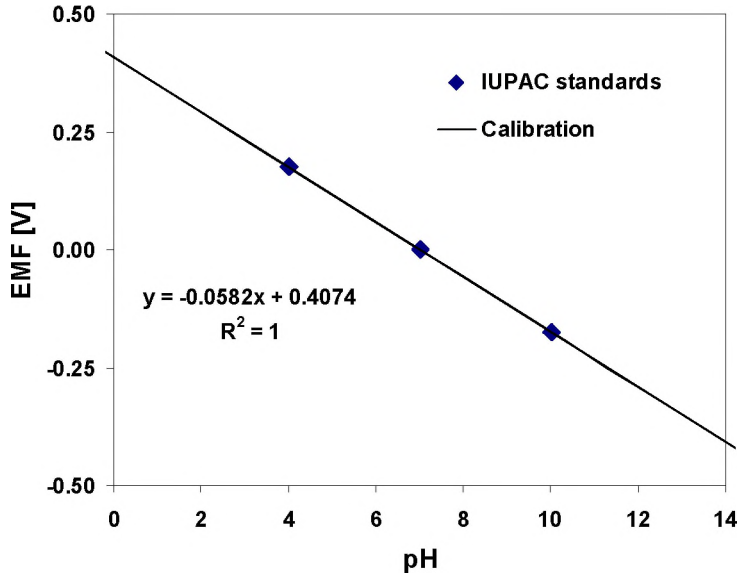

Fig. 7.1: Calibration of a pH electrode in aqueous IUPAC standard solutions at 22°C. Measured potential versus pH.

From a straight line regression, the sensitivity is found as the deviation from the Nernst slope. In this case, the sensitivity was 99.5%, which is very close to the Nernst slope (58.5mV/pH@ 22°C), showing almost ideal behaviour of the electrode. It is generally known that the glass membrane is imperfect in both ends of the pH scale[7], but in the pH range 2-12 the response is independent of pH i.e. the E versus pH slope can be regarded as constant. By assuming that $E°$ remains constant during calibration and measurement, Eq. 124 can be rearranged;

$$pH_{meas} = pH_S - \frac{sF}{R'T}(E_{meas} - E_S) \tag{125}$$

E_{meas} and E_S denote the measured potential in the unknown and standard solutions respectively. Eq. 125 can be used to calibrate in only one standard solution as long as the slope is known from a plot like Fig. 7.1. Eqs. 124-125 are included in automatic pH meters, thus the plot in Fig. 7.1 is usually not constructed by an operator. When an operator has calibrated in the aqueous standard solutions, the pH electrode gives pH_{meas}.

It is important to note that a pH meter always assumes that $E°$ is constant. This assumption is an important factor in pH measurements. It is useful to regard the standard potential $E°$ with an *inner* and *outer* contribution. The former corresponds to the inside of the electrode, and will depend on type of sensing and reference electrodes, as well as concentrations of the solutions. The latter describes the contact between the inner of the electrode and the test solution i.e. at the glass membrane and at the liquid junction. At a constant temperature the *inner* potential is truly a constant. It will remain constant as long as evaporation or other processes does not alter the KCl solution in the reference electrode (see Cell-I). The *outer* potential, however, depends on the composition of the test solution. Hence if the solution in question is much different than the calibration solution, the assumption of constant $E°$ can lead to errors. If e.g. the salinity of the test solution is much higher than in the standard (pH_S), the $E°$ changes due to a different potential across the liquid junction, $\Delta E_{LJ}°$ and possibly also over the glass membrane, $\Delta E_g°$. The actual pH of a solution can be expressed as;

$$pH = pH_S - \frac{sF}{R'T}\left[\left(E_{meas} - E_S\right) - \Delta E_g^o - \Delta E_{LJ}^o\right] \tag{126}$$

The Δ terms denote a change relative to the standard solution. It is reasonable to assume that when operating in aqueous solutions, $\Delta E_g°$, is negligible compared to $\Delta E_{LJ}°$. A pH responsive glass has a hydrated layer, thus MEG will probably have an impact on $\Delta E_g°$. Thorough discussions of these phenomena can be found in Bates[7] and Eisenman[13], but in the present work we are concerned with the net effect. Eq. 126 is combined with the pH_{meas} of Eq. 125 to obtain the expression;

$$\begin{aligned} pH &= pH_{meas} + \Delta pH_g + \Delta pH_{LJ} \\ &= pH_{meas} + \Delta pH \end{aligned} \tag{127}$$

Eq. 127 states that the actual pH of a solution equals the sum of pH_{meas} (measured pH) and the change introduced across the glass membrane, ΔpH_g, and liquid junction, ΔpH_{LJ}. During practical use it is impossible to separate the values arising at the glass membrane and liquid junction. Thus the influence of the solution on ΔpH_g, and, ΔpH_{LJ}, is included in a general ΔpH term. ΔpH describes the net effect i.e. the difference between *actual* and *measured* pH.

There exist several other types of electrodes than the KCl salt bridge type described above. Solid state electrodes will obviously not have a KCl salt bridge, while in another common type of reference the ceramic plug is replaced by a movable glass sleeve. The electrode operation is, however, the same with an *inner* and *outer* contribution to $E°$.

Solution chemistry affects the *outer* potential, which gives rise to ΔpH. In the calibration solution $\Delta pH=0$.

In this work there are two important sources for this ΔpH; salinity and MEG content. It is therefore valuable to divide the total ΔpH in two other contributions, one due to the salinity of the test solution, ΔpH_{Salt}, and one due to the MEG content, ΔpH_{MEG};

$$pH = pH_{meas} + \Delta pH_{Salt} + \Delta pH_{MEG} \tag{128}$$

Eq. 128 is used throughout this work to convert pH_{meas} to the actual pH. ΔpH_{Salt}, and ΔpH_{MEG} are determined from calibration as described in detail below. In this work it was chosen to let ΔpH_{Salt} be independent of MEG content i.e. has the same value in MEG containing solutions as in water. This is the same approach as used by Kan.et.al[4], and is discussed in further detail in section 7.3.3.

7.1.2 Salt dependence

If pH is measured in a solution with comparable ionic strength as in the calibration solutions (0.05-0.1M), ΔpH_{Salt} is virtually zero. In highly saline solutions, however, (>>0.1M) there will be a need for quantifying ΔpH_{Salt}. A change in salinity relative to the standard shifts the calibration line in Fig. 7.1 either up or down. It is not an option to add NaCl to the standard solution to obtain the desired ionic strength, since this will alter its pH_S. The ΔpH_{Salt} is given from the actual value, pH, and the measured, pH_{meas}, *as*;

$$\Delta pH_{salt} = pH - pH_{meas} \tag{129}$$

Experimentally ΔpH_{Salt} can be found by measuring pH_{meas} in a water+HCl solution as portions of NaCl are added to change the ionic strength. Thus the deviation due to salinity, ΔpH_{Salt}, is obtained given that the actual pH of the solution is either known or can be calculated.

7.1.3 MEG dependence

In a mixed solvent the issue of pH is more complex but the measuring difficulties are caused by the same problem as discussed above. The *outer* potential does not remain constant when the solvent varies. If an electrode is calibrated in aqueous solutions and thereafter used for measurements in MEG+water, the *outer* potential changes an unknown amount. If, however, the electrode is calibrated in a solution of the same MEG content (and ionic strength) as the test solution, the *outer* potential will obviously remain constant between calibration and measurement.

0.05m KHPh (Potassium Hydrogen Phtalate) buffer solutions have been extensively studied, and are designated the Reference Value pH Standard (RVS)[14]. Mussini et al.[1-3] have measured pH_{RVS} for the 0.05m KHPh buffer in MEG+water solutions. Their experimental measurements[1] have been revised in a more recent publication[3], and are the only standards available in MEG solutions at present. A function for pH_{RVS} must first of all model these measured values, as well as the pH_{RVS} of aqueous 0.05m KHPh in the desired temperature range. In addition the function must have a reasonable

extrapolation outside of the experimental data (0-70wt% MEG), since this work uses solutions of up to 99wt% MEG. The equation given by Mussini et.al[3], however, has an error in the temperature function, and a somewhat strange extrapolation at high MEG concentrations. Thus we chose to construct a new function from the aqueous data (0-95°C) given by Covington et al[10] and the above mentioned mixed solvent data[3]. Eq. 130 is of the same type as originally used by Mussini et al.[1] and generally reproduce the data within 0.005pH units.

$$\begin{aligned} pH_{RVS} &= 4.00249 + 1.0907 w_G + 0.9679 w_G^2 \\ &\quad + 0.3430 z + 0.03166 w_G z \\ &\quad - 0.8978 w_G^2 z + 7.7821 \left\{ \ln\left(\frac{T}{\theta}\right) - z \right\} \\ &\quad + 9.8795 w_G^3 \left\{ \ln\left(\frac{T}{\theta}\right) - z \right\} \end{aligned} \tag{130}$$

$z = \frac{T-\theta}{T}$, θ=298.15 and w_G is the weight fraction of ethylene glycol in the salt free solvent. The ΔpH_{MEG} term in Eq. 128 is found by measuring pH_{meas} in this KHPh standard solution, which has a given pH_{RVS} from Eq. 130;

$$\Delta pH_{MEG} = pH_{RVS} - pH_{meas} \tag{131}$$

7.1.4 Assignment of pH_{RVS}

For the purpose of further discussion it is valuable to look at how the KHPh solution is assigned a certain pH standard value, pH_{RVS}. Throughout discussion can be found in Covington et.al[10], Mussini et.al[3] and the IUPAC recommendations of 2002 from Buck et.al[11]. The silver chloride cell without transference is known as the Harned cell;

$$\mathrm{Pt} \mid \mathrm{H_2(g)} \mid \textit{solution, } H^+, Cl^- \mid \mathrm{AgCl} \mid \mathrm{Ag} \qquad \text{(Cell-II)}$$

The corresponding cell reactions are;

$$\frac{1}{2} H_2(g) = H^+ + e^- \tag{132}$$

$$AgCl(s) + e^- = Ag(s) + Cl^- \tag{133}$$

which yield the total cell reaction;

$$\frac{1}{2} H_2(g) + AgCl(s) = Ag(s) + HCl(aq) \tag{134}$$

Application of the Nernst equation yields the potential difference of the cell, E_{II}, given that the H_2 pressure is kept constant (1bar);

$$\begin{aligned} E_{II} &= E^o - \frac{RT\ln 10}{F}\log\left[a_{H^+}a_{Cl^-}\right] \\ &= E^o - \frac{RT\ln 10}{F}\log\left[\left(m_{H^+}\gamma_{H^+}/m^o\right)\left(m_{Cl^-}\gamma_{Cl^-}/m^o\right)\right] \end{aligned} \tag{135}$$

$m°=1mol/kg$ and is present simply to cancel dimensionality. $E°$ is the standard potential difference of the cell, and hence of the silver-silver chloride electrode since $\Delta G°$ for the reaction in Eq. 132 is set to 0 by definition. When $E°$ is known this cell directly measures the activity of HCl. $E°$ values determined by different groups, however, show significant inconsistencies arising from the design and preparation of the electrodes[3]. The potential difference E_{II}-$E°$ on the other hand is usually in good agreement. This is why it was decided to adopt a "reverse standardization" based on internationally accepted values of $\gamma_{\pm HCl}$. With this approach, the standard potential of Cell-II is found by filling it with HCl at a fixed molality (e.g. $m=0.01\ HCl\ mol\ kg^{-1}$);

$$\mathrm{Pt}\,|\,\mathrm{H_2(g)}\,|\,HCl(0.01m)\ |\,\mathrm{AgCl}\,|\,\mathrm{Ag} \qquad \text{(Cell-II-a)}$$

The cell gives the potential:

$$E_{II-a} = E^o - \frac{RT\ln 10}{F}\cdot 2\log\left[\frac{m_{HCl}\gamma_{\pm HCl}}{m^o}\right] \tag{136}$$

$E°$ is determined from the measured potential, $E_{II\text{-}a}$, and the mean activity coefficient of HCl, $\gamma_{\pm HCl}$, which can be obtained from the literature[11]. pH_{RVS} values of the standard KHPh buffer solution are found by filling the cell with 0.05m KHPh together with KCl;

$$\mathrm{Pt}\,|\,\mathrm{H_2(g)}\,|\,KHPh(0.05m)+KCl\ |\,\mathrm{AgCl}\,|\,\mathrm{Ag} \qquad \text{(Cell-II-b)}$$

To evaluate the measured potential of this cell, Eq. 135 is rearranged:

$$-\log\left(m_{H^+}\gamma_{H^+}/m^o\right) - \log\gamma_{Cl^-} = \frac{E_{II-b}-E^o}{k} + \log\left(m_{Cl^-}/m^o\right) \tag{137}$$

The right hand side of Eq. 137 is directly measurable and is recorded at various additions of KCl. The definition of pH (= -log a_{H+}) is usually introduced on the left hand side and the equation rewritten as;

$$pH - \log\gamma_{Cl^-} = \frac{E_{II-b}-E^o}{k} + \log\left(m_{Cl^-}/m^o\right) \tag{138}$$

Thus the quantity [pH-log γ_{Cl}] is directly obtainable, and this value is thereafter plotted versus m_{Cl} and extrapolated to $m_{Cl}=0$. The value at 0 chloride content is named "the acidity function" and written as $p(a_H\gamma_{Cl})°$ or $[pH\text{-}log\ \gamma_{Cl}]°$;

$$\left[pH-\log\gamma_{Cl^-}\right]_{m_{Cl^-}\to 0}=\left[pH-\log\gamma_{Cl^-}\right]^o=p\left(a_{H^+}\gamma_{Cl^-}\right)^o \qquad (139)$$

Then, pH_{RVS} is calculated from;

$$pH_{RVS}=\left[pH-\log\gamma_{Cl^-}\right]^o+\log\gamma^o_{Cl^-} \qquad (140)$$

$\gamma^o_{Cl^-}$ corresponds to the activity coefficient of Cl^- when the solution approaches 0 chloride content, and is an immeasurable quantity. In solutions of low ionic strength, however, it is possible to calculate it by use of a Debye Hückel equation. $\gamma^o_{Cl^-}$ is therefore by convention calculated from;

$$\log\gamma^o_{Cl^-}=\frac{-AI^{1/2}}{1+BaI^{1/2}}\ ;\ (I<0.1\ \text{mol kg}^{-1}) \qquad (141)$$

where A corresponds to the temperature dependent Debye Hückel limiting slope and I denotes ionic strength (mol/kg solvent). The factor Ba is set equal to $1.5(\text{mol kg}^{-1})^{-1/2}$ at all temperatures in the range 5-50°C, which is known as the Bates-Guggenheim convention.

The assignment of a pH standard can be summarized as follows:

- → Fill Cell-II with 0.01m HCl and measure the potential E_{II}
- → Use literature value (or calculate) for the mean ionic activity coefficient of HCl, $\gamma_{\pm HCl}$ and use this to obtain $E°$ from the measured E_{II}.
- → Fill Cell-II with 0.05m KHPh and measure [pH-log γ_{Cl}] of Eq. 138 for at least three molalities of added chloride (KCl)
- → Determine [pH-log γ_{Cl}]° by linear extrapolation to 0 chloride content
- → Calculate γ for Cl^- at zero KCl content using Eq. 141
- → Calculate pH_{RVS} by inserting log $\gamma°_{Cl}$ into Eq. 140

In water+MEG mixed solvents pH_{RVS} is measured in the exact same manner[1-3]. All solutions have the same concentrations in *mol / (kg solvent)*. The only difference is that the Debye-Hückel type equation (Eq. 141) will have different constants[1] (function of density and dielectric constant) for calculation of the activity coefficients i.e. $\gamma°_{Cl}$ and $\gamma_{\pm HCl}$ have different values than in water. $E°$ in Eq. 137-138 is written as $^{sol}E°$, when working in water+MEG solutions. The superscript, *sol*, denotes solvent. This is done to emphasize that $^{sol}E°$ has a different value for each MEG concentration, and $^{sol}E°$ is not equal to the value in water, $E°$.

7.1.5 Medium effect

When pH_{RVS} is measured in a water+MEG solution, it is done relative to the standard potential in the same water+MEG solution i.e. same MEG concentration. This potential is denoted ${}^{sol}E°$, as described above. A pH measured in water will have a different reference *(E°)* than a measurement in water+MEG *(*${}^{sol}E°$*)*. Because *pH* values at two different MEG concentrations have different references (${}^{sol}E°$) they are not directly comparable. A *pH* of 8 measured in 90wt%MEG cannot be said to be more or less acidic than a *pH* of 7 measured in 30wt%MEG or in water. It is emphasized that these measured *pH* values are actually numbers on different scales, much like measuring temperature both in terms of Centigrade and Fahrenheit without stating any connection between the two scales. Thus a direct comparison of *pH* at different MEG concentrations is meaningless. If the numbers are to be directly compared with each other, they have to be referred to the same reference. The obvious choice would be to refer all values to the pH scale in aqueous solutions. Before discussing this, it is useful to regard the activity of HCl measured in the Harned cell (Cell-II) above.

When $E°$ is known it is possible to measure the HCl activity in water i.e. relative to an *aqueous standard*. In the same way it is possible to measure the activity in a certain MEG concentration relative to ${}^{sol}E°$ *(medium standard)*. The difference between the standard *emf* in water, $E°$, and in the water+MEG mixture, ${}^{sol}E°$, defines the so-called primary medium effect[5,12,16] of the neutral HCl;

$$\ln\left({}^{w}_{sol}\gamma^{o}_{HCl}\right) = \frac{\left(E^{o} - {}^{sol}E^{o}\right)F}{RT} = \frac{\Delta G^{o}_{t}}{RT} \tag{142}$$

${}^{w}_{sol}\gamma^{o}$ corresponds to the *primary medium effect* where superscript *w* and subscript *sol* denotes that HCl is transferred from the solvent to water. This primary medium effect corresponds to a change in standard state from a *solvent* to an *aqueous* reference (see also section 2.2). This change in standard state is accompanied by a change in the Gibbs free energy, $\Delta G_t°$, where the subscript, *t*, denotes transfer. Fig. 7.2 shows the transfer of HCl from an aqueous standard state to an arbitrary water+MEG+HCl solution. This representation is equivalent with the treatment of NaCl in section 2.2. The first process going vertically down corresponds to a shift from an *aqueous* to a *solvent* standard state and is related with the *primary medium effect*. Going horizontally to the right, the activity coefficient in the water+MEG solution, ${}^{sol}\gamma$, (*=1* at infinite dilution) attains a value.

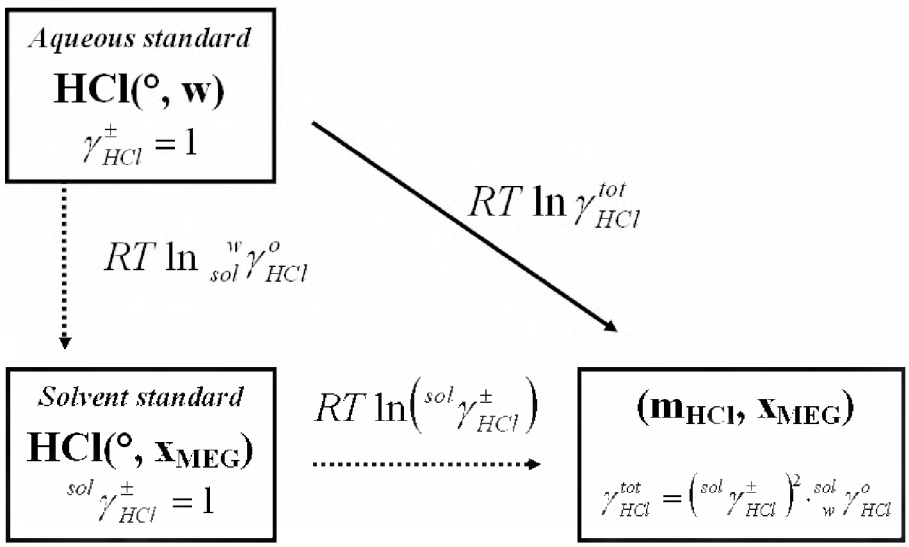

Fig. 7.2: Transfer of HCl from an aqueous standard state (°,w) to an arbitrary water+MEG+HCl solution. x_{MEG} and m_{HCl} denotes arbitrary concentrations of MEG and HCl, respectively.

The top left box (*aqueous standard)* in Fig. 7.2 is unaffected by MEG concentration, while the bottom left (*solvent standard)* changes with MEG concentration. The activities of HCl referred to a *solvent* standard, ${}^{sol}a_{HCl}$, and the *aqueous* standard, ${}^{w}a_{HCl}$, are given as:

$${}^{sol}a_{HCl} = \left(m_{HCl}\,{}^{sol}\gamma^{\pm}_{HCl}\right)^2 \tag{143}$$

$${}^{w}a_{HCl} = \left(m_{HCl}\,{}^{sol}\gamma^{\pm}_{HCl}\right)^2 \left({}^{w}_{sol}\gamma^{o}_{HCl}\right) \tag{144}$$

m_{HCl} denotes concentration (mol/ kg solvent), while the γ terms are defined above. All HCl activities can be referred to the same scale (*aqueous* scale) by introducing the *primary medium effect*, as given in Eq. 144. Activities (either ${}^{sol}a_{HCl}$ or ${}^{w}a_{HCl}$) of the neutral HCl are directly obtainable by measurements with Cell-II (relative to either ${}^{sol}E°$ or $E°$).

For pH the treatment is equivalent. The *primary medium effect* of the hydrogen ion, ${}^{w}_{sol}\gamma^{o}_{H^+}$, transforms the *solvent* referred pH, to an aqueous referred ${}^{w}pH$;

$${}^{w}pH = pH - \log {}^{w}_{sol}\gamma^{o}_{H^+} \tag{145}$$

However, at present it is impossible to use Eq. 145, because ${}^{w}_{sol}\gamma^{o}_{H^+}$ is unknown. The *primary medium effect* of the neutral HCl is measurable as described above. For pH purposes, however, this has to be separated into values for Cl^- and H^+. Thus the inability to compare pH at different MEG concentrations is due to the problem of separating ${}^{w}_{sol}\gamma^{o}_{HCl}$ into ${}^{w}_{sol}\gamma^{o}_{H^+}$ and ${}^{w}_{sol}\gamma^{o}_{Cl^-}$. No approach for this splitting is generally accepted at

present, and consequently there exists no route to directly compare *pH* at different MEG concentrations.

In the works of Bates et.al.[7,9] and Kan et.al.[4] the values measured in water+alcohol solutions are denoted *pH** to emphasize that *pH** is not directly comparable with a *pH* in water. In practical problems, however, it is usually not necessary to refer all measurements to an aqueous reference. Actual numerical values are of secondary importance as long as such data can be reproduced under identical conditions at different locations with different equipment.

7.2 Experimental

MEG (p.a. 99.9%, Acros) is hydroscopic and was analyzed for moisture with a Methrom 831 KF Karl-Fischer titration equipment. It contained less than 500ppm (0.05wt%) of water. At 4 and 25°C, combined glass electrodes of the 3M KCl ceramic bridge type (Mettler Toledo DG111-SC) and KCl(sat) type (Radiometer pHC2011-8) were used. At 50 and 80°C a special high temperature glass electrode from Innovative sensors (GT-DJ) was used.

The pH electrodes were first calibrated with standard aqueous IUPAC solutions from Radiometer (pH~ 4, 7 and 10) at temperatures 4, 25, 50 and 80°C. Then the electrodes were put into 0.05m (mole/kg solvent) solutions of Potassium Hydrogen Phtalate (KHPh) with known MEG+water concentration (0-100wt%). These MEG containing buffer solutions were prepared from dried (100°C, 3h) KHPh salt (p.a. 99.8% Merck). To evaluate ionic strength dependence of the electrodes a series of pH measurements in degassed aqueous 0.001M HCl solutions were performed. A 250ml round flask was filled with the HCl solution, equipped with a magnetic stirbar and put in a water bath at 25, 50 and 80°C. pH was measured continuously as portions (0.01-3m) of NaCl (p.a. 99.5% Merck) or KCl (p.a. 99.5% Merck) were added. The same experimental procedure was used for solutions containing MEG.

7.3 Results and Discussion

When the pH meter is calibrated in aqueous IUPAC standard solutions it measures the value pH_{meas}. Different electrode systems will give different pH_{meas} values, using otherwise identical conditions in water+MEG solutions i.e. pH_{meas} is principally not reproducible in water+MEG solutions. The following procedure therefore aims at describing a calibration method that enables reproducible measurements. It needs to be performed once for each electrode.

7.3.1 Calibration procedure

To take care of changes in MEG content the electrode is calibrated in the following way;

- → Calibrate the electrode in standard aqueous solutions (e.g. pH~4, 7 and 10). The pH electrode now gives pH_{meas}
- → Measure pH_{meas} in 0.05m KHPh solutions of varying MEG concentration e.g. 30, 50, 70 and 90wt% MEG.
- → Calculate the pH_{RVS} value of the KHPh buffer solutions from Eq. 130
- → Calculate the $\Delta pH_{MEG} = pH_{RVS} - pH_{meas}$,
- → Construct a function for ΔpH_{MEG} in an equivalent manner as given by Eq. 149

When this calibration has been performed once for a given electrode, the pH can be found from pH_{meas} using Eq. 146;

$$pH = pH_{Meas} + \Delta pH_{MEG} \tag{146}$$

The main simplification is that the procedure uses a single point calibration in MEG containing solutions. Thus it utilizes the same *pH-E* slope as obtained in water. If this does not hold it will lead to errors in pH by use of different electrode systems when well away from the pH of the buffer. The problem is solved if a second solution is defined in MEG+water solutions, but at present there is no such standard reference available. Several different electrodes were used in our laboratory, and the assumption of constant *pH-E* slope seemed to be reasonable. Temperature is another concern. pH is usually measured at room temperature, which seldom varies very much. ΔpH_{MEG} consequently remains virtually constant. At higher temperature (>40°C), however, ΔpH_{MEG} will be different. Thus for pH measurements well outside of room temperature, the calibration should be performed at the desired temperature.

Mussini et. al[1-3] did not do measurements of pH_{RVS} at concentrations higher than 70wt%MEG. This, however, does not render the approach described in this work useless at higher concentrations. Eq. 130 still gives a standard reference for the pH_{RVS} in any MEG concentration at any temperature. Reproducible results are obtained by use of any electrode as long as the same reference is used. It is noted that if other values of the KHPh buffer solution are recognised as *Standard Reference Values* (pH_{RVS}) we can simply adjust the calibration (Eq. 130), and hence also the scale model presented in this work.

At high salinities it is also necessary to quantify the salt/ionic strength effect. This effect can be found simply by measuring pH in a HCl solution as portions of NaCl are added. The solution containing 0.1mol NaCl /kg is denoted as *ref* and has a value pH^{ref}, while a solution of higher ionic strength is denoted *1* and has pH^{1}. The former gives the reference ionic strength and $\Delta pH_{Salt}=0$, but in the latter ΔpH_{Salt} has a certain value. When measuring pH_{meas} in these solutions the correlation is given as;

$$pH^{1}_{meas} - pH^{ref}_{meas} = pH^{1} - \Delta pH_{Salt} - pH^{ref} \tag{147}$$

By introducing concentration (mol/kg solvent), m, and activity coefficient, γ, of H^+ Eq. 147 is rewritten to obtain the desired ΔpH_{Salt} ;

$$\begin{aligned}\Delta pH_{Salt} &= \left(pH^{ref}_{meas} - pH^{1}_{meas}\right) + \left(pH^{1} - pH^{ref}\right) \\ &= \left(pH^{ref}_{meas} - pH^{1}_{meas}\right) + \log\frac{m^{ref}_{H^+}\gamma^{ref}_{H^+}}{m^{1}_{H^+}\gamma^{1}_{H^+}}\end{aligned} \tag{148}$$

Thus the deviation due to salinity, ΔpH_{Salt}, can be found given that the pH of the solutions are either known or can be calculated. In this work activity coefficients, γ, were calculated by a Pitzer ion interaction model as described in previous chapters. The salt dependence can be found in the following manner;

- → Prepare an aqueous HCl solution of approximately 1mM (pH~3)
- → Measure the electrode potential as portions of NaCl(s) (or KCl) are added
- → Calculate actual pH e.g. by using activity coefficients from Table 7.1 and Table 7.2.
- → Calculate ΔpH_{Salt} by use of Eq. 147-148, as relative change from a solution of 0.1mol NaCl /kg solvent.
- → Fit the measured values to an expression similar to Eq.152.

7.3.2 ΔpH_{MEG}

Each of the electrodes used during the experimental work, were given a ΔpH_{MEG} function. Eq. 149 was developed at 4-25°C for a Mettler Toledo 3M KCl bridge electrode of the ceramic disc type. For other electrodes or at higher temperatures the correlation will be slightly different.

$$\Delta pH_{MEG} = 0.327w - 0.233w^2 + 0.564w^3 \tag{149}$$

w denotes the weight fraction of mono ethylene glycol in the solvent. For practical use it is interesting to see how much variation different electrodes actually give. Fig. 7.3a) shows a comparison of the pH_{meas} and the actual pH (pH_{RVS}) of the KHPh standard solution as function of MEG. The measurements have been performed with different electrodes in our laboratory and at the Institute for Energy Technology (IFE)[15].

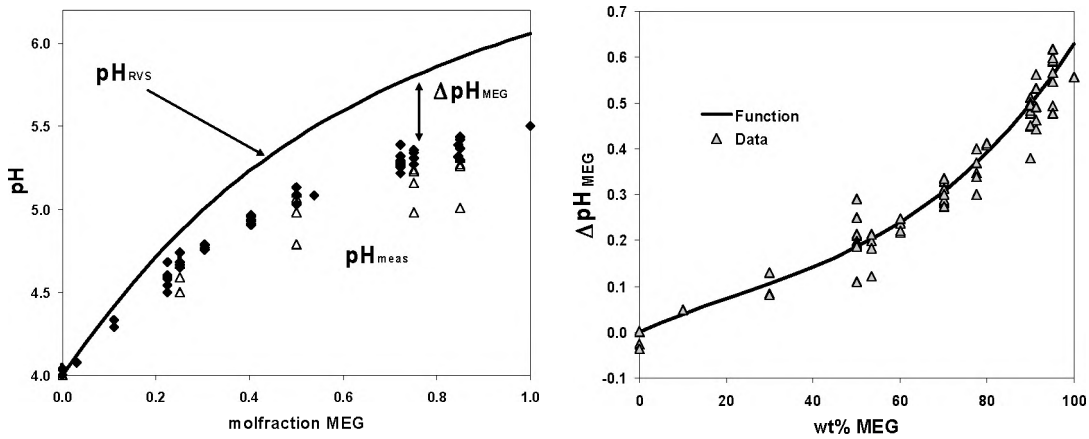

Fig. 7.3: *a)* measured pH compared to actual pH (pH_{RVS} solid line) of the KHPh standard solution at a temperature of 25°C for various glass electrodes as function of x_{MEG} ♦: Aqueous KCl bridge Δ: low temperature electrodes *b)* Corresponding ΔpH_{MEG} for KCl bridge types as function of wt% MEG.

In principle pH_{meas} varies between different electrodes. In Fig. 7.3a) this is seen as the variation between the experimental points. The solid diamonds corresponds to glass electrodes with a KCl bridge electrolyte, while the triangles are for special low temperature glass electrodes. The variations between the KCl bridge electrodes were not severe. Fig. 7.3b) shows the corresponding ΔpH_{MEG}, from the aqueous KCl electrodes of Fig. 7.3a). The solid line corresponds to the curve fit given by;

$$\Delta pH_{MEG} = 0.416w - 0.393w^2 + 0.606w^3 \qquad (150)$$

w denotes weight fraction of MEG in the solvent. Thus if no calibration is available for a given combined glass electrode with a KCl bridge, Eq. 150 provides a convenient approximation. Eq. 150 is developed for use at room temperature. Using this equation together with an arbitrary KCl salt bridge glass electrode should yield an accuracy of ±0.1-0.15pH units. There is obviously no guarantee that any glass electrode will comply with this function, and certainly not any other type of pH electrode e.g. a solid state electrode. This is clearly seen from Fig. 7.3a) where one of the low temperature electrodes shows a very different behaviour. Thus for other types than the KCl bridge glass electrode; a full calibration in the MEG containing KHPh standards should always be performed.

For some applications it may, however, be necessary to deal with pH at much higher temperatures. 10 different electrodes were used at 0-80°C in our own laboratory and at IFE[15]. These were all combined glass electrodes and from calibration of these it was developed a general ΔpH_{MEG} function;

$$\Delta pH_{MEG} = 0.7\left(\frac{T}{298.15}\right)^2 x_{MEG} \qquad (151)$$

x_{MEG} denotes molfraction of MEG in the solvent, while T corresponds to temperature in degree Kelvin. Eq. 151 should only be used if it is impossible to obtain any calibration data for a given electrode. For glass electrodes Eq. 151 is expected to give an accuracy of about ±0.3pH units at 0-100°C.

7.3.3 ΔpH_{Salt}

The electrodes are in addition influenced by a change in ionic strength; ΔpH_{Salt}. It is only necessary to quantify ΔpH_{Salt} when in a solution of high ionic strength, I>>0.1. Eq. 152 was developed at 4-25°C using combined glass electrodes of the KCl bridge type, where ionic strength was altered using NaCl. I denotes ionic strength (mole/kg solvent).

$$\Delta pH_{Salt} = -0.0467 + 0.146\sqrt{I} - 0.0224I \qquad (152)$$

The magnitude of the ionic strength dependence corresponded well with the findings of Bagg[17] and Kaasa[18]. Fig. 7.4a) shows a comparison of the measured, pH_{meas}, and actual pH of a water+HCl+NaCl solution. The difference between the lines is ΔpH_{Salt}.

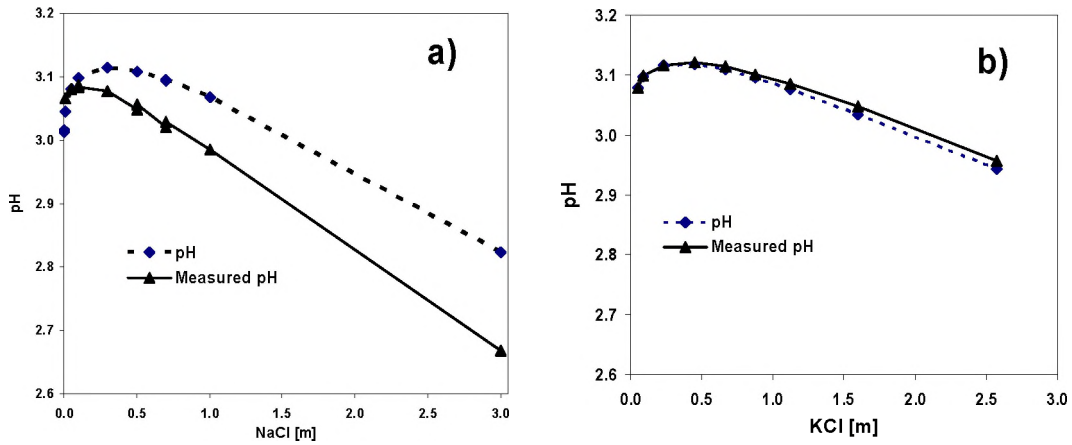

Fig. 7.4: Measured pH (pH_{meas} , ▲) compared to calculated pH (♦) in an aqueous HCl(0.001M) solution at a temperature of 22°C as function of salt content (mol/kg H_2O) *a)*NaCl from Table 7.1 *b)*KCl from Table 7.2

ΔpH_{Salt} is also salt dependent and not only ionic strength dependent as implied by Eq.152. Fig. 7.4b) shows that the pH measurement is much less influenced by KCl than NaCl. KCl additions give a measured pH that is slightly too high, contrary to NaCl where the opposite effect was observed. The solution inside the electrode is a 3M KCl solution, thus intuitively KCl should have a smaller impact on the liquid junction potential than NaCl. If many different species are present in solution, exact pH measurements at high salinities could consequently be a difficult task. When the salinity is very high, however, the salts are usually predominantly NaCl or KCl. Hence a calibration based on NaCl or KCl should give a good approximation.

The same experiments used for finding ΔpH_{Salt} in water, were also performed in water+MEG (see appendix 2). These experiments returned reproducible results that had similar magnitudes for the change in pH_{meas} as the results in water. However, the ΔpH_{Salt} cannot be found directly since the needed activity coefficients in the last term of Eq. 148 are unknown. Thus either ΔpH_{Salt} or γ_{H^+} must be known to establish the value of the other. There are two good choices to solve this problem and to obtain internal consistency in the model. Either a suitable value for γ_{H^+} is set, which will give ΔpH_{Salt} or ΔpH_{Salt} is set and γ_{H^+} follows from this choice. In this work the latter was used, hence ΔpH_{Salt} in a water+MEG solution was arbitrarily set to equal the value in water. This approximation was also used by Kan et.al.[4]. *pH* data could then be used to find the MEG dependence of the H^+ activity ($\gamma^N_{H^+}$) as described in detail in chapter 6 (see page 105-108).

7.3.4 Practical use; Reproducibility and accuracy

When the calibration has been performed once for a given electrode, the actual *pH* can be obtained from the measured pH_{meas} according to Eq. 153;

$$pH = pH_{meas} + \Delta pH_{Salt} + \Delta pH_{MEG} \tag{153}$$

The magnitude (@ 25°C) of ΔpH_{Salt} was found to be 0.07pH units at 1m of NaCl, while ΔpH_{MEG} was about 0.5 units at 90wt% MEG. Thus correct handling of the MEG dependence is regarded as the most important factor. pH measurements may vary with time, and certainly if the reference solution changed. In this work we propose that it is sufficient to determine ΔpH_{MEG} and ΔpH_{Salt} only once. The common aqueous calibration (to get pH_{meas}) is performed regularly. We have observed this to be a good procedure for electrodes that have been in use over a period of 1-2 years. The best practice would be to calibrate in a KHPh buffer with the same MEG content as the sample shortly before use. If calibration values in MEG standard solutions are not available it is possible to use the approximation of Eq. 150 (or Eq. 151). This is the less accurate approach but may, however, in some cases be the only possible option e.g. if old data are to be treated.

The response of a glass electrode is slower in water+MEG solutions than in water, and the electrode should be left at least 5-10 minutes in the solution. High salinity and high temperature makes pH measurements more difficult to reproduce, but the calibration method proposed in this work should minimize the error. During practical operation pH should generally be reproduced within 0.1-0.15pH units with any type of electrode. Best results are obtained at room temperature, but reproducibility much better than 0.05pH units (~±3mV) seems unattainable.

7.3.5 Application and testing

An important part of the scale model in this work is the calculation of the carbonic acid equilibria given in Eq. 154-155.

$$CO_2(g) = CO_2(aq) \tag{154}$$

$$CO_2(aq) + H_2O = H^+ + HCO_3^- \tag{155}$$

To verify the model pH was measured in MEG+water solutions of known $NaHCO_3$ content with continuous CO_2 bubbling of the solution (see Table 4.15). These measurements were performed with different electrodes than used for construction of the model. Such solutions with high concentration of bicarbonate are used for corrosion reduction in pipelines. The method is called *pH stabilization*[19].

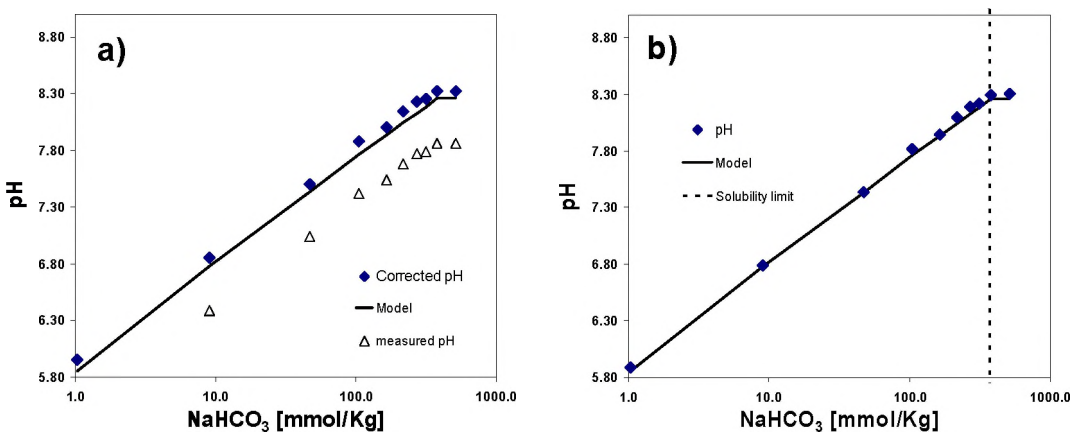

Fig. 7.5: pH in 90wt% MEG solution saturated with CO_2 at ~1atm total pressure and at a temperature of 25°C as function of $NaHCO_3$ content (mmol/kg solvent) *a)* Measured pH (pH_{meas}) compared with corrected pH from Eq. 150 *b)* pH from fully calibrated electrode (Table 4.15). Modelled pH is given by solid line, dotted line gives calculated solubility limit

Fig. 7.5 shows pH at 25°C in 90wt% MEG versus $NaHCO_3$ concentration on a logarithmic scale. In Fig. 7.5a) it is seen that pH_{meas} is systematically lower than the model line. When the pH is corrected with the ΔpH_{MEG} term of Eq. 150 it actually becomes slightly too high. This means that the electrode does not exactly follow the general Eq. 150. Fig. 7.5b) shows the results after the electrode was calibrated in MEG standards. Firstly the measurements closely resemble the model from 1mmol/kg and up to the solubility limit of sodium bicarbonate. Secondly it is noted that the breakpoint in the pH curve coincides with the scale model solubility limit.

In addition experiments with $NaHCO_3$ at 4, 50, and 80°C, and with $KHCO_3$ at 25°C were performed. The MEG concentration was either 60 or 90wt%, which are typical "rich" and "lean" MEG conditions in oilfield applications. All results are presented in chapter 10.2.1 (*see Fig. 10.2 and Fig. 10.3, Page 192*) and corresponded well with the model. Discrepancies were within 0.1pH units. Thus pH measurements were

reproduced and it was concluded that the calibration method was well suited for work in such solutions.

7.3.6 pH in corrosion models

pH is a critical parameter in many applications, and for corrosion evaluations it is very important. For corrosion rate prediction there exist several models, as described by Nyborg[20]. A common question is if the calculated *pH* in water+MEG systems from the present work can be directly used in the corrosion models. The answer is generally no because this work relies on calibration in special MEG containing KHPh solutions, and corrosion models probably do not do so. NORSOK M-506 is an empirical model[21], and requires pH as an input variable. NORSOK M-506 can adjust for the influence of glycol on the corrosion rate, because rate measurements have been performed in such solutions. When the model was made, the pH electrode was calibrated only in common aqueous standard solutions i.e. pH_{meas} was used for constructing the model. Hence pH_{meas} must also obviously be the input value, although it is principally not reproducible in water+MEG solutions. Eq. 150 (or Eq. 151) provides a convenient approximation for ΔpH_{MEG} i.e. the difference between pH_{meas} and the output *pH* of the scale model in this work. The scale model can consequently be used to calculate *pH,* which thereafter is corrected according to Eq. 146 to obtain an approximate value of pH_{meas}. This value can then be used in NORSOK M-506.

7.4 Summary chapter 7

All *pH* values in this work are referred to the 0.05m KHPh standard in the water+MEG solution at question. It is essential that a user of the model recognize this because a pH electrode calibrated only in common IUPAC aqueous standards will not give the pH value used in this work. An electrode calibrated in common aqueous standard solutions yields pH_{meas}. pH_{meas} is principally not reproducible in water+MEG solutions. This means that different electrodes will give different values for pH_{meas} in identical solutions. The actual *pH* can be found from pH_{meas} as;

$$pH = pH_{meas} + \Delta pH_{MEG} \qquad (156)$$

ΔpH_{MEG} is determined by calibration in MEG standards (0.05mol KHPh / kg solvent). This calibration has to be performed once for each electrode. For ordinary combined glass electrodes of the KCl bridge type, there are little variation between individual electrodes. Thus for such electrodes a convenient approximate for ΔpH_{MEG} has been given. Such a common ΔpH_{MEG} function gives a slightly decreased accuracy but is time saving. It also enables the use of old data in cases where it is impossible to obtain a calibration of the actual electrode that has been used.

At high salinities (>>0.1M) a pH measurement also has to be corrected for the salt/ionic strength impact on the electrode. This is included with a ΔpH_{Salt} term;

$$pH = pH_{meas} + \Delta pH_{Salt} + \Delta pH_{MEG} \qquad (157)$$

In this work it was chosen to set ΔpH_{Salt} equal to the value in water i.e. not a function of MEG concentration.

pH values are referred to the 0.05m KHPh standard with the MEG concentration at question. Theoretically this means that the numerical *pH* values obtained at different MEG concentrations are not directly comparable, because they are not on the same scale. Ideally all *pH* values should therefore be referred to the same reference. The aqueous standard state is an obvious choice. This problem is solved when internationally accepted values for the *primary medium effect* of the H^+ ion, ${}^{w}_{sol}\gamma^{o}_{H^+}$, have been set. In practical work this is not important. The primary concern is to measure the same *pH* under identical conditions at different locations with different equipment i.e. have a reproducible quantity. This is achieved with the described calibration method.

7.5 References chapter 7

1. Mussini, P. R., Marcolungo, I., Rondinini, S., Longhi, P."Acid-base equilibria and acidity scales in ethylene glycol/water solvent mixtures: recommended reference-value pH-metric standards and ionization constants for o-phthalic acid at normal and subzero temperatures" *Chim. Ind.(Milan)*, **73**, 262-268, (1991)
2. Mussini, P. R., Mussini, T. Rondinini, S. "Thermodynamics of HCl and recommendations for the standard emf of the cell hydrogen/silver chloride in ethylene glycol/water mixtures from -40 to 50°C" *Chim. Ind.(Milan)*, **73**, 190-194, (1991)
3. Mussini, P.R., Mussini, T., Rondinini, S. "reference value standards for pH measurements in D_2O and aqueous-Organic solvent mixtures: New accessions and assessments" *Pure & Appl. Chem.* **69(5),** 1007-1014, (1997)
4. Kan, A. T.; Fu, G.; Tomson, M. B. "Effect of Methanol on Carbonate Equilibrium and Calcite Solubility in a Gas/Methanol/Water/Salt Mixed System." *Langmuir*, **18(25),** 9713-9725, (2002)
5. Mussini, T., Mazza, F." Medium effects as key electrochemical variables for corrosion and electrochemistry studies in non-aqueous and mixed solvents", *Electrochimica Acta.* , **32(6)**, 855-862, (1987)
6. Mussini, T.,Covington, A. K., Longhi, P., Rondinini, S." Criteria for Standardization of pH measurements in Organic-Solvents and water+Organic solvent", *Pure Appl. Chem.* , **57(6)**, 865-876, (1985)
7. Bates, R. G., *Determination of pH. Theory and practice, 2.ed.*, (1973), John Wiley & Sons
8. Bates, R. G. "The modern meaning of pH" *Crit. rev. in analytical Chemistry,* **10(3)**, 247-278, (1981)
9. Bates, R. G., Paabo, M., Robinson, R. A." Interpretation of pH measurements in alcohol-water solvents", *J. Phys. Chem.*, **67**, 1833-38, (1963)
10. Covington, A. K., Bates, R. G., Durst, R. A." Definition of pH scales, standard reference values, measurement of pH and related terminology" , *Pure Appl. Chem.* , **57**, 531-542, (1985)
11. Buck, R.P., Rondinini, S., Covington, A.K., Baucke, F.G.K., Brett, C.M.A., Camoes, M.F., Milton, M.J.T., Mussini, T., Naumann, R., Pratt, K.W., Pitzer, P., Wilson, G.S., "Measurement of pH. definition, Standards, and Procedures" *Pure & Appl. Chem.* **74(11),** 2169-2200, (2002)
12. Elsemongy, M.M, Kenawy, I.M. "thermodynamics of hydrochloride acid in ethylene glycol+water mixtures from electromotive force measurements" *Zeit. Phys. Chemie. Neue. Folge.* **129,** 185-196, (1982)
13. Eisenman, G. *Glass Electrodes For Hydrogen and Other Cations,* (1967), Marcel Dekker Inc. New York
14. Durst, A., Koch, W.F., Wu, Y.C. "pH Theory and measurement", *Ion Selective Electrode. Rev.* **9,** 173-196, (1987)
15. Seiersten, M., Institute For Energy technology(IFE), Norway Private communications.
16. Popovych, O. "Estimation of medium effects for single ions and their role in the interpretation of nonaqueous pH" *Anal. Chem.* **38(4),** 558-563, (1966)
17. Bagg, J. "Computer calculation of liquid-junction potentials - I. Concentration profiles at junctions with concentrated potassium chloride", *Electrochim. Acta*, **35(2),** 367, (1990)

18. Kaasa, B., *Prediciton of pH, Mineral precipitations and multiphase equilibria during oil recovery*, Dr.Ing thesis, NTNU, (1998)

19. Seiersten, M., Dugstad, A., Gulbrandsen, E. "Conditions for scaling in pipelines-pH in glycol solutions", *SPE 80393, Int. Symposium on Oilfield Scale*, Aberdeen, (2003)

20. Nyborg, R. Dugstad, A. "Reliability and limitations of corrosion prediction tools for oil and gas pipelines", *EUROCORR no. 13-O-499,* Nice, France, Sept. (2004)

21. "CO_2 corrosion rate calculation model", NORSOK Standard M-506, Norwegian Technology Standard Institution, http:\\www.standard.no\petroleum, June (1998)

Table 7.1: Measured EMF and calculated ΔpH_{salt} at 25°C in water+NaCl solutions(mol/kg solvent). HCl concentration kept constant at about 0.001m

NaCl m	EMF mV	γ_{H^+}	ΔpH_{salt}
0.00	235.5	0.965	-0.060
0.01	235.4	0.901	-0.032
0.05	234.6	0.832	-0.011
0.07	234.4	0.816	-0.006
0.10	234.2	0.799	0.000
0.25	234.5	0.771	0.021
0.50	235.9	0.780	0.040
0.70	237.3	0.804	0.050
0.75	237.6	0.812	0.051
1.00	239.6	0.855	0.063
0.00	227.1	0.965	-0.062
0.10	225.9	0.799	0.000
0.50	228.2	0.781	0.049
0.70	229.9	0.808	0.063
0.00	229.0	0.972	-0.065
0.01	228.9	0.901	-0.034
0.05	228.1	0.832	-0.013
0.10	227.9	0.799	0.000
0.30	228.3	0.769	0.024
0.50	229.5	0.780	0.039
0.70	231.1	0.804	0.053
1.00	233.7	0.855	0.071
3.00	252.3	1.501	0.143

Table 7.2: Measured EMF and calculated ΔpH_{salt} at 25°C in water+KCl solutions(mol/kg solvent). HCl concentration kept constant at about 0.001m

KCl m	EMF mV	γ_{H^+}	ΔpH_{salt}
0.00	235.5	0.965	-0.024
0.04	233.4	0.835	0.002
0.09	232.2	0.801	0.000
0.23	231.2	0.766	0.002
0.45	230.9	0.763	-0.001
0.67	231.3	0.779	-0.003
0.87	232.1	0.804	-0.003
1.12	233.0	0.839	-0.006
1.60	235.2	0.924	-0.011
2.57	240.5	1.140	-0.011

8 A new method for estimation of MEG content

Transportation of hydrocarbons and water in long subsea flowlines results in new challenges to control hydrates, corrosion and scale. As the fluids cool down, water will condense and gas hydrates can form unless an inhibitor such as mono ethylene glycol (MEG) is present. To avoid hydrate formation, hence possible plug formation and transport problems, it is very important to have good control of the MEG concentration in the pipeline. The MEG concentration must therefore be regularly measured.

A commonly used method to measure MEG concentration is simply to measure the density of the solution. Since the density of MEG is greater than that of water, the MEG concentration can be found from a calibration curve. The density also depends on quantity of dissolved salts, with NaCl usually being the dominating compound. If dissolved salts are present, it will appear as if the MEG concentration is higher than it really is, and the system may not have proper hydrate protection. MEG concentration can be accurately measured by use of Gas Chromatography (GC), but usually requires that the samples are shipped to an external laboratory, unless a well equipped laboratory is available. This chapter presents a new and simple method where measurements of conductivity and density are combined to give an estimate of both MEG and salt concentration. In cases where pH stabilization[1] is used to control corrosion, the main salt component is often $NaHCO_3$ and not NaCl. If the alkalinity is measured, e.g. by titration, this can be corrected for. Most of the content in this chapter can also be found in Sandengen and Kaasa[2].

The new density data given in this chapter are also used in the model simply to recalculate concentration units i.e. *mol/L (or mg/L)* into *mol/kg*.

8.1 Theory

A density measurement is a fast, accurate and simple method for estimation of alcohol content in aqueous solutions. Fig. 8.1 shows the density of water/MEG solutions without salts at a temperature of 20 °C.

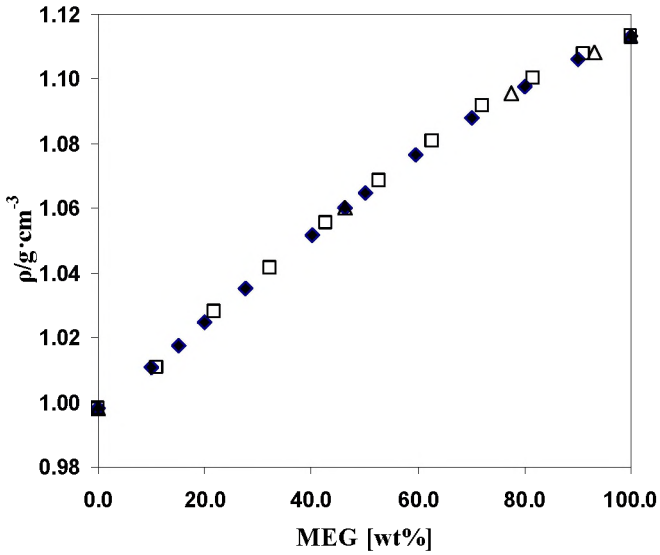

Fig. 8.1: Density of water/MEG mixtures at a temperature of 20 °C. Δ, This work; ♦, Tsierkezos et.al[3]; □, Corradini et.al[4].

From these data it is possible to relate density directly to the MEG concentration. The density of a solution is, however, also dependent on dissolved salt. Fig. 8.2 shows the density of water containing NaCl.

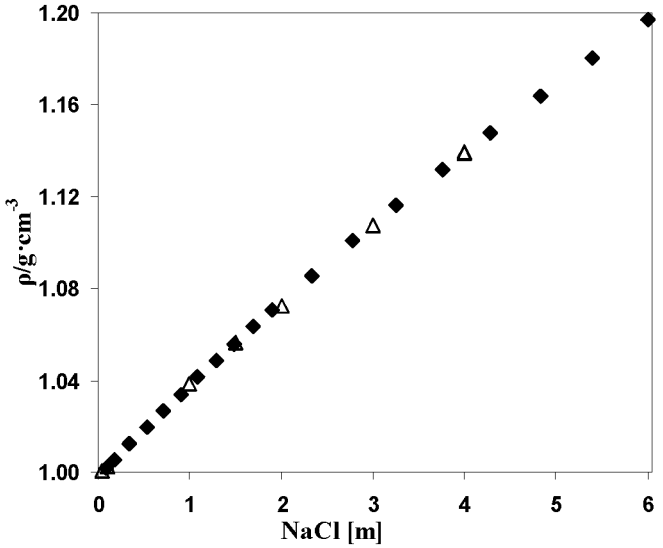

Fig. 8.2: Density of water as function of NaCl concentration(mol/kg solvent) at a temperature of 20 °C. Δ, This work; ♦, CRC Handbook[5].

Both NaCl and MEG increase the density, and a single density measurement is not sufficient to calculate the MEG concentration. One additional measurement is needed, and our choice is conductivity as it is fast and simple. Conductivity increase with the concentration of dissolved salt and is commonly used to measure salinity of waters. Fig. 8.3 shows the response in aqueous solutions as function of NaCl concentration.

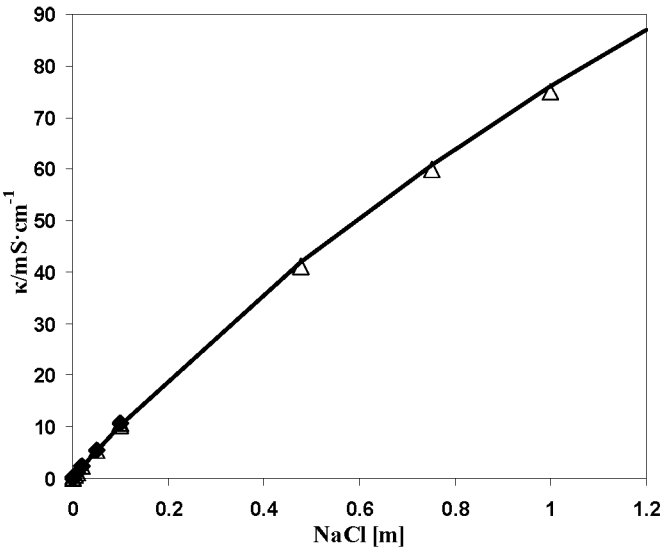

Fig. 8.3: Conductivity at a temperature of 25 °C in aqueous solutions of varying NaCl content (mol/kg solvent). The solid line gives the model in this work. Δ, This work; ♦, CRC Handbook[5].

The effect of MEG is, however, opposite as an increase in MEG concentration reduces the conductivity. Due to qualitatively different effects of MEG and salt on density and conductivity, the two measurements can be combined to calculate MEG and salt concentration in unknown samples. Refractive index measurements are also commonly used for estimation of MEG content in unknown samples. The change due to both MEG and salt is, however, very similar for density and refractive index such that a combination of the two is not suited for determination of MEG content in saline samples. It is noted that combination of refractive index and conductivity should yield good results.

8.2 Experimental

Moisture can be a problem because MEG is hydroscopic. The MEG(p.a. >99.5mass %) delivered by Merck was analyzed with a Methrom 831 KF Karl-Fischer titration equipment, and found to contain 720ppm (0.07 wt %) of water. MEG+Water solutions of concentrations between 0 and 100 weight % MEG were prepared gravimetrically in 1L screw cap bottles. These samples were thereafter degassed by use of a water jet pump. NaCl (p.a. >99.5 mass %, supplied by Merck) and MEG+water solutions were weighed into screw cap bottles with an internal volume of about 100ml to obtain samples of known salt and MEG content. Density measurements were performed with an Anton Paar DMA48(with an accuracy of ±0.1 $mg \cdot cm^{-3}$) at a temperature of (15, 20, 25 and 50) °C. The electrical conductivity was measured both by a pIONneer30 conductivity meter from Radiometer, equipped with a CDC 30T probe, and by a Hanna Instruments HI 9932. Both were calibrated with an aqueous NaCl solution having a conductivity of 1.000mS/cm at a temperature of 25 °C. The sensor was rinsed with deionised water and dried by use of pressured air, between each measurement. Temperature was measured with a built in sensor in the CDC 30T probe. The same experimental procedure was used when preparing mixtures containing $NaHCO_3$ (p.a. 99.8-100.2 %, supplied by Merck).

8.3 Results and Discussion

The uncertainties in the reported values are regarded as within ±1 mg/cm^{-3} and ± 5 % for the density and electrical conductivity respectively. This was estimated from separate measurements performed days apart by different operators. The observed variation between subsequent measurements on identical samples was similarly observed to be about ±0.3 mg/cm^{-3} and ± (2 to 3) %.

Table 8.1: Density in water(1)+MEG(2)+NaCl(3) at a temperature of (15, 20, 25 and 50) °C, and conductivity κ, at a temperature of 25°C. x=molfraction, m= mol/kg solvent.

x_2	m_3	ρ/g·cm^{-3}				κ/mS·cm^{-1}
		t=15 °C	t=20 °C	t=25 °C	t=50 °C	
0.000	0.000	0.9991	0.9982	0.9970	0.9880	0.00
0.000	0.050		1.0003			5.45
0.000	0.100	1.0033	1.0024	1.0011	0.9920	10.24
0.000	0.477					41.22
0.000	0.750					60.09
0.000	1.000	1.0392	1.0387	1.0361	1.0260	75.02
0.000	1.500	1.058	1.0563			100.21
0.000	1.953		1.0723		1.0594	118.29
0.000	2.500	1.0933			1.0779	137.74
0.000	3.000	1.1099	1.1075		1.0945	150.67
0.000	4.000	1.1414	1.1391		1.1243	175.35
0.000	5.000	1.1712		1.1662	1.1531	181.54
0.000	6.000	1.1992		1.1939	1.1810	192.94
0.000	6.000	1.1993		1.1938	1.1810	189.38
0.100	1.000		1.0735			47.35
0.100	0.500		1.0533			25.22
0.181	1.635		1.1156			48.11
0.196	2.398		1.1436			56.92
0.200	0.000	1.0627	1.0600			0.00
0.200	0.100	1.0666	1.0641			3.85
0.200	0.925	1.0974	1.0945			28.13
0.200	0.500		1.0789			17.52
0.200	1.000	1.0999	1.0968			29.67
0.200	1.014		1.0971			30.49
0.200	1.500	1.1175	1.1140			39.93
0.200	2.000	1.1343	1.1314			48.48
0.265	0.681		1.0972			17.89
0.284	1.000		1.1133			22.26
0.291	0.310		1.0872			8.38
0.310	0.970		1.1110			19.85
0.321	0.804		1.1088			16.97
0.350	0.500		1.1010			9.64
0.400	1.000		1.1236			15.65
0.409	0.559		1.1091			9.74
0.409	0.281		1.0992			5.30
0.499	0.000	1.0988	1.0954	1.0921	1.0749	0.00
0.499	0.100	1.1049	1.0992	1.0958	1.0784	1.62
0.499	0.500	1.1165	1.1146	1.1101	1.0929	6.73
0.499	1.000	1.1336	1.1308	1.1271	1.1107	11.68
0.499	1.500	1.1476	1.1472	1.1439	1.1259	14.93
0.599	1.000		1.1364			9.45
0.650	0.500		1.1213			4.64
0.650	1.000		1.1382			7.79
0.699	1.000		1.1404			7.67
0.798	0.000	1.1120	1.1082			0.00
0.798	0.100	1.1156	1.1118			0.89
0.798	1.000	1.1467	1.1432			6.11
0.998	0.000	1.1169	1.1132	1.1097	1.0921	0.00
0.998	0.100	1.1205	1.1170	1.1134	1.0960	0.73
0.998	0.250		1.1223		1.1016	1.55
0.998	0.500	1.1341	1.1310		1.1103	2.71
0.998	0.750		1.1395		1.1190	3.74
0.998	1.000	1.1507	1.1477	1.1441	1.1273	4.43

Table 8.2: Density ρ, in water(1)+MEG(2)+NaCl(3)+$NaHCO_3$(4) at a temperature of 20 °C, and conductivity κ, at a temperature of 25 °C[a]

x_2	m_3	m_4	ρ / g·cm^{-3}	κ / mS·cm^{-1}	x_2	m_3	m_4	ρ / g·cm^{-3}	κ / mS·cm^{-1}	x_2	m_3	m_4	ρ / g·cm^{-3}	κ / mS·cm^{-1}
0.000	1.000	0.050	1.0407	79.29	0.100	1.000	0.100		46.61	0.500	0.000	0.100	1.1007	1.00
0.000	1.000	0.075	1.0421	80.00	0.100	0.500	0.100	1.0601	26.93	0.500	0.900	0.100	1.1318	10.41
0.000	0.000	0.100	1.0042	6.95	0.200	1.000	0.050		29.28	0.500	0.000	0.251	1.1084	2.20
0.000	0.100	0.100	1.0083	15.73	0.200	0.000	0.100	1.0656	2.45	0.650	0.500	0.099	1.1260	4.88
0.000	0.500	0.100	1.0244	47.64	0.200	0.100	0.100		5.87	0.650	1.000	0.099	1.1429	7.83
0.000	0.900	0.100	1.0394	74.82	0.200	0.500	0.100		17.47	0.800	0.100	0.050	1.1148	1.06
0.000	1.000	0.100	1.0436	81.80	0.200	0.900	0.100	1.0988	27.16	0.800	1.000	0.050	1.1457	5.87
0.000	2.000	0.100	1.0791	135.30	0.200	1.000	0.100		30.43	0.800	1.000	0.075	1.1469	5.69
0.000	0.900	0.107	1.0398	80.48	0.200	0.000	0.250	1.0738	5.62	0.800	0.100	0.100	1.1173	1.32
0.000	0.100	0.150	1.0113	18.45	0.200	0.100	0.250		8.57	0.800	1.000	0.100	1.1480	6.01
0.000	1.000	0.150	1.0464	82.75	0.200	1.000	0.250		30.34	0.800	0.000	0.100	1.1137	0.53
0.000	2.000	0.200	1.0841	135.67	0.200	0.749	0.251	1.1010	25.17	0.800	0.900	0.100	1.1446	5.69
0.000	0.000	0.250	1.0131	15.65	0.200	0.500	0.100	1.0844	18.80	0.800	1.000	0.150	1.1505	5.86
0.000	0.100	0.250	1.0171	24.34	0.200	1.014	0.050	1.0995	31.46	0.800	0.000	0.250	1.1213	1.11
0.000	0.749	0.250	1.0421	70.46	0.200	0.100	0.100	1.0693	6.19	0.800	0.100	0.250	1.1248	1.77
0.000	1.000	0.250	1.0521	85.32	0.200	1.014	0.100	1.1020	31.81	0.998	1.000	0.050	1.1500	4.21
0.000	0.100	0.300	1.0200	26.11	0.200	0.100	0.250	1.0765	9.02	0.998	0.000	0.100	1.1183	0.39
0.000	2.000	0.300	1.0890	137.51	0.200	1.014	0.250	1.1106	33.80	0.998	0.100	0.100	1.1218	0.92
0.000	0.100	0.400	1.0257	30.91	0.200	0.100	0.400	1.0855	10.73	0.998	0.900	0.100	1.1489	4.06
0.000	1.000	0.400	1.0604	89.71	0.350	0.500	0.100	1.1062	10.33	0.998	1.000	0.100	1.1524	4.37
0.000	2.000	0.400	1.0939	139.39	0.350	1.000	0.100		17.42	0.998	0.000	0.250	1.1258	0.81
0.000	0.100	0.450	1.0286	32.91	0.500	0.100	0.050	1.1018	1.91	0.998	0.100	0.250	1.1293	1.32
0.000	0.000	0.500	1.0274	28.07	0.500	1.000	0.050	1.1333	11.06	0.998	0.750	0.250	1.1510	3.60
0.000	0.500	0.500	1.0467	61.23	0.500	1.000	0.075	1.1346	11.22	0.998	1.000	0.250	1.1597	4.21
0.000	0.100	0.600	1.0369	38.56	0.500	0.100	0.100	1.1043	2.21	0.998	0.100	0.400	1.1366	1.36
0.000	0.000	0.750	1.0413	37.25	0.500	0.500	0.100	1.1187	6.92	0.998	1.000	0.400	1.1668	4.07
0.000	0.100	0.750	1.0452	45.41	0.500	1.000	0.100	1.1358	11.22	0.998	0.000	0.500	1.1377	1.35
0.000	1.000	0.750	1.0795	96.65	0.500	0.100	0.250	1.1121	3.18	0.998	0.500	0.500	1.1543	3.06
0.000	0.000	1.000	1.0547	48.06										

[a] MEG concentration is given as mole fraction in the salt-free solvent, and the salt concentrations as molality m: mol/kg of solvent.

Table 8.3: Parameters for density ρ, and conductivity κ, functions

ρ/g·cm^{-3}	Value at 15 °C	Value at 20 °C	κ/mS·cm^{-1}	Value
ρ_{MEG}	1.1169	1.1134	p_1	107.5206
ρ_{water}	0.9991	0.9982	p_2	-28.6272
d	0.111916	0.109695	p_3	-0.0203
e	0.214501	0.209660	q_1	-3.7396
s_1	0.040247	0.040247	q_2	4.6799
s_2	-0.001214	-0.001214	r_1	8.0765
s_3	-0.005082	-0.005082	r_2	-3.7272
b_1	0.059715	0.059715	r_3	0.0714
b_2	-0.003501	-0.003501	h_1	2.9046
b_3	-0.009626	-0.009626	h_2	-3.0756
			l_1	64.2160
			l_2	-16.1611
			l_3	-0.7572
			l_4	7.0495

8.3.1 H_2O+MEG+NaCl

Experimental results for density and electrical conductivity for water+MEG+NaCl mixtures are given in Table 8.1. The MEG concentration is given as mole fraction and the NaCl molality as mol/kg solvent where the solvent is the salt free water+MEG.
Based on the experimental and literature data[3-9], functions for density and conductivity of (water+MEG+NaCl) mixtures were fitted. The density function is given in Eq.158.

$$\begin{aligned}\rho = &\left(x_{MEG}\rho_{MEG} + x_{H_2O}\rho_{H_2O}\right) \\ &+ dx_{MEG}x_{H_2O} + ex_{MEG}x_{H_2O}^3 \\ &+ \left(\left(s_1 + s_3\sqrt{x_{MEG}}\right)m_{NaCl} + s_2 m_{NaCl}^2\right)\end{aligned} \tag{158}$$

where x_i is the mole fraction of pure water or MEG. ρ_i is the density of pure water or MEG and m_{NaCl} is NaCl concentration(mol/kg solvent), which equals the ionic strength. The parameters d and e are used to calculate the density of the salt free (water+MEG) and the parameters $s_{1\text{-}3}$ include the effect of salt on the density. The values of all the parameters are given in Table 8.3. Temperatures of (15 and 20) °C were chosen because density is normally measured at one of these temperatures. Literature data and experimental data are generally reproduced by Eq.158 to within 0.001 g·cm^{-3}. The conductivity measurements were fitted to a 3-parameter equation.

$$\kappa = \left(K_1 \cdot e^{K_2}\right)x_{H_2O}^2 + K_3 x_{MEG}^2 \tag{159}$$

where K_1 is the conductivity of an aqueous solution, as given in Eq. 160 where the first two terms have the same form as the Debye-Hückel-Onsager equation[5], while the 3rd order term was added to fit the data at high concentrations. K_3 is a similar expression

that corresponds to conductivity in pure MEG, while K_2 gives the mixing of water/MEG. The curve fitted parameters *p, q* and *r* are given in Table 8.3.

$$K_1 = p_1 m_{NaCl} + p_2 m_{NaCl}^{3/2} + p_3 m_{NaCl}^3 \tag{160}$$

$$K_2 = q_1 x_{MEG} + q_2 x_{MEG}^2 \tag{161}$$

$$K_3 = r_1 m_{NaCl} + r_2 m_{NaCl}^{3/2} + r_3 m_{NaCl}^3 \tag{162}$$

Since conductivity is strongly temperature dependent, a reference temperature must be used. In this work it was chosen to refer all measurements to a temperature of 25 °C. The measured conductivity κ_t at temperature t, was therefore corrected using Eq. 163 to κ_{25} which is the conductivity if the measurements had been done at a temperature of 25 °C. Most commercially available conductivity meters have built in functions to do such temperature corrections from the actual temperature to a selected reference temperature.

$$\kappa_{25C} = \kappa_t + \frac{0.00054t^2 - 0.0669t + 3.381}{100} \kappa_t \cdot (25 - t) \tag{163}$$

Because of the strong temperature dependence, it is recommended to measure conductivity at a temperature close to the reference. It was observed that conductivity measurements were much more liable to give a random error than the density measurements. Two subsequent measurements in identical solutions could give a variation in conductivity of as much as 5 %.

With the above expressions for density and conductivity, 3-dimensional graphs of density and conductivity as function of MEG and salt concentration were constructed and are shown in Fig. 8.4.

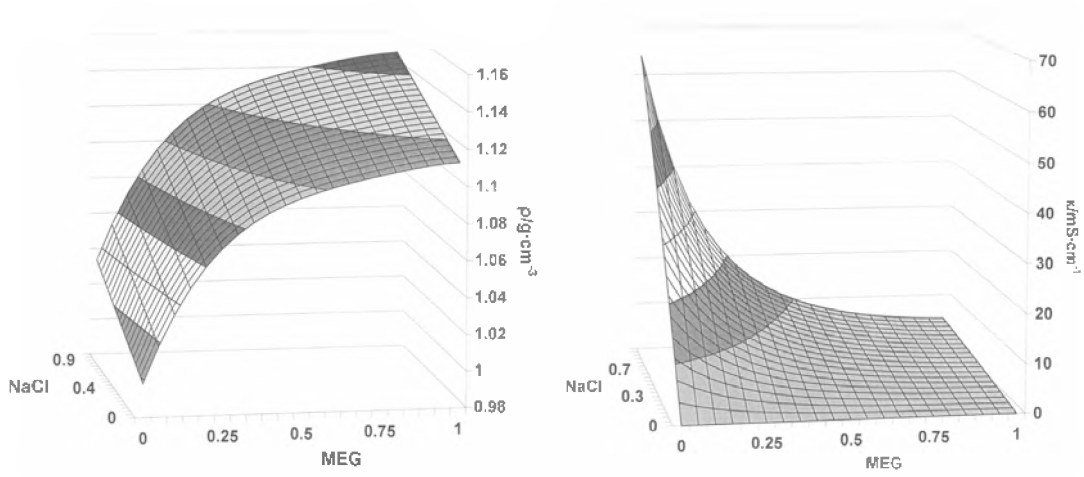

Fig. 8.4: Conductivity κ, at a temperature of 25 °C, and density ρ, at a temperature of 20 °C as function of MEG [molfraction] and NaCl [mol/kg solvent]

From the graphs, it is easy to see the qualitatively different behaviour in density and conductivity with respect to MEG and salt concentration. When the density is measured, this gives a line in the salt-MEG plane. The conductivity gives another line with opposite curvature in the salt-MEG plane. The point where these two lines intersect determines both the MEG and salt concentration of an unknown sample.

8.3.2 Computer modeling

When density and conductivity are measured, Eq. 158 and 159 have to be solved to find the MEG and salt concentrations. The simplest, but not very robust method is to use the "Solver" option in Excel. This gives fast and accurate results when a good start estimate is given. A more robust method is to solve Eq. 158 with respect to the NaCl concentration as a 2nd order equation and insert it into Eq. 159. The system is then easily solved using either the "Goal Seek" function in Excel or by performing numerical iteration with respect to the MEG fraction using the by section method.

8.3.3 Presence of other species

Formation waters contain several other species, typically K^+, Mg^{2+}, Ca^{2+}, Ba^{2+} etc. These species have different molecular weight and mobility, hence have a different quantitative impact on solution density and conductivity. However, in most formation waters, NaCl contributes with typically 90 % of the ions, thus the model is very little affected by other species. In addition it is noted that the output of the model should be interpreted in terms of ionic strength rather than NaCl concentration directly. Thus ionic strength will be a measure of all ions in solution as if they were NaCl i.e. NaCl equivalents. If for example some of the NaCl is replaced with $CaCl_2$, but keeping the ionic strength constant, the density and conductivity will change very little and in such a way that the calculated MEG concentration will remain virtually unaffected. This was confirmed by making a solution containing 77.5 wt% MEG, with an ionic strength of 1mol/kg where 10 % of this came from $CaCl_2$ and the rest from NaCl. From the measured density and conductivity, the model predicted the MEG concentration at 76.2 wt% and that the ionic strength was 0.965mol/kg. This is within the accuracy of the method. As a curiosity, it is noted that the density (1.1301 g·cm^{-3}) of this test solution is higher than the density for pure MEG (1.1169 g·cm^{-3}). Thus, using only density to estimate MEG concentration would in this case give a meaningless result. This clearly demonstrates the effectiveness of linking density and conductivity in a model to calculate MEG concentration and salt content.

8.3.4 H_2O+MEG+NaCl+$NaHCO_3$

One system will be given special attention. In cases where pH stabilization[1] is utilized for corrosion control there can be significant amounts of $NaHCO_3$ present, and perhaps very little other salts. Because $NaHCO_3$ has slightly different effect on both density and conductivity than NaCl, the model was expanded such that Na^+ is still the dominating cation, while both Cl^- and HCO_3^- are dominating anions. Table 8.2 summarizes additional measurements of density and conductivity with both NaCl and $NaHCO_3$ present in the solution. The presence of $NaHCO_3$ will shift the surfaces in Fig. 8.4 upwards, but their qualitative shape will remain unchanged.

The bicarbonate concentration can easily be found from an alkalinity titration[10] and can therefore be regarded as a known value. To model the effect of bicarbonate on the density, additional terms were added to Eq. 158.

$$\begin{aligned}\rho = &\left(x_{MEG}\rho_{MEG} + x_{H_2O}\rho_{H_2O}\right)\\ &+ dx_{MEG}x_{H_2O} + ex_{MEG}x_{H_2O}^3\\ &+ \left(s_1 + s_3\sqrt{x_{MEG}}\right)m_{NaCl} + s_2 m_{NaCl}^2\\ &+ \left(b_1 + b_3\sqrt{x_{MEG}}\right)m_{NaHCO_3} + b_2 m_{NaHCO_3}^2\end{aligned} \tag{164}$$

Where $b_{1\text{-}3}$ are empirical parameters given in Table 8.3 and m denotes concentration in mol/kg solvent. The expression for the conductivity in Eq. 159 is unchanged, but $NaHCO_3$ gives additional terms to parameters K_1 and K_3.

$$\begin{aligned}K_1 = &\, p_1 m_{NaCl} + p_2 m_{NaCl}^{3/2} + p_3 m_{NaCl}^3\\ &+ l_1 m_{NaHCO_3}\exp\left(l_3 m_{NaCl}\right) + \left(l_2 + l_4 m_{NaCl}\right)m_{NaHCO_3}^2\end{aligned} \tag{165}$$

$$\begin{aligned}K_3 = &\, r_1 m_{NaCl} + r m_{NaCl}^{3/2} + r_3 m_{NaCl}^3\\ &+ h_1 m_{NaHCO_3}\exp\left(h_2 m_{NaCl}\right)\end{aligned} \tag{166}$$

A measured alkalinity (HCO_3^- concentration) is normally in mol/litre solution or mol/kg solution. The above models, however, require the concentrations to be in mol/kg solvent. The following formula can be used to recalculate alkalinity from molarity to molality

$$alk[mol/Kg] = \frac{alk[mol/L]}{\rho - \sum C_i \cdot Mw \cdot 10^{-3}} \tag{167}$$

$\rho/g{\cdot}cm^{-3}$ denotes the density of the solution, while $C/mol{\cdot}L^{-1}$ and $Mw/g{\cdot}mol^{-1}$ corresponds to concentration and molecular weight of dissolved species respectively. This recalculation requires an estimate for the unknown concentration C of all species.

A simple iteration procedure is as follows; solve the model using the measured alkalinity; insert the calculated NaCl concentration and measured alkalinity in Eq. 167 to recalculate the alkalinity; and, reapply the model with the updated alkalinity; iterate until convergence (2-3 cycles). The effect of using the uncorrected alkalinity is, however, small and will give a slightly too high estimation of NaCl content, but MEG estimation will remain virtually unchanged.

8.4 Model testing and Application

Testing was performed on the 5 synthetic solutions and the oilfield sample given in Table 8.4. The oilfield sample had a MEG content known from Gas Chromatography (GC) analysis. Bicarbonate content was analyzed by use of an HCl alkalinity titration[10], and the MEG and salt concentration calculated using the above equations.

Table 8.4: Test solutions[a]. Density ρ, in water(1)+MEG(2)+NaCl(3)+$NaHCO_3$(4) at a temperature of 20 °C, and conductivity κ, at a temperature of 25 °C.

#	w_2	m_3	m_4	ρ/g·cm^{-3}	κ/mS·cm^{-1}
1	50.86	0.574	0.095	1.0929	17.17
2	17.32	0.698	0.118	1.0551	44.17
3	45.39	0.380	0.013	1.0743	13.12
4	73.74	0.585	0.046	1.1155	8.64
5	42.43	0.248	0.017	1.0671	9.79
6*	57.94	-	-	1.0745	0.13

*Oilfield sample from separator. MEG content measured with Gas Chromatography (GC). Salt content is unknown.
^ MEG concentration w_i is given as weight % in the salt free solvent, and the salt concentrations as molality m_i mol/Kg solvent.

Table 8.5: Results for test solutions; water(1)+MEG(2)+NaCl(3)+$NaHCO_3$(4). e_2 denotes error in MEG determination and e_3 error in the NaCl determination.

#	w_2/(wt %)	m_3/(mol·kg^{-1})	m_4/(mol·kg^{-1})	e_2/(wt %)	e_3/(%)
1	51.4	0.56	0.096	0.5	-3.0
2	19.1	0.66	0.117	1.8	-5.6
3	45.6	0.38	0.013	0.2	0.0
4	72.7	0.59	0.047	-1.0	0.3
5	43.5	0.25	0.017	1.1	2.5
6	57.1	0.01	-	0.8	-

From the results given in Table 8.5, it is seen that the calculated MEG content was within ± 2 wt %. Estimation of NaCl content was generally good, although one measurement showed as large error as (5 to 6) %. The accuracy of the model is generally ± (2 to 3) wt % for the estimation of MEG content, while it can vary as much as 10 % in the estimation of ionic strength. The most interesting systems typically have MEG concentrations of (40 to 90) wt %. In this range, the model has accuracy better than ± 2 wt% units and ionic strength is generally within (5 to 6) %. To obtain the best result density should be measured at a temperature of 20 °C and conductivity close to the reference temperature of 25 °C. Conductivity measurements are regarded as the most uncertain analysis. This is both due to random error, but also due to it being based on a one point calibration. Thus there exists a possibility for systematic error if the test solution is significantly different from the standard of 1ms/cm. It is noted that the model is developed for cases when NaCl and/or $NaHCO_3$ are the dominating salt species.

8.5 Summary Chapter 8

New experimental measurements of density and conductivity have been performed in mixed water+MEG+NaCl+$NaHCO_3$ solutions. A model based on this data set enables an estimate for both MEG concentration and salt content merely from the density and conductivity of a solution. If also the alkalinity is measured, the model can separate between $NaHCO_3$ and other salts. The model is valid in the whole concentration interval of 0 to 100 wt% MEG and with ionic strengths from zero to the solubility limits of NaCl and $NaHCO_3$. At intermediate MEG concentrations (40 to 90wt%) the accuracy of the model is regarded as ±2 wt % for calculation of MEG content.

8.6 References chapter 8

1. Olsen, S.; Lunde, O.; Dugstad, A.; Stabilizing pH in Troll pipelines solves glycol-regeneration problems, *Oil & Gas Journal* **1999**, 97(26), 59-62
2. Sandengen, K., Kaasa, B. "Estimation of Monoethylene Glycol (MEG) Content in Water + MEG + NaCl + $NaHCO_3$ Solutions", *J. Chem. Eng. Data* **2006,** 51, 443-447
3. Tsierkezos, N. G.; Molinou, I.E; Thermodynamic Properties of Water + Ethylene Glycol at 283.15, 293.15, 303.15, and 313.15 K. *J. Chem. Eng. Data* **1998,** 43, 989-993
4. Corradini, F.; Franchini, G.; Marcheselli, L.; Tassi, L.; Tosi, G; The ethane-1,2-diol/water solvent system: densities and excess molar volumes at various temperatures. *Aust. J. Chem* **1993,** 46, 243-251
5. Lide, D.R; *CRC Handbook of chemistry and physics*, 71st ed. Chemical Rubber Co. **1990**
6. Bagrovskaya, N. A.; Schmukler, L. E.; Lilin, S. A.; Physicochemical properties of water-alcoholic solutions of sodium chloride. *Russian Journal of Applied Chemistry* **1996,** 69(6), 914-915
7. Khimenko, M. T.; Gritsenko, N. N.; Volumetric and dielectric properties of ethylene glycol and diethylene glycol solutions in water, acetone, and methanol. *Russian Journal of Phys. Chem.* **1977,** 51(2), 275-277
8. Fogg, E. T; Hixon, N. A.; Thomson, A. R.; Densities and refractive indexes for ethylene glycol-water solutions *Anal. Chem.* **1955,** 27(10), 1609-11
9. Roberts, J. A.; Zhang, X.; Zheng, Y.; Determination of hydrogen bonding in water clusters through conductivity (dc) measurements of aqueous solutions of sodium chloride. *J. Chem. Phys.* **1994,** 100(2), 1503-10
10. Kaasa, B.; Østvold, T.; Alkalinity in Oil Field Waters. What alkalinity is and how it is measured. SPE37277, *Int. Symp. Oilfield Chemistry, Houston*, **1997**.

9 Magnesium Carbonate compounds

Reservoir waters may contain significant amounts of dissolved Mg^{2+}, but magnesium carbonate scales are normally not observed during oil recovery. When using MEG regeneration, solutions are circulated and salts accumulate in the system. Thus magnesium content may be high in the alkaline "lean MEG" stream. It was therefore decided to investigate magnesium carbonate solubility in water+MEG systems. "Lean MEG" refers to a solution lean in water i.e. with high MEG concentration, typically around 90wt%.

Magnesium carbonate solubility in water has been reported in the literature[1-8], but at present there are no data available in water + MEG solutions. The Mg-CO_2-H_2O-MEG system is complex, due to magnesium carbonate having several meta-stable phases. Pure magnesium carbonate ($MgCO_3$) is named magnesite, and is assumed to be the thermodynamically stable phase (0-80°C). Hydromagnesite ($3MgCO_3 \cdot Mg(OH)_2 \cdot 3H_2O$) is the second most stable in the same temperature range. Other phases have higher solubility in water.

In an attempt to measure the solubility of magnesium carbonate in water+MEG solutions, different phase modifications were bought from different commercial suppliers. An X-Ray diffraction (XRD) analysis did, however, show that the material claimed to be magnesite actually was hydromagnesite. It was therefore necessary to develop a method to synthesize magnesite.

9.1 Theory

Solid magnesium carbonate can exist in several modifications. The phases regarded in this work are:

→ **lansfordite**	$MgCO_3 \cdot 5H_2O$
→ **nesquehonite**	$MgCO_3 \cdot 3H_2O$
→ **hydromagnesite**	$3MgCO_3 \cdot Mg(OH)_2 \cdot 3H_2O$
→ **magnesite**	$MgCO_3$

Königsberger et.al[2] used the notation $4MgCO_3 \cdot Mg(OH)_2 \cdot 4H_2O$ for hydromagnesite, but in this work the $3MgCO_3 \cdot Mg(OH)_2 \cdot 3H_2O$ notation of Marion[1] was chosen. A literature survey[1-8] showed that the relative solubility in water is expected to change with temperature according to Fig. 9.1

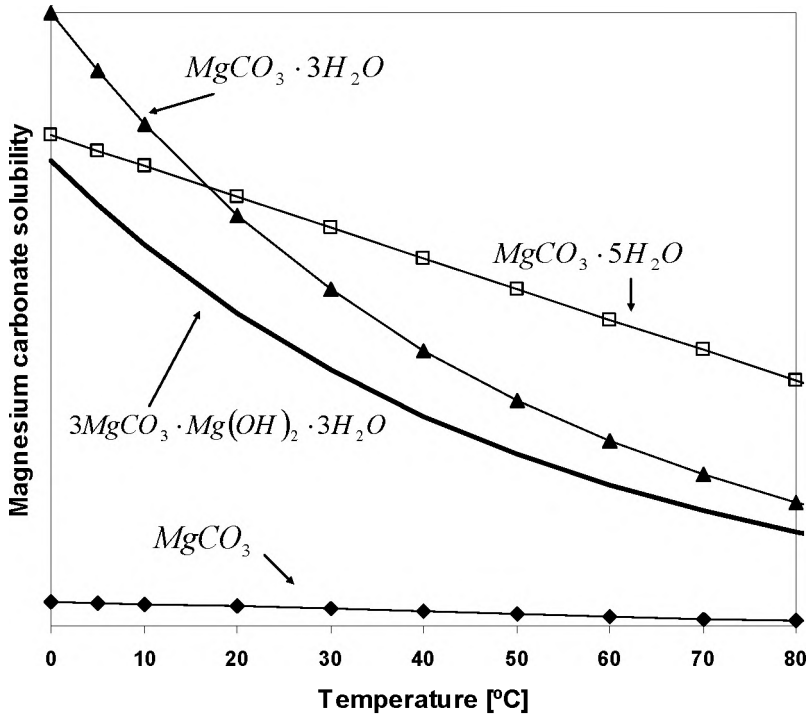

Fig. 9.1: Schematic of relative aqueous solubility[1-8] of various magnesium carbonate phases versus temperature. (P_{CO2} ~1 atm)

The lowest solubility gives the thermodynamically stable phase, which for all temperatures should be magnesite. Lansfordite and nesquehonite do not become more stable than hydromagnesite for $0 < T(°C) < 80$. It is, however, stated[1,2] that both lansfordite and nesquehonite are kinetically stabilized. Thus transformation to hydromagnesite does not occur at room temperature. Transformation in this work denotes simultaneous dissolution of the less stable and precipitation of the most stable solid phase. Kinetics of dissolution/precipitation is generally faster at high temperature[9]. Both nesquehonite and lansfordite should rapidly disappear at temperatures above 50-60°C. Precipitation of magnesite is similarly kinetically inhibited; thus hydromagnesite will be stable in aqueous solution for a long period of time, even at temperatures approaching 100°C. Solubility of magnesite at room temperature (P_{CO2}~1atm) has been found to be about 2-2.5mmol/kg water[5]. This solubility is actually much lower than Calcite ($CaCO_3$) and comparable to Siderite ($FeCO_3$). Sea water is generally slightly supersaturated with $CaCO_3$ but also contains a higher Mg^{2+} than Ca^{2+} concentration. Thus it should have a large magnesite supersaturation. Because $MgCO_3$ is normally not formed, this supports the statement that the reaction is kinetically inhibited.

Synthesis of magnesite[5] has usually involved temperatures above 100°C using steel autoclaves, although some investigators have been able to produce the solid down to 50-60°C. These low temperature methods usually involve either high pressure and/or high concentration of NaCl to lower the water activity.

9.2 Experimental

Three solid $MgCO_3$ phases were used during this work: magnesite ($MgCO_3$), nesquehonite ($MgCO_3 \cdot 3H_2O$) and hydromagnesite ($3MgCO_3 \cdot Mg(OH)_2 \cdot 3H_2O$). The latter was available from a manufacturer (Merck, z.a) while the other two were synthesized in our lab. The other chemicals were supplied by Merck (p.a. quality) unless otherwise stated. Titrisol ampoules from Merck were used for titration purposes. Phase analysis was performed using X-ray diffraction (XRD). MEG + water + NaCl stock solutions were prepared gravimetrically in 1L screw cap bottles (0 and 0.5m NaCl)

CO_2 was bubbled through the solutions with a flow rate of 20-50ml/min. The gas was passed through cleaning bottles with the same MEG+water+NaCl content as the sample before the inlet of the reaction flask. This was done to minimize evaporation of solvent during the experiments. CO_2 partial pressure was calculated by subtracting MEG+water vapour pressure from the atmospheric pressure. Literature data[13-17] for vapour pressure are only available in salt free solution. When salt was present it was decided to simply calculate the water+MEG vapour pressure according to Raoult's law. i.e vapour pressure is proportional to the mole fraction of solvent, which is slightly reduced in the presence of salts. The solutions in this work were not highly saline and the influence on the vapour pressure was therefore generally negligible. The uncertainty in the CO_2 pressure determination was estimated to ±0.01bar.

9.2.1 Nesquehonite synthesis

~80g $MgCl_2 \cdot 6H_2O$ was dissolved in 0.5L distilled water with continuous stirring and CO_2 (AGA, 4.0) bubbling at 25°C. ~60g solid $NaHCO_3$ was gradually added within a few minutes. The solution was magnetically stirred on a water bath (25°C) for approximately 24 h. The resulting precipitate was filtered using (Schleicher & Schuell, Black Ribbon paper) a Büchner funnel, and washed with distilled water and absolute ethanol. The precipitate was confirmed as nesquehonite using XRD analysis. No secondary phases were found.

9.2.2 Magnesite synthesis

Hydromagnesite (5-10g, solid) was added to a three-neck round flask containing a MEG + water solution (~250g,). Water cooled reflux was utilized to ensure that the solvent did not evaporate. The mixture was magnetically stirred under continuous CO_2 bubbling. Two successful experiments were performed: 90wt% MEG with 0.5m NaCl stirred for 7 days at 120±5°C and 95wt% MEG with 1m NaCl stirred for 3 days at 150±5°C. The resulting solid was collected as for nesquehonite, and confirmed to be magnesite by XRD.

Two other tests did not yield magnesite; 95wt% MEG with 1m NaCl stirred for 3 days at 160-163°C(boiling point) and ~100%MEG with no salt stirred for 4 days at 120±5°C. For the latter it was not necessary to use reflux due to the vapour pressure of the solvent being very low (~0.05bar)

9.2.3 Solubility

Solubility experiments were conducted in three-neck round flasks. The flasks were filled with 250-300g of the MEG+H_2O stock solution (0-97.5wt% MEG) and put on a water bath for temperature control (25-80°C). CO_2 was continuously bubbled through the solution with the flask being open to atmospheric pressure. Excess solid magnesium carbonate was added after the temperature had stabilised (~5g hydromagnesite or nesquehonite, ~0.5g magnesite) and stirred for 1-14 days. Precipitation of hydromagnesite (80°C) was achieved by dissolving the solid at 40°C and thereafter raising the temperature of the solution. Some solid hydromagnesite was left undissolved at the lowest temperature.

Precipitation of magnesite was attempted in aqueous solution of $NaHCO_3$ (~20mmol/kg) and $MgCl_2$ (~20mmol/kg) with CO_2 bubbling. Two samples were set up at each temperature; one with magnesite seed crystals (~0.1g) and one without. The solutions were stirred for 10 days at 25°C and 4 days at 80°C respectively.

Preliminary experiments (see Table 9.2) were conducted at room temperature using 500mL glass bottles. The solutions were prepared as above, but contained 0.5mol NaCl/ kg solvent. CO_2 was bubbled through the solution for about an hour at the start of the experiment. Thereafter the solutions were flushed with CO_2 for about ten minutes daily. Between CO_2 flushing, the solutions were corked and magnetically stirred.

9.2.4 Analysis

Samples (10-25g) were withdrawn with a plastic syringe and filtered through 0.2μm syringe mounted filters (Schleicher & Schuell). When the magnesium carbonates are dissolved, alkalinity equals twice the Mg^{2+} concentration. Alkalinity could be measured using Mettler Toledo DL50 automatic titration equipment. Thus alkalinity determination was easier and less work intensive than EDTA titration of Mg^{2+} that had to be done manually with a colour indicator. Alkalinity was therefore chosen as the primary analysis method, and measured using HCl(0.01M-0.1M) standard solutions. The analysis was standardized using solutions of known $KHCO_3$ and $NaHCO_3$ concentration, made from the solid salts. At 80°C the samples were quenched in about 20g distilled water to minimize evaporation during weighing.

To verify that alkalinity was equal to twice the Mg^{2+} concentration some of the samples were directly analysed for Mg^{2+} by EDTA titration. This titration was preformed on a hot plate (50-60°C) with a Calmagite(Acros, indicator grade) end point indicator. The analysis was standardized with solutions of known Mg^{2+} content (Titrisol ampoules, Merck).

9.3 Results and discussion

9.3.1 Magnesite synthesis

The reaction from hydromagnesite to magnesite in an aqueous solution under CO_2 gas bubbling can be written as;

$$\begin{aligned} &3MgCO_3 \cdot Mg(OH)_2 \cdot 3H_2O(s) + CO_2(g) \rightarrow 4MgCO_3 + 4H_2O(l) \\ &Hydromagnesite + CO_2 \rightarrow 4Magnesite + 4H_2O \end{aligned} \qquad (168)$$

The reaction has a certain equilibrium constant K which is a function of temperature and pressure. There are generally three parameters that can be varied to produce magnesite;

- → **Temperature**
- → **CO_2 pressure**
- → **Water activity**

An increase in temperature will shift the equilibrium to the right. More importantly it will generally increase the reaction rate and as mentioned above, magnesite is normally synthesized at high temperature. Both a higher CO_2 pressure and a lower water activity are advantageous since the reaction is shifted to the right.

Intuitively a MEG containing solution is advantageous for two reasons. Firstly MEG lowers the water activity, which should favour magnesite formation relative to the other $MgCO_3$ phases containing crystal water. Secondly it simply increases the boiling point of the solution and a higher temperature can be reached at atmospheric conditions. The MEG effect on the water activity is actually not as simple as indicated by Eq. 168, since MEG will also shift the equilibrium constant, K, of the reaction. The few measurements of magnesite solubility performed in this work actually indicated that the solubility ratio between hydromagnesite and magnesite *decreased* with MEG addition, which meant that the driving force actually decreased at high MEG conditions. Thus the most important effect of MEG is that it enables a higher temperature at atmospheric conditions.

Magnesite was in this work successfully synthesized from hydromagnesite by refluxing a solution of 90wt% MEG (120 ± 5°C) as described in the experimental section. It was desirable to keep the vessel at a temperature slightly lower than the boiling point to maintain a certain CO_2 pressure. The total pressure always equals the atmospheric pressure, and the CO_2 pressure(P_{CO2}) is therefore given as the difference between the atmospheric pressure (P_{tot}) and the vapour pressure of the solvent($P_{solvent}$). When approaching the boiling point $P_{solvent} \rightarrow P_{tot}$ thus P_{CO2} must approach zero. Because CO_2 is continuously bubbled through the solution there must be some gas present that gives a certain partial pressure. This will depend on the bubbling rate and cause some "steady

state" condition, but P_{CO2} will certainly have the lowest value at the boiling point of the solvent. Fig. 9.2 shows the X-ray diffraction pattern of the synthetic magnesite.

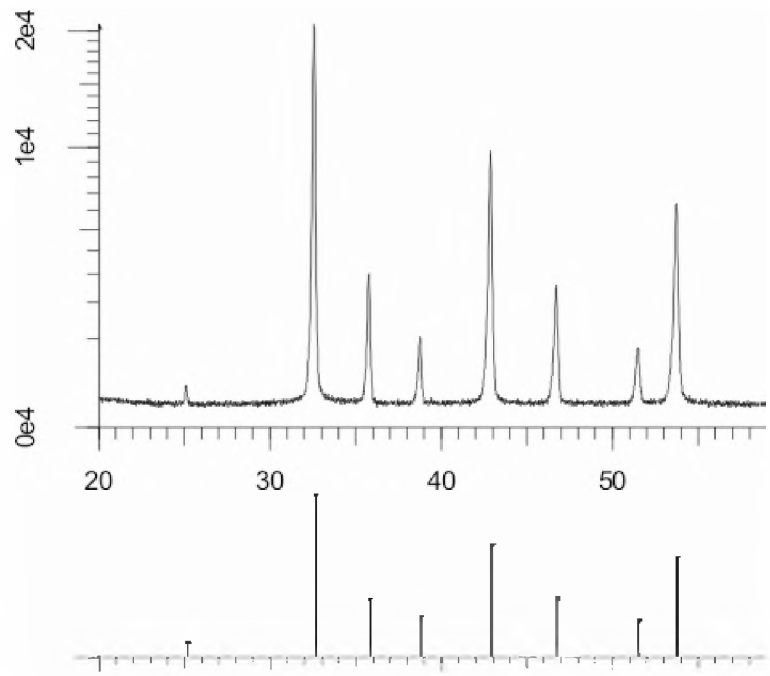

Fig. 9.2: XRD (2θ versus intensity from CuKα radiation) scan of synthesized magnesite in 90wt% MEG (0.5m NaCl, 120°C). Bars correspond to databank[12]

The X-ray diffraction (XRD) scan corresponded well with data in the databank[12], and showed no sign of impurities. With the method in this work, magnesite of good purity can easily be produced in common laboratory glassware, without the need of expensive steel bombs or other high pressure vessels.

Attempts were made to increase the NaCl and MEG concentrations further (95wt% MEG, 1mol NaCl / kg), as higher temperature should yield a higher reaction rate. When the reaction occurred at the boiling point of the solution (160-165°C) the product was an amorphous solid. This could be a result of the CO_2 pressure becoming small at the boiling point. CO_2 (or CO_3^{2-}) is needed to transform the hydroxide containing hydromagnesite into magnesite. At 150°C the attempt proved successful, and magnesite with an XRD pattern virtually identical with Fig. 9.2 was produced.

One experiment with ~100% MEG (120°C) was performed without reflux. Any water present should evaporate relative to MEG. The resulting solid, however, was gel like, not easily filtered, and gave a typical amorphous pattern during XRD analysis. In both the CO_2 dissociation and hydromagnesite dissolution reactions, water is included. It is therefore not obvious how these reactions occur in a solvent of virtually pure MEG.

Further optimisation of the synthesis should not include NaCl contents higher than 1.0-1.2m. This corresponds to the solubility limit at room temperature (>90wt% MEG), and it is desirable not to precipitate NaCl if the solution is cooled. A rough estimate is a

possible production of 50g of solid $MgCO_3$ per kg of solvent within a few days. The water + MEG + NaCl solution can be recycled and the amount of starting material (hydromagnesite) will determine the time before complete transformation into magnesite.

9.3.2 Solubility

When performing dissolution experiments the Mg^{2+} concentration always equals half the alkalinity. In the CO_2 saturated solutions of this work the total alkalinity virtually equals bicarbonate concentration i.e. $[HCO_3^-] >> [CO_3^{2-}]$ and $[OH^-]$. The error in the alkalinity determination for parallel measurements was generally within 1%. Samples withdrawn hours/days apart, however, showed larger variations, and the random error was estimated to ±5%.

Previous investigations in our lab concerning Ca, Ba and $SrCO_3$ solubility showed that the presence of MEG significantly lowered the reaction rate. MEG has a much higher viscosity than water, which implies a lower diffusivity[9] that can be rate determining for the dissolution process. To establish the time needed to reach equilibrium, the alkalinity was measured as function of time. The preliminary experiments at room temperature mentioned above, showed that at 90wt% MEG the solution should be left for at least 10-14 days. It was in addition performed an experiment in 50 wt% MEG at 25°C under continuous CO_2 gas flow. Fig. 9.3 shows the results for 50wt % MEG, where the discontinuity at about 2 days is due to too little hydromagnesite being present. More solid was added at this point. Some of the increase after 7 days can be attributed to a marked increase in atmospheric pressure during this period, as this in turn gives an increase in P_{CO2}.

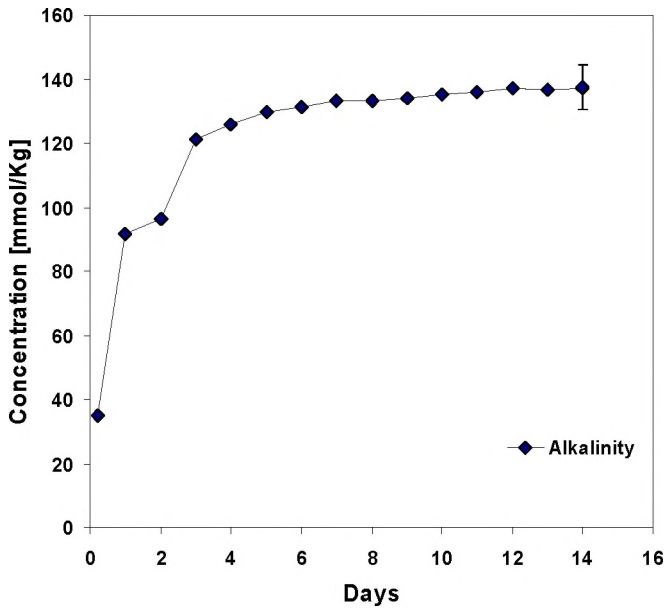

Fig. 9.3: Alkalinity (~HCO_3^- concentration) versus time in 50wt % MEG during dissolution of hydromagnesite at 25°C. Solution saturated with CO_2 at atmospheric pressure.

The error bar showed at 14 days corresponds to the estimated error of 5% in the data. Based on these measurements it was decided to leave solutions of 50-100wt% MEG for

14 days at 25°C. At lower MEG contents and higher temperatures shorter residence times were used as seen in Table 9.1. The solutions containing 95 and 97.5wt% MEG (25°C) were only run for 7 days. This was simply due to a problem with the CO_2 supply, thus the experiments had to be terminated. Ideally equilibrium should be reached from both under-saturation and supersaturation. This was done at 80°C, where precipitation does not give the meta-stable nesquehonite.

During this work only hydromagnesite was available as starting material, thus the other compounds had to be synthesized. It was decided to work in the range 25-80°C; hence lansfordite, that is stable relative to nesquehonite only below 20°C, should not be observed. Precipitation from an aqueous $MgCl_2$ / $NaHCO_3$ solution under CO_2 bubbling (P_{tot}= 1atm) yielded nesquehonite at 25°C and hydromagnesite at 80°C. The former was left in solution for 7 days (25°C) and the latter for 5 days (80°C). No transformation was observed, thus the two solid phases were kinetically stabilized for a long time under vigorous stirring. The produced nesquehonite was used as starting material at 80°C where, within 2 days, it had transformed into hydromagnesite. Thus the investigations were in good agreement with the literature findings described above.

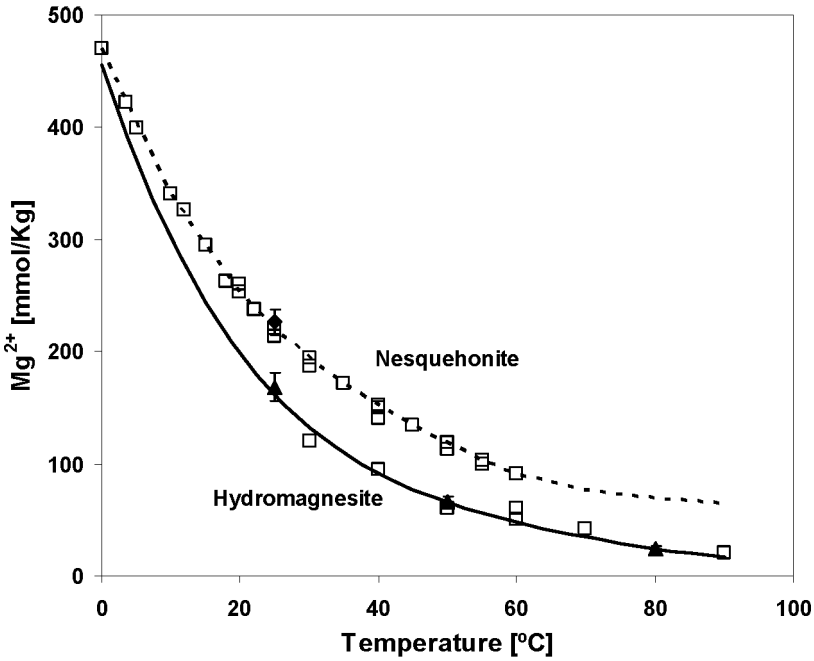

Fig. 9.4: Solubility as function of temperature [mmol/kg water] from Table 9.1 compared to literature values[2,3,6,8]. Solid line: Calculation from Eq. 178 in CO_2 saturated solutions with P_{tot}=1bar. ▲, hydromagnesite in this work; ♦, nesquehonite in this work; □, literature.

Fig. 9.4 compares literature data with the measurements of this work in water. There are two clear trends that correspond to the solubility of nesquehonite (dotted line extrapolation) and the less soluble hydromagnesite. $K°_{sp}$ of hydromagnesite ($3MgCO_3 \cdot Mg(OH)_2 \cdot 3H_2O$) is given from Eq. 169-170;

$$3MgCO_3 \cdot Mg(OH)_2 \cdot 3H_2O(s) = 4Mg^{2+} + 3CO_3^{2-} + 2OH^- + 3H_2O \quad (169)$$

$$K_{sp}^o = a_{Mg^{2+}}^4 a_{CO_3^{2-}}^3 a_{OH^-}^2 a_{H_2O}^3 \quad (170)$$

The solubility measurements gave Mg^{2+} concentration at a certain partial pressure of CO_2, thus carbonate and hydroxide as well as water activities, a, have to be calculated in Eq. 170. When the solubility is measured under CO_2 pressure the concentration of HCO_3^- is dominating i.e. much larger than both carbonate and hydroxide concentrations. Thus the results are best interpreted by an equation including only bicarbonate and Mg^{2+} concentrations, as well as the CO_2 pressure.

$$CO_2(g) = CO_2(aq) \qquad K_H^o \quad (171)$$

$$CO_2(aq) + H_2O = H^+ + HCO_3^- \qquad K_1^o \quad (172)$$

$$HCO_3^- = H^+ + CO_3^{2-} \qquad K_2^o \quad (173)$$

$$H_2O = H^+ + OH^- \qquad K_w^o \quad (174)$$

By combination of Eq. 169 with the carbonic acid equilibria (Eq. 171-173), and the self dissociation of water (Eq. 174) the desired relation is found;

$$3MgCO_3 \cdot Mg(OH)_2 \cdot 3H_2O(s) + 5CO_2 = 4Mg^{2+} + 8HCO_3^- \quad (175)$$

This reaction has a certain equilibrium constant, $K°_{comb}$, which is a combination of the constants from the reactions above;

$$K_{comb}^o = \frac{K_{sp}^o \left(K_H^o K_1^o\right)^5}{\left(K_w^o\right)^2 \left(K_2^o\right)^3} = \frac{a_{HCO_3^-}^8 a_{Mg^{2+}}^4}{f_{CO_2}^5} = \frac{m_{HCO_3^-}^8 \gamma_{HCO_3^-}^8 m_{Mg^{2+}}^4 \gamma_{Mg^{2+}}^4}{P_{CO_2}^5 \varphi_{CO_2}^5} \quad (176)$$

f, m, and γ denote fugacity, concentration (mol/kg solvent) and activity coefficients respectively. The fugacity is given as the product of partial pressure, P, and the fugacity coefficient, φ. Rearranging this equation gives the alternative expression for $K°_{sp}$ of hydromagnesite in Eq. 177.

$$K_{sp}^o = \frac{\left(K_w^o\right)^2 \left(K_2^o\right)^3}{\left(K_H^o K_1^o\right)^5} \cdot \frac{m_{HCO_3^-}^8 \gamma_{HCO_3^-}^8 m_{Mg^{2+}}^4 \gamma_{Mg^{2+}}^4}{P_{CO_2}^5 \varphi_{CO_2}^5} \quad (177)$$

This equation was used to calculate the solubility product $K°_{sp}$ in this work. Concentrations of HCO_3^- and Mg^{2+} were measured (Table 9.1 and Table 9.2) at a given partial pressure of CO_2, while the activity coefficients had to be calculated. This was done using the *Multiscale*[11] computer program that utilizes the Pitzer ion interaction[10] model for the aqueous phase. For the conditions in this work the fugacity coefficient, φ, is virtually 1 in all cases. $K°_{sp}$ was fitted by Eq. 178 and the function is shown in Fig.

9.5. The data point (22°C) from Table 9.2, seems to be too low compared to the other data. This experiment contained 0.5mol NaCl/kg solvent. Thus the discrepancy may actually be due to an inaccuracy in the activity coefficient model when substantial amounts of NaCl are present.

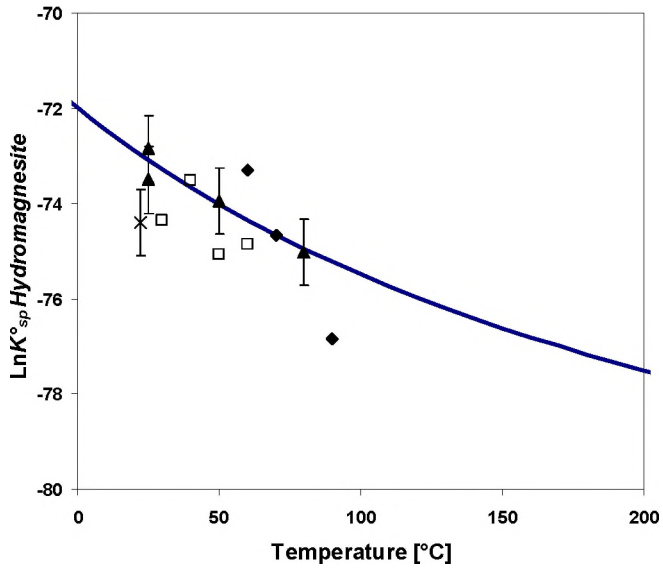

Fig. 9.5: Ln(K_{sp}°) of $3MgCO_3 \cdot Mg(OH)_2 \cdot 3H_2O$. ▲, this work (Table 9.1); X, this work (Table 9.2); ♦, Yanat'eva[3]; □, Königsberger et.al[5]; *solid line*, Eq. 178.

$$LnK^{o}_{sp} = \frac{3555.62}{T} - 85.022 \qquad (178)$$

Königsberger et.al[2] and Yanat'eva[3] claimed that the CO_2 pressure was about 1atm, but total pressures were not given. It is uncertain exactly how their measurements were performed, and therefore also exactly how to perform the calculation. In addition their data was only presented in the form of figures (Fig 3a from Königsberger et.al[2] and Fig 2 of Yanat'eva[3].), and the reading of values therefore introduces some uncertainty. The extrapolation to low temperature (0°C) was constructed such that it corresponded with the calculation in Fig.3a of Königsberger et.al[2]. The function given by Marion[1] can not be directly compared with Eq. 178, because Marion used a different activity coefficient model where the complexes $MgCO_3$° and $Mg(OH)^+$ were introduced.

9.3.3 Solubility in Water+MEG solutions

Hydromagnesite solubility (see Table 9.1) decreased with increasing MEG content, as seen in Fig. 9.6. The solid lines are calculated by the model of this work (see chapter 6)

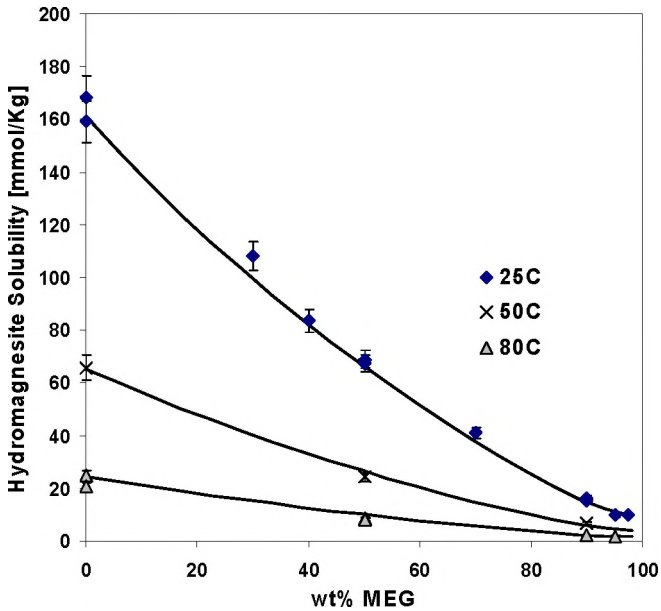

Fig. 9.6: Hydromagnesite ($3MgCO_3 \cdot Mg(OH)_2 \cdot 3H_2O$) solubility in solutions saturated with CO_2 at p_{tot}=1atm (25-80°C) versus wt% MEG in solvent. Solid line: Model of this work

Hydromagnesite ($3MgCO_3 \cdot Mg(OH)_2 \cdot 3H_2O$) contains crystal water, thus an increased solubility at high MEG concentrations was expected. Measurements of e.g gypsum solubility (see chapter 4) showed a steep solubility increase at high MEG contents where the water activity is low. Hydromagnesite has a complex solid structure with a mixture of carbonate and hydroxide. Combination of equilibria gave the relation in Eq. 175. Although the solid phase includes crystal water, Eq. 175 describes the dissolution equilibrium merely by the CO_2 pressure and the dissolved ions Mg^{2+} and HCO_3^-. Thus the solubility is not directly dependent on water activity. This corresponds with the data presented in Fig. 9.6 at high MEG contents.

Magnesite was synthesized as described in detail above and the solubility thereafter determined. The aqueous measurement in Table 9.3 showed the same magnitude as found in the literature[5]. Fig. 9.7 compares the measured magnesite solubility with calculations of calcite($CaCO_3$), strontianite($SrCO_3$) and siderite ($FeCO_3$) solubility. The solubility is comparable to that of siderite but actually shows a much larger decrease with MEG addition. This may, however, be slightly misleading due to that the solubility was measured by dissolution. A very slow reaction rate may therefore have given too low values in 50 and 90wt% MEG.

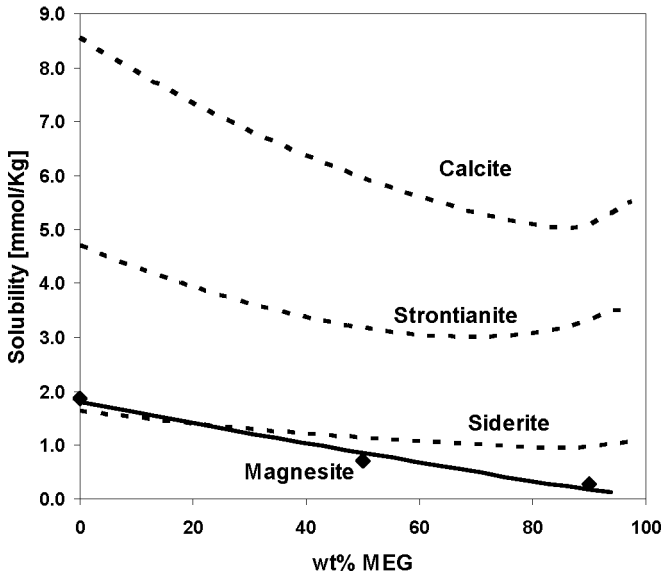

Fig. 9.7: Solubility at 25°C as function of wt% MEG. P_{CO2}~1atm no added NaCl. ♦, $MgCO_3$ from Table 9.3; *Lines,* model calculations

Although the solubility is very low precipitation of $MgCO_3$ is, as mentioned above, kinetically inhibited. Magnesite precipitation was not observed in the hydromagnesite dissolution experiments (25-80°C), which was run for 2-14 days. To investigate this kinetic inhibition further, supersaturated solutions at 25 and 80°C were made. These were under-saturated with respect to hydromagnesite, but had SR of 90-100 with respect to magnesite. Two parallels were run at each temperature, where one solution was seeded with magnesite and the other was not. After 10 days at 25°C and 4 days at 80°C magnesite precipitation was not detected in any of the solutions. Even the seeded solution at 80°C did not show any precipitation.

It was decided to include Hydromagnesite as the only solid magnesium carbonate phase in this work. The scale model is a thermodynamic model, such that principally should only the thermodynamically stable phase be included even though a different phase may initially form. The omission of the less stable nesquehonite and lansfordite is therefore founded on the same argument that aragonite and vaterite are omitted for $CaCO_3$ precipitation. The thermodynamic approach is a conservative one, where a precipitate may form if the solution is supersaturated relative to the stable phase. From this argument should, however, also hydromagnesite be omitted and magnesite included as the only stable phase. Because even the seeded system at 80°C did not show any precipitation, it is reasonable to assume that the kinetics is so slow that it will normally not form during oilfield operation. From this observation it was decided to omit magnesite from the model, as the user would only be unnecessary confused by the always high SR of this salt. It would be even worse if actions were made to avoid $MgCO_3$ (magnesite) formation since it most likely would not form.

9.4 Summary chapter 9

A method for synthesizing magnesite from hydromagnesite at atmospheric conditions has been suggested. Mono Ethylene Glycol (MEG) is used to lower the solvent vapour pressure at temperatures above 100°C. The solubility of magnesite in water at 25°C was found to be about 1.9mmol/kg in a solution saturated with CO_2 at atmospheric conditions.

The solubility of hydromagnesite ($3MgCO_3 \cdot Mg(OH)_2 \cdot 3H_2O$) has been measured at temperatures (25-80)°C and MEG + water solution containing 0-97.5 wt% MEG. A steady decrease in solubility (mol/kg solvent) with increasing MEG content was observed. Hydromagnesite is included as the only magnesium carbonate mineral in the scale model of this work. Hydromagnesite is actually a meta-stable phase, but the thermodynamically stable magnesite has been omitted due to its formation being kinetically inhibited.

9.5 References

1. Marion, M.G.; Carbonate mineral solubility at low temperatures in the Na-K-Mg-Ca-H-Cl-SO_4-OH-HCO_3-CO_3-CO_2-H_2O system; *Geochim. Cosmochim. Acta*, **65(12),** 1883-1896, (2001)
2. Königsberger, E.; Königsberger, L.; Gamsjäger, H.; Low-temperature thermodynamic model for the system Na_2CO_3-$MgCO_3$-$CaCO_3$-H_2O; *Geochim. Cosmochim. Acta*, **63(19/20),** 3105-3119, (1999)
3. Yanat'eva, O.K. "The metastable equilibrium in the system $CaCO_3$-$MgCO_3$-H_2O", translation of *Izvestiya Akademii Nauk SSSR,* **1,** 180-182, (1960)
4. Johnston, J. "The solubility constant of calcium and magnesium carbonates", *J. Am. Chem. Soc.*, **37,** 2001-20, (1915)
5. Langmuir, D. "Stability of carbonates in the system MgO-CO_2-H_2O", *Journal of Geology,* **73,** 730-754, (1965)
6. Linke, W. F. *Solubilities, Inorganic and metal-organic compounds* 4th ed. (1965) Am. Chem. Soc. WashingtonD.C
7. Christ, C.L. Hostetler, P.B., "Studies in the system MgO-SiO_2-CO_2-H_2O: the activity product constant of magnesite", *Am.J.Sci.* **268,** 439-453, (1970)
8. Stephen H., *Solubilities of inorganic and organic compounds*, Vol.1, (1963) , Pergamon Press
9. Mullin, J. W. *Crystallization 4th ed.*, (2001), Butterworth Heinemann
10. Pitzer, K. S. *Thermodynamics* 3rd ed., (1995), McGraw-Hill
11. Kaasa, B., Prediciton of pH, Mineral precipitations and multiphase equilibria during oil recovery, Dr.Ing thesis, Norwegian University of Technology and Science-NTNU, ISBN 82-471-0339-7 (1998)
12. International Centre for Diffraction Data, Powder Diffraction File, Release 1999
13. Trimble, H.M., Potts, W. "Glycol-water mixtures. Vapor pressure-boiling point-composition relations." *Ind. and Eng. Chem,* 27, 66-68, (1935)
14. Villamanan, M., A., Gonzalez, C., Van Ness, H.C. "Excess thermodynamic properties for water/ethylene glycol." *J. Chem. Eng. Data,* 29(4),427-429, (1984)
15. Gonzalez, C., Van Ness, H.C. "Excess thermodynamic functions for ternary systems. 9. Total-pressure data and GE for water/ethylene glycol/ethanol at 50°C.", *J. Chem. Eng. Data*, **28(4)**, 410-412, (1983)
16. Nath,A., Bender,E., "Isothermal vapor-liquid equilibriums of binary and ternary mixtures containing alcohol, alkanolamine, and water with a new static device." *J.Chem.Eng.Data*, **28(4),** 370-375,(1983)
17. Lancia,A., Musmarra,D., Pepe,F., "Vapor-liquid equilibria for mixtures of ethylene glycol, propylene glycol, and water between 98° and 122°C." *J. Chem. Eng of Japan,* **29(3),** 449-455, (1996)

Table 9.1: Solubility measurements of hydromagnesite and nesquehonite in MEG + water solutions.

D[a]	Wt% MEG[b]	T / °C	$[Mg^{2+}]$ / mol·kg^{-1}	P_{CO2} /bar	Start[c]	XRD[d]
6	0	25	159.1	0.97	H	**H**
5	0	25	168.2	0.97	H	**H**
7	30	25	112.2	0.99	H	**H**
3	40	25	83.5	0.99	H	**H**
7	50	25	67.4	1.00	H	**H**
14	50	25	68.9	1.02	H	
14	70	25	41.0	0.98	H	
7	90	25	15.3	0.99	H	**H**
14	90	25	16.3	1.00	H	
7	95	25	9.8	0.99	H	
7	97.5	25	9.9	0.99	H	
7	0	25	226.2	0.97	N	**N**
7	30	25	147.5	0.98	N	**N**
5	0	50	65.8	0.88	H	**H**
5	50	50	24.3	0.91	H	**H**
5	90	50	6.8	0.96	H	**H**
1	0	80	24.9	0.53	H	
4	0	80	20.6	0.50	H	**H**
3	50	80	8.4	0.64	H	**H**
9	50	80	7.9	0.64	H	**H**
2	90	80	2.1	0.87	H	**H**
4	90	80	2.0	0.86	PT	
4	95	80	2.0	0.93	PT	
4	90	80	6.9	0.87	H	
2	0	80	29.6	0.53	N	**H**
2	90	80	8.2	0.87	N	

[a] Number of days in solution. [b] Weight % MEG in solvent
[C] Starting materials: H = Hydromagnesite N = Nesquehonite. PT = precipitated from 40 °C
[d] Phase determined by XRD after the experiment: H = Hydromagnesite, N = Nesquehonite.

Table 9.2: Solubility of hydromagnesite in MEG + water+ NaCl (0.5 mol /kg solvent) solutions saturated with CO_2 (not continuous gas flow). T=22±2°C, P_{tot}~1atm.

D[a]	Wt% MEG[b]	$[Mg^{2+}]$ / mol·kg^{-1}
13	0	156.3
28	40	83.0
67	50	77.4
29	60	50.3
19	90	23.2
22	90	24.7

Table 9.3: Solubility of magnesite[c] in MEG + water solutions at 25°C.

D[a]	Wt% MEG[b]	$[Mg^{2+}]$ / mol·kg^{-1}	P_{CO2} /bar
7	0	1.86	0.96
7	50	0.71	0.98
7	90	0.28	0.99

[a] Number of days in solution. [b] Weight % MEG in solvent [c] Phase confirmed (by XRD) to be magnesite in all experiments.

10 The computer program

The investigations of this work have been used to upgrade the *Multiscale*[1] computer program with additional salts and the ability to handle MEG as a co-solvent. The new model is called *MultiMEGScale*, has good flexibility and can do exactly the same type of calculations as the aqueous model. MEG is commonly introduced in the aqueous phase, but the model also accepts MEG input in the gas or oil phase.

10.1 Model operation

The multiphase equilibrium model is described schematically in Fig. 10.1. An equation of state is used to describe the oil and gas equilibrium condition in the *hydrocarbon phase*. The *aqueous phase* contains all the ions and usually most of the water and MEG in the system. Salts forming scale are obviously present in the *solid phase*. At a certain point in an oilfield production process there can consequently be equilibrium between all phases i.e. oil-gas-aqueous-solid. How such a model performs the calculation, both principally and mathematically, is described in detail by Kaasa[1,2].

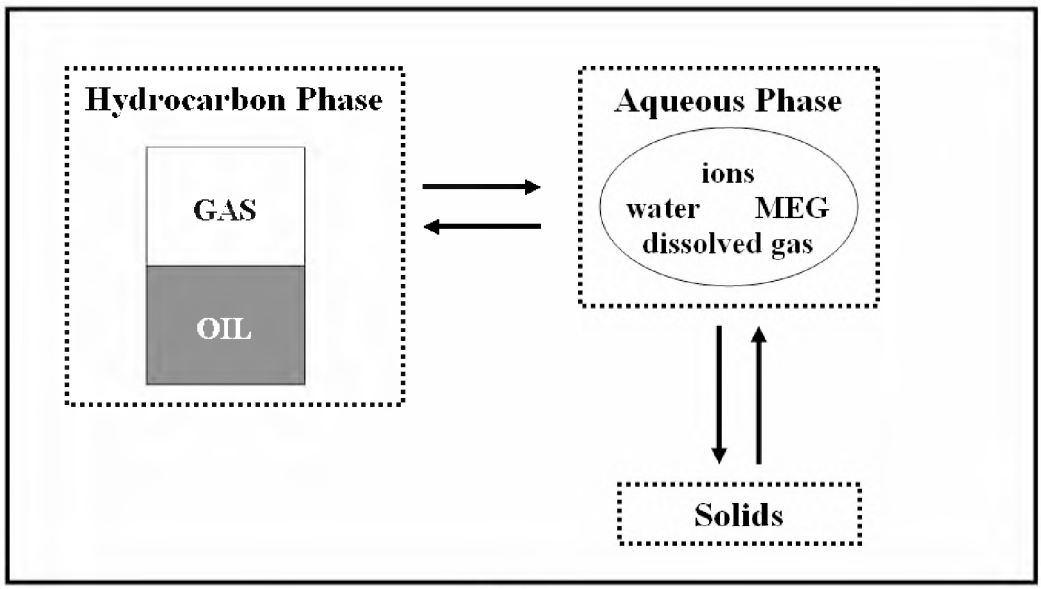

Fig. 10.1: Schematic of the multiphase equilibrium.

MEG is not present in any of the solids, and must consequently only be included in the *hydrocarbon* and *aqueous* phases. The equation of state is expanded with an additional component, MEG, and chapter 6 describes in detail how MEG is included in the aqueous phase.

Most species are present either only in the *hydrocarbon* phase, or only in the *aqueous+solid* phases. Precipitation of NaCl is such an example, where the ions Na^+ and Cl^- are present in the *aqueous* phase and the solid NaCl obviously in the *solid* phase. Heavy hydrocarbons like C_{10+} does not dissolve in the aqueous phase, and are therefore present only in the *hydrocarbon* phase. Thus the equilibrium distributions of C_{10+} in *oil-gas*, and NaCl in *water-solid,* are principally independent.

Some species can exist in both the *hydrocarbon* and *aqueous (+solid)* phases. These species are:

→ CO_2, CH_4, H_2S, and organic acids
→ H_2O and MEG

Henry's constant $K°_H$ gives the equilibrium distribution of CO_2, CH_4, H_2S, and the organic acids between the *hydrocarbon* and *aqueous* phases. The MEG effect on the distribution of these species is therefore included in the aqueous phase model as described in detail in chapter 6. At equilibrium the composition of the aqueous phase gives the activities of H_2O and MEG. These values lead to certain partial pressures (fugacities) of H_2O and MEG. Thus the MEG concentration in the *aqueous* phase determines how much water and MEG that will be present in the *hydrocarbon* phase (or vice versa). Water is much more volatile than MEG, such that the "moisture" in the gas phase will mostly consist of water and very little MEG.

Empirically fitted MEG dependences are introduced as described in detail in chapter 6. The model has a "MEG calculation" routine that uses these functions to calculate new equilibrium constants and activities. Thereafter the model calculates the whole multiphase equilibrium as before[1,2]. This is best explained by an example. Regard the thermodynamic equilibrium constant for NaCl;

$$K^o_{sp}\left(NaCl\right) = m_{Na^+} m_{Cl^-} \gamma^S_{Na^+} \gamma^S_{Cl^-} \left(\gamma^{N\pm}_{NaCl}\right)^2 \tag{179}$$

All parameters are defined in previous sections, but it is emphasized that γ^S denotes the activity coefficient valid in water and m concentration as *mol/(kg solvent)*. Eq. 179 can be rewritten to introduce a new equilibrium constant, K^{MEG}, from the $\gamma^{N\pm}$ values as:

$$\frac{K^o_{sp}\left(NaCl\right)}{\left(\gamma^{N\pm}_{NaCl}\right)^2} = K^{MEG} = m_{Na^+} m_{Cl^-} \gamma^S_{Na^+} \gamma^S_{Cl^-} \tag{180}$$

The right hand side is now exactly the same as for calculation in water, thus the scale model can perform the calculation as "if the solvent was water" simply by changing the equilibrium constant from $K°$ to K^{MEG}.

This pH independent salt is obviously the simplest case. Salts containing crystal water and pH dependent salts are much more complicated but the principle is the same as for NaCl. Mode of operation can be summarized as:

- → MEG content is an input from the user, which can be measured as described in chapter 8. Other input data are water/gas/oil analysis, pressure, temperature, rates etc.
- → Input MEG concentration and temperature, together with calculated ionic strength, are sent to the "MEG calculation" routine.
- → The deviations from the aqueous model are calculated as described in chapter 6
- → These data are used to calculate new equilibrium constants and activities in the water+MEG solvent.
- → The new equilibrium constants and activites are sent to the *Mulitscale* model, which simply calculates as "if the solvent was water". MEG activity is only used for calculation of partial pressure (fugacity) that is used in the PVT part of the model.

It is impossible to use the model in 100% MEG due to the choice of an aqueous standard state (see chapter 2). The activity of water is a key parameter both in the PVT model and in the calculation of carbonic acid equilibria. Because water activity approaches 0 in pure MEG, the model is valid only up to ~99wt% MEG (in the solvent). To reach 100% MEG it is probably necessary to introduce a self dissociation of MEG.

Generally the functions providing MEG dependence have been fitted from data in the 0-100°C range. Thus using the model well outside of this range (>120°C) will give uncertainties. Flow in MEG containing production pipelines is usually covered by the 0-100°C range, but in process plants the temperature may be higher than this. Predictions in process plants with high temperature, sometimes combined with extremely high salinities, are outside the scope of this work.

10.2 Model application

10.2.1 Testing of pH prediction

To test how pH is predicted by the model, pH was recorded as function of added $NaHCO_3$ (4-80°C) and $KHCO_3$ (25°C) under continuous CO_2 bubbling. The measurements were performed with 60 and 90wt% MEG, corresponding to typical "rich" and "lean" MEG conditions for oilfield use. Details can be found in section 4.3.5 and all results are given in Table 4.15-Table 4.19. These experiments were performed using different electrodes than those used for construction of the model.

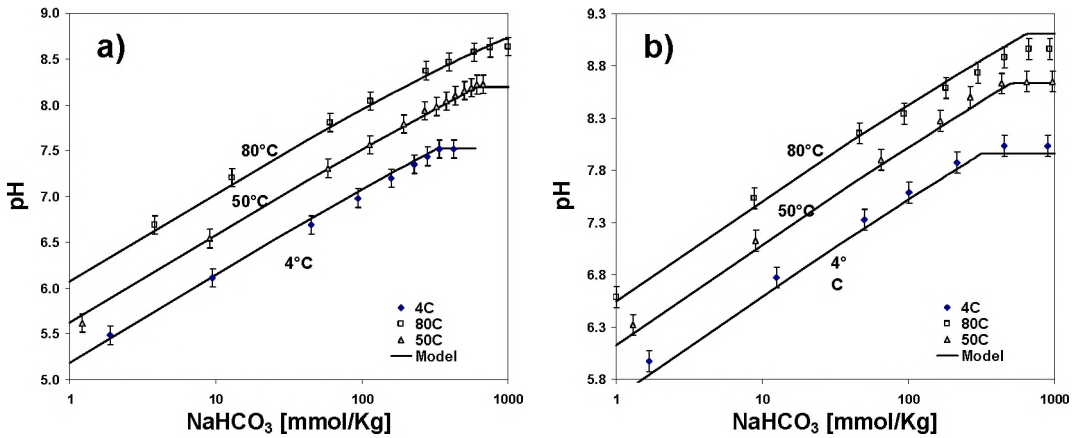

Fig. 10.2: Measured *pH* (Table 4.15-Table 4.19) in water+MEG+$NaHCO_3$ solutions saturated with CO_2 at atmospheric pressure versus $NaHCO_3$ concentration at three temperatures (4, 25 and 80°C). *a)* 60wt% MEG. *b)* 90wt% MEG. *Solid lines:* Model prediction

Fig. 10.2 compares results at 4, 50 and 80°C with model predictions. The break in the curve corresponds to the solubility limit of $NaHCO_3$. Generally the results correspond well with the model, the exception being 80°C in 90wt% MEG. Fig. 10.2b) shows that the model gives a too high pH at high contents of $NaHCO_3$ in this case. The discrepancies may be due to measuring difficulties, as the different pH electrodes show much larger individual variation and drift at high temperature. Secondly it should be noted that the model is fitted using data from measurements with only about 10mmol/kg of $NaHCO_3$. It is therefore not surprising that some variations are observed at 0.5-1mol/kg. Another reason could be that the calculated solubility limit is too high, thus the break in the curve should have occurred at a lower pH. This can also be the case for the 80°C series at 60wt% MEG (Fig. 10.2a)

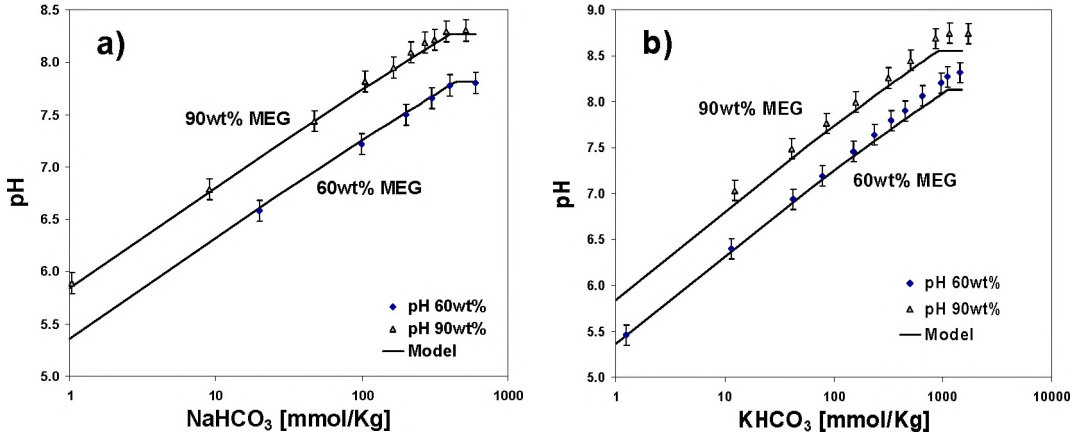

Fig. 10.3: Measured *pH* (Table 4.15 and Table 4.19) in 60 and 90wt% MEG solutions (P_{CO2}~1bar) as function of a)$NaHCO_3$ and b)$KHCO_3$ concentration (mmol/kg solvent) at 25°C. *Solid lines*: Model prediction

Fig. 10.3a) shows that the measurements in water+MEG+$NaHCO_3$ at 25°C corresponded well with the model. This was expected since the bulk of the measurements that the model is based on were performed at this temperature. In addition all common combined pH electrodes function well at 25°C and the solubility is not high enough for ionic strength to be of any significant influence. Fig. 10.3b) on the other hand shows a variation between the model and the measurements at high concentrations of $KHCO_3$. The ionic strength is significantly higher than for $NaHCO_3$, and it is possible that the model is inaccurate at such conditions. At 90wt% MEG the results are, however, systematically slightly higher than the model and it also seems that the break in the curve occurs at a too low value. The modeling of the $KHCO_3$ solubility is discussed in section 6.6.1.

10.2.2 Salting out

If to a saturated solution of NaCl in water a small amount of alcohol is added, two things may happen. The solution may be supersaturated, due to a lower solubility of NaCl in the new water+alcohol solution, or it may be unsaturated. The former leads to precipitation of NaCl and is called *salting-out*, while the latter is called *salting-in*. Fig. 10.4 shows NaCl solubility as function of alcohol content for MEG, Methanol and Ethanol. NaCl solubility is seen to decrease with type of alcohol as MEG>MeOH>EtOH.

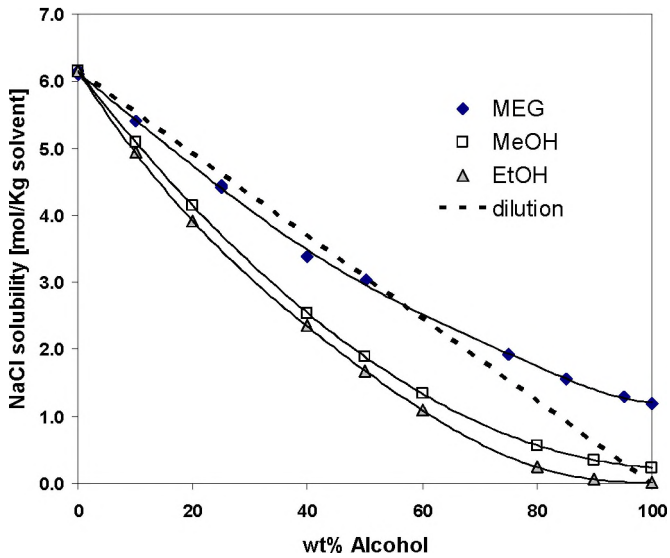

Fig. 10.4: NaCl solubility[3-5] as mol/(kg solvent) at 25°C as function of alcohol concentration (wt% in salt free solvent). EtOH= Ethanol, MeOH=Methanol.

The dotted line denotes the resulting NaCl concentration, before a possible precipitation, when pure alcohol is added to a saturated aqueous solution of NaCl. A saturated solution (25°C) with 1kg of water contains 6.16mole NaCl. Addition of 1kg alcohol to this solution gives an alcohol concentration of 50wt%, while NaCl concentration is reduced to ½ of the original, =3.08mol/kg solvent. Addition of 9kg alcohol (90wt%) reduces the concentration to 1/10 and so on. If the solubility is lower than the "dilution" line the solution will be supersaturated with NaCl. It is seen that addition of MEG gives a slight supersaturation i.e. salting-out up to 50wt% MEG, while above this point the solubility is higher than the dotted line i.e. salting-in. The other two alcohols have a much larger adverse effect on the NaCl solubility and salting-out is observed over nearly the whole concentration interval.

Another way of graphically illustrating the concept of salting-out is to make the same plot, but now as *mol/kg water*. When adding alcohol the amount of water will remain the same, thus solubility lower than 6.16*mol/kg water* indicate the possibility for salting-out. Fig. 10.5 shows this plot, where the solubility goes to infinity when the alcohol concentration approaches 100%.

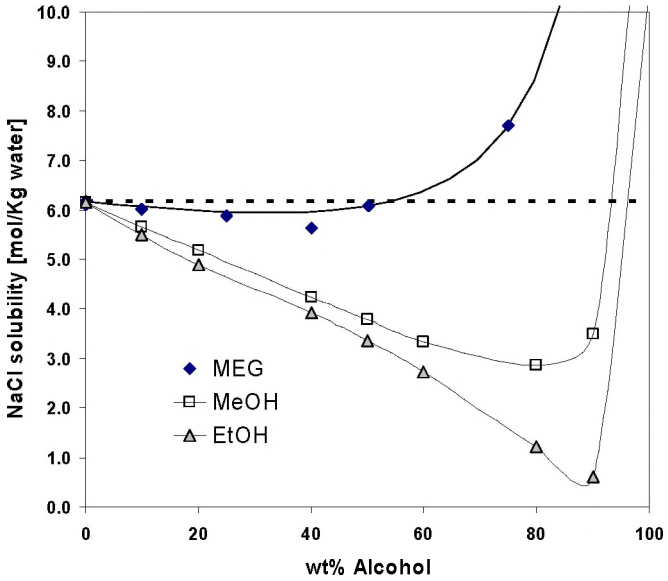

Fig. 10.5: NaCl solubility[3-5] as mol/(kg water) at 25°C as function of alcohol concentration (wt% in salt free solvent). EtOH= Ethanol, MeOH=Methanol.

In oilfield applications it is important to know if supersaturation is reached in a mixing point where saline waters meet MEG. Fig. 10.6 shows the predicted relative change (*per kg water*) in solubility rather than its actual value. Thus solubility less than 100% means that there is a possibility for salting-out, while above 100% there is obviously no chance of precipitation.

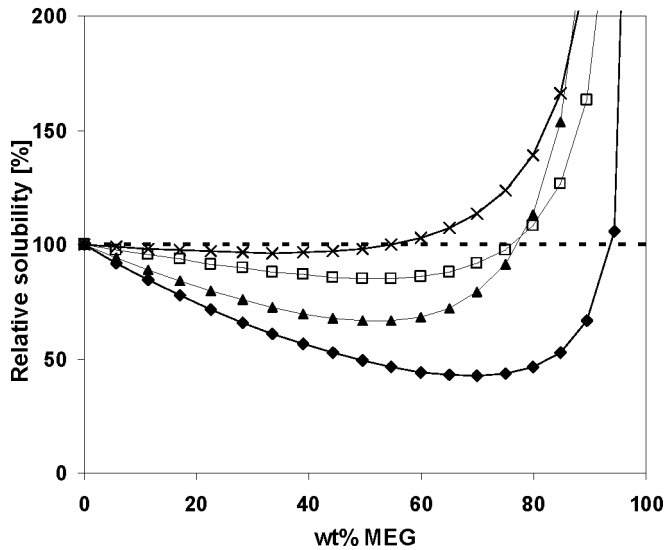

Fig. 10.6: Calculated relative solubility (*mol/kg water*) as function of MEG at 25°C. ×, NaCl; □, KCl; ▲, $BaSO_4$; ♦, $CaSO_4$

All salts have a relative solubility higher than 100% at high MEG contents. This is simply due to a much larger amount of solvent (water+MEG) being present. Thus the solubility *per kg water* becomes very high, as described earlier. It is seen that MEG has a severe adverse effect on the solubility of $CaSO_4$, while the topmost curve of NaCl has an insignificant solubility reduction. MEG is in other words an efficient *antisolvent* for sulphates but not for NaCl.

10.2.3 Practical use in gas well

To present the models ability to calculate scale potential of carbonate salts under practical conditions an example is considered below; Assume that a gas well is producing 9million Sm^3 of natural gas(1% CO_2, mainly CH_4). At a certain point (120bar, 80°C) this gas meets a hydrate inhibitor stream (100m^3/day) containing 90wt% MEG and 4200mg/kg of $NaHCO_3$. Sodium bicarbonate is present to reduce corrosion[6] of the pipeline. At a certain time the well starts to produce the formation water given in Table 10.1 from the reservoir (260bar, 93°C).

Table 10.1: Sample of typical formation water

Ion	mg/l	Ion	mg/l
Na^+	58000	Cl^-	91900
K^+	730	Br^-	0
Mg^{2+}	920	SO_4^{2-}	0
Ca^{2+}	300		
Ba^{2+}	6		
Sr^{2+}	0		
Fe^{2+}	0		
Organic acid		0	mg/l
Total alkalinity		410	mg/l
Pressure		1	bar
Temperature		15	°C
pH		NA	

Using this information *MultiMEGScale* can calculate the scaling risk at a given formation water production. Fig. 10.7a) shows the calculated saturation ratio (SR) versus amount of produced formation water for $CaCO_3$ and for Hydromagnesite ($3MgCO_3 \cdot Mg(OH)_2 \cdot 3H_2O$).

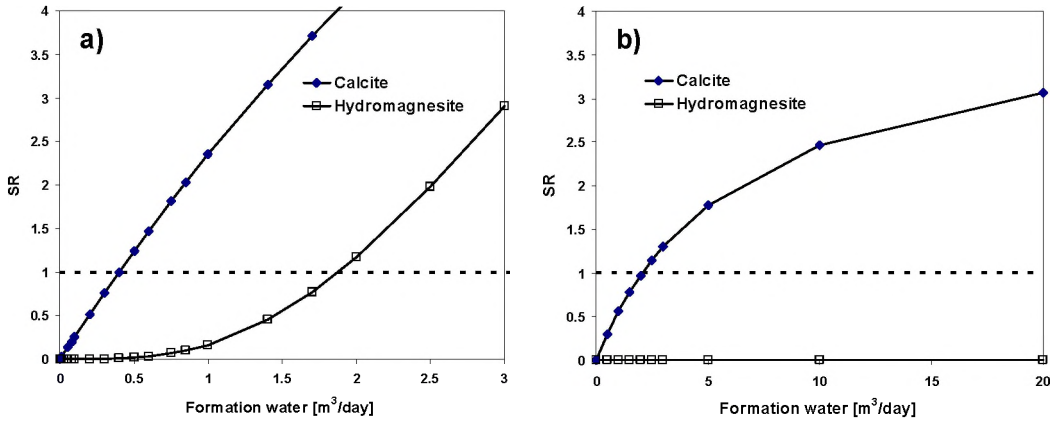

Fig. 10.7: SR versus rate of formation water for a gas well. □; Hydromagnesite, ♦; $CaCO_3$ a) Model prediction with *MultiMEGScale* b) Prediction with the aqueous *Multiscale* model. T=80°C P=120bar

It is seen that $CaCO_3$ becomes supersaturated with a rate of formation water of only about $0.4m^3$/day and hydromagnesite at about 1.8 m^3/day. It should be noted that the model is strictly thermodynamic and does not provide any information about kinetics i.e. how high SR that can be tolerated before precipitation really occurs. Fig. 10.7b) shows the same calculation with *Multiscale* i.e. the aqueous scale model without the MEG capability. In this case the calculation gives that calcite is supersaturated at about $2m^3$/day, while SR of hydromagnesite is virtually zero. Hydromagnesite has a very high solubility in water, but the solubility is severely reduced in the presence of MEG as presented in chapter 5 and 6.

10.3 Improvement of the model

New experimental data in water+MEG systems will evidently make further improvements of the model possible. Because several oil companies have started to use MEG for hydrate inhibition in a large scale, it is most likely that more gas-liquid equilibrium data soon will be available. Such data are vital for water and MEG activities in the aqueous phase and tuning of the PVT part of the model. Especially for gas wells correct vapour pressures are important. This is due to the large gas volumes acting as a reservoir that can either provide free water through condensation, or absorb water through evaporation. Temperature and pressure changes in such systems will determine how much solvent (water+MEG) that is present at each (P,T) point of the process. The solvent volumes will thereafter determine salt concentrations and therefore the scaling risk.

10.3.1 Methanol

The method used in this work can in an equivalent manner be used to include Methanol as co-solvent in the model. For water+MeOH solutions much data are available in the elaborate works of Kan et.al[7-8]. These data can be used directly to expand the model; hence there is not a need for much new data for the most common scaling materials. However, there is still a need for e.g. $BaCO_3$ and $SrCO_3$ data collection and some modelling work. Thus the introduction of Methanol still requires an extensive study.

10.4 References chapter 10

1. Kaasa, B., *Prediciton of pH, Mineral precipitations and multiphase equilibria during oil recovery,* Dr.Ing thesis, Norwegian University of Technology and Science-NTNU, (1998)
2. Kaasa, B., Sandengen, K. and Østvold, T. " Thermodynamic Predictions of Scale Potential, pH and Gas Solubility in Glycol containing Systems", SPE 95075, Int. Symposium on Oilfield Scale, Aberdeen, (2005)
3. Pinho, A.P., Macedo, E.A, "Presentation of salt solubility in mixed solvents; A comparison of thermodynamic models", *Fluid Phase Eq.* **116**, 209-216, (1996)
4. Kraus, K.A., Raridon, R.J. and Baldwin,W.H. "Properties of organic-water mixtures." *J.Am.Chem.Soc.,* **86(13),** (1964)
5. Masoudi, R., Tohidi, B., Anderson, R., Burgass, R.W., Yang, J. "Experimental measurements and thermodynamic modeling of chlathrate hydrate equilibria and salt solubility in aqueous ethylene glycol and electrolyte solutions" *Fluid Phase Equilibria*, **219**, 157-163, (2003)
6. Olsen, S., Lunde, O., Dugstad, A., "Stabilizing pH in Troll pipelines solves glycol-regeneration problems", *Oil & Gas Journal*, **97(26),** 59-62, (1999)
7. Kan, A.T Fu,G. Tomson, M.B "Effect of Methanol and Ethylene Glycol on Sulfates and halite Scale Formation" *Ind. Eng. Chem. Res.* **42**, 2399-2408, (2003)
8. Kan, A. T.; Fu, G.; Tomson, M. B. "Effect of Methanol on Carbonate Equilibrium and Calcite Solubility in a Gas/Methanol/Water/Salt Mixed System." *Langmuir*, **18(25)**, 9713-9725, (2002)

11 Conclusions

A model to predict scale formation in water+MEG (MonoEthylene Glycol) mixed solutions has been developed. Scale forming minerals included in the model are: $CaSO_4$, $CaSO_4 \cdot 2H_2O$, $BaSO_4$, $SrSO_4$, NaCl, KCl, $CaCO_3$, $FeCO_3$, $BaCO_3$, $SrCO_3$, $3MgCO_3 \cdot Mg(OH)_2 \cdot 3H_2O$, FeS, $Mg(OH)_2$, $NaHCO_3$, $KHCO_3$, Na_2CO_3, K_2CO_3, and NaAc. The latter three can in addition contain various amounts of crystal water. CO_2, H_2S and the most common organic acids found in an oilfield have MEG dependent phase distribution and dissociation. The solubility of $CH_4(g)$ in water+MEG has also been included.

An already existing aqueous multiphase scale model forms the basis of the new model. The capability of performing scale calculations in MEG containing solutions has been empirically constructed from new experimental data together with literature data. The mathematical functions used for curve fitting were generally arbitrarily chosen polynomials i.e. they do not have any physical/theoretical basis.

Principally there is a difference between pH dependent and independent salts in the model. For pH independent salts like $CaSO_4$ and NaCl, a MEG dependence has been constructed for each precipitation equilibrium. Such MEG dependences are fitted from solubility data. For description of pH dependent species, the model must also include phase distribution of CO_2, H_2S and the usual organic acids found in oil field waters. These species can exist both in the gas+oil phase and in the water+MEG phase, contrary to ions that are present only in the water+MEG phase. The phase distribution is accounted for by introducing a MEG dependence for the activities of the dissolved gases. These gases dissociate in water+MEG forming H^+ and the corresponding anions. A pH measurement gives the *activity* of H^+. The activity of the H^+ ion has a certain MEG dependence, and e.g. in the $CO_2(aq)$ equilibria the corresponding HCO_3^- and CO_3^{2-} ions will also have certain MEG dependences. Thus pH *independent* species have a MEG dependence fitted for each *salt,* while pH *dependent* species have MEG dependences for each *ion.* For scale purposes cations do, however, always appear in equilibria with anions and eventually form neutral salts. Thus the model can be described as having a certain MEG dependence for each precipitation reaction, irrespective of the equilibrium containing a pH dependent specie or not.

All equilibria are dependent on temperature, pressure, MEG concentration and concentrations of dissolved species. In pure water solutions the Pitzer ion interaction model adjusts for the deviations from ideality. At present, however, it is impossible to extend the Pitzer model such that is valid also in MEG containing solutions. The basic idea in this work is to let the effect of temperature, pressure and that of dissolved species (ionic strength) be the same in water+MEG solutions as in water. Introduction of MEG simply shifts all equilibrium constants and the model performs the calculation "as if the solvent was water". This approach has the advantages that it gives a simple and robust model with reasonable extrapolations outside the range of experimental data.

Most importantly it can be fitted from a limited amount of solubility data e.g. only 5 MEG concentrations at one temperature. Such a model is not strictly correct, however. To adjust for the oversimplification in the model, the MEG dependences of equilibria and activity coefficients are allowed to be functions of MEG concentration, temperature and ionic strength when data allows for such a refinement. Generally the MEG dependences in this work are given by functions that are only dependent on MEG concentration and temperature. The amount of available data is in most cases not sufficient to thoroughly investigate the combined effect of ionic strength and MEG.

A coupled effect between ionic strength and MEG should be most pronounced at low ionic strength (<0.1mol/kg solvent). CO_2 dissociation and modelling of low soluble carbonates are probably the most important aspects of the model. For these equilibria it was not observed any systematic coupled ionic strength-MEG effect from an ionic strength of 0.01mol/kg solvent to 0.7mol /kg solvent. This means that the simplification of using the same ionic strength effect in water+MEG mixtures as in water, satisfactory adjusted the results within the experimental scatter.

For conditions encountered in oil and gas transport pipelines and at well heads, the model should function well. The MEG dependences are empirically fitted, generally in the range 0-100°C and covering the whole interval 0-100% MEG in the solvent. Solubility data have been used to fit the model. Hence if the model predicts precipitation of a salt, the ionic strength is normally in the same range as in the data used for constructing the model. The exceptions are points in the process facility where the temperature is high, and/or several highly soluble species like Na^+, K^+, CO_3^{2-}, Cl^- etc. are present yielding a high salinity (>1mol/kg). Such conditions can typically be encountered in MEG regeneration boilers. The model is not suited for calculations at such conditions.

The activity of water, a_{H_2O}, in the solvent determines the amount of moisture in the gas (and oil) phase. a_{H_2O} has been fitted from partial pressure data, and is important in scale calculations as it is included in acid equilibria reactions. Salts that contain crystal water are directly influenced by water activity.

Much new data have been gathered for the water+MEG system, mainly concerning the first dissociation constant of CO_2, the solubilities of the carbonates; $CaCO_3$, $BaCO_3$, $SrCO_3$ and $3MgCO_3 \cdot Mg(OH)_2 \cdot 3H_2O$ as well as the sulphates, $CaSO_4$ and $CaSO_4 \cdot 2H_2O$. These experiments were confined to 20-80°C and ionic strengths of 0-0.7mol/kg.

Special attention has been given to the Mg-CO_3-H_2O-MEG system, due to solid magnesium carbonate appearing in several meta-stable phases. Hydromagnesite ($3MgCO_3 \cdot Mg(OH)_2 \cdot 3H_2O$) has been included as the only magnesium carbonate mineral in the scale model. Hydromagnesite is actually a meta-stable phase, but the thermodynamically stable magnesite ($MgCO_3$) has been omitted due to its formation being kinetically inhibited. Even seeded aqueous solutions at 80°C with an SR of 90-100 with respect to magnesite, did not give any precipitation within 4 days.

A method for synthesizing magnesite from hydromagnesite at atmospheric conditions has been suggested. Mono Ethylene Glycol (MEG) is used to lower the solvent vapour pressure at temperatures above 100°C.

Generally MEG severely reduces salt solubility, on a mol/kg solvent basis, but to a lesser extent than methanol. Salts containing crystal water usually show a marked solubility increase at >90wt% MEG in the solvent. This can be attributed to a decrease in water activity as MEG concentration increases.

A new method for the measurement of MEG concentration has been developed. The advantages are that it is fast, easy and inexpensive. Merely density and conductivity of the solution are used to estimate both MEG and Salt contents. If also the alkalinity is measured, the model can separate between $NaHCO_3$ and other salts for improved accuracy. The method is based on new data of density and conductivity in mixed *water+MEG+NaCl+*$NaHCO_3$ solutions. It is valid in the whole concentration interval of 0 to 100 wt% MEG and with ionic strengths from zero to the solubility limits of NaCl and $NaHCO_3$. At intermediate MEG concentrations (40 to 90wt%) the accuracy of the method is regarded as ±2 wt % for calculation of MEG content. Na^+ must be the dominating cation, and Cl^- and/or HCO_3^- the dominating anions for the method to function properly.

The determination and meaning of pH in water+MEG solutions have been discussed. All *pH* values in this work are referred to the 0.05m KHPh (Potassium Hydrogen Phtalate) standard in the water+MEG solution at question. It is essential that a user of the model recognize this because a pH electrode calibrated only in common aqueous standards will not give the pH value used in this work. The measured value from an electrode calibrated in common aqueous standard solutions is denoted pH_{meas}. pH_{meas} is principally not reproducible in water+MEG solutions, but the actual *pH* can be found from pH_{meas} as;

$$pH = pH_{meas} + \Delta pH_{Salt} + \Delta pH_{MEG}$$

ΔpH_{MEG} is determined by calibration in MEG standards (0.05mol KHPh / kg solvent). This calibration has to be performed once for each electrode. At high salinities (>>0.1M) a pH measurement also has to be corrected for the salt/ionic strength impact on the electrode. This is included with the ΔpH_{Salt} term.

The main area of application for this model is prediction of carbonate scale and hence for control of the alkalinity in the MEG injection stream. pH prediction in alkaline solutions in contact with CO_2 is therefore vital. pH prediction was tested at 4-80°C in CO_2 saturated solutions (60 and 90wt% MEG) at a total pressure of ~1bar. pH was measured as function of added $NaHCO_3$ or $KHCO_3$ (only at 25°C). Salt concentrations were varied from 0.1mmol/(kg solvent) and up to the solubility limits. The calculations were generally within 0.1pH units of the measurements.

APPENDIX 1: Symbols and abbreviations

a	activity
A	Anhydrite ($CaSO_4$)
A	Debye Hückel limiting slope
A_T	Total alkalinity (mol/kg)
C_p	Heat capacity (J/K mole)
E	Potential (V)
$E°$	Standard potential (V)
E_{LJ}	Electrode potential at Liquid Junction
E_g	Electrode potential at glass membrane
EtOH	Ethanol
f_i	Fugacity of comp *i* (bar)
F	Faraday's constant (96484.6 $C \cdot mol^{-1}$)
G	Gypsum ($CaSO_4 \cdot 2H_2O$) (*or* Gibbs free energy)
$\overline{G}$	Partial Gibbs free energy (J/mole)
H	Enthalpy (kJ/mole)
ΔpH_{MEG}	Calibration value from measurements in MEG containing 0.05m KHPh standard solutions
ΔpH_{Salt}	Calibration value for ionic strength/Salt influence on pH electrode
ΔG^E_{Salt}	Excess Gibbs energy due to change in salt content (J/mole)
ΔG^E_{MEG}	Excess Gibbs energy due to addition of MEG (J/mole)
I	Ionic strength (mol/kg)
K°	Thermodynamic equilibrium constant
K'	Stochiometric equilibrium constant
M	Molarity (mol/L solution)
m	Molality (mol/kgsolvent)
$m°$	$=1 mol\ kg^{-1}$
MEG	Monoethylene Glycol
MeOH	Methanol
n	number of moles *or* the number of electrons transferred in half reaction (Nernst equation)
pH	"actual pH" = -log (a_{H+})
pH_{meas}	Measured pH. Electrode calibrated in aqueous standard solutions
pH_{RVS}	pH-metric Reference Value Standard (0.05m KHPh)
pH_S	pH-Standard
$p(a_H\gamma_{Cl})$	Acidity function. Measurable quantity used for pH standard determination
$p(a_H\gamma_{Cl})^\circ$	Acidity function extrapolated to 0 chloride content
P	Pressure (bar)

PVT	Pressure Volume Temperature (Model calculating phase behaviour of gas and condensed phases)
T	Temperature (Kelvin)
R	Gas constant (8.314 $J \cdot K^{-1}$ mol^{-1})
R'	$R \cdot ln10$
s	sensitivity of pH electrode (variation from Nernst' slope)
S	Entropy (J/K mole)
V	Volume (cm^3)
wt%	Weight % (Concentration in salt free solvent)
$\bar{v}$	Partial molar volume (cm^3/mole)
w	Water
w_{MEG}	weight fraction MEG
x,y,z	Molefraction in water/oil, gas and total
XRD	X-ray Diffraction

Greek

φ	Fugacity coefficient
$\bar{\kappa}$	Partial molar compressibility (cm^3/mol bar)
γ	Activity coefficient
$\gamma^{\pm}$ or $\gamma_{\pm}$	Mean activity coefficient. e.g. $\gamma^{\pm}_{NaCl} = \sqrt{\gamma_{Na^+}\gamma_{Cl^-}}$ and $\gamma^{\pm}_{Na_2CO_3} = \sqrt[3]{\left(\gamma_{Na^+}\right)^2 \gamma_{CO_3^{2-}}}$
$\gamma^{o}_{Cl^-}$	Activity coefficient of Cl^- at zero chloride concentration
γ^{N}	Activity coefficient due to MEG
γ^{S}	Aqueous activity coefficient
$\gamma^{o,N}_{H^+}$	Primary medium effect of H^+
${}^{w}_{sol}\gamma^{o}_{H^+}$	Primary medium effect of H^+
${}^{w}_{sol}\gamma^{o}_{HCl}$	Primary medium effect of HCl (from *solvent* to *water*)
${}^{sol}_{w}\gamma^{o}_{HCl}$	Primary medium effect of HCl (from *water* to *solvent*)
μ_i^j	Chemical potential of comp i in phase j (J/mole)

Symbols, superscripts and subscripts

°	in standard state
sol *or* s	Solvent; usually for denoting a *solvent* based standard state
w	Water; usually for denoting an *aqueous* based standard state
ID	Ideal
E	Excess
ref	reference ionic strength = 0.1mol/kg solvent
∞	Infinite dilution

APPENDIX 2: pH in saline water+MEG solutions

To investigate salt influence on a pH electrode, the pH_{meas} was measured in HCl+NaCl+Water+MEG solutions relative to a solution with ionic strength of 0.1mol/kg. The experiments were performed in solutions containing ~1mmol HCl/kg, where portions of NaCl were added to change the ionic strength. Data were obtained with a Mettler Toledo DG111-SC combined 3M KCl electrode at 25°C (two series) and a special high temperature electrode from Innovative sensors (GT-DJ) at 50°C. Table A1-A3 gives the change relative to the 0.1m NaCl solution i.e. pH_{meas} – (pH_{meas} with 0.1m NaCl)

Table A 1: Change in pH_{meas} relative to 0.1 mol NaCl/kg solution at 25°C.

NaCl m	MEG / wt%			
	0	**30**	**50**	**90**
0	-0.022	-0.068	-0.088	-0.080
0.01	-0.020	-0.048	-0.057	-0.063
0.05	-0.006	-0.015	-0.017	-0.016
0.07	-0.003	-0.008	-0.009	-0.007
0.1	**0.000**	**0.000**	**0.000**	**0.000**
0.25	-0.005	0.004	0.008	0.013
0.5	-0.029	-0.018	-0.015	-0.003
0.7	-0.053	-0.044	-0.041	-0.045
0.75	-0.058	-0.050	-0.047	
1	-0.092	-0.087	-0.085	

Table A 2: Change in pH_{meas} relative to 0.1 mol NaCl/kg solution at 25°C.

NaCl m	MEG / wt%				
	0	**50**	**50**	**90**	**90**
0	-0.020	-0.082	-0.085	-0.076	-0.075
0.01	-0.018				
0.05	-0.004	-0.017	-0.018	-0.021	-0.021
0.1	**0.000**	**0.000**	**0.000**	**0.000**	**0.000**
0.3	-0.008	0.007	0.005	0.011	0.017
0.5	-0.028	-0.014	-0.013	-0.006	0.000
0.7	-0.056	-0.039	-0.039	-0.032	-0.019
1	-0.100	-0.085	-0.085	-0.078	
3	-0.417				

Table A 3: Change in pH_{meas} relative to 0.1 mol NaCl/kg solution at 50°C.

NaCl m	MEG / wt%			
	0	**30**	**50**	**90**
0	-0.007	-0.061	-0.094	-0.098
0.01	-0.018	-0.048	-0.068	-0.088
0.05	-0.005	-0.016	-0.017	-0.041
0.07	-0.001	-0.009	-0.009	-0.020
0.1	**0.000**	**0.000**	**0.000**	**0.000**
0.25	-0.005	0.010	0.013	0.014
0.5	-0.013	-0.020	-0.003	-0.005
0.7	-0.053	-0.042	-0.027	-0.016
0.75	-0.055	-0.048	-0.033	
1	-0.089	-0.082	-0.067	

APPENDIX 3: $CaSO_4$ solubility data

The first investigation[1] of $CaSO_4$ (anhydrite) solubility gave values in water (see chapter 6.3.1) that were too high compared with other data. In the solutions containing MEG, however, the results were generally consistent and corresponded well with the data given in chapter 4. These data are given in the table below, although the values at ~100% MEG and temperature 25-40°C are questionable. Accuracy is regarded as ±5% but never less than ±0.2mmol/kg solvent.

Table A 4: $CaSO_4$ (Anhydrite) solubility. Salt concentrations given per kg *solvent* and MEG concentration as wt% in solvent.

Temp [°C]	MEG wt%	NaCl mol/kg	Ca^{2+} mmol/kg	Temp [°C]	MEG wt%	NaCl mol/kg	Ca^{2+} mmol/kg
25	50	0	3.08	65	20	0	6.39
25	80	0	1.24	65	40	0	3.27
25	90	0	1.02	65	50	0	2.05
25	95	0	0.81	65	60	0	1.25
25	100	0	0.41	65	80	0	0.50
25	50	0.1	5.84	65	90	0	0.38
25	80	0.1	2.23	65	95	0	0.31
25	90	0.1	1.88	65	100	0	0.51
25	100	0.1	1.55	65	50	0.1	4.62
				65	80	0.1	1.16
40	20	0	8.94	65	90	0.1	1.04
40	40	0	4.00	65	100	0.1	1.48
40	50	0	3.16	65	100	0.1	1.11
40	50	0	3.18	65	20	0.5	18.73
40	50	0	3.19	65	40	0.5	10.75
40	60	0	1.86	65	50	0.5	7.91
40	80	0	0.78	65	60	0.5	5.76
40	90	0	0.55	65	80	0.5	2.91
40	95	0	0.64	65	90	0.5	2.06
40	100	0	0.17	65	95	0.5	2.04
				65	100	0.5	1.97
85	20	0.7	17.63	65	20	0.7	21.43
85	50	0.7	8.10	65	50	0.7	9.43
85	80	0.7	2.55	65	80	0.7	3.48
85	90	0.7	2.35	65	90	0.7	2.60
85	95	0.7	1.83	65	95	0.7	2.54

[1] Kaasa, B., Sandengen, K. and Østvold, T. " Thermodynamic Predictions of Scale Potential, pH and Gas Solubility in Glycol Containing Systems", SPE 95075, Int. Symposium on Oilfield Scale, Aberdeen, (2005)